JOURNAL OF ENGINEERING SCIENCES

(cc) BY-NC

ЖУРНАЛ ІНЖЕНЕРНИХ НАУК

ЖУРНАЛ ИНЖЕНЕРНЫХ НАУК

(cc) BY-NC

JOURNAL OF ENGINEERING SCIENCES

ЖУРНАЛ ІНЖЕНЕРНИХ НАУК

ЖУРНАЛ ИНЖЕНЕРНЫХ НАУК

Scientific Journal

Науковий журнал

Научный журнал

Founded in 1994

Заснований у 1994 році

Основан в 1994 году

The Journal of Engineering Sciences is an open access scientific journal that covers urgent issues of the up-to-date high-tech production, development of new engineering trends and future technologies. General topics of the journal concerns manufacturing, mechanical and chemical engineering. The main publication language presented for papers is English. The editorial board represented by scientists from different European research institutions allows covering the journal's topics and qualitatively evaluate all the submitted papers. The system of double blinded reviewing process provides a high-quality presentation of papers. The editorial police including the submitting, reviewing, acceptance and publication of the materials are completely transparent.

Recommended for publication
by the Academic Council of Sumy State University,
(minutes No. 6 of 15.11.2018)

The Journal is the scientific professional edition of Ukraine in the field of Engineering Sciences (ordered by the Ministry of Education and Science of Ukraine, July 13, 2015, No. 747): http://old.mon.gov.ua/img/zstored/files/747.rar).

The Journal of Engineering Sciences is published with the support of the following partners:
− Faculty of Technical Systems and Energy Efficient Technologies of Sumy State University (Sumy, Ukraine): http://teset.sumdu.edu.ua;
− Faculty of Mechanical Engineering, University of West Bohemia (Pilsen, Czech Republic): http://www.fst.zcu.cz;
− Faculty of Mechanical Engineering and Management, Poznan University of Technology (Poznan, Poland): https://www.put.poznan.pl.

CrossRef
https://search.crossref.org

Directory of Open Access Journals (DOAJ)
https://doaj.org

Index Copernicus International Journals Master List
https://journals.indexcopernicus.com

Google Scholar
https://scholar.google.com

International Institute of Organized Research
http://www.i2or.com

Scientific Indexing Services (SIS)
http://www.sindexs.org

Academic Resource Index (Research Bible)
http://researchbib.com

Directory of Research Journals Indexing (DRJI)
http://www.drji.org

World Cat
http://www.worldcat.org

Eurasian Scientific Journal Indexing (ESJI)
http://esjindex.org

Journal Impact Factor
http://jifactor.org

Impact Factor Services for International Journals (IFSIJ)
http://ifsij.com

Journal Factor
http://www.journalfactor.org

Open Academic Journals Index (OAJI)
http://oaji.net

Academic Keys
http://academickeys.com

International Society for Research Activity (ISRA)
Journal Impact Factor (JIF):
http://www.israjif.org

Advanced Science Index (ASI):
http://journal-index.org

International Scientific Indexing (ISI):
http://isindexing.com

Global Digital Publishing Platform
https://issuu.com

Vernadsky National Library of Ukraine
http://www.nbuv.gov.ua

Electronic Sumy State University Institutional Repository
http://essuir.sumdu.edu.ua

TOPICS

OF THE "JOURNAL OF ENGINEERING SCIENCE":

1. MANUFACTURING ENGINEERING:

- (A) Machines and Tools;
- (B) Technical Regulations and Metrological Support;
- (C) Materials Science.

2. MECHANICAL ENGINEERING:

- (D) Dynamics and Strength of Machines;
- (E) Computational Mechanics.

3. CHEMICAL ENGINEERING:

- (F) Processes in Machines and Devices;
- (G) Energy Efficient Technologies;
- (H) Environmental Protection.

CONTENTS

MANUFACTURING ENGINEERING

MECHANICAL ENGINEERING

CHEMICAL ENGINEERING

Processes in Machines and Devices ○ ○ ○ ○ ○ ● ○ ○ **F**

Energy Efficient Technologies ○ ○ ○ ○ ○ ○ ● ○ **G**

Environmental Protection ○ ○ ○ ○ ○ ○ ○ ● **H**

DSMIE 2019

2nd International Conference on Design, Simulation, Manufacturing: The Innovation Exchange

June 11-14, 2019 | Lutsk, Ukraine

http://dsmie.sumdu.edu.ua

- English language
- Keynote Speakers
- Keynote & Technical Sessions
- Industrial companies
- Industry Tour
- Universities

DSMIE-2019

Important Dates

Date	Event
November 20, 2018	Paper Submission
December 20, 2018	Paper Notification
January 15, 2019	Final Paper Submission
February 1, 2019	Registration & Fee Payment

About

DSMIE-2019 focuses on a broad range of research challenges in the fields of **Manufacturing Engineering**, **Mechanical Engineering** and **Chemical Engineering**, addressing current and future trends in design approaches, simulation techniques, computer-aided systems, software development, ICT tools and Industry 4.0 strategy implementation for engineering tasks solving.

DSMIE-2019

Sumy State University · ЛНТУ · TECHNICKÁ UNIVERZITA V KOŠICIACH · Kielce University of Technology · UNIVERSITY OF WEST BOHEMIA · InnovativeFET · Промышленность в Фокусе

Contacts

- Sumy State University, 2 Rymskogo-Korsakova St., Sumy, 40007, Ukraine
- E-mail: dsmie@teset.sumdu.edu.ua
- Tel.: +38-066-488-03-19

Together we can do more for science, technology, engineering and education
© DSMIE Team

Finite Element Analysis of Orthogonal Cutting Forces in Machining AISI 1020 Steel by Using a Carbide Tip Tool

Bashistakumar M.[1], Pushkal B.[2*]

[1] B. R. Ambedkar National Institute of Technology, Grand Trunk Road, Jalandhar, 144011 Punjab, India;
[2] L. Narain College of Technology, Kalchuri Nagar, Raisen Road, Bhopal, 462021 Madhya Pradesh, India

Abstract. Force modeling in metal cutting is important for various purposes, including thermal analysis, tool life estimation, chatter prediction, and tool condition monitoring. Numerous approaches have been proposed to model metal cutting forces with various degrees of success. In addition to the effect of work piece materials, cutting parameters, and process configurations, cutting tool thermal properties can also contribute to the level of cutting forces. The process of orthogonal metal cutting is studied with the finite element method under plane strain conditions. A numerical procedure has been developed for simulating orthogonal metal cutting using a general-purpose finite element method. The focus of the results presented in this work is on the effect of forces on the tool by variation of cutting parameters. The result is simulated with the analytical value for evolution of effective force for cutting material under various cutting condition.

Keywords: AISI 1020 steel, shaping, analytical model, finite element model, orthogonal cutting.

1 Introduction

Being the fundamental model for all cutting processes, modelling of the orthogonal cutting has been one of the most important problems for machining researchers for decades. Understanding the true mechanics and dynamics of the orthogonal cutting process would result in solution of major problems in machining such as parameter selection, accurate predictions of forces, stresses, and temperature distributions. In order to optimize machining processes three-dimensional models are indispensable that are capable to simulate three-dimensional chip flow using one cutting edge.

2 Literature Review

Both analytical and numerical methods have been used in the literature to model orthogonal cutting processes. The first successful mathematical attempt for understanding of the mechanics of orthogonal cutting is made by Merchant [1]. He studied the continuous type chips and formulated the deformation zone, i.e. the shear plane that is responsible for the formation of the chip by force equilibrium and the minimum energy principle. Although his work has several important assumptions, it is still widely used to understand the basics of the cutting process. Later,

many researchers [2–7] worked on the modeling of the orthogonal cutting. After some deceleration in the research on cutting process mechanics due to the developments in CNC and CAD/CAM technologies, the process research regained some momentum in recent years. Many predictive models have been proposed by means of analytical, semi-analytical or completely numerical methods up to now. Semi-analytical models, where some of the values are identified from the cutting tests, usually yield high prediction accuracy, however they may not always provide insight about the process [8–10]. In addition, the cutting tests can be time consuming depending on the number of variables and their ranges. Some analytical models may provide sufficient insight about the process and the solution times are usually very short. They can be grouped in some categories such as Johnson Cook material model [13], the slip-line models [15–19], and thin and thick shear zone models [20–22]. There are also several studies where the friction in machining is investigated. However, there are still issues in modeling the rake contact zone which involves the friction between the tool and the work piece due to the complex nature of the chip-tool contact. The objective of this study is to propose an orthogonal cutting model that integrates the primary

Journal of Engineering Sciences, Volume 5, Issue 2 (2018), pp. A 1–A 10

A 1

and secondary deformation zones' effects on the cutting process. In modeling of the primary shear zone the study of Dudzinski and Molinari [21] is used. The model uses a thermo-mechanical constitutive relationship which is transformed to a Johnson-Cook type material model in this study. The shear plane is modeled having a constant thickness. In their later model, they modelled the friction on the rake face as a temperature dependent value. However, they just considered sliding contact conditions which may be valid for very high cutting speeds.

On the other hand, numerical models, such as FEM, [11–14] could provide much more detailed information about the process, such as temperature and pressure distribution on the rake face, however their accuracy is questionable and the solution times can be very long. A three-dimensional FEM model was developed by Fang and Zeng [26] based on coupled thermo-elastic-plastic material flow. The model utilized a rigid tool and hence unable to simulate stresses inside the cutting tool. Cutting forces were measured at different inclination angles of the tool. The model was however, not validated experimentally. Zou et al. [27] made a new Orthogonal cutting model by using an upper bound approach. They introduced two new variables based on process kinematics that replaces chip flow angle and coefficient of friction in the traditional scheme. The chip flow angles predicted from the new model were found to be comparable with the experimental results. In numerical modeling methods, both finite difference methods (FDM) and finite element methods (FEM) have been used to model orthogonal cutting processes. An FDM model to predict temperature fields in orthogonal cutting was developed by Lazoglu and Islam [28]. The proposed a new method based on elliptical structural grid generation and the computational expense was found to be much less as compared to the conventional FE models. The temperature predictions were found to be in good agreement with the experimental data using the proposed finite difference method. Li and shih [29] developed a 3D finite element model (FEM) using AdvantEdge to simulate orthogonal turning of titanium. The model can predict cutting forces, temperature at the tool-chip interface and chip thickness and the effect of various process parameters and cutting geometries can be investigated. In addition to continuous chip formation, serrated chips were also modeled. All the results are found to be in close agreement with the experimental observations. In addition to traditional Lagrangian scheme, Arbitrary Lagrangian Eulerian (ALE) method was also employed by researchers to model orthogonal cutting processes. An ALE model for orthogonal cutting of AISI 4340 with cemented carbide tools was developed by Llanos et al. [30]. Chip flow angles and cutting forces were predicted with different cutting parameters and tool geometries. Overall a good correlation was found with the experimental findings. The outputs of the proposed model are the cutting forces, the stress distributions on the rake face. Although the model is still under development, the final aim of the model is to develop a cutting process model which needs minimum amount of calibration tests. The friction and material constants can be obtained from or-thogonal cutting tests. After the calibration, the model can be applied for all machining operations using the same tool and work piece material.

This study aims to model orthogonal cutting process in shaping operations for AISI 1020 steel. Unlike ALE models which are computationally expensive, the developed model uses a Lagrangian approach technique. The model is able to predict initial chip formation, chip growth and steady state chip formation and does not need any prior assumption regarding the chip flow. The accuracy of the model is verified by comparing depth of cut, feed and radial forces with the analytical data. In addition tool performance and surface integrity of the work piece is analyzed using stress distribution in the work piece and the cutting tool.

3 Research Methodology

3.1 Johnson–Cook material model

The flow stress models that describe the work material behaviour as a function of temperature, strain and strain rate are considered highly necessary to represent work material constitutive behaviour under high-speed cutting conditions for work materials. Unfortunately sound theoretical models based on atomic level material behaviour are far from being materialized as reported by Jaspers and Dautzenberg [9]. Therefore, semi empirical constitutive models are widely utilized. Among such models, the constitutive model proposed by Johnson and Cook [13] describes the flow stress of a material with the product of strain, strain rate, and temperature effects that are individually determined as given in the following equation:

$$\sigma_{AB} = \left[A + B \left(\bar{\varepsilon}_{AB} \right)^{n} \right] \left[1 + c \ln \left(\frac{\dot{\bar{\varepsilon}}_{AB}}{\dot{\bar{\varepsilon}}_{0}} \right) \right] \left[1 - \left(\frac{T - T_{0}}{T_{m} - T_{0}} \right)^{m} \right] \quad (1)$$

In the Johnson-Cook (JC) constitutive model, the parameter A is the initial yield strength of the material at room temperature and a strain rate of 1 s^{-1} and $\bar{\varepsilon}$ represents the plastic equivalent strain. The equivalent plastic strain rate $\dot{\bar{\varepsilon}}_{AB}$ is normalized with a reference strain rate $\dot{\bar{\varepsilon}}_{AB}$. The temperature term in the JC model reduces the flow stress to zero at the melting temperature of the work material, T_m leaving the constitutive model with no temperature effect. In general, the constants A, B, C, n, and m of the model are fitted to the data obtained by several material tests conducted at low strains and strain rates and at room temperature as well as the split Hopkinson pressure bar (SHPB) tests at strain rates up to 10^4 s^{-1} and at temperatures up to 600 °C [8, 9].

The JC model provides a good fit for strain-hardening behavior of metals and it is numerically robust and can easily be used in FEM simulation models [13]. Zerilli and Armstrong (ZA) derived an alternative constitutive model for metals with a crystal structure distinction by using dislocation-mechanics theory [14].

The orthogonal cutting tests results for AISI 1020 are adopted from Oxley [6] that are performed for 0.2 % carbon steel. The cutting conditions are given in Table 1. The flow stress data of SHPB tests adopted from Jasper and Dautzenberg [18] is combined with the flow stress determined under the orthogonal cutting conditions. The constants of the JC material model for work flow stress are computed as $A = 333$, $B = 737$, $C = 0.008$, $n = 0.15$, and $m = 1.46$ for the extended ranges of strain (0.051–1.070), strain-rate (1–17 766 s^{-1}) and temperature (20–721 °C).

Those constants are found in close agreements with the ones determined by Jasper and Dautzenberg [9], as given in Table 1, indicating the success of the proposed methodology.

The details of the computed process variables in the primary and secondary deformation zones are given in Table 2. The parameters of the tool-chip interface friction model are also computed by using the methodology proposed in this study as shown in Table 1.

Table 1 – Material constants for the Johnson-Cook model obtained from SHPB tests [9]

Material	Reference	T_m, °C	A, MPa	B, MPa	c	n	M
AISI 1045	[9]	1 460	553.1	600.8	0.0134	0.234	1.00
AISI 1020	[9]	1 525	333.0	737.0	0.0080	0.150	1.46
AL 6082 T-6	[9]	582	428.5	327.7	0.0075	1.008	1.31
Ti6Al4V	[17]	1 630	862.5	331.2	0.0120	0.340	0.80
Ti6Al4V	[16]	1 630	782.7	498.4	0.0280	0.280	1.00

Table 2 – Orthogonal test mild steel [9]

V, m/min	t_1, mm	t_2, mm	T_{AB}, s	T_{int}, s	K_{chip}	$\bar{\varepsilon}_{AB}$	$\dot{\bar{\varepsilon}}_{AB}$	$\bar{\varepsilon}_{int}$	$\dot{\bar{\varepsilon}}_{int}$	τ_{AB}, N/mm^2
100	0.125	0.4	428	627	223.8	1.07	5 488	1.55	1.50	558.5
200	0.125	0.3	474	681	128.6	0.87	16 488	1.28	5.35	648.6
100	0.250	0.6	447	701	214.9	0.87	17 766	1.28	10.70	579.5
200	0.250	0.7	467	662	193.6	0.97	5 861	1.42	0.98	579.3
100	0.500	1.1	494	721	206.6	0.82	10 632	1.21	3.18	624.4
200	0.500	1.2	450	674	211.9	0.78	12 653	1.14	7.70	614.0
100	1.000	2.3	458	649	192.9	0.82	3 399	1.21	0.79	634.0
200	1.000	2.4	453	635	191.3	0.73	4 814	1.07	2.37	647.0

3.2 The primary shear zone model

The plastic deformation is assumed to take place only at the shear plane, and with plane strain conditions. Also the shear plane is modeled as a thin plane but having a thickness of 0.025 mm. Moreover, the shear stress distribution at the outer boundary of the shear plane is assumed to be uniform. With the assistance of the equations of conversation of momentum and energy, and the constitutive law, Dudzinski and Molinari [21] proposed to solve a compatibility condition with an iterative procedure in order to calculate the shear stress at the entry of the shear plane, τ_0. Moreover again from the equations of motion for a steady state solution and continuous type chip. The shear stress at the exit of the shear plane is calculated as presented in works [21, 22].

3.3 Oxley's analysis of machining

A simplified illustration of the plastic deformation for the formation of a continuous chip when machining a ductile material is given in Figure 1. There are two deformation zones in this simplified model a primary zone and a secondary zone. It is commonly recognized that the primary plastic deformation takes place in a finite-sized shear zone. The work material begins to deform when it enters the primary zone from lower boundary *CD*, and it continues to deform as until it passes the upper boundary *EF*. Oxley et al. [6] assumed that the primary zone is a parallel-sided shear zone.
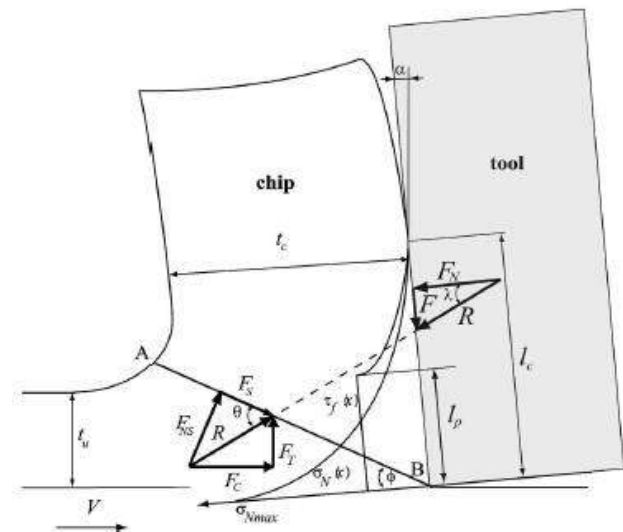
Figure 1 – Forces acting on the shear plane and the tool with resultant stress distribution on tool rake surface [6]

There is also a secondary deformation zone adjacent to the tool chip interface that is caused by the intense contact pressure and frictional force. After exiting from the primary deformation zone, some material experiences further plastic deformation in the

secondary deformation zone. Using the quick-stop method to experimentally measure the flow field, Oxley [6] proposed a slip-line field similar to the one shown in Figure 1. Initially, Oxley and co-authors assumed that the secondary zone is a constant thickness shear zone. In this study, we assume that the secondary deformation zone is triangular shape and the maximum thickness is proportional to the chip thickness.

3.4 Numerical experiment finite element modelling of shaper tool

Numerical simulations with FEA were performed using the ABAQUS FE modeling software Advantage. Features to model machining processes in the software include adaptive remeshing capabilities for resolution of multiple length scales; multiple body deformable contact for tool–work interface, and transient thermal analysis. The material properties model contains deformation hardening, thermal softening and rate sensitivity associated with a transient heat conduction analysis for finite deformations. A constant coefficient of friction 0.2 is assumed in the simulations. The numerical simulations were performed with the commercial code ABAQUS/Explicit. The tool geometry and the cutting conditions are listed in Table 1. Two minor differences are: element layer of 2 μm in the lagrangian mesh acting as an interface between the upper part of the work piece (which will be cut forming the chip) and the lower part of the work piece (which will be the machined surface) to minimize the losses of material due to erosion and allow separation assuming a von Mises type yield criterion and an isotropic strain hardening rule for the work piece material, the yield stress σ_y is given by the Johnson-Cook equation.

The tool was assumed to behave as an elastic solid. Table 4 shows the detail properties of the work piece. Table 5 shows the mechanical parameters and Table 6 the thermal parameters of both material models. An element deletion criterion based on a critical value of the equivalent plastic strain was considered in the lagrangian mesh for the work piece material. This serves to erode the thin layer keeping the material at the chip. Previous work showed small influence of this criterion in cutting forces and temperature distribution, when critical value ranged from equivalent plastic strain 0.5 to 3.5. No distortion was observed in the mesh with this criterion.

An initial temperature of 293 K was fixed for both solids. Although friction phenomena produce an intense heating at the tool-chip interface, friction .3 was considered as a first approximation to the problem. Numerical model was used to analyze influence of several parameters in model results (cutting forces and chip formation mainly).

Table 3 – The cutting condition and tool geometry used in Lagrangian approach

Clearance angle	Rake angle	Velocity, m/min	Depth of cut, mm	Cutting environment
0.5	0.10	100	0.5; 1.0	Dry

Table 4 – Workpiece properties of 1020 low carbon steel (mild steel)

Minimum properties	Ultimate tensile strength, Psi	87 000
	Yield strength, Psi	72 000
	Elongation	10 %
	Rockwell hardness	B89
Chemical composition	Iron (Fe)	99.08–99.53 %
	Manganese (Mn)	0.3–0.6 %
	Carbon (C)	0.18–0.23 %
	Phosphorus (P)	0.04 % max
	Sulphur (S)	0.05 % max

Table 5 – Mechanical parameters of the workpiece and tool material models

Material	ρ, kg/m^3	E, GPa	υ	A, MPa	B, MPa	n	c	ε	m	B
WP:AISI1020 mild steel	7 833	210	0.30	333	737	0.15	0.0080	1	1.46	0.9
Tool: CNMG 120404 (carbide tip)	14 500	450	0.19	896	656	0.50	0.0128	–	0.80	–

Table 6 – Thermal parameter of the work piece and tool

Material	Specific heat, J/(kg·K)	Thermal conductivity, W/(m·K)
WP:AISI1020 mild steel	586	52.0
Tool: CNMG 120404 (carbide tip)	234	33.5

4 Results and Discussion

4.1 Numerical simulation results

Analytical approach to calculate cutting force, feed force and stress generation on the tool and work piece was calculated from taking the value from Tables 2–3. The analytical calculation was considered for 100 m/s. For this velocity the different data were taken from previously conducting experiment that is Table 2 [9]. The chip thick-ness ratio and shear stress generated on the work piece were used to calculate shear angle, co-efficient of friction and cutting force generated on the work piece. Similarly Tables 1–2 used together to find out the stress generated on the chip during orthogonal cutting operation. The various models like Johnson-Cook material model, Oxley's analysis of machining were used to find out the cutting force, feed force and stress generated in cutting process.

Table 7 – Analytical results

Depth of cut, mm	Clearance angle	Rake angle	Cutting forces and flow stress			
			F_s	F_c	F_t	σ_{AB} , MPa
0.5	0	0	195.1	299.8	55.01	704.7
		10	285.9	382.0	196.63	
	5	0	195.1	299.8	55.01	
		10	285.9	382.0	196.63	
1.0	0	0	416.1	659.8	175.55	755.1
		10	483.7	552.4	202.80	
	5	0	416.1	659.8	175.55	
		10	483.7	552.4	202.80	

In all the above cases depth of cut, clearance angle and rake angle are very according to requirement. When depth of cut increases cutting force and feed force value all so increases. The result of the cutting force and feed force directly depend upon the depth of cut and rake angle. The Johnson–Cook material model, primary shear zone model, Oxley's machining model, and analytical model were used to find out the result by using analytical equation. The clearance angle has no effect on calculating cutting forces. Its value remains same for same depth of cut and rake angle for whatever the clearance angle. The stress generated on tool chip interference remains same for individual depth of cut. The clearance and rake angle has no effect on the calculation of Stress generation. The resultant stress calculation was derived from Johnson–Cook material model equation and material parameters.

Finite element validation of cutting force, feed force and stress in machining of the AISI 1020 steel was addressed in present work. The finite element analysis is done by ABAQUS mechanical explicitly software. A work piece block was prepared with a dimension of (50×4×15) mm³. The material properties assignment was given from Johnson-Cook material model. A solid homogeneous section was assigned to the model. The proper meshing was done over the work piece model to evaluate good result. The meshing is here up to 12 000 elements. The fix boundary condition was given to the model except the cutting zone. The same process maintained for the tool also.

The material properties for the tool were calculated from Johnson–Cook material model. Material section and meshing was also given to the tool model. In boundary condition tool movement direction was given, velocity 100 m/s was maintained.

The different depth of cut maintained with different rake and clearance angle in this analysis. Detail analysis described below with graphical result.

For depth of cut 0.5 mm, 0° clearance angle and 0° rake angle, the maximum cutting force was found as 365 N at the starting point of the tool in X direction and minimum force was 302 N at the end point of the tool. The maximum feed force in this analysis was 105 N at the starting point of the tool in Y direction and minimum feed force was 38 N at the end point of the tool in the same direction. The maximum stress generated in this analysis was $8.5 \cdot 10^8$ Pa and minimum stress was $6.2 \cdot 10^8$ Pa. The result of this analysis was given in Figures 3–6 in terms of graphical view.
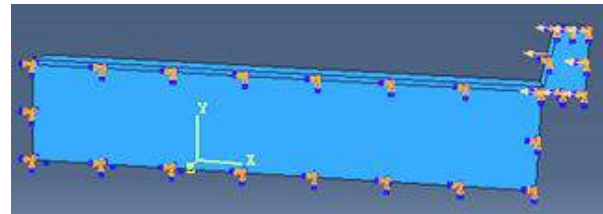
Figure 2 – Showing boundary conditions of tool and workpiece

For depth of cut 1.0 mm, 0° clearance angle and 10° rake angle, the maximum cutting force was found as 580 N at the starting point of the tool in X direction and minimum force was 524 N at the end point of the tool. The maximum feed force in this analysis was 238 N at the starting point of the tool in Y direction and minimum feed force was 176 N at the end point of the tool in the same direction. The maximum stress generated in this analysis was $8.1 \cdot 10^8$ Pa and minimum stress was $6.8 \cdot 10^8$ Pa. The result of this analysis was given in Figures 7–10 in terms of graphical view.

The above process of finite element experiment was conducted for two different depths of cut 0.5 and 1.0 mm, two different rake angles 0° and 10° and two different clearance angles 0° and 5°. Likewise 8 experiments have been carried out to find out the result. The result table is given in Table 8.
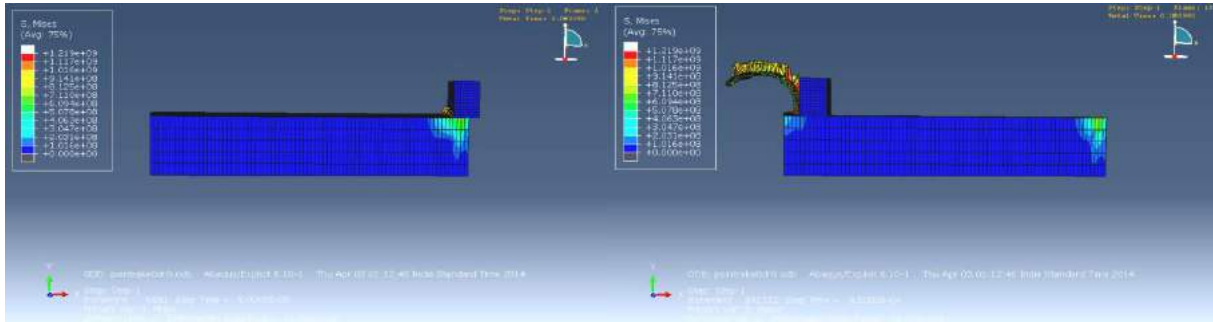
Figure 3 – Showing tool movement over work piece from start to end point
for depth of cut 0.5 mm, 0° clearance angle and 0° rake angle
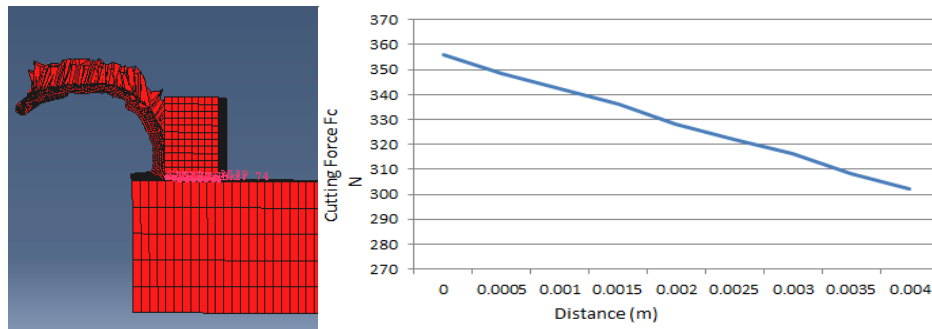
Figure 4 – Showing cutting force generated in *X* direction for
depth of cut 0.5mm, 0° clearance angle and 0° rake angle
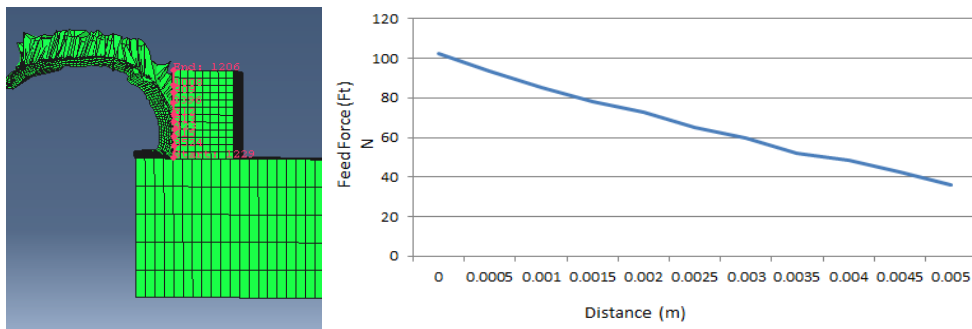
Figure 5 – Showing feed force generated in *Y* direction for
depth of cut 0.5mm, 0° clearance angle and 0° rake angle
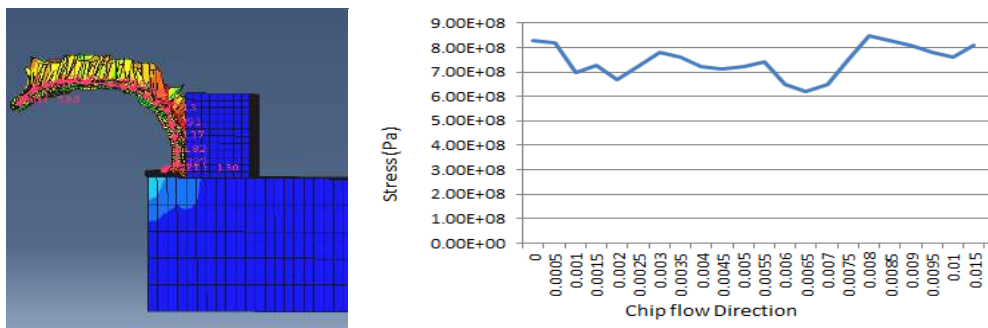
Figure 6 – Showing von Mises stress generated along chip flow direction
for depth of cut 0.5mm, 0° clearance angle and 0° rake angle
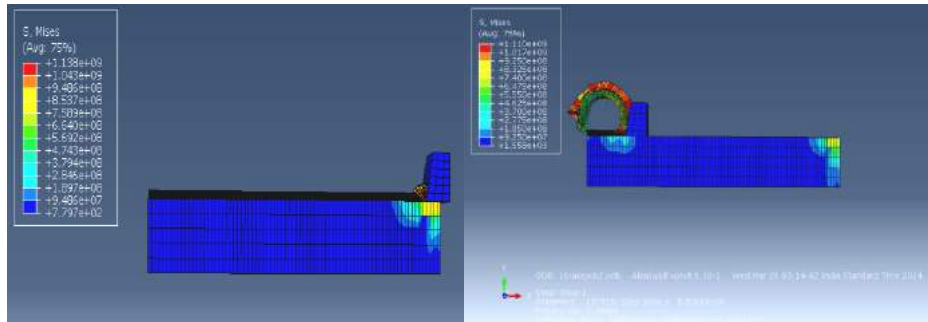
Figure 7 – Showing tool movement over work piece from start to end point
for depth of cut 1.0 mm, 0° clearance angle and 10° rake angle
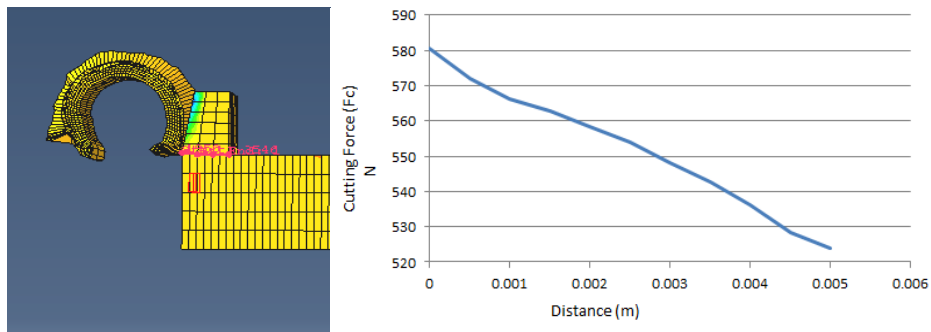
Figure 8 – Showing cutting force generated in *X* direction for
depth of cut 1.0 mm, 0° clearance angle and 10° rake angle
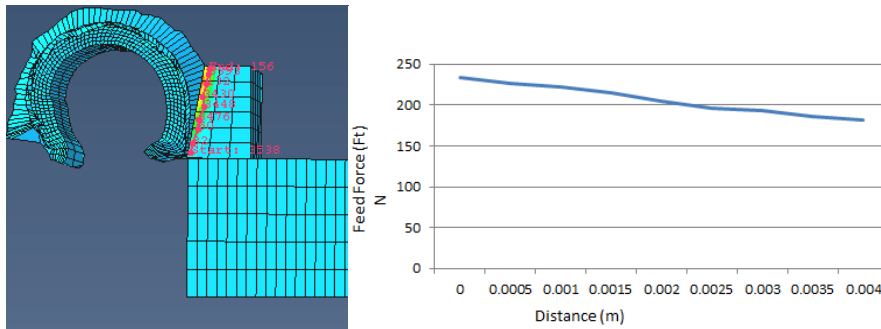
Figure 9 – Showing feed force generated in *Y* direction for
depth of cut 1.0 mm, 0° clearance angle and 10° rake angle
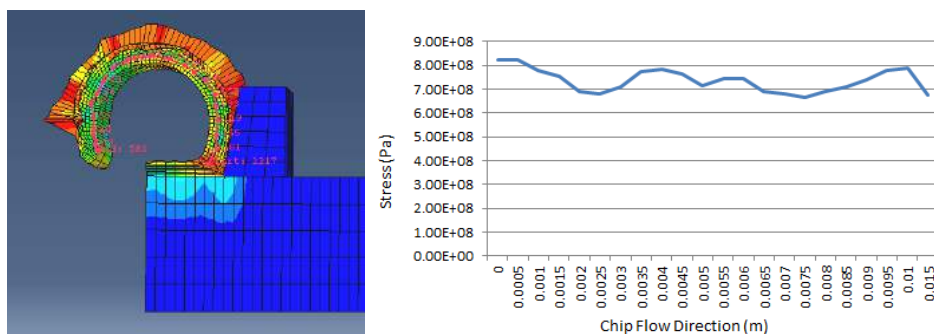
Figure 10 – Showing von Mises stress generated along chip flow direction
for depth of cut 1.0 mm, 0° clearance angle and 10° rake angle

Table 8 – Finite element analysis result

Depth of cut, mm	Clearance angle	Rake angle	Cutting force F_c, N		Feed force F_t, N		Stress σ_{AB}, 10^8 Pa	
			max	min	max	min	max	min
0.5	0	0	365	302	105	38	8.50	6.20
		10	450	382	238	170	8.20	6.50
	5	0	318	279	85	38	8.40	4.50
		10	423	365	225	175	8.30	4.80
1.0	0	0	691	622	200	152	8.53	6.32
		10	580	524	238	176	8.10	6.80
	5	0	715	635	239	179	8.32	6.82
		10	614	539	220	175	8.51	4.90

4.2 Comparison of the results

In this paragraph, a comparison between analytical results using the model reported in Table 8 and FE simulation presented in Table 9. The detail result was given below.

In this comparision the analytical rasult and the finite element result were not equal in any perticular point. The value of cutting force and feed force were maximum at the tool point or edge. The value were gradually decreases to wards the end point of the tool.

Stress generation on tool chip interference very with in the range of $(5.0–8.5) \cdot 10^8$ Pa. From the graph it was clear that numerical approach (FEM) result for cutting force, feed force and stress generated on the tool chip interference is more than the analytical result. There was a varition of 20–100 N on feed force and cutting force by comparision of both the process. Stress generated on chip flow direction also very from point to point. By taking the maximum resultant case on each observation it was found that a diiference of $(0.5–1.0) \cdot 10^8$ Pa between both the process.

Table 9 – Comparisons between analytical result and finite element result

Depth of cut, mm	Clearance angle	Rake angle	Analytical result			Finite element analysis result		
			F_c, N	F_t, N	σ_{AB}, 10^8 Pa	F_{c1}, N	F_{t1}, N	σ_{AB1}, 10^8 Pa
0.5	0	0	299.8	55.01	7.04	365	105	8.50
		10	382.3	196.63	7.04	450	238	8.20
	5	0	299.8	55.01	7.04	318	85	8.40
		10	382.0	196.63	7.04	423	225	8.30
1.0	0	0	659.8	175.55	7.55	691	208	8.53
		10	552.4	202.80	7.55	580	238	8.10
	5	0	659.8	175.55	7.55	715	239	8.32
		10	552.4	202.80	7.55	614	220	8.51

Reasons for significant difference in analytical and FEM model results:

1. Material parameters.

The material properties which are used to calculate analytical result for AISI 1020 steel is different from Johnson-Cook model material parameters. In FEM Johnson-Cook parameters with material properties are used to validate the FE experiment. These parameters are considered from previous experiment data. These are depend upon material flow rate, melting temperatue of material, properties of body and working condition.

2. Adiabatic heating.

Heat generated in the metal cutting can have a significant effect in the difference between the model result. The heat generation also directly affect the result of cutting forces and stress generation. The heat generation mechanism are the plastic work done in the primary and secondary shear zone and the sliding friction along the tool chip interference. In metal cutting process heat generated in the work piece and chip does not have sufficient time to diffuse away. Therefore temperature rise in work piece and chip is mainly due to localized adiabatic heating. Due to this reason also there is a significant difference between both the models.

3. Separation criterion.

This criterion states that chip separation occur when the stress along the cutting path reach a critical combination at a specified distance in front of the tool tip. To implement this criterion in ABAQUS the cutting path in work piece is defined by contact surface. Paired finite element nodes on the contact surface are initially in the perfect bond. When the chip separation criterion is met at the specified

distance in front of the tool tip, the pair of finite elements above and below the contact surface immediately before the tool tip will separate thus this process also partially affect the difference between the model results.

4. Friction generation.

Friction plays a very important role in metal cutting. It not only determine the power requirement for removing a given volume of metal but also controls the surface quality of the finish product and the rate of wear of cutting tool. Friction is also difficult to model in the metal cutting. In analytical model friction is solely depends upon the frictional angle 'β' and frictional angle depend upon chip thickness ratio. Chip thickness ratio already determined from experimental data. For a particular cutting, a frictional angle is fixed. So for a particular operation a particular result is developed. The friction is depend upon the rake angle and clearance angle which are used in the operation. So the resultant forces and stress generation inanalytical process solely depend upon the friction coefficient, rake angle and clearance angle which are used in the analytical model equation to find out the result. On the other hand in FEM simulation by ABAQUS friction is taken as a constant from 0.2–0.9 which is vary from material to material. In this case I have used frictional constant as 0.3. During material cutting operation basically friction changes time to time due to material behaviour in cutting zone. Therefore frictional constant also affect the cutting forces for finding out the result.

5 Conclusions

The proposed finite element model can be used quite satisfactorily to predict cutting forces, Stresses and chip morphology to a reasonable degree of accuracy.

Rake angle effect in orthogonal cutting can be simulated using the developed FEM model.

Depth of cut has the largest effect on the cutting forces, whereas clearance angle has no significance influence in cutting process.

The stress and force field predicted by the FE model are in accordance with the experimental findings and theoretical knowledge.

Chip flow can easily be predicted by observing the direct stress contour at the rake face of the tool.

References

1. Ernst, H., & Merchant, M. E. (1941). Chip Formation, Friction and High Quality Machined Surfaces. *Trans. Am. Soc. Met.*, Vol. 29, pp. 299–378.
2. Lee, E. H., & Shaffer, B. W. (1951). The Theory of Plasticity Applied to a Problem of Machining. *J. Appl. Mech.*, Vol. 18, pp. 405–413.
3. Zorev, N. N. (1963). Inter-Relationship Between Shear Processes Occurring Along Tool Face and Shear Plane in Metal Cutting. *International Research in Production Engineering*, ASME, New York, pp. 42–49.
4. Tay, A. O., Stevenson, M. G., & de Vahl Davis, M. G. (1974). Using the Finite Element Method to Determine Temperature Distributions in Orthogonal Machining. *Proceedings of the Institution for Mechanical Engineers*, Vol. 188, pp. 627–638.
5. Usui, E., & Shirakashi, T. (1982). Mechanics of Machining: From Descriptive to Predictive Theory. *On the Art of Cutting Metals – 75 Years Later*, ASME, New York, PED 7, pp. 13–35.
6. Oxley, P. L. B. (1989). *Mechanics of Machining, an Analytical Approach to Assessing Machinability*. Ellis Horwood Ltd.
7. Özel, T., & Altan, T. (2000). Determination of Workpiece Flow Stress and Friction at the Chip-Tool Contact for High-Speed Cutting. *Int. J. Mach. Tools Manuf.*, Vol. 40/1, pp. 133–152.
8. Childs, T. H. C. (1998). Material Property Needs in Modeling Metal Machining. *Proceedings of the CIRP International Workshop on Modeling of Machining Operations*, Atlanta, Georgia, May 19, pp. 193–202.
9. Jaspers, S. P. F. C., & Dautzenberg, J. H. (2002). Material Behavior in Conditions Similar to Metal Cutting: Flow Stress in the Primary Shear Zone. *J. Mater. Process. Technol.*, Vol. 122, pp. 322–330.
10. Adibi-Sedeh, A. H., Madhavan, V., & Bahr, B. (2003). Extension of Oxley's Analysis of Machining to Use Different Material Models. *ASME J. Manuf. Sci. Eng.*, Vol. 125, pp. 656–666.
11. Davies, M. A., Cao, Q., Cooke, A. L., & Ivester, R. (2003). On the Measurement and Prediction of Temperature Fields in Machining 1045 Steel. *CIRP Ann.*, Vol. 52 (1), pp. 77–80.
12. Özel, T., & Altan, T. (2000). Process Simulation Using the Finite Element Method: Prediction of Cutting Forces, Tool Stresses and Temperatures in High-Speed Flat End Milling Process. *Int. J. Mach. Tools Manuf.*, Vol. 40/5, pp. 713–738.
13. Johnson, G. R., & Cook, W. H. (1983). A Constitutive Model and Data for Metals Subjected to Large Strains, High Strain Rates and High Temperatures. *Proceedings of the 7th International Symposium on Ballistics*, Hague, Netherlands, pp. 541–547.
14. Zerilli, F. J., & Armstrong, R. W. (1987). Dislocation-Mechanics-Based Constitutive Relations for Material Dynamics Calculations. *J. Appl. Phys.*, Vol. 61 (5), pp. 1816–1825.
15. Hamann, J. C., Grolleau, V., & Le Maitre, F. (1996). Machinability Improvement of Steels at High Cutting Speeds – Study of Tool/Work Material Interaction. *CIRP Ann.*, Vol. 45, pp. 87–92.
16. Lee, W. S., & Lin, C. F. (1998). High-Temperature Deformation Behavior of Ti6AL4V Alloy Evaluated by High Strain-Rate Compression Tests. *J. Mater. Process. Technol.*, Vol. 75, pp. 127–136.
17. Meyer Jr, H. W., & Kleponis, D. S. (2001). Modeling the High Strain Rate Behavior of Titanium Undergoing Ballistic Impact and Penetration. *Int. J. Impact Eng.*, Vol. 26, pp. 509–521.

18. Shatla, M., Kerk, C., & Altan, T. (2001). Process Modeling in Machining. Part I: Determination of Flow Stress Data. *Int. J. Mach. Tools Manuf.*, Vol. 41, pp. 1511–1534.

19. Tounsi, N., Vincenti, J., Otho, A., & Elbestawi, M. A. (2002). From the Basic Mechanics of Orthogonal Metal Cutting toward the Identification of the Constitutive Equation. *Int. J. Mach. Tools Manuf.*, Vol. 42, pp. 1373–1383.

20. Adibi-Sedeh, A. H., & Madhavan, V. (2002). Effect of Some Modifications to Oxley's Machining Theory and the Applicability of Different Material Models. *Mach. Sci. Technol.*, Vol. 6 (3), pp. 379–395.

21. Lee, L. C., Liu, X., & Lam, K. Y. (1995). Determination of Rake Stress Distribution in Orthogonal Machining. *Int. J. Mach. Tools Manuf.*, Vol. 35 (3), pp. 373–382.

22. Huang, Y., & Liang, S. Y. (2003). Cutting Forces Modeling Considering the Effect of Tool Thermal Property-Application to CBN Hard Turning. *Int. J. Mach. Tools Manuf.*, Vol. 43, pp. 307–315.

23. Moufki, A., Devillez, A., Dudzinski, D., & Molinari, A. (2004). Thermomechanical modelling of oblique cutting and experimental validation. *International Journal of Machine Tools and Manufacture*, No. 44:971.

24. Molinari, A., & Moufki, A. (2005). A new thermomechanical model of cutting applied to turning operations. Part I. Theory. *International Journal of Machine Tools and Manufacture*, Paper no. 45:166.

25. Moufki, A., & Molinari, A. (2005). A new thermomechanical model of cutting applied to turning operations. Part II. Parametric study. *International Journal of Machine Tools and Manufacture*, Paper no. 45:181.

26. Fang, G., & Zeng, P. (2005). Three-dimensional thermo–elastic–plastic coupled FEM simulations for metal orthogonal cutting processes. *Journal of Materials Processing Technology*, Paper no. 168:42.

27. Zou, G. P., Yellowley, I., & Seethaler, R. J. (2009). A new approach to the modeling of orthogonal cutting processes. *International Journal of Machine Tools and Manufacture*, Paper no. 49:701.

28. Lazoglu, I., & Islam, C. (2012). Modeling of 3D temperature fields for oblique machining. *CIRP Annals – Manufacturing Technology*, Paper no. 61:127.

29. Li, R., & Shih, A. J. (2006). Finite element modeling of 3D turning of titanium. *The International Journal of Advanced Manufacturing Technology*, Paper no. 29:253.

30. Llanos, I., Villar, J. A., Urresti, I., & Arrazola, P. J. (2009). Finite element modeling of oblique machining using an arbitrary Lagrangian–Eulerian formulation. *Machining Science and Technology*, Paper no. 13:385.

Скінченноелементний аналіз ортогональних сил різання при обробці сталі AISI 1020 з використанням твердосплавного різального інструменту

Башистакумар М.[1], Пушкал Б.[2]

[1] Національний технологічний інститут ім. Б. Р. Амбедкара, Гранд Транк роуд, 144011, м. Пенджаб, Індія;
[2] Технологічний коледж ім. Л. Нараяна, Райзен роуд, 62021, м. Мандх'я Парадеш, Індія

Анотація. Моделювання сил різанні металу має важливе значення для різних цілей, включаючи термічний аналіз, оцінку ресурсу інструменту, прогнозування ресурсу і моніторинг стану інструменту. Запропоновано числові методи моделювання сил різання металевих заготовок. Додатково встановлені параметри процесу різання деталей, що обробляються, теплові властивості різального інструменту. Процес ортогонального різання металу досліджується методом скінченних елементів за умов плоскої деформації. Розроблена числова процедура, що реалізує метод скінченних елементів для моделювання ортогонального різання сталей загального призначення. Основна увага приділена результатам щодо впливу сил різання на інструмент при зміні параметрів різання. Результати визначаються як аналітично так і числовими методами для заданої сили різання матеріалу з різними параметрами процесу.

Ключові слова: сталь AISI 1020, формування, аналітична модель, скінченноелементна модель, ортогональне різання.

Analysis of the Theories for Assessment of the Quality Management Product Efficiency

Zaloga V.[1], Yashyna T.[1*], Dynnyk O.[2]

[1] Sumy State University, 2 Rymskogo-Korsakova St., 40007 Sumy, Ukraine;
[2] Konotop Institute of Sumy State University, 24 Myru St., 41600 Konotop, Ukraine

Abstract. In the article the advantages of introduction and reasons of low efficiency of the quality management system at the machine-building enterprises are determined. The methods and tools of the quality management system are considered. The conducted analysis of publications has made it possible to distinguish areas in which studies are carried out on the implementation and effective use of the quality management system at machine-building enterprises. A comparative analysis of two versions of ISO 9001 standards has been performed. A functional scheme of product quality management has been developed. The work of domestic and foreign authors on the assessment of the effectiveness of the quality management system is considered. The proposed method will allow controlling the quality of products at all stages of theirs production. The application of this method makes it possible to assess the functioning of the processes of the machine-building enterprise to determine the most critical ones in terms of quality, as well as can be used to assess both the basic processes of production and the assessment of elements or operations.

Keywords: quality, quality management system, assessment, efficiency, measuring system.

1 Introduction

In the context of the rapid development of the international trade, the quality of products becomes an important tool for increasing competitiveness. The success of domestic machine-building enterprises (ME) in the external and domestic markets depends entirely on how their products meet the requirements of customers and international standards of ISO 9000 series [1].

DSTU ISO 9000:2015 states "a quality-oriented organization promotes a culture that results in behavior, attitudes, activities and processes that add value by meeting the needs and expectations of customers and other relevant stakeholders" [2].

Today, there is no doubt, the quality is impossible to provide only by the control method. One should pay essential attention to quality management (QM). An efficient QM product makes it possible to avoid various failures in the work, to detect and eliminate them in a timely manner with the least losses for the enterprise.

Worldwide practice has shown in order to increase the company's competitiveness, the application of international standards of ISO 9000 series today is a reliable tool for building an effective quality management system (QMS). It provides an opportunity to objectively evaluate the wishes of consumers, turn them into requirements for products, establish production opportunities, find weaknesses that impede the achievement of the required quality, choose the correct corrective and preventive actions, assess the level of customers satisfaction and other participants in the production, and outline ways its development.

According to the results of the annual survey of the International Organization for Standardization [3] among the 191 countries which received ISO 9001:2008 certificates by 2017, Ukraine ranks the 60th place (601 certificates) and ISO 9001:2015 – 57th place (702 certificates). Among the CIS countries, Ukraine ranks the third place yielding only to Belarus and Russia.

Domestic enterprises are actively implementing QMS, however, as surveys of employees show, about 60–80 % of QMS are ineffective. The reasons for this are the formal approach to their creation (not for the sake of quality, but for the sake of the certificate, confirmation of its existence), the inattention of the enterprise managers to such a system, the low qualification of the enterprises personnel in the field of quality management, the attempts to solve new tasks by trials and errors, by the forces of service quality only and so on [4].

Thus, increasing the efficiency of QM products, and therefore ensuring the competitiveness of MEs in both domestic and foreign markets, can be attributed to the today priorities.

Journal of Engineering Sciences, Volume 5, Issue 2 (2018), pp. B 1–B 6

B 1

2 Literature Review

Many publications have been devoted to the question of QM products. Significant contribution to the development of the theoretical and methodological recommendations made both overseas and domestic scientists. Among them, one can note the researches of E. Deming, J. Juran, F. Crosby, K. Ishikawa, A. Feigenbaum, G. Taguchi, J. Harrington, V. Shapiro, M. Shapoval, R. Bychkivsky. But despite the significant contribution to the theory of QM, the practical aspects of the formation of an effective QMS, taking into account the specifics of the Ukrainian MEs, still remain insufficiently researched.

The purpose of this paper is to summarize the experience with product quality management, to analyze the existing methods of assessing the effectiveness of the QMS, to identify insufficiently researched issues and to formulate prospects for further work in this direction.

3 Research Methodology

The continuous improvement of the quality and competitiveness of products have caused the rapid development of the systems, methods and tools of the QMS.

An invaluable contribution to the development of QM has been made by American scientists E. Deming and J. Juran. The well-known Deming cycle PDCA, used in quality systems, is the Deming chain reaction, which indicates the linkage of product quality with the company's core performance indicators, the 14 principles of Deming, which underlie the successful work of QM [5, 6].

In the guidelines for small and medium-sized enterprises of the International Organization for Standardization [7] and several other sources [4, 8–10] it was stated seven simple tools for quality control were developed by K. Ishikawa, known as "father of quality control circles". Japanese experience has shown 95 % of problems in the workshop can be solved by using seven simple means of quality control: process flow charts; check sheets; graphs; Pareto analysis; cause and effect diagrams; scatter diagrams; control charts. They are intended to analyze quantitative data on quality and allow relatively simple, but at the same time scientifically grounded methods to solve 95 % problems of analysis and QM in the various fields.

However, when new products create, not all facts have a numerical nature. There are factors that are subject only to verbal descriptions. Accounting for these factors is about 5 % of quality problems. These problems arise mainly in the management of processes, systems, teams, and when solving them, along with statistical methods, it is necessary to use the results of operational analysis, optimization theory, psychology, etc. Therefore, a powerful and useful set of tools was developed, which made it possible to ease the task of QM when analyzing these factors, which are called seven new quality control tools. They are systematized and generalized by S. Mizuno [7]: affinity diagram; communication diagram; tree diagram; matrix diagram; arrows chart; diagram of the program implementation process; matrix of priorities.

Proven by time, they are increasingly applied to domestic MEs. However, the results of their application do not always coincide with the expectations of managers. Therefore, a lot of attention is paid to the problems of implementation and effective use of QMS at Ukrainian enterprises.

The analysis of publications made it possible to select the directions in which the research is conducted.

For example, Dryzyuk V. and Fedak O. [4] determined the advantages of QMS implementation and analyzed the reasons for their ineffective implementation at domestic enterprises. Problems, ways of overcoming them and the prospects for the implementation of QMS are considered by Dolgaleva O. V., Orlov P. A., and Boychuk N. Ya. [8–10]. Rudenko L. studied the international experience in QM and prospects of its use at Ukrainian enterprises. Dragnova N. I. in her work considered the directions of the development of QMS and analyzed their advantages and disadvantages. Chekmasova I. A. and Marchenko T. B. offer a methodology for the implementation of QMS in the enterprise [11–12].

A considerable experience in the field of QM theory and the concept of building an integrated QMS has been accumulated. The importance of their implementation at the ME is reflected in works by Valyavsky S. M., Momota O. I., Filipova S. V., et al. [13–15].

The results of scientific research in the field of QM from the point of view of the process approach are presented in the works of Podvyshennoy N. V., Kubishin N. S., Klavdienko N. V., et al. consider QMS as an element of innovative enterprise development [16, 17].

Shvets V. Ya., and Ivanova M. I. provide practical guidance on the formation of an effective integrated QMS. They propose the creation of a special structural subdivision at the enterprise, which will ensure the continuing suitability, adequacy and effectiveness of QMS products [18].

During the research, a comparative analysis of two versions of the standards the previous ISO 9001:2008 and the new ISO 9001:2015 was performed. It showed the new version contains a number of significant changes. More attention is paid to the principles of process approach, leadership, employee involvement and risk-oriented thinking. In our opinion, the main objective of the change in the standard is the need to focus on process management, which will provide insight and continuous satisfaction of requirements, achievement of efficient functioning of processes; improving processes based on the evaluation of data and information [2].

The author's vision of the structure of the QMS, which takes into account the whole life cycle of products, the PDCA cycle, principles, meets the requirements of ISO 9001:2015, are presented in Figure 1.
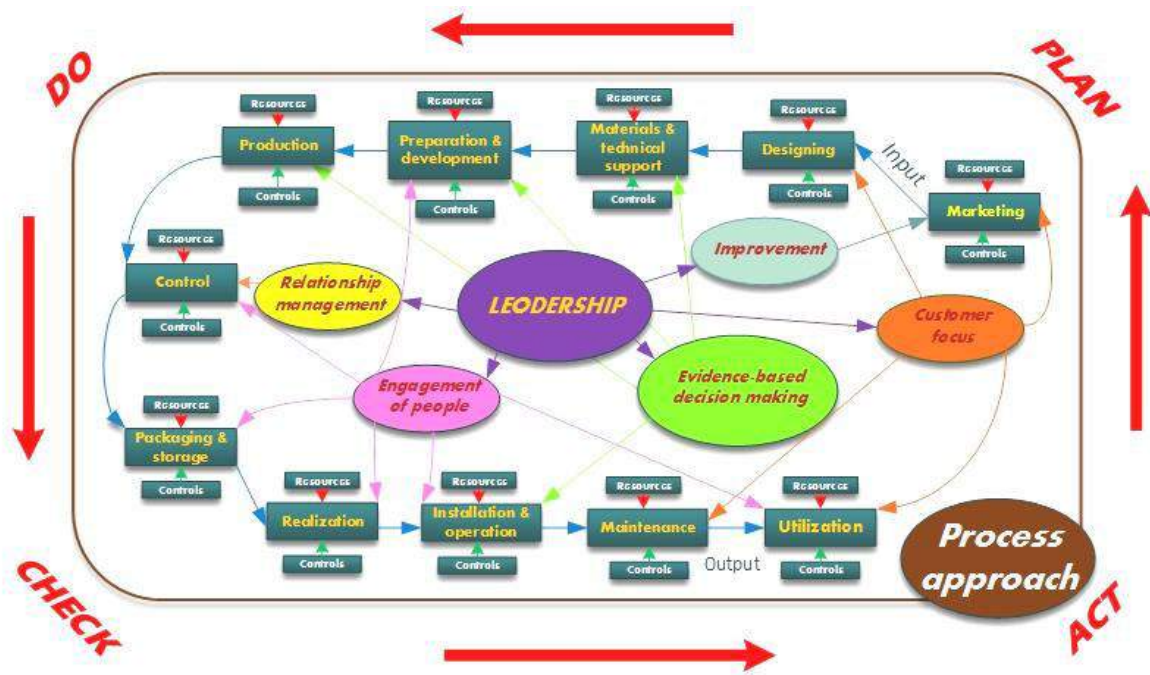
Figure 1 – Functional scheme of product quality management

According to [2, 19], the QMS is based on the seven principles of QM. One of the principles is to improve: successful organizations are constantly improving.

ISO 9001 standards state one of the main tools for improving the organization's performance in the field of quality is the assessment of the effectiveness of the existing QMS. "It is important for the organization to regularly monitor and assess both the implementation of the plan and the effectiveness of the QMS". Another principle of QM involves making decisions based on factual data. Solutions which are based on the analysis and evaluation of data and information likely give the desired results [2, 19].

Thus, the assessment of the effectiveness of the QMS is an important but rather difficult task. On the one hand, there is an obvious need to receive an actual confirmation that the implemented QMS is really functioning and ensures the achievement of the goals of the organization. On the other hand, the effectiveness of processes is constantly affected by a large number of heterogeneous factors, the consideration and accounting of which is a major problem, which critically complicates the task of assessing the effectiveness of the QMS in general and the effectiveness of its individual processes in particular.

However, the standards [1, 2] do not propose a mechanism for a comprehensive assessment of the effectiveness. Therefore, issues related to the problem of adequate and objective evaluations, as well as further analysis of the effectiveness of the QMS, become a problem of both theoretical and practical significance.

The analysis of existing methods for assessing the effectiveness and efficiency of QMS showed there are a large number of methods described in the scientific literature and those applied in practice by domestic and foreign enterprises. For example, the methods of balancing the system of indicators and self-assessment of key elements of the QMS are widely used according to the recommendations of the standard ISO 9004:2009, the Malcolm Boldridge Grant Rating Scale, the method for determining the perfection based on EFQM criteria, benchmarking (comparative assessment with leading companies), etc.

In works [20, 21] authors have recommended to use the system of Norton and Kaplan balanced indicators to assess the effectiveness of the QMS, which allows at the same time to take into account the interests and the degree of satisfaction of all interested parties.

Gorbenko N. A. based on the of the proposed classification of optimal quality indicators, has developed a unified system of dependencies of the evaluation of the processes of enterprise QMS, which can be carried out in one of twenty variants, depending on the compliance of the individual quality indices with one of the four characteristics of the proposed classification and the importance of the process in the QMS [22].

Gunkalo A. V. proposed to prioritize the QMS processes during its evaluation (based on quality policy and goals) to ensure the development of corrective and preventive actions and their timely implementation, according to the degree of significance, taking into account available costs, by developing a process management model using the system of controlled process indicators [23].

Authors [24] recommend using two types of rating methods for the assessment of QMS. The rating is in absolute form and in a comparative form by changing the parameters of the work of QMS in time or at individual enterprises. Such approaches require an as-

sessment of a significant number of indicators that may change as a result of the implementation or improvement of the QMS.

Chaban O. P. proposed a vector method for assessing the products quality and services that takes into account the broad set of unit quality indices and, through the modules and the quality phase, allows one-to-one numerical integral estimation to be obtained [25].

In work [26] Trish G. N. developed a unified system of dependencies of single quality indicators of heterogeneous processes with a dimensionless scale of evaluation, which allows one to evaluate processes in one of twenty variants, depending on the types of the processes quality indicators and the importance of the process itself in QMS. The algorithm of estimation of dynamic characteristics of processes quality with the use of criteria of nonparametric statistics is developed, which allows to obtain an estimation of the process quality taking into account the time of its functioning.

Zubretskaya N. A. [27] focused on solving the problem of ensuring the reliability of multicriteria assessment and prediction of the quality of industrial products at the stages of design, manufacturing and operation using adaptive methods and intelligent decision support systems. She proposed a conceptual model of the information system of multicriteria assessment, forecasting and quality management of industrial products.

Morteza R. Z. has developed a toolkit to assess the compliance of the standards of management systems based on the use of "expert ranking", followed by "Pareto compromise" by choosing a rational solution that allows to classify the degree of compliance with the standards used to integrate the standards and determine the standard, the main requirements of which accepted as the basis of the integration process.

In [28] N. V. Tereschenko noted that any newly made decision and, accordingly, the change in the number of implemented actions is reflected in the dynamics of the relevant performance indicators. That is why it is proposed to use the rate of indicators' growth assigns of the ordering indicators. In accordance with these requirements, he proposed using the model of index valuation of performance (MINOR) to measure the effectiveness of the QMS and to determine measures to improve it. The offered model allows to reveal critical areas of enterprise activity, which directly influence the quality of production and competitiveness of the enterprise.

Ol'khovskaya O. L., Zaika A. A., and Bal'zan M. V. [29, 30] suggest the use of an automated evaluation of the effectiveness of QMS, based on the method of fuzzy multicriteria analysis, which involves the use of expert evaluation of project indicators, the accounting of pair comparisons instead of quantitative estimates, the consideration of varying importance criteria, which is evaluated by experts.

While Kovalev O. I. in his work [31], for the automating evaluation process, he considers the model of the quality of activity and functioning of the enterprise (English activity and functioning, A&F) from the point of view of all possible results, which implies observance of the

efficiency of the logical sequence of "resources – direct results – direct and indirect end results".

K. Szczepanska and M. Urbaniak indicate that the methods for assessing the effectiveness of the QMS improvement should be incorporated into a coherent measurement system and offer tools that allow organizations to assess the effects of improvements in the QMS, such as internal and external audits; risk management, performance indicators and process efficiency, customer satisfaction assessment, qualitative cost analysis; analysis of best practices and self-esteem [31].

R. Ginevicius and V. Petraskevicius on the basis of the proposed classification of the process quality indicators, created a system of interconnections between different sizes of individual quality indices and their values on an immensely large scale, which, in their opinion, allows us to obtain a quantitative assessment of the quality of any process at an enterprise, given its importance in the QMS at a certain point in time and to analyze the situation during this time [33].

There is, therefore, a sufficiently large number of methods for assessing the effectiveness of the QMS, but the vast majority of them are used after the product has been manufactured, which makes it possible to determine the quantity of the defect and not to control it at all stages of the product life cycle. A method is needed to assess the impact of various factors directly on the quality of processes and to obtain objective information about their functioning.

4 Conclusions

Assessment of the effectiveness of QMS products is an important and rather difficult task, as the effectiveness of processes is constantly influenced by a large number of various factors, which complicate the task of assessing the effectiveness and efficiency of QMS. The conducted analysis of publications has made it possible to select the areas in which studies are conducted on the implementation and effective use of the quality management system at the ME and to consider the work of domestic and foreign authors on the evaluation of the effectiveness of the QMS. It is established that for today there is no single method for conducting an assessment of the effectiveness of the QMS, therefore the issue remains relevant and requires further research.

A method is proposed that will allow controlling the quality of products at all stages of its production. The application of this method makes it possible to assess the functioning of the ME processes to determine the most critical in terms of quality and can be used to assess both the basic processes of production and the evaluation of elements and operations.

In our opinion, the practical use of the proposed method allows solving several problems at once: to carry out a quick and effective assessment of all MP processes; to study in detail the structure of processes operating in the enterprise; it is reasonable to choose the process for improvement.

References

1. DSTU ISO 9000:2015, IDT (2016). *Quality management systems. Basic Provisions and Dictionary*. UkrNDNTS, Kyiv, Ukraine.
2. DSTU ISO 9001:2015, IDT (2016). *Quality management systems. Requirements*. UkrNDNTS, Kyiv, Ukraine.
3. Executive Summary (2017). *The ISO Survey of Management System Standard Certifications 2017*. Retrieved from: http://www.iso.org/iso/home.html.
4. Druzyuk, V., & Fedak, O. (2009). Quality Management System – Investing in the Future. *Standardization, Certification, Quality*, No. 1, pp. 51–54.
5. Deming, E. (1994). *Out of the crisis*. Alba Publishing, Tver, Russia.
6. Lapidus, V. A. (1996). Statistical methods, general quality management, certification, and more. *Standards and Quality*, No. 4–6.
7. Product quality (2006). *A guide for small and medium sized enterprises*. UNIDTO, Vienna, Austria.
8. Dolgalova, O. V., & Stepanov, A. D. (2017). *Product quality management system at the enterprise and development of measures on its improvement*. Collection of scientific works of DonNACEA, Vol. 2, No.4, pp. 72–78.
9. Orlov, P. A. (2013). Implementation of quality management systems: state, problems, perspectives. *Standardization, Certification, Quality*, No. 6, pp. 59–63.
10. Boychuk, N. Ya., & Holtobina, I. O. (2013). Problems and modern state of the system of quality management of products at the enterprises. *Modern Problems of Economy and Entrepreneurship*, No. 12, pp. 149–155.
11. 11 Chekmasova, I. A., & Shatilo, D. M. (2013). Management of the quality of the enterprise: development and implementation problems. *Bulletin of NTU KhI*, No. 7, pp. 167–173.
12. Marchenko, T. B. (2007). Methodology for introducing a quality management system in an enterprise. *Current Problems of the Economy*, No. 12, pp. 152–156.
13. Prodius, O. I., & Illinchuk, O. I. (2017). Quality management as a factor for increasing the competitiveness of products. *Prychornomorah Economic Studies*, No. 18, pp. 89–93.
14. Momot, O. I. (2014). The Possibilities of Using International Standards for the Construction of Integrated Management Systems. *Bulletin of the Kiev National University of Technology and Design*, No. 5 (37), pp. 133–138.
15. Filippova, S. V. (2005). Mechanism of formation of integrated production systems as an instrument of preventive management of transformation of industrial production. *Development Economics*, No. 2 (34), pp. 42–45.
16. Simkova, T. O., & Kirichenko, A. I. (2016). Trends in the development of quality management systems in Ukraine due to the introduction of world standards. *Economy and Society*, No. 7, pp. 482–489.
17. Popova, O. Yu., & Skibenko, G. G. (2014). Quality management as an element of innovative enterprise development. *Economics and Management Organization*, No. 3 (19) – 4 (20), pp. 194–198.
18. Shvets, V. Ya., & Ivanov, M. I. (2013). Formation of an Efficient Integrated Quality Management System for Machine Building Products. *Economic Bulletin*, No. 2, pp. 147–156.
19. ISO Central Secretariat Chemin de Blandonnet Case Postale 401 (2014). *Quality Management Principles*. Geneva, Switzerland.
20. Khimicheva, G. I., & Kalinuk, N. V. (2015). Application of the concept of BSC for assessing the effectiveness and efficiency of the quality management system. *Journal of the KNUTD, Metrology and certification*, No. 6 (92), pp. 142–149.
21. Bogachenko, O. P. (2013). *Theory and practice of evaluating the effectiveness of using the quality management system: monograph*. ZNTU, Zaporizhzhia, Ukraine.
22. Gorbenko, N. A. (2014). *Development of methodology for evaluating quality management systems of enterprises taking into account the requirements of international standards: Ph.D. thesis*. Kharkiv, Ukraine.
23. Gunkalo, A. V. (2007). *Development of normative and methodological principles of evaluation of quality management systems: Ph.D. thesis*. Ukraine.
24. Stolyarchuk, P., Baytsar, R., & Gunkalo, A. (2008). Methods for assessing quality management systems. *Measuring Technique and Metrology*, No. 68, pp. 244–247.
25. Chaban, O. P. (2009). *Development of methods for assessing the quality of products and services by single and aggregate indicators: Ph.D. thesis*. Ukraine.
26. Trysh, G. N. (2013). *Development of methodology for evaluating processes of quality management systems of enterprises taking into account the requirements of international standards: Ph.D. thesis*. Lviv, Ukraine.
27. Zubretskaya, N. A. (2013). *Development of scientific bases of multicriterion estimation and forecasting of quality of industrial products: Ph.D. thesis*. Kyiv, Ukraine.
28. Tereshchenko, N. V., & Yashin, N. V. (2006). Model of complex evaluation of the effectiveness of the SMK. Methods of estimation and calculation. *Methods of Quality Management*, No. 4. pp. 38–46.
29. Olkhovskaya, O. L., & Zayka, A. A. (2017). System of evaluation of the quality management of the organization of the production process at the machine-building enterprise. *Economic Bulletin of the Donbas*, No. 1 (47), pp. 106–109.

30. Olkhovskaya, O. L., & Zayka, A. A. (2016). Assessment of the quality management system of the production process. *Economic Bulletin of the Donbas*, No. 3 (45), pp. 154–157.
31. Kovalev, A. I. (2018). How to Assess the Performance of an Enterprise. *Journal of Engineering Sciences*, Vol. 5, Issue 1, pp. B1–B6.
32. Szczepanska, K., & Urbaniak, M. (2011). Evaluation of Effect of Quality Management System Improvement. *Foundations of Management*, Vol. 3, No. 1, pp. 97–108.
33. Ginevicius, R., Petraskevicius, V., & Trishch, H. (2015). Quantitative evaluation of quality management systems processes. *Economic Research*, Vol. 28, No. 1, pp. 1096–1110.
34. Application of applied static methods in production of products (2001). *Practical Guide*. SMC "Priority", Novgorod, Russia.

Аналіз існуючих теорій та концепцій оцінювання ефективності управління якістю продукції

Залога В. О.[1], Яшина Т. В.[1], Динник О. Д.[2]

[1] Сумський державний університет, вул. Римського-Корсакова, 2, 40007, м. Суми, Україна;
[2] Конотопський інститут Сумського державного університету, вул. Миру, 24, 41600, м. Конотоп, Україна

Анотація. У статті визначені переваги впровадження та причини низької ефективності системи управління якістю на вітчизняних машинобудівних підприємствах. Розглянуті методи та інструменти системи управління якістю. Проведений аналіз публікацій дав змогу виокремити напрямки, в яких ведуться дослідження щодо впровадження та ефективного використання системи управління якістю на машинобудівних підприємствах. Виконано порівняльний аналіз двох версій стандартів ISO 9001. Розроблена функціональна схема управління якістю продукції. Розглянуті роботи вітчизняних і зарубіжних авторів щодо оцінювання ефективності систем управління якістю. Запропоновано метод, який дозволить контролювати якість продукції на всіх етапах її виготовлення. Застосування цього методу дає можливість здійснити оцінку функціонування процесів машинобудівних підприємств для визначення найбільш критичного за рівнем якості та може застосовуватись для оцінювання як основних процесів виробництва, так і елементів та операцій.

Ключові слова: якість, система управління якістю, оцінювання, ефективність, вимірювальна система.

Research of Non-metallic Inclusions Removal in Teeming Ladles of Various Design

Molchanov L. S.[1], Synehin Y. V.[1*], Lantukh O. S.[1], Ryshkova I. S.[2]

[1] National Metallurgical Academy of Ukraine, 4 Gagarina Av., 49600 Dnipro, Ukraine;
[2] Dniprovsk State Technical University, 2 Dniprobudivska St., 51918 Kamianske, Ukraine

Abstract. It was studied in the article the possibility of intensification of removal of non-metallic inclusions in a teeming ladle during holding without any additional external influences on the metal (argon blowing or electromagnetic stirring). Increasing the efficiency of removal of non-metallic inclusions is achieved by creating in a teeming ladle during tapping a circulation pattern that accelerate the floating of inclusions. The described effect is achieved by using a rational shape of the workspace of the teeming ladle, which has been found as a result of "water" modelling. To carry out the experiment, the authors have proposed the similarity numbers describing the floating of non-metallic inclusions in the ladle during the tapping and for some time after its completion. On the basis of the proposed similarity numbers, an experimental facility and the experimental method were developed. In the course of the experiment, the construction of linings of several types was studied. Ladles of the best design provide by 16–19 % faster removal of non-metallic inclusions from steel than in ladles of conventional design. The results of the research can be useful for mini-plants and enterprises with ladles of small capacity, where the use of argon blowing and electromagnetic stirring is technologically and economically unreasonable.

Keywords: "water" modelling, floating, non-metallic inclusions, damping devices.

1 Introduction

It is well known, that non-metallic inclusions (NI) in steel are not only concentrators of internal stresses, but also under certain conditions can cause corrosion destroying of steel [1]. The main sources of steel pollution by NI at the stage of tapping from BOF into the ladle are furnace slag, fragments of the ladle lining and products of deoxidation.

Usually NI are removed from steel by floating up due to the Archimedean force and the convection in liquid steel. At the same time for the small NI prevails the influence of convection, and for large – the Archimedean force [2]. Intensification of this process is carried out by accelerating upward flow of the melt by means of inert gas blowing or electromagnetic stirring. However, the application of these measures for teeming ladles of low-capacity is inappropriate due to the significant thermal losses and the risk of getting the slag inclusions from the cover slag back into the metal with the injection of argon. Electromagnetic stirring requires significant capital expenditures for its implementation.

Therefore, the only technologically expedient way for NI removing from steel is to hold the metal melt in the ladle for optimal time.

2 Literature Review

Sang-Ik Chung *et al.* [3] were exploring the removal of NI during the processing of steel in ASEA-SKF. By using mathematical modeling and statistical analysis of industrial data they have determined that the removal of NI with the diameter of 10–100 μm is the most effective under the condition of combined stirring of upward induction stirring of 400 A and gas blowing of 5 l/min.

The similar research has been carried out by Lidong Teng [4] on stainless steel. He has determined that during Ar injection and simultaneous EMS inclusions with a size of more than 5.4 μm after LF-EMS is reduced by 50 % compared to that after argon gas stirring ladle station. Inclusions with a size of more than 5.4 μm after LF-EMS is reduced by more than 70 % compared to that after argon gas stirring.

3 Research Methodology

3.1 Formularization of similarity numbers

Based on the results of the preparatory stage [5], the authors, using the π-theorem, established that the process of NI floating after filling the ladle can be described by the Archimedes number (Ar), the modified homochronality number (Ho_m) and the linear simplex (D):

$$Ar = \frac{\Delta\rho \cdot g \cdot d_{NI}^3}{\rho_{liq} \cdot v_{liq}^2}; \qquad (1)$$

$$Ho_m = \frac{g \cdot \tau^2}{h_{liq}}; \qquad (2)$$

$$D = \frac{d_{NI}}{h_{liq}}, \qquad (3)$$

where ρ_{liq}, $\Delta\rho$ – respectively the density of the liquid and the density difference of the liquid and NMI, kg/m^3; g – acceleration of gravity, m/s^2; d_{NI} – diameter HB, m; v_{liq} – the kinematic viscosity of the liquid, m^2/s; τ – time, s; h_{liq} – the level of liquid in the ladle, m.

However, calculating the scales of simulation, the authors have encountered the problem of choosing model substances that would satisfy the condition:

$$\begin{cases} Ar = idem, \\ Ho_m = idem, \\ D = idem. \end{cases} \qquad (4)$$

The material that imitates NI must have a spherical shape and also not dissolve and not form a conglomeration in water. Polyethylene and stearin good satisfy these requirements. However, the linear scale for these materials is 1.8. It means that the model of a ladle must be 1.8 times larger than the original. Using a smaller linear scale requires the application of a liquid with low density and/or viscosity instead of water.

According to Markov [6], in case of too incomparable linear parameters in a similarity number, it can be neglected as not essential. Based on this statement and considering the small value of the linear simplex $D = 10^{-6}–10^{-3}$, authors have put forward the hypothesis of self-similarity of the linear simplex D. It means that for simulation of the process it is need only to provide the value of linear simplex less than particular value.

3.2 Methodology of "water" modeling

For experimental confirmation of the hypothesis, an experimental facility was assembled and a series of 15 experiments was carried out. The experimental facility is shown in Figure 1.

The facility consisted of a set of ladle models 1 of different sizes. The necessity of use several models of different sizes is caused by the need to vary the magnitudes of the Archimedes number and the linear simplex within ranges of their definition independently of each other.
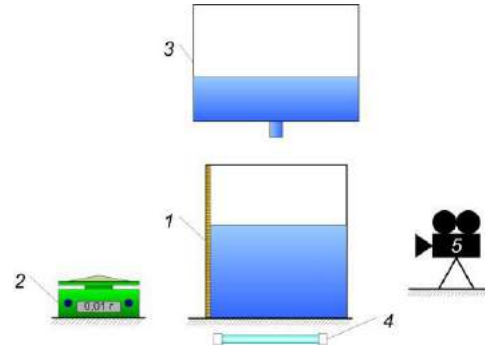
Figure 1 – The scheme of the experimental facility:
1 – model of the ladle; 2 – electronic scales; 3 – buffer vessel;
4 – halogen lamp; 5 – video camera

Before the experiment a charge of the stearin was weighed on an electronic scale 2 with an accuracy limit of 0.01 g. The weight of the charge is based on the similarity of the volumetric concentration of powder in the liquid on the model and the original of $2.88 \cdot 10^{-3}$ m^3/m^3 [7]. The weighed powder sample was gently loaded onto the bottom of the ladle, after which water was poured from the buffer vessel 3. The height of the drain hole above the bottom of the ladle model was changed according to the linear scale for each experiment. From the bottom, the ladle was illuminated by a 150 W halogen lamp 4. The duration of floating was determined from the video of the experiments that were taking by the video camera 5 in the HD mode.

According to Markov [6], the self-similarity of a dimensionless number can be confirmed in following condition:

$$\frac{d \lg \pi_y}{d \lg \pi_x} = 0, \qquad (5)$$

where π_y and π_x – respectively the dimensionless function and its dimensionless argument.

Condition (5) is observed for $\lg D < -2$ ($D < 0.01$). This means that to fulfil semblance of the floating NI during holding steel in the ladle the diameter of the NI must be at least 100 times smaller than the level of liquid steel in the ladle.

As a result of following statistical analysis it has been determined that the duration of NI floating can be calculated by using following equation:

$$Ho_m = 42420 Ar^{-0,51} D^{-0,86} \qquad (6)$$

The results of equation (6) and Stocks equation are different. According Frolov [8] his difference might be caused by turbulence during simultaneous floating of large group of NI.

3.3 Effect of lining design on duration of NI floating up

On the next stage of research authors have varied the shape of model workspace in order to determine the optimal for decreasing of floating duration. The following shapes of model's bottom have been offered (Figure 2).
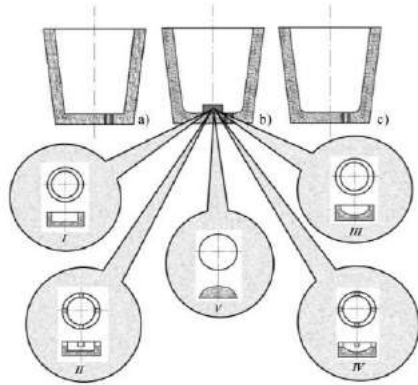
Figure 2 – Types of the shape of model workspace:
a – common design of the ladle; b – ladle equipped with fillet and various damping device; c – ladle equipped with fillet

Figure 3 – Comparison of various types
of the shape of model workspace

Type (a) is common design. Type (c) has fillet between ladle's bottom and wall with various rounding radius. Type (b) has besides fillet also damping device of various design in the place of steel jet impact. Offered measures have to provide change of flow pattern in ladle in a way to decrease duration of NI floating up.

The experiments were carried out on the model with linear scale 1:10 and using the stearin granules average size 750 μm. In condition of these experiments stearin granules simulate NI average size 320 μm.

The experiment on each type of the shape of model workspace was carried out three times. So for analysis average value of duration of NI floating up were taken.

4 Results and Discussion

Considering that a time scale is about 1:3 the results of experiment were converted for original teeming ladle of 60 t capacity. Comparison of average duration of NI floating up for each type of the shape of model workspace is shown on Figure 3.

It is clearly seen that the best results were achieved with using damping device in form of hemisphere ("b V") and bowl ("b I"). Model equipped only with fillet has shown the worst result ("c").

Another important feature is the height of splash after impact of metal jet with the bottom of teeming ladle. The large splash leads to increase of metal surface that interacts with atmospheric oxygen. This causes to secondary oxidation of steel.

On the Figure 4 it was shown the splash after impact of metal jet with the bottom of teeming ladle of type "b" design (Figure 2). The largest splashes can be seen at the ladles of types "b II, III, IV". The splashes in these cases reached almost to the edge of the ladle. For "b I" types the splash was quite small and almost as the same height as for the common ladle design. The shape of damping device in form of hemisphere ("b V", Figure 3) has provided no splash at all, only little turbulences at the fillet between ladle's bottom and wall.

Thus the "b V" type of the teeming ladle provides both most efficient of NI remove from steel and the lowest level of secondary oxidation during the tapping.

Figure 4 – Splash after impact of metal jet with the bottom of teeming ladle of various design

Obviously increase of efficiency of NI removal is a consequence of flow pattern which is induced during steel tapping. Increase of duration of NI floating up for some types of the shape of model workspace can be explained by creating in liquid dead zones that keep NI inside.

5 Conclusions

Authors have proved that to fulfill semblance of the floating NI during holding steel in the ladle the diameter of the NI must be at least 100 times smaller than the level of liquid steel in the ladle. It makes possible to get accurate results in research of NI removal on "water" models.

By using "water" modeling, authors have found the shape of teeming ladle's workspace that change the flow pattern in ladle during the steel taping in a way to decrease duration of NI floating up.

The use of teeming ladle equipped with damping device in form of hemisphere and bowl provides decrease of duration of NI floating up by 16–19 %.

References

1. Filippov, G. A., Rodionova, P. G., & Baklanova, O.N. (2004). Korrozionnaya stoykost stalnyih truboprovodov [Corrosion resistance of steel pipelines]. *Tehnologiya metallov [Technology of metals]*, Vol. 2, pp. 24–27 [in Russian].

2. Okhotskyi, V. B., Kostolov, O. L., Cimonov, V. K., Kovalov, D. A., Tarakanov, A. K., Kucher, A. H., et al. (1997). *Teoriia metalurhiinykh protsesiv [Theory of metallurgical processes]*. Kyiv, IZMN [in Russian].

3. Chung, S.-I., Shin, Y.-H., Yoon, J.-K. (1992). Flow Characteristics by Induction and Gas Stirring in ASEA-SKF Ladle. *ISIJ International*, Vol. 32, Issue 12, pp. 1287–1296.

4. Teng, L. (2017). Effect of EMS on Inclusion Removal in Ladle Furnace for Specialty Steel Production. *Proceedings of AISTech 2017*, pp. 1395–1402.

5. Lantukh, O. S., Molchanov, L. S., & Synehin, I. V. (2018). Metodyka fizychnoho modeliuvannia splyvannia ansambliu nemetalevykh vkliuchen u stalerozlyvnomu kovshi [Method of physical modeling of floating of the nonmetallic inclusions group in a teeming ladle]. *Matematychne modeliuvannia [Mathematical modelling]*, Vol. 1 (38), pp. 95–99.

6. Markov, B. L. (1984). *Fizicheskoe modelirovanie v metallurgii [Physical modeling in metallurgy]*. Moscow, Metallurgy [in Russian].

7. National Metallurgical Academy of Ukraine (2017). *Rozrobka teoretychnykh zasad enerho- ta resursozaoschadzhuiuchykh tekhnolohij vyplavky ta bezperervnoho rozlyvannia iakisnykh marok stalej [Development of theoretical foundations of energy and resource saving technologies of melting and continuous casting of qualitative grades of steels]*. Dnipro, NMetAU, State registration No. 0116U008351 [in Ukrainian].

8. Frolov, J. G. (1988). *Kurs kolloidnoj himii. Poverhnostnye javlenija i dispersnye sistemy [Course of colloid chemistry. Surface phenomena and dispersed systems]*. Moscow, Chemistry [in Russian].

Дослідження процесу вилучення неметалевих включень в сталерозливних ковшах різної конструкції

Молчанов Л. С.[1], Синегін Є. В.[1], Лантух О. С.[1], Ришкова І. С.[2]

[1] Національна металургійна академія України, просп. Гагаріна, 4, 49600, м. Дніпро, Україна;
[2] Дніпровський державний технічний університет, вул. Дніпробудівська, 2, 51918, м. Кам'янське, Україна

Анотація. У статті досліджена можливість інтенсифікації видалення неметалевих включень у ковші без будь-якого додаткового зовнішнього впливу на метал (продування аргоном або електромагнітне перемішування). Підвищення ефективності видалення неметалевих включень досягається за рахунок створення циркуляції, що прискорює плавання включень. Описаний ефект досягається використанням раціональної форми робочого простору ковша, отриманої у результаті моделювання. Для проведення експериментальних досліджень авторами запропоновані критерії подібності, що описують плавучість неметалевих включень у ковші під час заливання і впродовж деякого часу після його завершення. На основі запропонованих критеріїв подібності розроблено відповідний експериментальний метод. Під час експеримента вивчено конструкцію декількох видів футеровок. Ковші найкращої конструкції забезпечують на 16–19 % швидше вилучення неметалевих включень зі сталі, ніж у ковшах традиційної конструкції. Результати дослідження можуть бути корисними на малих підприємств, що використовують ковші малої потужності, де застосування технологій аргонного продування та електромагнітного перемішування є економічно необґрунтованими.

Ключові слова: водне моделювання, плавання, неметалеве включення, демпферний пристрій.

Systematic Presentation of Ritz Variational Method for the Flexural Analysis of Simply Supported Rectangular Kirchhoff–Love Plates

Ike C. C.[*]

Enugu State University of Science and Technology, P.M.B. 01660, Enugu, Nigeria

Abstract. In this work, the Ritz variational method for solving the flexural problem of Kirchhoff–Love plates under transverse distributed load has been presented systematically in matrix form. An illustrative application of the matrix presentation was done for simply supported rectangular Kirchhoff–Love plate under uniformly distributed load. The application used a one term Ritz approximating displacement (coordinate, or basis) function. A one term Ritz approximate solutions obtained for center displacement of square plates showed a difference of 1.9 % from the exact solution for displacement. Solution obtained for the bending moment at the center showed a difference of 7.9 % from the exact solution for bending moment. The one term Ritz approximation for the maximum shear force showed a difference of –10.7 % from the exact solution. The results obtained for a one term Ritz approximation of the displacement shape function was reasonably close for practical purposes.

Keywords: Ritz variational method, Kirchhoff–Love plate, shape function, total potential energy, principle of minimization.

1 Introduction

Plates are three dimensional structures having one transverse dimension that is very small in comparison with the other (in-plane) dimension. They are usually subjected to forces applied perpendicularly to their plane. They therefore resist applied load by the development of bending moments in two in-plane directions, and a twisting moment. They can also be submitted to forces in the plane of the plate. They are thus commonly encountered structural forms used in floor slabs, bridge decks, foundations, and naval and aerospace structural panels.

The mathematical problems of plate analysis belongs to the three dimensional theory of elasticity governed by the simultaneous satisfaction of the requirements of the material stress-strain laws, the kinematic (geometric) relations between strain and displacements, the differential equations of equilibrium and the loading and restraint boundary conditions [1–4].

However, the full three dimensional theory of elasticity problem has often been approximated to two dimensional idealizations owing to the disparity in the scale of the dimensions, especially in thin plates. The analysis and theories of plates have been broadly categorized into two using the thickness to breadth ratios, namely thick plate theories (analysis) and thin plate theories (analysis). The

ratio of the maximum deflection to the thickness has also been used as criterion in the classification of plates as plates with small deflection, and plates with large deflection.

This study uses the Kirchhoff–Love plate theory also called the classical thin plate theory. The Kirchhoff–Love plate theory, is based on three assumptions (Kirchhoff's hypothesis) which reduce the equations of the three dimensional theory of elasticity to two dimensions. They are [5–7]:

1. Cross-sections that are perpendicular to the neutral surface of the plate before bending remain straight and normal after bending deformation.

2. The normal stress in the transverse (thickness) direction is so small as to be insignificant, and is neglected. Thus $\sigma_{zz} = 0$. This simplifies the three dimensional stress-strain relations into a two dimensional problem.

3. The transverse shearing strains γ_{xz} and γ_{yz} are assumed to be zero. Thus the thickness of the plate does not change during flexural deformation.

Apart from the Kirchhoff–Love plate theory, other plate theories commonly used in the literature to analyse plates are: Mindlin plate theory [8], Reissner plate theory [9], Levinson plate theory, shear deformation plate theories, and Reddy's plate theory.

Methods used in the analysis of plates are broadly classified as: analytical (or mathematical) methods, and numerical (or approximate) methods. The analytical methods, which seek to obtain closed form mathematical solutions to the plate problem at every point in the plate domain include: Eigen function expansion methods, integral transform methods, separation of variables methods, etc. The numerical methods seek to obtain approximate solutions to the plate problem. Some of the numerical methods are: variational methods [10], finite element methods, finite difference methods [11], finite grid methods, residual methods, and boundary collocation methods.

The research aim is to present systematically, the Ritz variational method for the flexural analysis of simply supported Kirchhoff plates under transverse distributed load. The objectives include:

a) to present the flexural problem of Kirchhoff plates under transverse distributed load as a variational problem, and state the problem in variational form;

b) to apply the principle of minimization of the total potential energy functional for the plate and find the equations of static equilibrium in equivalent variational form as the minimum total potential energy functional.

c) to find suitable coordinate shape functions for the simply supported ends of the plate.

2 Research Methodology

The total potential energy functional Π of a Kirchhoff plate under distributed transverse load is the sum of the strain energy and the potential energy of the distributed load, and is given by the integral over the plate domain R^2:

$$\Pi = \iint_{R^2} \left\{ \frac{D}{2} \left[(\nabla^2 w)^2 + 2(1-\mu) \left(\frac{\partial^2 w}{\partial x^2} \frac{\partial^2 w}{\partial y^2} - \left(\frac{\partial^2 w}{\partial x \partial y} \right)^2 \right) \right] - qw \right\} dxdy$$

where $w(x, y)$ – the deflection of the plate middle surface; μ – the Poisson's ratio of the plate; D – the flexural rigidity of the plate; $q(x, y)$ – the intensity of distributed transverse load on the plate; ∇^2 – the Laplacian operator in the x-y coordinates; R^2 – the plate domain defined as $0 \leq x \leq a, 0 \leq y \leq b$.

Let the deflection be approximated in terms of a linear combination of n basis (or coordinate or shape) functions of the space coordinates that apriori satisfy the end support conditions thus:

$$w_n(x, y) = \sum_{i=1}^{n} c_i \varphi_i(x, y) \tag{1}$$

$$w_n(x, y) = c_1\varphi_1(x, y) + c_2\varphi_2(x, y) + \ldots + c_n\varphi_n(x, y) \tag{2}$$

where c_i are the n undetermined parameters of the displacement function $\varphi_i(x, y)$ are the coordinate, shape or basis functions that are chosen to satisfy the boundary conditions at the ends.

The total potential energy functional can be expressed in general as follows:

$$\Pi = \iint_{R^2} \left\{ \frac{D}{2} \left(\left(\nabla^2 \sum_{i=1}^{n} c_i \varphi_i \right)^2 + 2(1-\mu) \left(\frac{\partial^2}{\partial x^2} \left(\sum_{i=1}^{n} c_i \varphi_i \right) \frac{\partial^2}{\partial y^2} \left(\sum_{i=1}^{n} c_i \varphi_i \right) - \left(\frac{\partial^2}{\partial x \partial y} \sum_{i=1}^{n} c_i \varphi_i \right)^2 \right) \right) - q \sum_{i=1}^{n} c_i \right\} dxdy$$

$$\tag{3}$$

where

$$\delta_{ik} = \delta_{ki} = \int_0^a \int_0^b D \left\{ \frac{\partial^2 \varphi_i}{\partial x^2} \frac{\partial^2 \varphi_k}{\partial x^2} + \frac{\partial^2 \varphi_i}{\partial x^2} \frac{\partial^2 \varphi_k}{\partial y^2} + \frac{\partial^2 \varphi_i}{\partial y^2} \frac{\partial^2 \varphi_k}{\partial x^2} + \frac{\partial^2 \varphi_i}{\partial y^2} \frac{\partial^2 \varphi_k}{\partial y^2} - (1-\mu) \left(\frac{\partial^2 \varphi_i}{\partial x^2} \frac{\partial^2 \varphi_k}{\partial y^2} + \frac{\partial^2 \varphi_i}{\partial y^2} \frac{\partial^2 \varphi_k}{\partial x^2} - 2 \frac{\partial^2 \varphi_i}{\partial x \partial y} \frac{\partial^2 \varphi_k}{\partial x \partial y} \right) \right\} dxdy$$

$$\tag{4}$$

$$\Delta_{ip} = \int_0^a \int_0^b q(x, y) \varphi_i(x, y) dxdy \tag{5}$$

The principle of minimization of the total potential energy functional leads to the Ritz variational equation:

$$\frac{\partial \Pi}{\partial c_i} = 0 \tag{6}$$

for $i = 1, 2, \ldots, n$. In matrix form, the Ritz variational equations become the system of $n \times n$ equations in c_i given by:

$$\delta_{11}c_1 + \delta_{12}c_2 + \ldots + \delta_{1n}c_n - \Delta_{1p} = 0$$
$$\delta_{21}c_1 + \delta_{22}c_2 + \ldots + \delta_{2n}c_n - \Delta_{2p} = 0 \tag{7}$$
$$\text{M}$$
$$\delta_{n1}c_1 + \delta_{n2}c_2 + \ldots + \delta_{nn}c_n - \Delta_{np} = 0$$

or in matrix form,

$$\begin{pmatrix} \delta_{11} & \delta_{12} & L & \delta_{1n} \\ \delta_{21} & \delta_{22} & L & \delta_{2n} \\ M & & & \\ \delta_{n1} & \delta_{n2} & L & \delta_{nn} \end{pmatrix} \begin{pmatrix} c_1 \\ c_2 \\ \\ c_n \end{pmatrix} = \begin{pmatrix} \Delta_{1p} \\ \Delta_{2p} \\ \\ \Delta_{np} \end{pmatrix} \tag{8}$$

A rectangular Kirchhoff-Love plate simply supported on the edges $x = 0$, $x = a$, $y = 0$, and $y = b$ and carrying uniformly distributed transverse load of intensity q was considered in this study. A one unknown deflection parameter assumption was considered as the simplest case of representation of the deflection function given in general as the equation (2). Thus, $w(x, y) = c_1\varphi_1(x, y)$, $w(x, y) = c_1 F_1(x)G_1(y)$, where $F_1(x)$ and $G_1(y)$ are the coordinate shape functions of the plate in the x and y coordinate directions respectively. The displacement and loading boundary conditions are:

$$F_1(x = 0) = F_1(x = a) = 0$$
$$G_1(y = 0) = G_1(y = b) = 0$$
$$\frac{\partial^2}{\partial x^2} F_1(x = 0) = \frac{\partial^2}{\partial x^2} F_1(x = a) = 0$$
$$\frac{\partial^2}{\partial y^2} G_1(y = 0) = \frac{\partial^2}{\partial y^2} G_1(y = b) = 0$$

Suitable coordinate (basis or shape) functions that satisfy the boundary conditions can be obtained using the polynomial shape functions as:

$$F_1(x) = x^4 - 2ax^3 + a^3 x$$
$$G_1(y) = y^4 - 2by^3 + b^3 y$$

The Ritz variational equation then simplifies to $\delta_{11} c_1 = \Delta_{1p}$, where

$$\delta_{11} = D \int_0^a \int_0^b \left((F_1''(x))^2 (G_1(y))^2 + 2F_1''(x)F_1(x)G_1''(y)G_1(y) + (F_1(x))^2 G_1''(y) \right)$$
$$- (1-\mu)\left(2F_1''(x)F_1(x)G_1''(y)G_1(y) - 2(F_1'(x))^2 (G_1'(y)^2) \right) dxdy \qquad (9)$$

where

$$F_1''(x) = \frac{d^2 F_2(x)}{dx^2}$$
$$G_1'(y) = \frac{dG_1(y)}{dy^2}$$
$$G_1''(y) = \frac{d^2 G_1(y)}{dy^2}$$
$$\Delta_{1p} = \int_0^a \int_0^b q F_1(x)G_1(y)dxdy$$

By differentiation,

$$F_1'(x) = 4x^3 - 6ax^2 + a^3$$
$$F_1''(x) = 12x^2 - 12ax = 12(x^2 - ax)$$
$$G_1'(y) = 4y^3 - 6by^2 + b^3$$
$$G_1''(y) = 12y^2 - 12by = 12(y^2 - by)$$

$$\delta_{11} = D\left\{ \int_0^a (F_1''(x))^2 dx \int_0^b (G_1(y))^2 dy + 2\int_0^a F_1''(x)F_1(x)dx \int_0^b G_1''(y)G_1(y)dy \right.$$
$$+ \int_0^a (F_1(x))^2 dx \int_0^b (G_1''(y))^2 dy - 2(1-\mu)\left(\int_0^a F_1''(x)F_1(x)dx \int_0^b G_1''(y)G_1(y)dy \right.$$
$$\left. - \int_0^a (F_1'(x))^2 dx \int_0^b (G_1'(y))^2 dy \right) \right\}$$

$$\Delta_{1p} = q\int_0^a F_1(x)dx \int_0^b G_1(y)dy$$
$$\delta_{11} = D\{I_1 I_2 + 2I_3 I_4 + I_5 I_6 - 2(1-\mu)(I_3 I_4 - I_7 I_8)\}$$
$$\Delta_{1p} = q I_9 I_{10}$$

where

$$I_1 = \int_0^a (F_1''(x))^2 dx \quad I_2 = \int_0^b (G_1(y))^2 dy \quad I_3 = \int_0^a F_1''(x)F_1(x)dx$$
$$I_4 = \int_0^b G_1''(y)G_1(y)dy \quad I_5 = \int_0^a (F_1(x))^2 dx \quad I_6 = \int_0^b (G_1''(y))^2 dy$$
$$I_7 = \int_0^a (F_1'(x))^2 dx \quad I_8 = \int_0^b (G_1'(y))^2 dy \quad I_9 = \int_0^a F_1(x)dx$$
$$I_{10} = \int_0^b G_1(y)dy$$

The integrals are evaluated to yield:

$$I_1 = \int_0^a (F_1''(x))^2 dx = \frac{24}{5}a^5 \quad I_2 = \frac{31}{630}b^9 \quad I_3 = -\frac{17}{35}a^7$$
$$I_4 = -\frac{17}{35}b^7 \quad I_5 = \frac{31}{630}a^9 \quad I_6 = \frac{24}{5}b^5 \quad I_7 = \frac{17}{35}a^7$$
$$I_8 = \frac{17}{35}b^7 \quad I_9 = \frac{a^5}{5} \quad I_{10} = \frac{b^5}{5}$$

Hence,

$$\delta_{11} = D\left(\frac{744a^5 b^9}{3150} + \frac{744}{3150}a^9 b^5 + \frac{578a^7 b^7}{1225} \right)$$
$$\Delta_{11} = \frac{1}{25}q a^5 b^5 \quad c_1 = F\frac{q}{D}$$
$$F = \left(\frac{744}{126}(b^4 + a^4) + \frac{578}{49}a^2 b^2 \right)^{-1}$$
$$w_1(x, y) = \frac{Fq}{D}(x^4 - 2ax^3 + a^3 x)(y^4 - 2by^3 + b^3 y)$$

Deflection at the centre ($x = a/2$; $y = b/2$):

$$w_c = \frac{25}{256}\left(\frac{744}{126}(1 + \alpha^4) + \frac{578}{49}\alpha^2 \right)^{-1} \frac{qa^4}{D} \qquad (10)$$

where $\alpha = a/b$.

3 Results

3.1 Square Kirchhoff–Love plates

For square Kirchhoff-Love plates, $a = b$, $\alpha = 1$:

$$\delta_{11} = 0.944 D a^{14}; \quad \Delta_{1p} = \frac{qa^{10}}{25};$$
$$c_1 = 0.0378\frac{qa^4}{D}; \quad w_c = 0.004\frac{qa^4}{D}.$$

3.2 Bending moment and shear force

Using the bending moment-deflection relations and the shear deflection relations, the maximum bending moments occur at the plate centre, and is given for square plates by:

$$M_{xx} = 0.0517qa^2. \qquad (11)$$

The exact solutions obtained by Timoshenko and Woinowsky–Krieger [12] is:

$$M_{xx_{max}} = 0.0479qa^2. \qquad (12)$$

Similarly,

$$Q_x = 0.420qa. \qquad (13)$$

4 Discussion

The Ritz variational method which is based on the principle of minimization of the total potential energy functional for a structure has been presented in a systematic way for the flexural problem of Kirchhoff–Love plates under distributed load. The presentation relied on the approximation of the unknown deflection function $w(x, y)$ using approximating displacement shape functions with unknown displacement parameters, and constructed from basis (shape) functions that satisfied apriori the boundary conditions of the loading and the deformation. This yielded the total potential energy functional given in general as equation (3). Application of the extremum condition gave the system characteristic equations in matrix form as equation (8). The use of the method was illustrated for rectangular Kirchhoff–Love plates with simply supported edges using a one term displacement approximation. For a square thin plate, the centre deflection was obtained as equation (10) giving a relative error of 1.9 %. The bending moment at the centre was obtained using the bending moment-deflection relations as equation (11) giving a relative error of 7.9 %. The maximum shear force was obtained from the shear force-deflection relation as equation (13), giving a relative error of −10.7 %.

5 Conclusions

The following conclusions are made from this study.

1. The Ritz variational method can be presented in systematic form using matrices in a displacement based procedure.

2. The stiffness influence coefficients are determined from the shape function by integration.

3. The unknown displacement parameters of the deflection function are evaluated by solving the matrix algebraic equation.

4. A one unknown parameter choice of the deflection function that satisfied the geometric and force boundary conditions yielded seasonally accurate prediction of the maximum deflection at the center with a relative error of 1.9 %. This is reasonable considering the ease of computation offered by the method.

5. A one parameter choice of the deflection function that satisfied the natural and force boundary conditions was less accurate in the estimation of the maximum bending moments and shear force, yielding relative errors of 7.9 % for maximum bending moment and −10.7 % for the shear force.

References

1. Ike, C. C., Nwoji, C. U., Ikwueze, E. U., & Ofondu, I. O. (2017). Bending analysis of simply supported Kirchhoff plates under linearly distributed transverse load. *Explorematics Journal of Innovative Engineering and Technology*, Vol. 1, No. 1, pp. 28–36.

2. Ike, C. C., Nwoji, C. U., & Ofondu, I. O. (2017). Variational formulation of Mindlin plate equation and solution for deflection of clamped Mindlin plates. *International Journal for Research in Applied Sciences and Engineering*, Vol. 5, Issue 1, pp. 340–353.

3. Nwoji, C. U., Onah, H. N., Mama B. O., & Ike, C. C. (2017). Theory of elasticity formulation of Mindlin plate equations. *International Journal of Engineering and Technology*, Vol. 9, No. 6, pp. 4344–4352, doi: 10.21817/ijet/2017/v9i6/170906074.

4. Ike, C. C. (2017). Equilibrium method in the derivation of differential equations for homogeneous isotropic Mindlin plates. *Nigerian Journal of Technology*, Vol. 36, No. 2, pp. 346–350.

5. Ike, C. C. (2017). Kantorovich Euler–Lagrange–Galerkin method for bending analysis of thin plates. *Nigerian Journal of Technology*, Vol. 36, No. 2, pp. 351–360.

6. Mama, B. O., Nwoji, C. U., Ike, C. C., & Onah, H. N. (2017). Analysis of simply supported rectangular Kirchhoff plates by the finite Fourier sine transformation method. *International Journal of Advanced Engineering Research*, Vol. 4, Issue 3, pp. 285–291.

7. Nwoji, C. U., Mama, B. O., Ike, C. C., & Onah, H. N. (2017). Galerkin–Vlasov method for the flexural analysis of rectangular Kirchhoff plates with clamped and simply supported edges. *IOSR Journal of Mechanical and Civil Engineering*, Vol. 14, Issue 2, pp. 61–74, doi: 10.9790/1654-1402.16174.

8. Mindlin, R. D. (1951). Influence of rotary inertia and shear on flexural motions of isotropic elastic plates. *Journal of Applied Mechanics*, Vol. 18, No. 1, pp. 31–38.

9. Reissner, E. (1945). The effect of transverse shear deformation on the bending of elastic plates. *Journal of Applied Mechanics*, Vol. 12, pp. 69–77.

10. Aginam, C. H., Chidolue, C. A., & Ezeagu, C. A. (2012). Application of direct variational method in the analysis of isotropic thin rectangular plates. *ARPN Journal of Engineering and Applied Sciences*, Vol. 7, No. 9, pp. 1128–1138.

11. Eze, J. C., Ibearugbulem, O. M., & Onyechere, C. I. (2013). Pure bending analysis of thin rectangular flat plates using ordinary finite difference method. *International Journal of Emerging Technology and Advanced Engineering*, Vol. 3, Issue 3, pp. 20–23.

12. Timoshenko, S., & Woinowsky-Krieger (1959). *Theory of plates and shells*. McGraw Hill, Tokyo.

Систематичне викладення варіаційного методу Рітца для аналізу жорсткості шарнірно опертої прямокутної пластини Кірхгофа–Лява

Іке Ч. Ч.

Державний університет науки і технології м. Енугу , П.М.Б. 01660, м. Енугу, Нігерія

Анотація. У роботі у матричній формі представлений узагальнений спосіб застосування варіаційного метода Рітца для розв'язання задачі про вигин навантаженої пластини Кірхгофа-Лява. Наведено приклади застосування шарнірно опертої прямокутної пластини під рівномірно розподіленим навантаженням, використовуючи функції форми у базисі прямокутної системи координат. Один з прикладів наближеного розв'язку за методом Рітца отримано для переміщення центра квадратної пластини плит. При цьому, відносна похибка відносно точного значення складає 1,9 %. Отримане значення для згинального моменту у центрі пластини відрізняється від існуючого точного рішення на 7,9 %. Значення перерізувального зусилля дає похибку
–10,7 %. Таким чином, одержані результати для апроксимації функції форми із подальшим застосуванням методу Рітца, є достатньо близькими для практичних цілей.

Ключові слова: варіаційний метод Рітца, пластина Кірхгофа-Лява, функція форми, загальна потенціальна енергія, принцип мінімізації.

Comprehensive Approach for Identification of Nonlinear Stiffness Characteristics of Bearing Supports for the Oxidizer Turbopump of the Liquid Rocket Engine

Pavlenko I.[1*], Demyanenko M.[1], Edl M.[2], Simonovskiy V.[1], Pitel' J.[3], Pavlenko V.[4], Verbovyi A.[1]

[1] Sumy State University, 2 Rymskogo-Korsakova St., Sumy, 40007, Ukraine;
[2] University of West Bohemia, 8 Universitni St., 306 14 Pilsen, Czech Republic;
[3] Technical University of Košice, 1 Bayerova St., Prešov, 08001, Slovakia;
[4] Machine-Building College of Sumy State University,
17 Shevchenka Av., 40022, Sumy, Ukraine

Abstract. This article dials with the refinement of the mathematical and computational models of the oxidizer turbopump rotor considering bearing gaps, axial preloading, compliance of the housing parts and the effect of rotation. The loading scheme consists of four substeps is proposed considering preliminary displacement of the outer cage, axial displacement as a result of the support deformation due to the axial preloading force, radial displacement due to the support deformation, as well as centrifugal forces of inertia caused by rotation of the rotor with an inner cage. Modelling of contacts interactions using ANSYS software is carried out according to the appropriate models of contact behaviour. The contact areas between the rolling elements, inner and outer cases are obtained. The contact angle is determined. Isosurfaces of axial and radial displacements for the bearing supports are built. Nonlinear stiffness of bearing supports is determined as the tangent of the angle of inclination for the curve "radial load – radial displacement". The proposed approach, which used for designing turbopump units for liquid rocket engines, will allow refining the reliable mathematical and computational models of rotor dynamics for turbopump units and providing appropriate computer simulation of forced oscillations of the rotor systems for given permissible residual imbalances considering nonlinear stiffness characteristics of bearing supports.

Keywords: compliance of housing, initial clearance, axial preloading, radial load, contact angle, radial stiffness, axial stiffness.

1 Introduction

The creation of reliable models of rotary systems is an urgent problem that allows designing high-power rotary machines including turbopump units of liquid rocket engines. The process of modelling should be based on the existing experience in designing of reliable equipment the requirements for which are permanently increased.

Based on the experience of the Faculty of Technical Systems and Energy Efficient Technologies (Sumy State University, Ukraine) in mathematical modelling of rotary systems, and the Faculty of Mechanical Engineering (University of West Bohemia, Czech Republic) in providing numerical simulations, as well as the Faculty of Manufacturing Technologies with a seat in Prešov (Technical University of Košice, Slovakia) in carrying out experimental research, this paper is devoted to refine the computational model of rotor dynamics for turbopump units

and further computer simulation of forced oscillations of the rotor systems for given permissible residual imbalances considering the nonlinear stiffness of bearing supports.

The proposed clarifications are related to effect of rotation on deformation of moving parts of bearings, compliance of the housing, as well as gaps and axial preloading of the bearing supports.

The clarification of the stiffness parameters of the bearing supports is carried out by a combination of 2D and 3D finite element models using up-to-date computational means.

The proposed approach will allow refining the reliable mathematical and computational models of rotor dynamics for turbopump units and providing computer appropriate simulation of forced oscillations of the rotor systems for given permissible residual imbalances considering nonlinear stiffness characteristics of bearing supports.

2 Literature Review

The problem of identification of the nonlinear bearing stiffness is highlighted in recent research works. Particularly, the paper [1] dials with the investigation of nonlinear reactions in rotors' bearing supports of turbopump units for liquid rocket engines. However, this work does not consider the impact of initial bearing gap and axial preloading.

The problem of dynamics and diagnostics of vertical rotors with nonlinear supports stiffness is solved in the doctoral thesis [2].

Clarifications considering the impact of gap seals with floating rings are presented in monograph [3]. Additionally, it is shown that the presence of gaps in the bearing supports reduces the bearing stiffness. However, gap seals with floating ring, axial preloading and rotation of the rotor cause an increasing dependence of the bearing stiffness on the rotor speed. Consequently, the critical frequencies of the rotor increase.

A review of investigations of nonlinear dynamic on bearings with rolling element is presented in the research work [4].

The calculation of forced oscillations under the system of imbalances (direct synchronous precession) performed using the computer program [5] considers the dependences of the bearing stiffness on the rotor speed and impact of the gyroscopic moments of inertia of bushing parts.

Paper [6] is aimed at theoretical and experimental study of spindle ball bearing nonlinear stiffness.

General scientific and methodological approach for the identification of mathematical models of mechanical systems using artificial neural networks is delivered in paper [7].

Nonlinear dynamic response for the system "cylindrical roller bearing – rotor system" is presented in the paper [8]. The proposed mathematical model with 9 degrees of freedom allows considering combined localized defect at inner–outer races of bearings.

The need to consider clarified mathematical model of rotor dynamics for investigation of critical frequencies considering stiffness of bearings and seals is justified in the work [9] on the example of on examples of the centrifugal compressor's rotor.

The influence of bearing stiffness on the nonlinear dynamics of a shaft-final drive system is presented in the research paper [10].

3 Research Methodology

The connection of shafts of the turbopump unit causes a weak dynamic interaction between them. In this case, the partial critical frequencies of separate rotors do not differ much from the corresponding frequencies, obtained as a result of calculations for the entire rotor. This fact is confirmed by the calculations presented in the work [2]. Therefore, the oxidizer turbopump and fuel pump rotor systems should also be considered as the separate dynamic systems. The design scheme of the oxidizer turbopump rotor is presented in Figure 1.

The ANSYS software with the modules "Static Structural" and "Transient Structural" is used for determining the bearing stiffness considering initial gaps, axial preloading, rotation effect and compliance of the housing. The basic design schemes for loading bearing supports are presented in Figure 2.
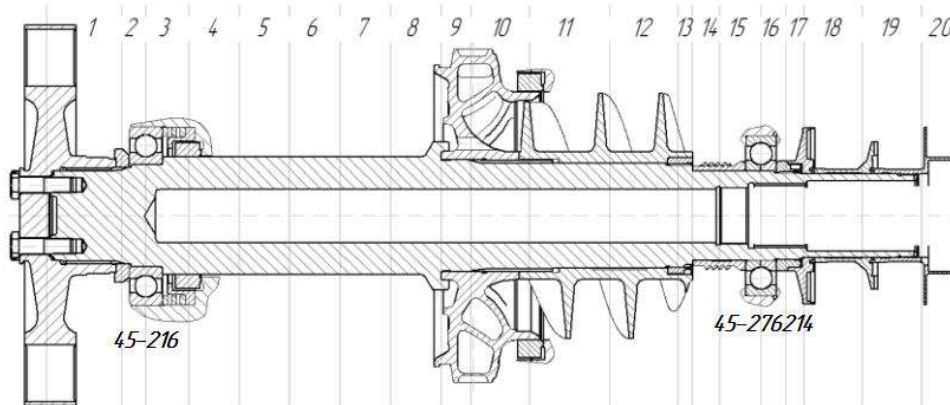
Figure 1 – Design scheme of the oxidizer turbopump rotor
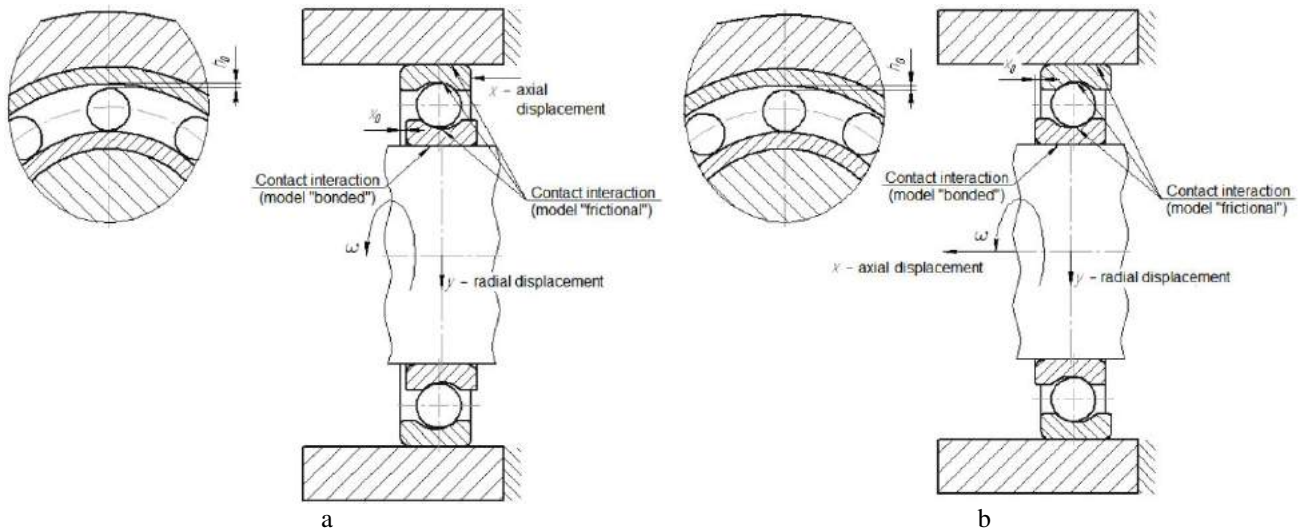
Figure 2 – Design scheme of the bearing supports 45-216 (a) and 45-276214 (b)

The loading scheme consists of four substeps:

1. Preliminary displacement of the outer cage (for the bearing support 45-216) and the shaft (for the bearing support 45-276214) towards the application of axial pre-loading force. Axial displacement x_0 is determined due to the maximum radial gap $h_0 = 0.095$ mm [11].

2. Determination of the axial displacement x as a result of the support deformation due to the axial preloading force $T = 4,5$ kN [11]. Investigation of forced oscillations of the rotor on ball bearings.

3. Numerical calculation of the radial displacement y of the shaft axis as a result of the support deformation due to the radial force $R = 10$ kN.

4. Considering centrifugal forces of inertia caused by rotation of the rotor with an inner cage of the bearing support.

Modelling of contacts by using ANSYS software is carried out according to Table 1.

Table 1 – Models of contact interaction between the mating surfaces

Mating surfaces		Contact model
Shaft	Inner cage	"bonded"
Inner cage	Rolling elements	
Rolling elements	Outer cage	"frictional"
Outer cage	Housing	

The contact areas between the rolling elements and cases are shown in Figure 3. The loading schemes accogding to substeps 2–4 of bearing loading are presented on Figures 4–6.

Isosurfaces of axial and radial displacements for the bearing supports are presented on Figures 7–8.
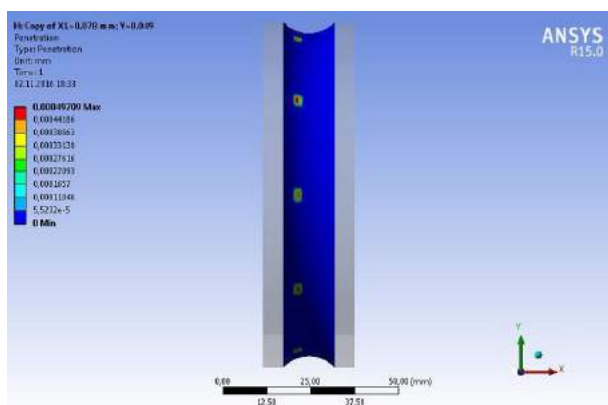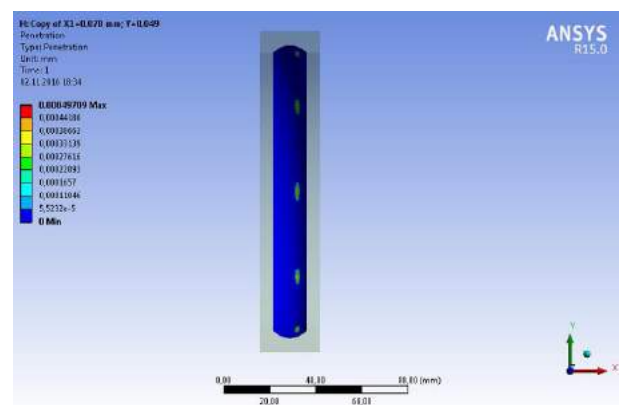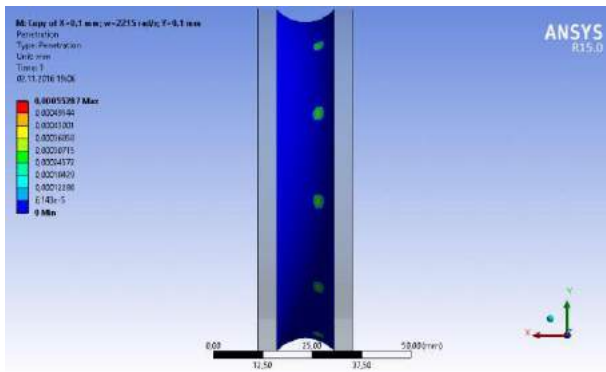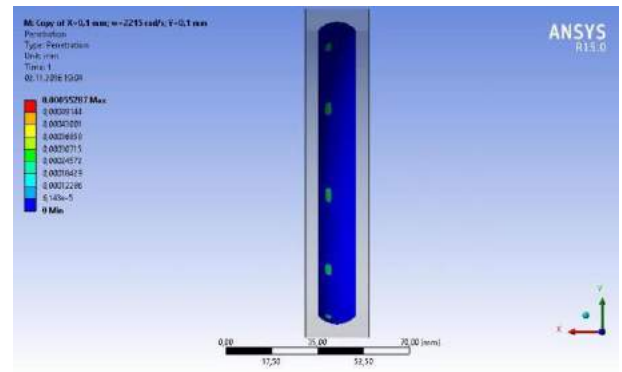
Figure 3 – Contact areas between the rolling bodies, inner (a, c) and outer (b, d) cages
for the bearin supports 45-216 (a, b) and 45-276214 (c, d)
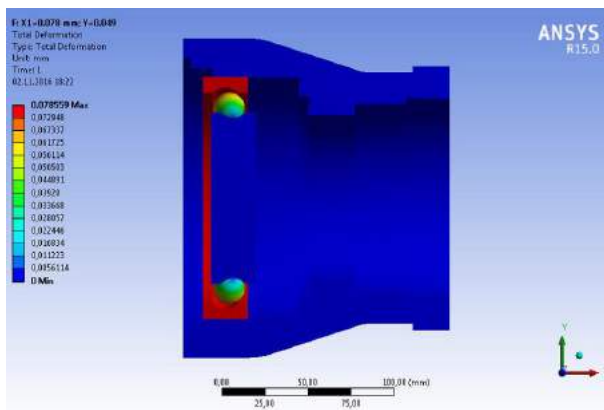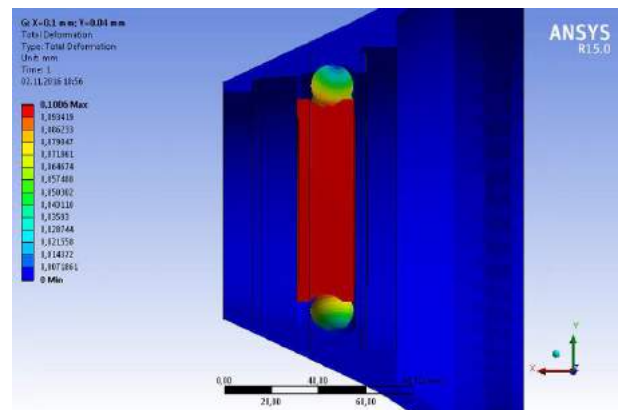
Figure 4 – Deformations of the bearing supports 45-216 (a) and 45-276214 (b) as a result of axial preloading
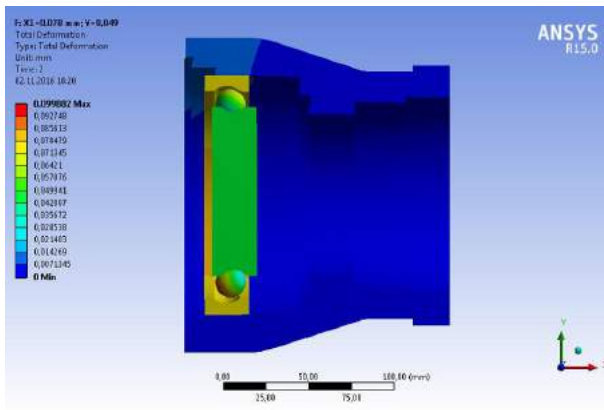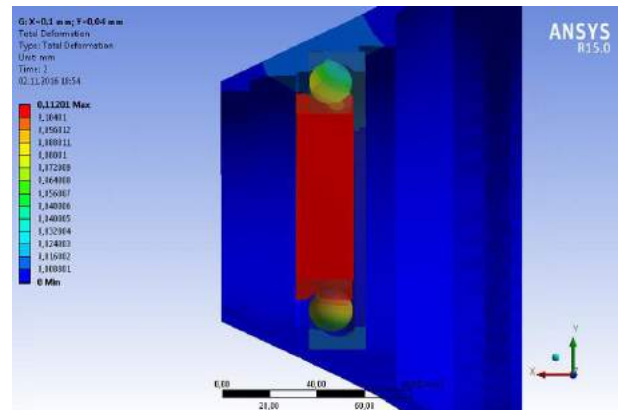
Figure 5 – Deformations of the bearing supports 45-216 (a) and 45-276214 (b) as a result of axial preloading and radial force
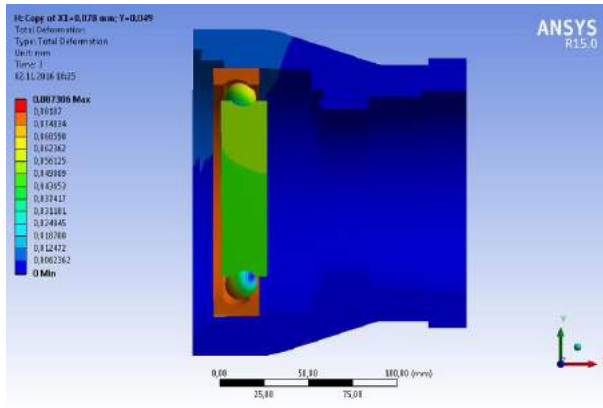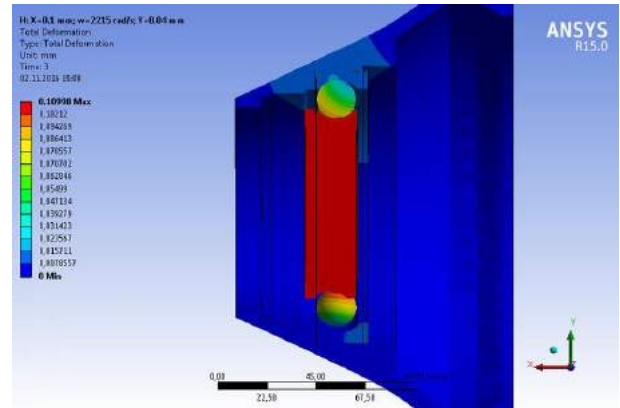
a   b

Figure 6 – Deformations of the bearing supports 45-216 (a) and 45-276214 (b)
as a result of axial preloading, radial force and rotation of the rotor
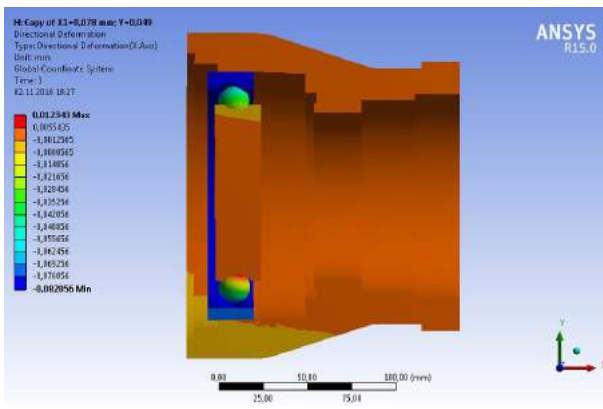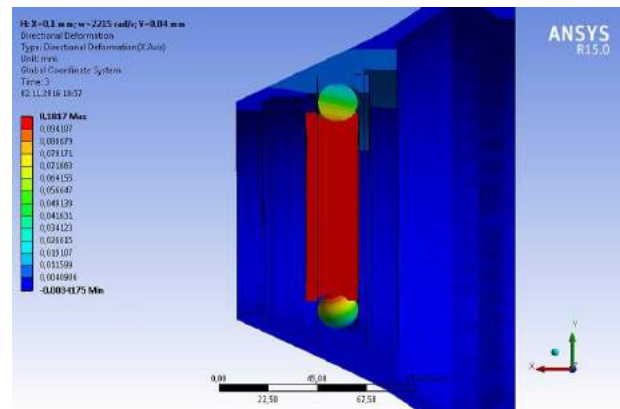
a   b

Figure 7 – Isosurfaces of axial displacements for the bearing supports 45-216 (a) and 45-276214 (b)

a   б
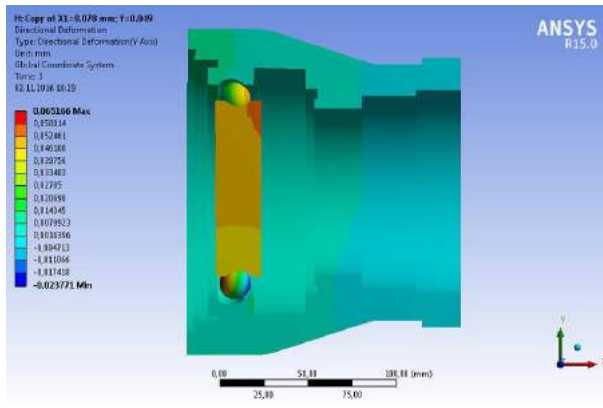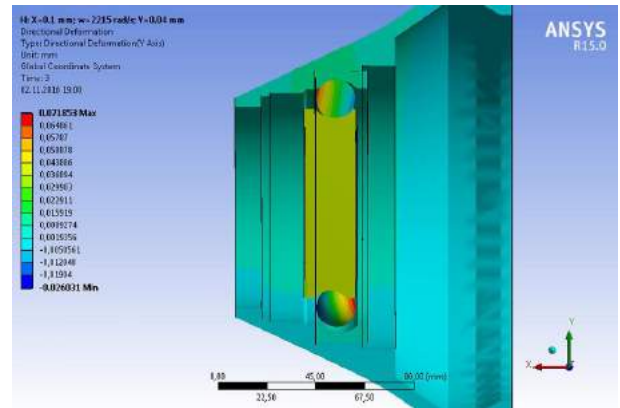
Figure 8 – Isosurfaces of radial displacements for the bearing supports 45-216 (a) and 45-276214 (b)

4 Results

The results of numerical simulation are summarized in Table 2.

The stiffness c of the bearing support is determined due to the following formula:

$$c = \partial R / \partial y, \qquad (1)$$

where R – radial force; y – radial displacement.

As a result of numerical simulation (the determination of radial displacements of the rotor axis under the discrete values of the radial force), the approximated curves "radial load – radial displacement" are defined (Figure 9).

Analytical expressions describing the dependence "radial load – radial displacement" determined as a result of approximation of the experimental data are summarized in Table 3.

Table 2 – The results of numerical simulation

Bearing	Displacement, μm						
	h_0	x_0	x	Rotor speed, 10^3 rad/s			
				0	1.1	2.0	2.2
45-216	95	620	80	51	50	48	47
45-276214	95	620	100	40	40	39	39

a   b
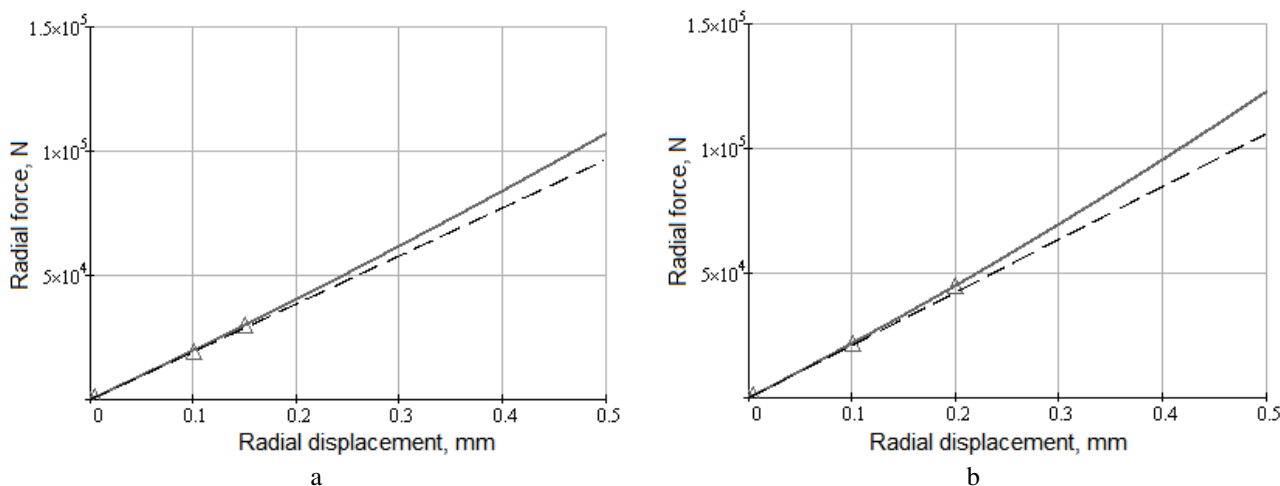
Figure 9 – Dependence "radial force – radial displacement" for the bearing supports 45-216 (a) and 45-276214 (b)

Table 3 – Analytical dependences "radial load – radial displacement"

Bearing support	45-216			45-276214		
Radial displacement y, μm	5	100	150	5	100	200
Radial force R, kN	0.9	1.95	30	1	22	45
Approximated curve (R, N; y, m)	$R(y) = 1.94 \cdot 10^8 \cdot y + 4.0 \cdot 10^{10} \cdot y^2$			$R(y) = 2.12 \cdot 10^8 \cdot y + 6.7 \cdot 10^{10} \cdot y^2$		
Nonlinear radial stiffness (c, N/m; y, m; R, N)	$c(y) = 1.94 \cdot 10^8 + 8.0 \cdot 10^{10} \cdot y$			$c(y) = 2.12 \cdot 10^8 + 1.34 \cdot 10^{11} \cdot y$		
	$c(R) = 1.94 \cdot 10^8 \cdot (1 + 4.2 \cdot 10^{-6} R)^{0.5}$			$c(R) = 2.12 \cdot 10^8 \cdot (1 + 6.0 \cdot 10^{-6} R)^{0.5}$		

The linear radial stiffness of the support is defined as the tangent of the initial angle of inclination of the curve "radial load – radial displacement" (Figures 9, dash line):

$$c_0 = \left(\frac{\partial R}{\partial y} \right)_0. \qquad (2)$$

Taking into account the expressions given in Table 2, the values of the bearing stiffness c_0 of the supports 45-216 and 45-276214 are equal $1.94 \cdot 10^8$ N/m and $2.12 \cdot 10^8$ N/m respectively. Exceeding the bearing stiffness of the support 45-276214 in comparison with the bearing support 45-216 is explained by the relatively large number of rolling bodies.

Similar values of the bearing stiffness, determined without the rotor speed for the supports 45-216 and 45-276214 are equal $1.88 \cdot 10^8$ N/m and $2.10 \cdot 10^8$ N/m respectively.

For further designing the mathematical models of free and forced oscillations of the rotor systems for turbopump unit considering the impact of the rotor speed on bearing stiffness, the following analytical dependence is proposed:

$$c(\omega) = c_0 + \alpha \omega^2. \qquad (3)$$

In this case, the estimation of the coefficient α is carried out by the linear regression formula [1]:

$$\alpha = \frac{\sum_{k=1}^{3} (c_k - c_0) \omega_k^2}{\sum_{k=1}^{3} \omega_k^4}, \qquad (4)$$

where c_k – bearing stiffness, determined as a result of the numerical simulation for the rotor speed ω_k (Table 2); k – number of the experimental point.

As a result, values of the coefficient α are obtained (Table 4), as well as the approximated curves are built (Figure 10).

The obtained data allows determining the dependence of the bearing stiffness on the radial force (Figure 11).

Table 5 and Figures 12–13 contain the data presenting the axial stiffness of the bearing supports.

Table 4 – Parameters of the nonlinear bearing stiffness

Bearing support	Parameter	
	c_0, N/m	α, N·s^2/m
45-216	1.88	1.223
45-276214	2.10	0.408
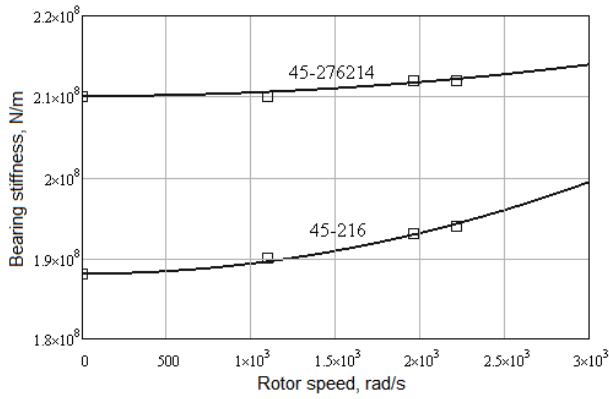
Figure 10 – Dependence of the bearing stiffness
on the rotor speed
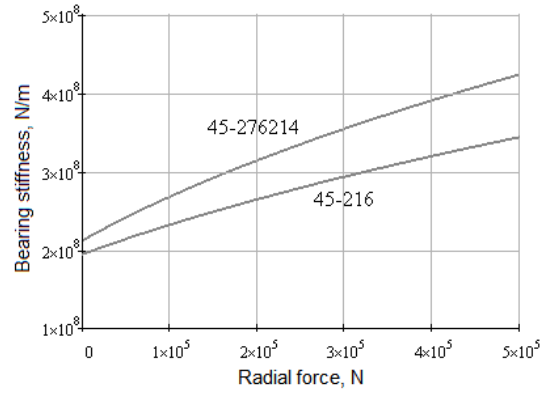
Figure 11 – Dependence of the bearing stiffness
on the radial force

a

a
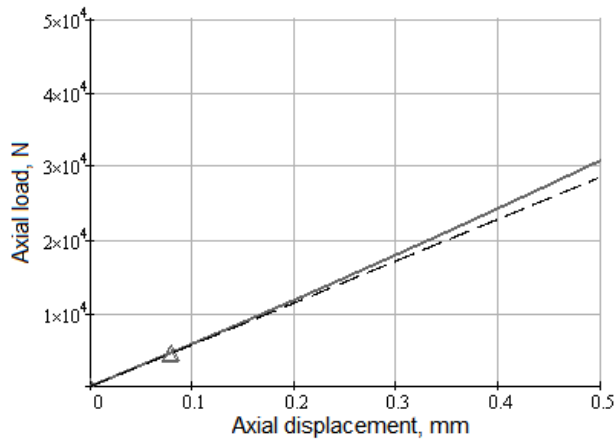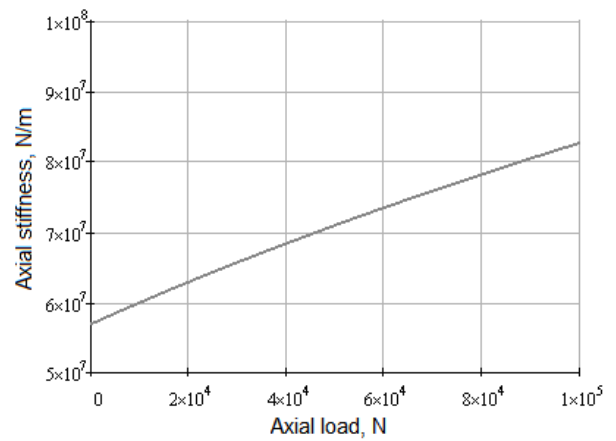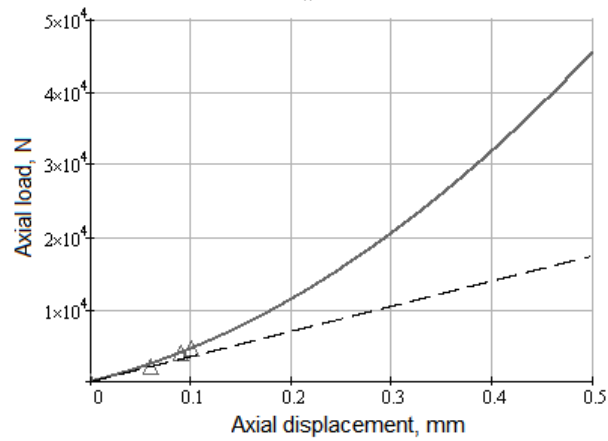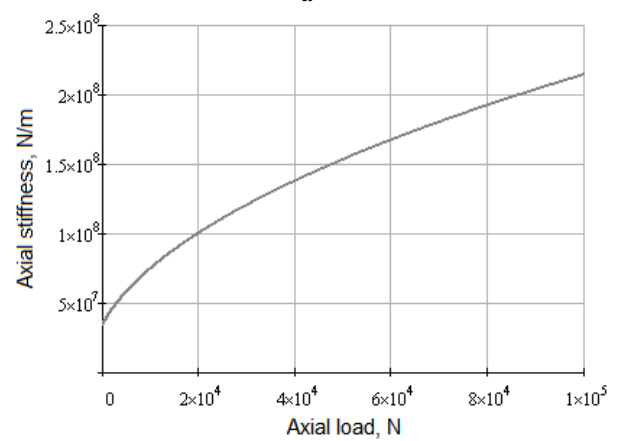
b

Figure 12 – Dependence "radial load – radial displacement"
for the bearing supports 45-216 (a) and 45-276214 (b)

b

Figure 13 – Dependence "axial load – axial displacement"
for the bearing supports 45-216 (a) and 45-276214 (b)

Thus, the proposed comprehensive approach is approved on the example of the oxidizer turbopump's rotor for the liquid rocket engine that will allow refining the reliable mathematical and computational models of rotor dynamics for turbopump units and providing appropriate computer simulation of forced oscillations of the rotor systems for given permissible residual imbalances considering nonlinear stiffness characteristics of bearing supports.

Further research will be aimed at obtaining spectrums of critical frequencies and related mode shapes for the rotor systems in abovementioned bearing supports, as well as at the detailed analysis of forced oscillations of the turbopump rotor for the nonlinear stiffness of the bearing supports considering radial gaps, initial clearance, axial preloading, maximum rotor speed and compliance of the housing for the system of residual imbalances, which led to the maximum values of centrifugal forces.

5 Conclusions

As a result of numerical simulation (the determination of radial displacements of the rotor axis under the discrete values of the radial force), the approximated curves "radial load – radial displacement" are defined. Analytical expressions describing the mentioned dependence are determined as a result of approximation of the experimental data.

The results of more precise calculations of rotor dynamics for the turbopump considering bearing gaps, axial preloading, rotor speed and compliance of the housing parts will allow clarifying the detuning from the resonance.

6 Acknowledgements

References

1. Pavlenko, I. V., et al. (2018). Investigation of non-linear reactions in rotors' bearing supports of turbo-pump units for liquid rocket engines. *Journal of Engineering Sciences*, Vol. 5, Issue 1, pp. D6–D14, DOI: 10.21272/jes.2018.5(1).d2.
2. Tadzijevas, A., (2015). *Dynamics and diagnostics of vertical rotors with nonlinear supports stiffness*. Doctoral thesis, Kaunas University of Technology.
3. Pavlenko, I., Simonovskiy, V., Pitel', J., & Demianenko, M. (2018). *Dynamic analysis of centrifugal machines rotors with combined using 3D and 2D finite element models*. Lüdenscheid, RAM-VERLAG.
4. Sharma, A., Upadhyay, N., & Kunkar, P. K. (2018). Nonlinear dynamic investigations on rolling element bearings: A review. *Advances in Mechanical Engineering*, Vol. 10(3), pp. 1–15, DOI: 10.1177/1687814018764148.
5. Pavlenko, I., & Simonovskiy, V. (2015). *Computer program "Forced oscillations of the rotor"*. Certificate of the authorship, Ukraine, State reg. no. 61788.
6. Madoliat, R., & Ghanati, M. F. (2013). Theoretical and Experimental Study of Spindle Ball Bearing Nonlinear Stiffness. *Journal of Mechanics*, Vol. 29, pp. 633–642, DOI: 10.1017/jmech.2013.48.
7. Pavlenko, I., Trojanowska, J., et al. (2018). Scientific and methodological approach for the identification of mathematical models of mechanical systems by using artificial neural networks. *Lecture Notes in Electrical Engineering*, Vol. 505, pp. 299–306, DOI: 10.1007/978-3-319-91334-6_41.
8. Patel, U. K. A., & Upadhyay, S. H. (2014). Nonlinear Dynamic Response of Cylindrical Roller Bearing–Rotor System with 9 Degree of Freedom Model Having a Combined Localized Defect at Inner–Outer Races of Bearing. *Tribology Transactions*, Vol. 60, Issue 2, pp. 284–299.
9. Pavlenko, I. V., Simonovskiy, V. I., Pitel, J., et al. (2017). Investigation of critical frequencies of the centrifugal compressor rotor with taking into account stiffness of bearings and seals. *Journal of Engineering Sciences*, Vol. 4, Issue 1, pp. C1–C6, DOI: 10.21272/jes.2017.4(1).c1.
10. Jinli, X., Lei, W., & Wenxin, L. (2016). Influence of Bearing Stiffness on the Nonlinear Dynamics of a Shaft-Final Drive System. *Shock and Vibration*, Vol. 2016, Article ID 3524609, DOI: 10.1155/2016/3524609.
11. Martsynkovskyy, V. A., Zahorulko, A. V., et al. (2016). *Numerical simulation of rotor dynamics for liquid rocket engines with considering dynamic characteristics of bearings and seals*. Sumy, Sumy State University, State reg. no. 0115U000679.

Комплексний підхід до ідентифікації нелінійних жорсткісних характеристик підшипникових опор турбонасоса окислювача рідинного ракетного двигуна

Павленко І.[1*], Дем'яненко М.[1], Едл М.[2], Симоновський В.[1], Пітель Я.[2], Павленко В.[4], Вербовий А.[1]

[1] Сумський державний університет, вул. Римського-Корсакова, 2, 40007, м. Суми, Україна;
[2] Західночеський університет, вул. Університетська, 8, 306 14, м. Пльзень, Чехія;
[3] Технічний університет м. Кошице, вул. Баєрова, 1, 08001, м. Прешов, Словаччина;
[4] Машинобудівний коледж Сумського державного університету, просп. Шевченка, 18, 40022, м. Суми, Україна

Анотація. Стаття присвячена уточненню математичних та обчислювальних моделей ротора турбонасоса окислювача з урахуванням зазорів у підшипниках, попереднього осьового навантаження, податливості корпусних елементів та впливу обертання вала. Запропонована схема навантаження складається з чотирьох шагів з урахуванням попереднього зміщення зовнішньої обойми, осьового зміщення у результаті переміщення опори внаслідок попереднього осьового навантаження, радіального переміщення внаслідок деформації підшипникової опори, а також відцентрових сил інерції, викликаних обертанням ротора разом із внутрішньою обоймою. Моделювання контактної взаємодії з використанням програмного забезпечення ANSYS здійснюється відповідно до достовірних моделей. Встановлені зони контакту між тілами кочення і внутрішньою та зовнішньою обоймами, а також визначений кут контакту. Побудовано ізоповерхні осьових та радіальних переміщень підшипникових опор. Нелінійна жорсткість опор визначається як тангенс кута дотичної до кривої, що описує залежність «радіальне навантаження – радіальне зміщення». Запропонований підхід, який використовується для проектування турбонасосних агрегатів рідинних ракетних двигунів, дозволить уточнити достовірні математичні та обчислювальні моделі динаміки ротора і забезпечити якісне моделювання вимушених коливань роторних систем для заданої системи допустимих залишкових дисбалансів з урахуванням нелінійних характеристик жорсткості підшипникових опор.

Ключові слова: податливість корпуса, початковий зазор, попереднє осьове навантаження, радіальне навантаження, кут контакту, радіальна жорсткість, осьова жорсткість.

Design and Analysis of Connecting Tie Rod Assembly for Automotive Application

Aravindaraj E.[1], Natrayan L.[2*], Santhosh M. S.[3], Kumar M. S.[2]

[1] Sri Manakula Vinayagar Engineering College, Mannadipet, 605 107 Pudicherry, India;
[2] VIT University, Chennai, 600 127 Tamil Nadu, India;
[3] Selvam College of Technology, Salem Road (NH 7), Pappinaickenpatti, Namakkal, 637 003 Tamil Nadu, India

Abstract. The tie rod end is one of the most elementary parts of a steering mechanism, which has direct and crucial importance in terms of driving safety. The tie rod end is used to ensure that the wheels are aligned. It provides the adjustment for the wheel to align and keeps the tires free from wearing out on the inner as well as outer edges. Hence the functioning of the tie rod is crucial for steering as well as suspension performance of the vehicle. Today's world is competitive. Market demands the advanced technology at a lower price. This reflects in making the technology cheaper. Hence every industry determined for the cost-effective product at a lower price and within minimum period for 'time to market. This puts a lot of pressure on engineers to consistently strive to design the more effective products at the lower price. The work is focused on the functioning of the tie rod. Generally, tractor connecting tie rod gets failed due to the overload applications. This paper focuses on modifying the old tie rod design and material. Finally, analysis the load causes of existing and modified design using ANSYS software. This modelling approach, the stress variations and deformation characteristics of each component are investigated for high operational loading conditions.

Keywords: thru-hole, clamp structure, front axle, ANSYS, deformation.

1 Introduction

Tie rod ends support (Figure 1) thru the steering of a vehicle and variety it possible to capture a tire. These devices occur in pairs on each tire. This sanctions for cornering and angling of the tire minus affecting too much torque on the trundlenopestaple how deep the seizure [1]. Tie-rod is certain as driving adherent for slanting the panel (along with panel mounting frame) from horizontal to vertical position and vice versa. In principal, tie-rod will have essential coupler with nail rods on sides, one through left hand thread and another through right hand thread [2]. The coupler has identical threads to put up these eased tie rods [3]. On spinning the coupler is turned, together the rods will spread or withdraw based on the trend of rotation of coupler. The ends of the rods are moreover eye or fork expiration type [3, 4].

Further research will be aimed at research the adjustable front axle with adjustable tie rod (Figure 1).

This origination relays to a tractor and more specifically to unregulating front axle for a row crop farm tractor. In farm tractors of the row produce type it is crucial to afford for widening and narrowing the stamp of the ambi-

tion wheels where a three wheel tractor is fretful [5]. A four wheel rumpus crop tractor requires that both front and rear wheels be adjustable squarely, in directive to travel between the plants in the rows [6]. The peak common scheme of varying the width of the wheel tread on ruckus crop tractors currently is to dispose the wheels hubs and tire rims in such routine that by reversing the wheels in relative to the hubs the stamp may be amplified or narrowed [7]. While the development above described may perform to be artlessearnings of amending the stride of the wheels of the tractor, however such amending mechanism fills a long desired want of stingily and easily altering the width of the tread of façade wheels of row crop tractors [8].

Figure 1 – Adjustable tie rod

2 Research Methodology

2.1 EN8 carbon steel material

EN8 is typically abounding organic but can be supplied to edict in the stabilized or finally heat salted (appeased and tempered to "*Q*" or "*R*" properties for off-putting ruling subdivisions up to 63 mm), which is ample for a widespread range of applications. EN8 is suitable for the assembly of quantities such as general-tenacity axles and shafts, gears, bolts and studs [6, 9]. It can be auxiliary hardboiled typically to 50–55 HRC by initiation processes, producing modules with enriched wear resistance. For such tenders the use of EN8D (080A42) is prudent. EN8 in its heat frozen rehearses possesses virtuous homogenous metallurgical structures, philanthropic unfailing machining properties [9]. Virtuous heat treatment grades on segments grander than 63 mm may still be attainable, but it should be illustrious that a fall-off in mechanical properties would be superficialpotential the epicentre of the bar [10, 11]. Table 1 gives mechanical properties of material.

Table 1 – Material Properties

Material	Yield strength, N/mm^2
EN8	465
EN8D	443
EN5D	451
EN5C	438

When compared to mechanical property and cost EN8 is the best one for design the product and economical one [12].

2.2 Existing thru-hole design parts

The previous research papers are useful for deciding the analysis strategy. There were numerous conference papers, reference manuals, book by Robert cook Concepts and applications of FEA will be helpful for the project. From some of the research work it is being observed that the existing thru hole design model.

The existing geometrical model is created as a solid works 2016 software and analysis in ANSYS Workbench, The geometrical model constitutes of the socket (Figure 2), radial ball joint (Figure 3), tube (Figure 4) and axle ball joint (Figure 5).

While neglecting the parts that are thought as negligible in the analysis. Figure 6 shows that existing tie rod design using solid works software.

2.3 Problem identification

In the existing design nut and bolt joints are used to connect the socket and tube, so it can't withstand more compressive load and tensile load. It leads to bend which causes breakage in the tie rod. Also, the thru-hole design is applicable to load only below 2 000 kg and when the load increases the tie rod bends. So it cannot withstand more than 2 500 kg tensile load and compressive load.

Figure 2 – Socket
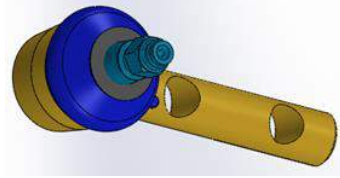
Figure 3 – Radial ball joint

Figure 4 – Tube
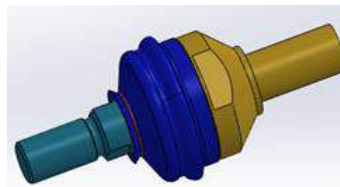
Figure 5 – Axle ball joint
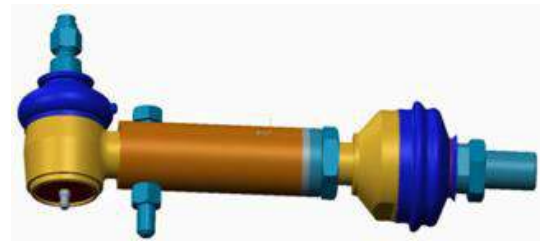
Figure 6 – Existing tie rod design

2.4 Designs of tie rods

2.4.1 Proposed new design

The tie rod is continuously under random loading there can be more chances of developing the cracks at the critical areas and chances of failure. Also the manufacturing process of this existing design is critical and time consuming. Hence it is necessary to make the design simple and cost effective such that it gives overall effectiveness in terms of weight, cost, load carrying capacity and easy of manufacturing process. The main task in this study is to find the critical buckling load for the existing design. Observe the deformation and stresses induced in the Tie rod. Set up the benchmark for the proposed design.

Figure 7 shows proposed new connecting tie rod design, thru-hole clamped design used to connect the tube and socket. Because of groove and clamp withstands more compressive and tensile load compare to exiting design.

Figure 7 – Proposed new design

2.4.2 Existing model tie rod analysis

The existing tie rod model has carried out static analysis using EN8 carbon steel material, while applied the load upto 2 000 kg in exiting model, it's can't shows any deformation. Figures 8–9 show that thru-hole design applicable only below 2 000 kg load.
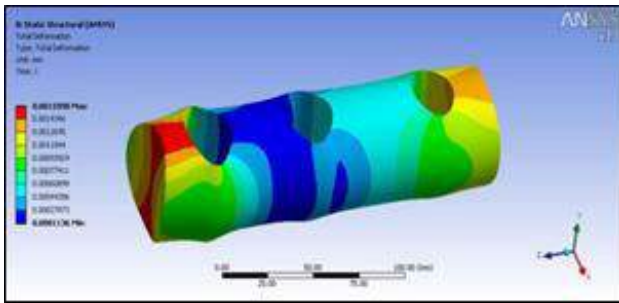
Figure 8 – Compressive load
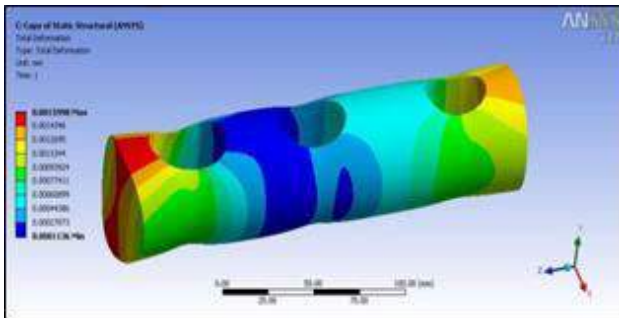
Figure 9 – Tensile load

Increasing the tensile compression loads up to 2 500 kg, existing model tie rod getting failure and its goes to deformation. Figures 10–11 show failure action of tie rod during 2 500 kg load.
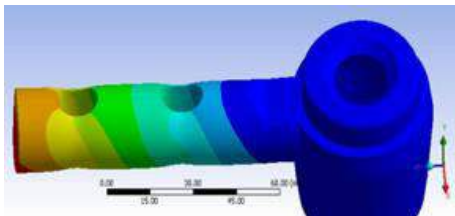
Figure 10 – During tensile load

Figure 11 – During compressive load

2.4.2 Sample groove design with hollow construction (Existing Design)

When compared to thru hole this groove design withstands more load during compression load. From the Figure 12, groove design with hollow construction cannot withstand more than 2 500 kg of compressive load. So, this designs also not suitable for the tie rod.
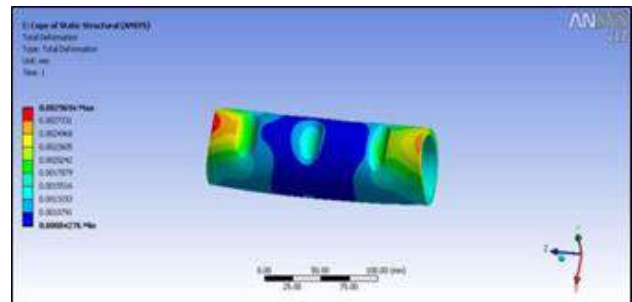
Figure 12 – Compressive load test for hollow groove design

2.5 Proposed new design analysis

2.5.1 Sample solid groove design

The solid groove design has analysis using EN8 carbon steel in Figures 13–14. Hence, Solid groove design withstands more loads when compared to both hollow groove and thru-hole design. It cannot withstand up to 3 500 kg of compressive load and tensile load. So this the suitable design for the adjustable tie rod.
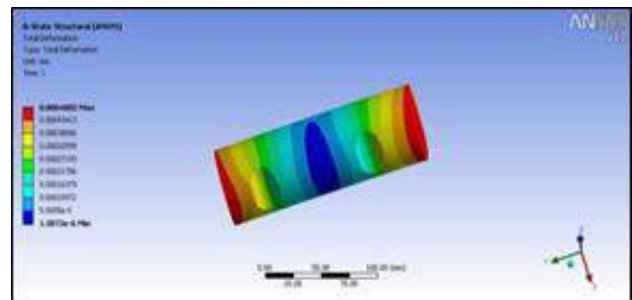
Figure 13 – Compressive load test on solid groove design
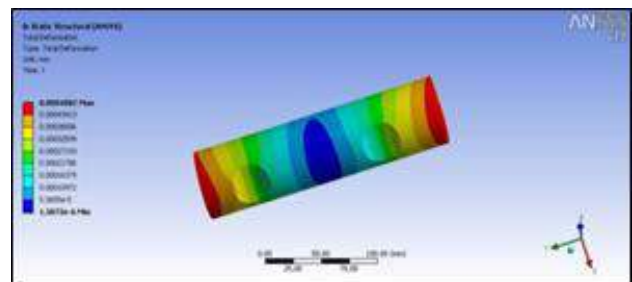
Figure 14 – Tensile load test solid groove design

2.5.2 Tensile and compression load analyses of adjustable tie rod

Below Figures 15–16 show the thru hole design failed to withstand the 3000kg tensile load, but grooved design can withstands more load when compared to thru hole design in tie rod.
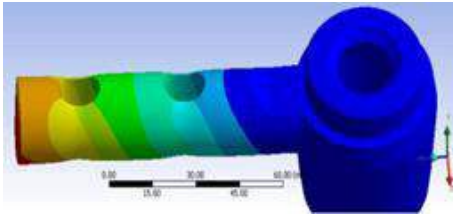
Figure 15 – Thru hole design
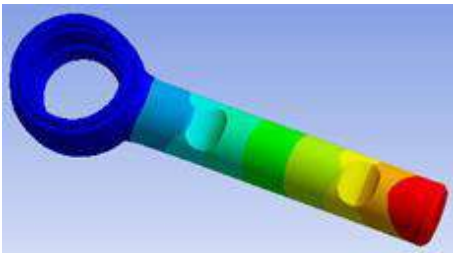
Figure 16 – Clamped design

2.6 Comparison of analysis result

Tables 2–3 show static analysis results for existing and proposed new design using EN8 Carbon steel.

Table 2 – Socket with through hole

Load, kgf	Max stress, N/mm^2	FOS
2 500	365	0.77
3 000	438	0.64
4 000	583	0.48

Table 3 – Socket with groove

Load, kgf	Max stress, N/mm^2	FOS
2 500	151.7	1.85
3 000	182.4	1.54
4 000	243.2	1.15

From the results, maximum stress has acted on the through hole design, and proposed design has less deformation is obtained compare to exiting tie road model. Tie rods are merely subjected with more compressive forces. From the above analysis shows that proposed design has more damping capacity and can withstand more compressive forces. This is due to because of carbon flake distribution in the material. Carbon flake distribution is better in EN8 carbon steel.

2.7 Buckling of thin cylindrical shells subject to axial loads

Clarifications of Donnell's eight order differential equation provides the innumerable buckling approaches of a thin cylinder underneath compression. But this analysis, which is in harmony with the slight refraction theory

bounces much sophisticated morals than shown from tryouts [13]. So it is habitual to find the precarious buckling load for countless erections which are cylindrical in silhouette from pre-existing design cambers where perilous buckling load FCR is intrigued along side the ratio R/t, where R is the radius and t is the thickness of the cylinder for innumerable values of L/R, where L is the length of the cylinder. If cut-outs are modern in the cylinder, life-threatening buckling loads as well as pre-buckling slants will be exaggerated [14–15].
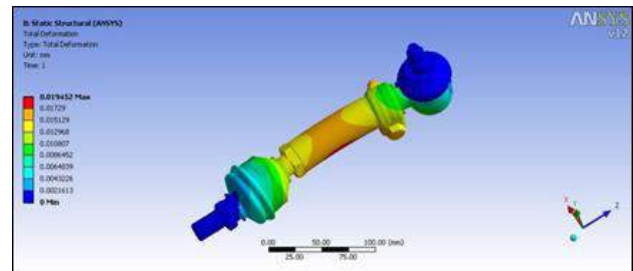
Figure 17 – Buckling load test on adjustable connecting tie rod

Examination of this formula reveals the following interesting facts with regard to the load-bearing ability of slender columns.

Bending load in both ends hinged is given by the following Euler's formula:

$$BL = \frac{\pi^2 EI}{L^2}, \tag{1}$$

where E – Young's modulus; L – length of the tie rod; I – moment of inertia:

$$I = \frac{\pi \left(D^4 - d^4 \right)}{64}. \tag{2}$$

E. g., for inner diameter d = 22.5 mm and outer diameter D = 30 mm, moment of inertia I = 2.72·10^4 mm^4.

Figure 18 shows that bending load calculation for proposed design, it is enough for the rod to withstand compressive and tensile load. When compared to previous design clamped design having more bending loads capacity. Previous design bending load is 25.9 kN. This design bending load is 31.6 kN. So, this design is good when compared to existing design.
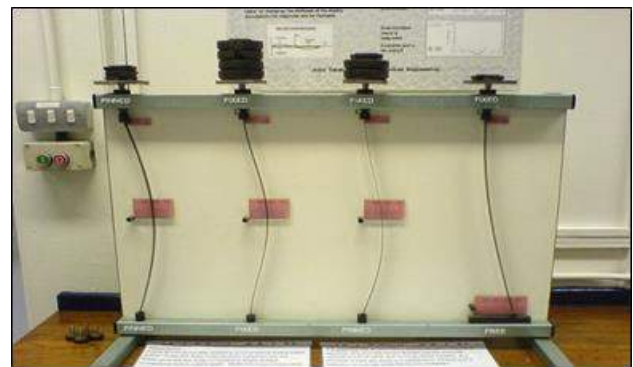
Figure 18 – Failure of struts or columns

3 Results and Discussion

Tie rod plays an important role in the steering system and should be carefully selected. EN8 Carbon Steel material selected for this design. Existing and proposed model has done in solid works software in the form of a multibody system, after that solid structure was produced where all interconnected essentials supposed to be perfectly inflexible, and in absolute stage of taxing finite element analysis was executed consuming ANSYS software package. From the accessible results we can arrange that the dissemination of deformation and stress do not overdo the yield strength value and that there are neither indemnities nor failure of Tie rod. The load 2 000 kg has applied in exiting model, it's can't shows any deformation. While increasing the load up to 2 500 kg, thruhole design getting bend because it cannot withstand the over load, so that thru hole design model has applicable only below 2 000 kg load. The maximum load of 4 000 kgf has acting on thru hole and groove design model.since, the thru hole design results shows stress has act 583.3 N/mm^2, Factor of safety is 0.48, and Groove design model results show that stress has act 243.2 N/mm^2 and Factor of safety is 1.15. Thru-hole design bending load is 25.9 kN and clamp design bending load is 31.6 kN.

4 Conclusions

In this study, existing thru-hole design model has modified toclamp groove design with EN8 carbon steel material. From the static analysis results shows deformation of the proposed tie rod model is lower than existing tie rod, the critical buckling load of proposed tie rod is more than existing tie rod in buckling analysis. From the presented results we can conclude that deformation and stress do not exceed the yield strength value that there are neither damages nor failure to new proposed groove design tie rod. So the proposed tie rod is suitable for tractor.

References

1. M. Senniappan, R. More, S. Bhide and S. Gowda, S. (2016). Optimization of Commercial Vehicle's Steering Tie Rod Arm Design Based on Strain Life Approach. SAE Technical Paper, 2016-01-0381.DOI: 10.4271/2016-01-0381.
2. L. Natrayan and M. Senthil Kumar. (2018). Study on Squeeze Casting of Aluminum Matrix Composites-A Review. Advanced Manufacturing and Materials Science. Springer, Cham, 2018. 75-83. DOI: 10.1007/978-3-319-76276-0_8.
3. U. Kulkarni, M. Gowda and H. Venna. (2016). Effect of Tie Rod Length Variation on Bump Steer. SAE Technical Paper, 2016-28-0201.DOI :10.4271/2016-28-0201.
4. Wei Duan and Suraj Joshi. (2011). Failure analysis of threaded connections in large-scale steel tie rods. Engineering failure analysis, 18(8); 2008-2018.DOI: 10.1016/j.engfailanal.2011.06.002
5. L.Natrayan et al.(2018). Optimization of squeeze cast process parameters on mechanical properties of Al$_2$O$_3$/SiC reinforced hybrid metal matrix composites using taguchi technique. Mater. Res. Express; 5: 066516. DOI: 10.1088/2053-1591/aac873
6. Darwish Mohamed, Ahmed YehiaElsayed and KhaledNassar. (2018). Design and constructability of a novel funicular arched steel truss false work. Journal of construction engineering and management, 144.3: 04018002. DOI: 10.1061/(ASCE)CO.1943-7862.0001449.
7. Young-Chul Park, Seung-KulBaek, Bu-KyoSeo, Jong-Kyu Kim, and Kwon-Hee Lee. (2014). Lightweight design of an outer tie rod for an electrical vehicle, journal of applied mathematics, vol. 2014, Article ID 942645, 6 pages. DOI:10.1155/2014/942645.
8. Betül Sultan Yıldız and Ali RızaYıldız. (2018). Comparison of grey wolf, whale, water cycle, ant lion and sine-cosine algorithms for the optimization of a vehicle engine connecting rod. Materials Testing: 60(3); 311-315. DOI:10.3139/120.111153.
9. J. K. Kim, Y. J.Kim,W.H. Yang, Y. C. Park, and K.-H. Lee. (2011). Structural design of an outer tie rod for a passenger car, International Journal of Automotive Technology, 12(3); 375−381.DOI: 10.1007/s12239−011−0044−6.
10. M. Senthil kumar, Ajithgopinath and Natrayan.L (2017). Evaluation of mechanical properties of E-Glass and Coconut fiber reinforced with polyester and Epoxy resin matrices, Inter J Mech Prod Engi Res Develop, 7(5), pp.13-20.
11. Natrayan L et al. (2017). An experimental investigation on mechanical behaviour of SiCp reinforced Al 6061 MMC using squeeze casting process. Inter J Mech Prod Engi Res Develop., 7(6):663–668.
12. C.E. Megharaj, P.M. Nagaraj and K.J. Pasha. (2016). Design and analysis of a forging die for manufacturing of multiple connecting rods. In IOP Conference Series: Materials Science and Engineering, 149(1), pp 012145.
13. T. Zhao, W. Ding,L.Wei, W.Wu, Y.Qiao. (2018).Thebehavior analysis of a cofferdam constructed by double sheet pile wall above muck. In: Zhang D., Huang X. (eds) Proceedings of GeoShanghai 2018 International Conference: Tunnelling and Underground Construction. GSIC 2018. Springer. DOI: 10.1007/978-981-13-0017-2_3.
14. M. S. Santhosh, R. Sasikumar, L. Natrayan, M. Senthil Kumar, V. Elango and M. Vanmathi. (2018). Investigation of mechanical and electrical properties of kevlar/E-glass and basalt/E-glass reinforced hybrid Composites. . Inter J Mech Prod Engi Res Develop., 8(3): 591-598.

Конструкція та аналіз вузлів з'єднувальних тяг для застосування в автомобілебудуванні

Аравіндараж Е.[1], Натраян Л.[2], Сантош М. С.[3], Кумар М. С.[2]

[1] Інженерний коледж Шрі Манакула Вінаягар, Маннадіпет, 605 107, м. Пудічеррі, Індія;
[2] Університет VIT, 600 127, м. Ченнай, Індія;
[3] Технологічний коледж Селвам, Салем шлях, 637 003, м. Намаккал, Індія

Анотація. Кінцева тяга є однією з найпростіших частин рульового механізму, що має безпосереднє і найважливіше значення з точки зору безпеки руху. Кінцевий штифт використовується для того, щоб колеса були вирівняні. Це забезпечує регулювання, щоб колесо вирівнялось, і воно не знімається як на внутрішніх, так і на зовнішніх краях. Отже, функціонування гальмівного важеля має вирішальне значення для керування, а також для підвіски автомобіля. Сьогоднішній світ є конкурентоспроможним. Ринок вимагає передових технологій за більш низькою ціною. Це відображається у виборі дешевших технологій. Отже, кожна галузь визначається для рентабельного продукту за більш низькою ціною і в межах мінімального періоду часу на момент продажу. Це створює великий тиск на інженерів, які постійно прагнуть розробляти більш ефективні продукти за більш низькою ціною. Робота зосереджена на функціонуванні стяжок. Узагалі існують з'єднання із перевантаженням. Ця стаття зосереджена на модифікацію традиційної конструкції тяги. Наведено аналіз причин завантаження існуючої та модифікованої конструкцій за допомогою програмного забезпечення ANSYS. Цей підхід ґрунтується на дослідженні навантажень і деформацій кожного компонента для високих експлуатаційних умов навантаження.

Ключові слова: монтажний отвір, затискний пристрій, передня вісь, ANSYS, деформація.

Application of Rough TOPSIS Technique for the Analysis of Engineering System Failure Causes

Emovon I.[*], Nwaoha T. C.

Federal University of Petroleum Resources, P.M.B. 1221, Effurun, Delta State, Nigeria

[*]**Corresponding Author's Address:**
emovon.ikuobase@fupre.edu.ng

Abstract. The prioritization of the causes of engineering system failure posed to be a challenge. Therefore, there is a need to develop a tool that will be used to identify critical problems of an engineering system to facilitate decision making in allocation of available resources in ensuring optimal system performance. In this paper, a rough technique for order preference by similarity to the ideal solution (Rough-TOPSIS) is proposed, which combines rough set theory and TOPSIS for the prioritization exercise in uncertain engineering environment. The technique is exemplified with a numerical example and advanced using information from experts. From the result of the analysis, factors/causes hampering the optimal performance of the engineering system have been revealed in order of importance. The proposed approach have comparative advantages over other hybrid methods as it can easily be implemented with hand calculation/spreadsheet, without requiring additional tools to evaluate decision criteria weights and aggregate experts opinions.

Keywords: rough set theory, Rough TOPSIS, engineering system, failure causes, decision criteria.

1 Introduction

Many developing countries are characterized with ineffective water transportation system, poor telecommunication system, poor health care delivery system, ineffective rail way system and ineffective power generation system. These have hampered their economic and social growth. The engineering systems failures have been attributed to ineffective maintenance, misappropriation of fund among other reasons. The level of impact of the different failure causes on engineering system varies. The analysis of the various failure causes in the order of importance is therefore imperative.

However, in the literature, most of the authors have been mainly worried with the bane of power generation with specific reference to Nigeria. Ohajianya et al. [1] in their studies, identified factors such as inept manpower and deficient power reform as the causes of epileptic electricity supply in Nigeria. Olaoye et al. [2] in a similar research work, examined the bases of power crisis in Nigeria and recommended the use of renewable energy as means of reducing and / or eliminating the crisis. Sambo et al. [3] identified elements such as deficiency of fund and low involvement of private sector, as the reason for

energy predicament in their paper. The above papers only identified the causes of engineering system failure, without prioritizing them in order of importance.

Only limited papers are found in existing literature with respect to prioritization of the causes of engineering system failure but specifically for power generation system problems. Emovon and Nwaoha [4] utilised an integrated AHP and MOORA method for ordering the problems of power generation in Nigeria. Emovon and Samuel [5] applied a combination of entropy and Multi-Attribute utility Theory (MAUT) methods in the ranking of alternative solutions to power generation problems.

Nevertheless, the methods utilized by the above authors have shortcomings, which are addressed in the approach suggested in this paper, for the prioritization of engineering system failure causes. The method proposed is the Rough TOPSIS technique, which is an integration of the Rough Set Theory and the TOPSIS method. Furthermore, the analysis in this paper is not limited to power generation system but addresses majority of engineering system.

The causes of engineering system failure in most developing countries are numerous and the resultant effects are poor sea transport delivery, low power generation,

Journal of Engineering Sciences, Volume 5, Issue 2 (2018), pp. E 1–E 6

E 1

poor telecommunication and poor health care service delivery. Some common causes of the system failure are ineffective maintenance, misappropriation of fund, insufficient fund, insufficient skilled manpower and wrong industrial setting location and are described as follows:

1. Ineffective maintenance (AT1): the engineering system is poorly safeguarded and in most scenarios, the system is allowed to fail before being fixed. This approach has resulted to collapse of engineering system.

2. Misappropriation of fund (AT2): the meagre fund available for engineering system maintenance and expansion are misappropriated by bodies entrusted with the management of the systems.

3. Insufficient funding (AT3): the fund available for sustainability of the engineering system in most cases is grossly insufficient.

4. Insufficient skilled manpower (AT4): the skilled manpower needed for effective operation and maintenance of engineering system are lacking or inadequate.

5. Wrong location (AT5): the engineering systems are in most scenarios sited in wrong location, and this is generally due to nepotism and ethnicity. The locations are normally far away from energy sources and skilled manpower which do result to industries incurring extra cost in terms of moving materials and human resources to system sites.

The above factors were carefully selected from the nine factors, Emovon and Nwaoha [4] identified as the problems of power generation in Nigeria. The five factors were selected and modified because they affect all engineering system.

The different engineering system failure causes are ranked in this paper with reference to some decision criteria. The decision criteria are listed and described as follows:

1. Damages (DC1): the failure of engineering system can damage firm image, cause personnel death or injuries and product or services delay. The different failure causes have vary degree of damaging effect and the one with the greatest effect is generally the most critical.

2. Environmental degradation (DC2): the failure of engineering system can produce reversible and irreversible damages to the environment. The engineering system failure cause with greater negative effect on the environment is considered most critical.

3. Engineering system efficiency (DC3): the failure cause that will impact more negatively on the system service delivery is considered as most critical failure cause. The decision criteria are the modified version of Emovon and Nwaoha [4] to make them applicable to all engineering system rather than limiting it to power generation.

2 Research Methodology

2.1 Rough set theory

The approach commonly applied in overcoming vagueness of human mind which generally have negative impact on group decision making is the Rough Set Theory (RST) [6]. The approach was introduced by Pawlak [7]. RST resolve the challenges of uncertainty in group decision making, by applying lower and upper approximation [8].

Supposing U is the universe, comprising all elements and Y a random elements of U. R is defined as a set of classes organized as $D_1 < D_2 \ldots < D_n$ [6]. The lower approximation, $\underline{APM}(D_i)$ upper approximation, $\overline{APM}(D_i)$ and boundary region, are thereforeexpressed as [9]:

$$\underline{APM(D_i)} = U\left\{Y \in \frac{U}{R(Y)} \leq D_i\right\} \tag{1}$$

$$\overline{APM(D_i)} = U\left\{Y \in \frac{U}{R(Y)} \geq D_i\right\} \tag{2}$$

$$BD(D_i) = U\left\{Y \in \frac{U}{R(Y)} \neq D_i\right\} =$$
$$= \left\{Y \in \frac{U}{R(Y)} > D_i\right\} \cup \left\{Y \in \frac{U}{R(Y)} < D_i\right\} \tag{3}$$

D_i can be denoted in the form of Rough number, $RN(D_i)$, with the lower limit and upper limit expressed as equations 4 and 5 respectively [10]

$$\underline{Lim(D_i)} = \frac{1}{P_L}\sum \frac{R(Y)}{(Y)} \in \underline{APM(D_i)} \tag{4}$$

$$\overline{Lim(D_i)} = \frac{1}{P_U}\sum \frac{R(Y)}{(Y)} \in \overline{APM(D_i)} \tag{5}$$

The difference between the upper limit and the lower limit of $RN(D_i)$, is $BD(D_i)$ expressed as

$$BD(D_i) = \left[\overline{Lim}(D_i) - \underline{Lim}(D_i)\right] \tag{6}$$

where P_L and P_U denote number of elements in $\underline{APM}(D_i)$ and $\overline{APM}(D_i)$ respectively.

The interval arithmetic operation such as addition and division is also applicable to rough numbers, the operation can be found in the work of [10].

2.2 Rough TOPSIS

The Rough TOPSIS is a hybrid approach for analyzing group decision problem which combines Rough Set Theory with TOPSIS method. The RST is applied in operating vague data from experts involves in the group decision making process. The analyzed data then serve as input information into the TOPSIS method for final ranking of alternatives.

The analysis steps in the Rough TOPSIS are expressed as follows [9]:

Step 1. Decision matrix X, formation, having m number of alternatives AT_i ($i =1, 2, \ldots, m$) and n number of decision criteria, DC_i ($j = 1, 2,\ldots , n$). Z representing number of experts that partakes in the prioritization process. The decision matrix produced is indicated as:

$$X = \begin{bmatrix} x_{11}^r & x_{12}^r & x_{13}^r & \cdots & x_{1n}^r \\ x_{21}^r & x_{22}^r & x_{23}^r & \cdots & x_{2n}^r \\ x_{31}^r & x_{32}^r & x_{33}^r & \cdots & x_{3n}^r \\ \vdots & \vdots & \vdots & \ddots & \vdots \\ x_{m1}^r & x_{m2}^r & x_{m3}^r & \cdots & x_{mn}^r \end{bmatrix} \tag{7}$$

where $r = 1, 2, \ldots, z$, and x_{ij}^r ($i = 1, 2, \ldots, m$) denote rating of r-th expert for i-th alternative with respect to criterion j.

Step 2. The decision matrix is transformed into rough decision matrix S using the equations (1) – (6), and the details of the transformation process can be found in the work of [10]:

$$S = \begin{bmatrix} [x_{11}^L, x_{11}^U] & [x_{12}^L, x_{12}^U] & \cdots & [x_{1m}^L, x_{1m}^U] \\ [x_{21}^L, x_{21}^U] & [x_{22}^L, x_{22}^U] & \cdots & [x_{2m}^L, x_{2m}^U] \\ \vdots & \vdots & \ddots & \vdots \\ [x_{n1}^L, x_{n1}^U] & [x_{n2}^L, x_{n2}^U] & \cdots & [x_{nm}^L, x_{nm}^U] \end{bmatrix} \tag{8}$$

where x_{ij}^L and x_{ij}^U indicate lower and upper limits of rough number

Step 3. Evaluation of standardized decision matrix with regard to rough number as follows:

$$Nx_{ij}^L = \frac{x_{ij}^L}{\left(\max_i \left[x_{ij}^L; x_{ij}^U \right]\right)} \tag{9}$$

$$Nx_{ij}^L = \frac{x_{ij}^L}{\left(\max_i \left[x_{ij}^L; x_{ij}^U \right]\right)} \tag{10}$$

where Nx_{ij}^L and Nx_{ij}^U denote the upper and lower limits of the standardized rough matrix.

Step 4. Determination of the weighted standardized rough matrix expressed as:

$$Y_{ij}^L = W_{ij}^L . Nx_{ij}^L \tag{11}$$

$$Y_{ij}^U = W_{ij}^U . Nx_{ij}^U \tag{12}$$

The rough weights of decision criteria; W_{ij}^L and W_{ij}^U analytical steps based on the equations (1) – (6) can be found in [9].

Step 5. Definition of positive ideal solution (PS) and negative ideal solution (NS) as follows:

$$V_j^+ = \max_i \left(Y_{ij}^U\right), If\ J \in B; \min_i \left(Y_{ij}^L\right) If\ J \in C \tag{13}$$

$$V_j^- = \min_i \left(Y_{ij}^L\right), If\ J \in B ; \max_i \left(Y_{ij}^U\right), \tag{14}$$

where V_j^+ and V_j^- denote the values of PS and NS respectively while B and C represent the beneficial criterion and non-beneficial criterion respectively.

Step 6. The evaluation of each alternative separation from the PS and NS respectively as follows:

$$Z_j^+ = \left\{ \sum_{J \in B} \left(Y_{ij}^L - V_j^+\right)^2 + \sum_{J \in C} \left(Y_{ij}^U - V_j^-\right)^2 \right\}^{\frac{1}{2}} \tag{15}$$

$$Z_j^- = \left\{ \sum_{J \in B} \left(Y_{ij}^L - V_j^+\right)^2 + \sum_{J \in C} \left(Y_{ij}^U - V_j^-\right)^2 \right\}^{\frac{1}{2}} \tag{16}$$

where Z_j^+ and Z_j^- represent the separation of each alternative from PS and NS respectively

Step 7. The rough TOPSIS performance value of each alternative, ZA_i, is evaluated as follows:

$$ZA_i = \frac{Z_i^-}{(Z_i^- + Z_i^+)} \tag{17}$$

3 Results and Discussion

3.1 Numerical Example

The proposed Rough TOPSIS suitability in analyzing different causes of engineering systems failure is illustrated with a numerical example. In the numerical example, twoexperts assigned score to each causes of engineering system failurebased on 3 decision criteria whilst utilizing 5-point likert scale. The assigned rating which form the decision problem is shown in Table 1.The two experts also assigned rating to the three decision criteria; DC1, DC2 and DC3 in the order of importance based on 5 point likert scale, as shown in Table 2.

Table 1 – Experts assigned rating to alternatives

S/N	Expert 1			Expert 2		
	DC1	DC2	DC3	DC1	DC2	DC3
AT1	5	4	5	4	3	5
AT2	4	3	3	3	4	3
AT3	4	3	2	2	3	2
AT4	3	4	2	3	3	4
AT5	2	2	1	1	4	1

Table 2 – Ratings for decision criteria importance

Expert	DC1	DC2	DC3
1	4	2	5
2	4	2	3

3.2 Rough TOPSIS Analysis

In the Rough TOPSIS, the rough weights of the decision criteria are needed as part of the analysis process. On this basis, decision criteria are evaluated using the equations (1) – (6) and the detailed procedure on the analysiscan be found in the work of [9], and results produced are indicated in Table 3.

Table 3 – Decision criteria rough weights

S/N	Rough weights	Normalized rough weights
DC1	[4, 4]	[0.889, 0.889]
DC2	[2, 2]	[0.444, 0.444]
DC3	[3.5, 4.5]	[0.778, 1.000]

The above process is proceeded with Rough TOPSIS analysis which begins with the formation of the group rough decision matrix. To form the matrix, the individual expert ratings in Table 1 is aggregated using the equations (1) – (6) with the detailed procedure in the reference [10]. The group rough matrix developed from the analysis is indicated in Table 4.

The assigned rating for alternative, AT2 against decision criteria, DC1 (AT2 / DC1) [3–4] is applied to demonstrate the analysis:

$$\underline{Lim}(4) = \frac{3+4}{2} = 3.5$$

$$\underline{Lim}(3) = 3$$

$$\overline{Lim}(4) = 4$$

$$\overline{Lim}(3) = \frac{3+4}{2} = 3.5$$

The lower limits and upper limits values are now averaged to form rough number $RN\left(\dfrac{AT2}{DC2}\right)$ as follows:

$$\left(\frac{AT2}{DC2}\right)^{L} = \frac{3.5+3}{2} = 3.25$$

$$\left(\frac{AT2}{DC2}\right)^{U} = \frac{4+3.5}{2} = 3.75$$

$$RN\left(\frac{AT2}{DC2}\right) = [3.25, 3.75]$$

Table 4 – Group rough decision matrix

S/N	DC1		DC2		DC3	
AT1	4.25	4.75	3.25	3.75	5.0	5.0
AT2	3.25	3.75	3.25	3.75	3.0	3.0
AT3	2.50	3.50	3.00	3.00	2.0	2.0
AT4	3.00	3.00	3.25	3.75	2.5	3.5
AT5	1.25	1.75	2.50	3.50	1.0	1.0

After the formation of the group rough decision matrix, the next step is the development of the normalized form of it using the equations (9) – (10), and the generated result is shown in Table 5. The is followed with the formation of the weighted normalized matrix in Table 6, applying the equations (11) – (12) on data in Tables 3, 5. The values of PS and NS is then evaluated, applying the equations (13) – (14) on data in Table 6, and the results obtained are shown in Table 7. Applying the equations (15) – (17) Z^+, Z^- and rough TOPSIS performance index, ZA, are evaluated respectively and the results produced

are shown in Table 8. The engineering system failure causes; AT1, AT2, AT3, AT4 and AT5 are ranked based on their respective rough performance scores. The rank orders of the alternatives are shown in Table 8 and Figure 1.

Table 5 – Normalized rough decision matrix

S/N	DC1		DC2		DC3	
AT1	0.895	1.000	0.867	1.000	1.000	1.000
AT2	0.684	0.789	0.867	1.000	0.600	0.600
AT3	0.526	0.737	0.800	0.800	0.400	0.400
AT4	0.632	0.632	0.867	1.000	0.500	0.700
AT5	0.263	0.368	0.667	0.933	0.200	0.200

Table 6 – Weighted normalized rough decision matrix

S/N	DC1		DC2		DC3	
AT1	0.796	0.889	0.385	0.444	0.778	1.000
AT2	0.608	0.701	0.385	0.444	0.467	0.600
AT3	0.468	0.655	0.355	0.355	0.311	0.400
AT4	0.562	0.562	0.385	0.444	0.389	0.700
AT5	0.234	0.327	0.296	0.414	0.156	0.200

Table 7 – Values of PS and NS

Parameter	DC1	DC2	DC3
PS	0.889	0.444	1.000
NS	0.234	0.296	0.156

Table 8 – Rough TOPSIS performance score (*ZA*) and rank

S/N	Engineering system failure causes	Z^+	Z^-	ZA	Rank
AT1	Ineffective maintenance	0.248	1.079	0.813	1
AT2	Misappropriation of fund	0.606	0.661	0.522	2
AT3	Insufficient fund	0.812	0.490	0.376	4
AT4	Insufficient skilled manpower	0.696	0.652	0.484	3
AT5	Wrong location	1.079	0.157	0.127	5

From Table 8 and Figure 1, the most critical cause of engineering system failure in most developing countries is ineffective maintenance; AT1 having the highest value of rough TOPSIS performance score of 0.813. The least cause of the systems failure is wrong location AT5 having the least rough TOPSIS performance score and ranked fifth position among the five alternative causes of failure.

For developing countries to improve on telecommunication, health care delivery, water transportation, power generation among others, there is the need for them to put in place, an effective maintenance scheme that will guarantee safe and reliable operation of the machinery of an engineering system.
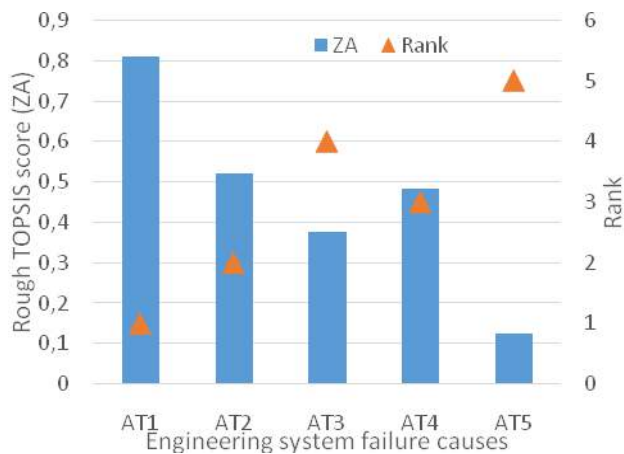
Figure 1 – Rough TOPSIS performance score (Z*A*) and rank

3.3 Rough TOPSIS comparison with other existing MCDM tools in literature

Although, other multi-criteria decision making (MCDM) tools such as, PROMETHEE, AHP, ELECTRE and DEMATEL when applied as stand alone or in conjunction with other techniques can produce similar result with that of Rough TOPSIS. However, the choice of tools generally depends on the analysts' which is normally guided by appropriateness and computational effort required [11]. In the light of this, a similar technique applied by Emovon [12] in comparing different MCDM tools is utilized in this paper to compare Rough TOPSIS with other hybrid MCDM tools.

Hand calculation / spreadsheet: tick – easy to calculate using hand calculation / spreadsheet, and cross – difficult to calculate using hand calculation / spreadsheet.

Software code: tick – easy to code and cross – difficult to code.

Additional tool: Tick- no additional tool required to implement & Cross- additional tool is required for implementation.

From Table 9, it is clearly shown that the Rough TOPSIS can be more easily analyzed and implemented than other hybrid methods due to the fact that the methodology process can be solved with either hand calculation or spreadsheet with less effort. Furthermore, from the Table, no additional tool is required, in the implementation of the tool and this is as a result of the Rough Set Theory capability of evaluating decision criteria weights and at the same time managing the uncertainty of different experts' opinions.

Table 9 – Level of computational effort required of MCDM tools

Program / Approach	Rough TOPSIS	FUZZY-AHP	FUZZY-DEMATEL	AHP-DEMATEL	AHP-ELECTRE	AHP-PROMETHEE
Hand calculation	✓	×	×	×	×	×
Spreadsheet	✓	✓	×	×	×	×
Easy to code	✓	×	×	×	×	×
Additional tool	✓	✓	✓	×	×	×

4 Conclusion

This paper presented a technique for analyzing engineering system failure causes. The technique utilized Rough TOPSIS which integrate Rough Set Theory and TOPSIS method for evaluating causes of engineering system failure causes. The result of the analysis indicate that ineffective maintenance is the most critical cause of engineering system failure in most developing countries.

The Rough TOPSIS approach used in the analysis is simpler in terms of implementation when comparedto other hybrid techniques, as the approach is easier to code and implement with the use of hand calculation/spreadsheet. Furthermore, the approach does not require the use of additional tools for it implementation as opposed to most other approaches which require additional tool for decision criteria weights analysis and experts information aggregation.

References

1. Ohajianya, A. C., Abumere, O. E., Owate, I. O., & Osarolube, E. (2014). Erratic Power Supply in Nigeria: Causes and Solutions. *International Journal of Engineering Science Invention*, Vol. 3, No. 7, pp. 51–55.
2. Olaoye, T., Ajilore, T., Akinluwade, K., Omole, F., & Adetunji, A. (2016). Energy crisis in Nigeria: Need for renewable energy mix. *American Journal of Electrical and Electronic Engineering*, Vol. 4, No. 1, pp. 1–8.
3. Sambo, A. S., Garba, B., Zarma, I. H., & Gaji, M. M. (2012). Electricity generation and the present challenges in the Nigerian power sector. *Journal of Energy and Power Engineering*, Vol. 6, No. 7, pp. 1050.
4. Emovon, I., & Nwaoha, T. (2018). Power generation problems ranking using a combination of AHP AND MOORA techniques. *Research in Logistics and Production*, Vol. 8, No. 2, pp. 155–168.
5. Emovon, I., & Samuel, O. D. (2017). Prioritising alternative solutions to power generation problems using MCDM techniques: Nigeria as case study. *International Journal of Integrated Engineering*, Vol. 9, No. 3, pp. 11–17.

6. Stević, Ž., Tanackov, I., Vasiljević, M., & Rikalović, A. (2017). Supplier evaluation criteria: AHP rough approach. *27th International Scientific Conference on Industrial Systems*, pp. 298–303.
7. Pawlak, Z. (1982). Rough sets. *International Journal of Computer and Information Sciences*, Vol. 11, No. 5, pp. 341–356.
8. Abu-Donia, H. M. (2012). Multi knowledge based rough approximations and applications. *Knowledge-Based Systems*, Vol. 26, pp. 20–29.
9. Song, W., Ming, X., Wu, Z., & Zhu, B. (2014). A rough TOPSIS approach for failure mode and effects analysis in uncertain environments. *Quality and Reliability Engineering International*, Vol. 30, No. 4, pp. 473–486.
10. Zhai, L. Y., Khoo, L. P., & Zhong, Z. W. (2009). A rough set based QFD approach to the management of imprecise design information in product development. *Advanced Engineering Informatics*, Vol. 23, No. 2, pp. 222–228.
11. Löken, E. (2007). Use of multicriteria decision analysis methods for energy planning problems. *Renewable and Sustainable Energy Reviews*, Vol. 11, No. 7, pp. 1584–1595.
12. Emovon, I. (2016). *Multi-criteria decision making support tools for maintenance of marine machinery systems*. PhD thesis, School of Marine Science and Technology, Newcastle University, UK.

Застосування засобів Rough TOPSIS для аналізу причин відмов інженерних систем

Емовон І., Нваоа Т.

Федеральний універсетет нафтових ресурсів, P.M.B. 1221, м. Еффурун, Нігерія

Анотація. У роботі розглянута проблема визначення пріоритетів причин відмов інженерних систем. Відповідно, є потреба у розвитку інструмента для ідентифікації критичних проблем в інженерних системах для полегшення прийняття рішень при розподілі наявних ресурсів у забезпеченні оптимальної продуктивності системи. У роботі запропонована теорія грубих множин шляхом застосування засобів Rough-TOPSIS для упорядкування за подібністю до досягнення ідеального рішення. Такий підхід дозволяє поєднати теорію грубих множин і TOPSIS для визначення пріоритетів у заданому інженерному середовищі. Наведені числовий приклад використання запропонованого методу та вдосконалена методика використання інформації від експертів. Як результаті дослідження, були виявлені фактори (причини), що перешкоджають оптимальному функціонуванню інженерної системи, у порядку їх значущості. Запропонований підхід має відносні переваги над іншими гібридними методами, що легко можна здійснити за допомогою ручного розрахунку або електронної таблиці, не вимагаючи додаткових інструментів для оцінювання критеріїв прийняття рішень та сукупних думок експертів.

Ключові слова: теорія грубих множин, Rough TOPSIS, інженерна система, причини відмови, критерії прийняття рішення.

Development of the Computer Graphics Management System Using Text of Natural Language

Al Salaimeh S.

Aqaba University of Technology, 79 Wasfi al-Tal St., Aqaba, Jordan

Abstract. The computer has been an integral part of our life. We cannot imagine complicated mathematical and technological calculation without using computer, but we are at this stage in the development of computing systems, when is not enough computer obedience. We needed an assistant. In this paper, we can see the predicate presentation of the text of the natural language personal computer is able to understand person and obey his command. As for the scope of this method of representing natural language text, it is seen the first time that is the use spectrum is very large; firstly, it can be used for research and educational purposes, as well as to study algebra of predicates. Secondly, use as an assistant in the word a user with a computer (is a good addition to the programs engaged in speech recognition). Thirdly, in the regions associated with artificial intelligence.

Keywords: predicate, natural language, mathematical calculation, human speech, artificial intelligent.

1 Introduction

Since of this century, the human way of life has undergone serious changes. The computer has been an integral part of our life. We cannot imagine complicated mathematical and technological calculation without using computer, but we are at this stage in the development of computing systems, when is not enough computer obedience. We needed an assistant.

So that computer can carry out nonstandard tasks, it is necessary to teach to thing and communicate with person, in other words. Technical systems, mechanized mental work, got the name of artificial intelligence systems [1–4].

2 Research Methodology

One of the tasks of the artificial intelligence is developing systematic methods for translating the meaning of human speech into the language of predicate algebra. Make sense in the form of concepts into computer. But, how it can be done? What is the meaning of the utterance? It is not difficult to answer it. As is known, the meaning of utterance is a function of the dependence of variables of this statement. It

remains only to find the text of the natural language object variable. We will consider finding object variable in the text of natural language in comparison with the detection of these variable in mathematical statements.

Consider an example, mathematical statement $(x + y = z)$, where x, y, z – object variables by which and in this case is variables definition on set $N = \{0, 1, 2, …\}$ all nonnegative integers, in this form the mathematical statement is not true, not false. But if you imagine this expression as a function $\xi = f(x, y, z)$, where f – function that returns true or false mathematical expression turns into a true function, since the function ξ indicates the truth of the mathematical expression. So, the meaning of a mathematical statement is a predicate $\xi = f(x_1, x_2, …, x_n)$ representing the dependence of the true of a variable ξ on n subject variables $x_1, x_2, …, x_n$ of this utterance.

We have consider, what is the meaning of the mathematical statement. Now, guided by hypothesis of a close relationship of natural and mathematical language, suppose, that such an interpretation of the meaning apply and to assumption of natural language [3].

The text of the natural language consists of word and the interrelations between them. We will leave the

relationship for now, get special attention to words. Single words, from which a proposal is drawn up, we will consider as the basic elements of linguistics algebra. What do individual words mean? Suppose, that the express some predicate.

It is not difficult to see, what it is really. Let us take a word, for example: the word cube. Enter object variable x. turn to a person and we use it as a test subject, it is easy to see what is carrier of predicate. Expressed in word cube, really showing the subject a variety of subjects x from any set A asking him, is it the subject x cube? If x is a cube, then theanswer is truth, otherwise false.

By it is behaviour, the subject is implemented by some predicate, dependent on x and defined on the set A. we write down it is types cube(x). it plays the role of the elementary formula of linguistics algebra. The word cube serves as predicate name, reproducible subjects. So, the introduced elementary predicates can be formed by means of Boolean operations; "–", "^", "ˇ" more difficult predicates: cub _ or ellipse (x) = cub (x) ˇ ellipse (x); _cub (x) = No _ cub (x); cub (x) ^ ellipse (y) = cub _ and _ ellipse (x, y). In the latter case, it is no longer one subject x, cube, a second one is ellipse, we see, that language uses negations as basic, disjunction and conjunctive, linguistic algebra refers to class of Boolean algebra [5–9].

Formalization of the text is subject to situational suggestions. For example: (in cube there is an ellipse). The relationship between objects cube and the ellipse is described _stand _ on (x, y), it can be subjected to dismemberment. We introduce predicate stand _ (y), understandable in the sense of an (object y stand) a predicate on (y, x), corresponding to utterance (subject y situated on subject x), it is clear that the predicate stand _ on $(y, x)$and stand y ^ on (y, x) match. It allows further splitting and predicate stand (y). It can be represented as a conjunction predicates present _ time (y) and stand (y). The first predicate means: "subject y it is observed at the current time" second one: "subject y presence is a state of standing" (irrespective of time).

Combining the conjunction of introduced predicates, we write the sentence in question in the following form. Cube(x) ^ ellipse (y) present _ time (y) stand (y) ^ on (y, x), we will not move further in the analysis of the semantic structure of this statement. To do this, it will be necessary to penetrate onto the semantic structure of words "cube" "and" "ellipse" "," "present""time" "stand" "and" "on". For this you can refer to the explanatory dictionary, express the meaning of each of these word using the given in its different, the roles of which are phrases, made up of other words. When will this process end, you need to collect words, remaining not expression, and tie them to each other of utterances system bearers of the natural language as true. The utterances system performs the role of analysis in the system of axiom. Defining the primary concepts of mathematics. In the language it abstractly defines the meaning of the word, which cannot express using direct definition through other words. Above we demonstrate the subdivision of the verb, but the same division is allowed and nouns (object).

For example, the word cubes. These items consist of faces, which in turn consist of a set of points, united in the face. It means that if we denote all faces of the cube as:
face _ 1(x), face _ 2 (x), …, face _ 6 (x), then cube (x) = face _ 1 (x) ^ face _ 2 (x) ^ … ^ face _ 6(x), and each side can be represented in the following form:
face _ 1 (x) = point _ 1 _ 1 (x) ^ point _ 1 _ 2 (x) ^ … … ^ point _ 1 _ n (x), face _ 2 (x) = point _ 2 _ 1 (x) ^ point _ 2 _ 2 (x) ^ … ^ point _ 2 _ n (x), … …, face _ 6 (x) = point _ 6 (x) ^ point _ 6 _ 2 (x) ^ … … ^ point _ 6 _ n (x).

3 Results

It can be shown, that almost all elements of the text of natural language can be divided into more primitive predicate, it means, that having identified all elementary predicates of the text there is natural language. We can express any situation with a semantic expression. Up to this point, we have considered the text there is a written natural language in terms of view of understanding the computer.

But for interaction IBM and human need computer management. For this purpose predicates of action, which unlike ordinary predicates, performs some kind of action and return of truth, if the specified action was successful, and false if not? Example: predicate highlight (x). This predicate object, highlight (cube (x)), then the predicate of the action is checked for truth.

Predicate cub (x) and if the subject cube exists, so the predicate highlight this subject. As you see, the predicate of action being given another predicate, which take on the function of checking for the presence of the environment of the object, of course, the possibility of applying a predicate is not ruled out in form highlight (x), but in this case complexity of the fulfillment of the predicate is doubled (check for presence of the object x among the selection of the object if it exists). The first cases are preferable, since at many levels of testing of action predicates the perform duplicate functions (check for existence of object among) example: move (highlight (cube (x))).

Action predicate are also subject to dismemberment, for example: a cube is drawn on the screen of the monitor, the user givers the command move (cube (x)). This expression will correspond to the structure of predicates, draw "recount _ coordinates (erase (cube (x))", this partitioning of the action predicate result from the specifics of the display of objects on the monitor. Also its possible to note, what happens when objects are dismembered as cube, the predicate of action acts to dismemberment, draw(cube(x)) = draw(edge_(x)) ^ draw(edge_2(x)) ^ … ^ draw(edge_6(x)) = draw(point 1_1(x)) ^ … ^ draw(point_1_$n(x)$) draw(point_2_1(x)) ^ … ^ draw(point_2_2(x)) ^ … … ^ draw(point_6_1(x)) ^ … ^ draw(point_6_$n(x)$).

4 Conclusions

Summing up, we can say that thanks to predicate presentation of the text of the natural language personal computer is able to understand person and obey his command.

As for the scope of this method of representing natural language text, it is seen the first time that is the use spectrum is very large; firstly, it can be used for educational purposes to study algebra of predicates.

Secondly, use as an assistant in the word a user with a computer (is a good addition to the programs engaged in speech recognition).

Thirdly, in the regions associated with artificial intelligence and so on.

References

1. Ohajianya, A. C., Abumere, O. E., Owate, I. O., & Osarolube, E. (2014). Erratic Power Supply in Nigeria: Causes and Solutions. *International Journal of Engineering Science Invention*, Vol. 3, No. 7, pp. 51–55.
2. Al Salaimeh, S., & Pushkarev, A. N. (2011). Preliminary assessment for the effectiveness of the principles of logistics information management system. *International Journal of Computer Science and Telecommunications*, Vol. 2, Issue 9.
3. Manning, C., & Schütze, H. (2009). *Foundations of Statistical Natural Language Processing*, MIT Press, Cambridge.
4. Bird, S., Klein, E., & Loper, E. (2009). *Natural Language Processing with Python: Analyzing Text with the Natural Language Toolkit*, O'Reilly Media.
5. Batiha, K., Al Salaimeh, S., & Besoul, K. (2006). Digital Art and Design, *Leonardo Journal of Science*, pp. 1–8.
6. Al Salaimeh, S., & Jabber, H. (2008). Weights Adjustment Neural Networks. *European Journal of Scientific Research*, Vol. 21, No. 2, pp. 314–318.
7. Al Salaimeh, S. Quality Assurance of Logistics Information System. *American Journal of Scientific Research*, Issue 1, pp 34–36.
8. Al Salaimeh, S., Makadmeh, Z., Avramenko, V. P., & Shtangee, S. V. (2012). Optimal Resource Allocation under Bad Compatibility of Functional Limitations. *International Journal of Computer Science and Technology*, Vol. 3, Issue 1.
9. Al-Shatnawi, A. M., Zawaideh, F., Al Salaimeh, S., & Khairuddin, O. (2011). Offline Arabic Text Recognition – An Overview. *World of Computer Science and Information Technology Journal*, Vol. 1, No. 5, pp. 184–192.

Розроблення системи керування комп'ютерною графікою з використанням тексту природної мови

Аль Салаймех С.

Технологічний університет м. Акаба, вул. Васфі аль-Тал 18, м. Акаба, Йорданія

Анотація. Без комп'ютера як невід'ємної частини життя людства неможливо уявити складний математичний і технологічний розрахунок сучасних систем. Проте, на даному етапі розвивитку обчислювальних системи недостатньо комп'ютерного грамотності без відповідного програмного супроводу. У зв'язку із вищезазначеним, у статті викладено текст природної мови персонального комп'ютера, здатного зрозуміти людину і виконувати його команди. Стосовно обсягу запропонованого підходу, пов'язаного із поданням тексту природної мови, то показано різноманітний спектр її використання, по-перше, для наукових і освітніх цілей та вивчення алгебри предикатів. По-друге, даний підхід може бути використаний як помічник у зв'язку користувача із комп'ютером шляхом створення відповідних додатків до програмного забезпечення, у тому числі для розпізнаванням мови. По-третє, така методика може бути використана в областях, пов'язаних із створенням і застосуванням систем штучного інтелекту.

Ключові слова: предикат, природна мова, математичний розрахунок, людське мова, штучний інтелект.

Selection of the Optimal Software for Designing Expert Systems

Mukhoid O. V.[*], Kostornoi O.S., Shyfrin D. M.

Research and Design Institute for Atomic and Power Pumpbuilding JSC "VNIIAEN", 2 2nd Zaliznychna St., 40003 Sumy, Ukraine

Abstract. This article deals with the problems of information processing, searching and finding the solutions in the related fields of scientific knowledge. One of the solutions to this kind of problem is the software like expert systems. The aim of the article is to test the existing software tools for constructing expert systems, to make the assessment of the existing feature set, to determine the set of criteria that influences on the selection of software, to analyze the possible ways of using it regarding to structuring, storing, searching and changing of the accumulating knowledge bases. The article provides a comprehensive analysis of existing expert system shells. As a result of the analysis, the lifecycle phase of the expert system are considered, the basic criteria are selected for each phase. Focusing on the most popular criteria, the best software for constructing the expert system is selected. A prototype of the expert system was developed in the selected shells. The complexity of the prototype development is estimated. The shortcomings of the software are identified. The analysis parameters are summarized in a comparative table. The best shell for the construction of expert systems is selected considering the selected criteria.

Keywords: expert system, production system, ES shells, analysis.

1 Introduction

The total amount of information that an average employee uses in work has significantly increased lately. The problem of processing a large array of data comes to the fore in many areas of activity

According to Sviridov S. S., a developer or researcher spends about half of working time searching for necessary information [1]. For example, in the field of customer support for software use, a consultant is guided by about 10 technical standard documents and about 40 instructions of various types (the total volume of documentation is several hundred pages). Information in the above mentioned documents is periodically updated and supplemented. And if the consultant supports several software products or several groups of users solving various tasks, then the situation becomes much more complicated

To reduce the time for finding a solution, searching for answer from several knowledge areas and choosing several alternative solutions, it is recommended to use expert systems (ES). According to Doctor of Technical Science, Professor Gavrilova TA, the expert systems shall be used "... where the main difficulty relates to the use of weakly-structured knowledge of practitioners and where the logical (semantic) processing of information prevails over the computational" [2]. In other words, the expert system

must take up the "bottlenecks" of standard search: to provide a substantive adaptation of the problem, the ability to consider the consultant skill and qualification level. In the case of a significant discrepancy in the levels of knowledge between the system and the consultant, an explanation module is mandatory. In addition, the ES should be able to learn enriching a knowledge base, check the available knowledge for correctness, consistency and completeness.

It should be noted that the task of selecting the expert system for search does not have a unique solution at present. This makes it urgent to study a variety of evaluation criteria, methods of construction and methods of using various expert systems.

The purpose of this paper is to select the best software for constructing the ES relative to CAD tasks.

2 Research Methodology

2.1 Procedure

In the process of studying the problem of selecting the best software, we will:

— determine the set of criteria that influence on the selection of software for the implementation of the ES;
— select the software that meet the selected criteria;

— prepare a "basic prototype" for testing the functionality of the selected software;
— develop the "basic prototype" in the selected software;
— identify potential difficulties in the development of the ES;
— evaluate the complexity of the ES development.

Let us dwell upon the stage of defining a set of criteria for selecting software for constructing the ES.

Factors for selecting the best ES can be conditionally attributed to three different stages of the life cycle of the ES: construction, usage and updating.

When selecting the ES, it is important to consider construction methods that influence on the speed and ease of system construction. According to P. Jackson [3], "... if the success of the project depends on the development term, then you should select a shell with embedded legend tools and advanced user interface. Interface development is one of the most time-consuming stages of system design, and the more of this work can be shifted to the shell, the faster the project will be completed".

To construct the ES, it is necessary to pay attention to the following parameters:

— work with a convenient method of knowledge representation (logical, problem frame, rule-based etc.);
— ability to work with the knowledge base;
— general approach to all domains;
— presentation of peculiarities of the design model, the design methodology;
— consideration of the qualification of the ES user;
— modularization of the knowledge base;
— level of description details of the domain;
— task execution in the conditions of data lacking;
— availability of an inference machine;
— availability of the event log (record of system malfunction);
— ability to process the exceptional conditions;
— availability of a search mechanism of disambiguation;
— configuration of the necessary auxiliary software and equipment for the operation of the ES;
— adaptive properties (ability to customize for a specific domain);
— knowledge representation method.

In terms of the ES use, it is necessary to analyze following evaluation criteria:

— functionality (finding the answer, inquiry qualification, explanation, training, etc.);
— speed of operation (speed of answer search);
— cost of acquisition, implementation, owning;
— ease of use of the ES (ease of editing tools, accessibility of the help system, user-friendly interface of the shell, ease of learning, etc.);
— availability of the Russian version;
— possibility to study the scheme of obtaining (finding) the answer;
— availability of a thesaurus (dealing with synonyms);

— possibility of searching a "negative" answer;
— logging of use cases (history of hits and search results).

When using the ES, there may be a need to improve the existing functionality or introduce new capabilities. Therefore, it is also important to consider the following parameters:

— compatibility with other computer-aided design software (integration);
— possibility of self-improvement of the ES (open source, availability of an applied programming interface);
— completeness and ease of use of technical documentation for the ES;
— reliability and perspectivity of the software company, as well as the availability of qualified technical support;
— access security, delineation of rights.

To develop the most important criteria for us to select software for constructing the ES, we will carry out a practical study using "Basic prototype".

On a provisional basis, the "basic prototype" model contains 3 basic elements: the question, the answer, the recommendation. The ES for the "basic prototype" will solve the problem of finding recommendations for some malfunctions during user's work with the software.

At the beginning of the program, the user will be asked what the error is related to - the file, the system start or application software. Depending on the choice, a recommendation will be offered or questions will be asked to clarify the problem. The user can be offered solutions - for example, contact customer support professionals (ACS sector), send e-mail to the developer or find a defective element.

To solve such problems, an important criterion is the method of knowledge representation based on rules because they:

— allow us to create a knowledge base in "If-Then" form which is familiar to user;
— possess modularization – each unit of information can be deleted, changed or added independently of the rest;
— have self-explanatory function - it is possible easily trace the set of rules used for output.

So our intermediate conclusion is that in order to solve our task regarding the best software for constructing the ES with respect to our conditions, the following criteria are of practical interest:

— availability of the graphical interface of the program;
— ease of creating the ES;
— convenient tool for debugging the created system;
— possibility of self-improvement (open source, availability of an applied programming interface);
— necessity for installation of additional software to run the program;
— cost.

Based on the above criteria for developing the "Basic prototype", the following software products were selected to implement the required functionality of the ES.

2.2 CLIPS

The software environment for the development of expert systems is a rule-based system, the Rete algorithm is used as inference engine. The main competitive advantages of CLIPS are:

— acceptable performance;
— explicit syntax;
— availability of calling external functions written in other programming languages;
— modules written in CLIPS can be called by programs written in other languages.
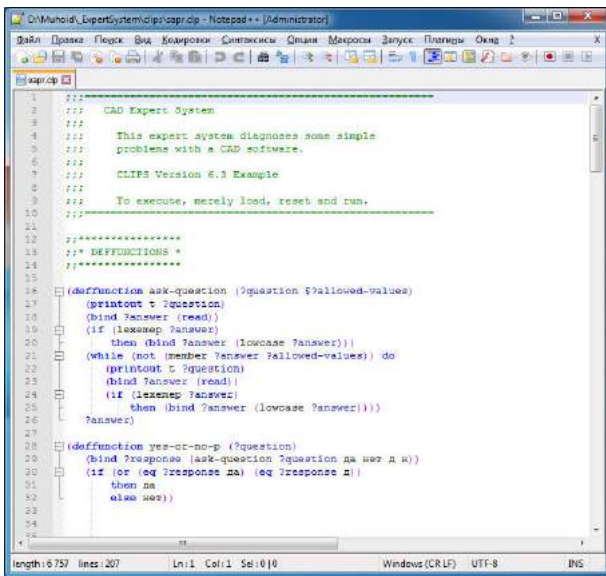
Figure 1 – Sample code written in CLIPS

Figure 2 – Graphical interface of CLIPS

2.3 Java Expert System Shell

Java Expert System Shell (JESS) is a shell for developing expert systems; the system was developed by Sandia National Laboratory.

Intelligent system Jess allows you to create a Java application providing the ability to process data based on knowledge represented as rules.

At the moment, Jess is one of the easiest and fastest shells for expert systems. Like CLIPS, the Jess kernel uses the Rete algorithm to match the facts to the rules, which is very efficient and fast in solving multiple comparison problems. It remembers the result of the last testing of knowledge and re-tests only newly appeared facts. Jess has a closed source code, unlike CLIPS.
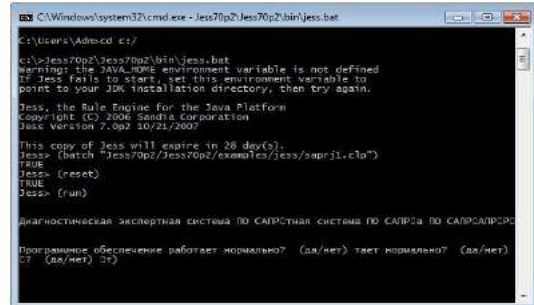
Figure 3 – Graphical interface of JESS

2.4 Prolog

Prolog is a declarative language or predicate calculus language. A predicate is a logical formula from one or more arguments. Prolog involves a set of facts and rules that ensure the finding of solutions based on these facts. Inference mechanism of Prolog is based on a comparison of facts and is the backward chaining inference. It extracts the stored (known) information by choosing answers to requests.
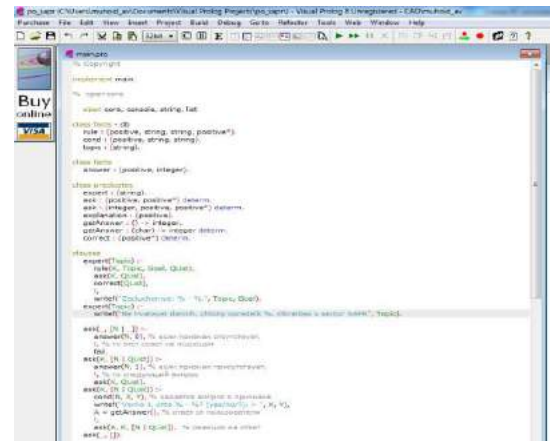
Figure 4 – Interface of IS development
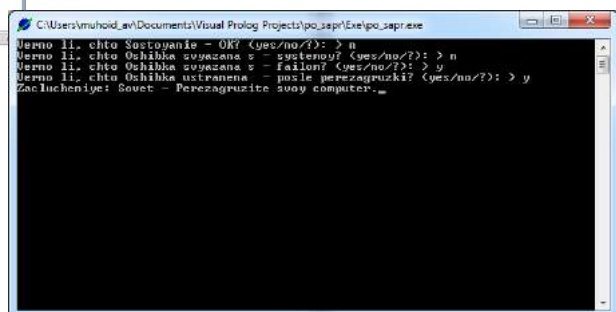
Figure 5 – Window with output of results

2.5 Expert Developer Pro

The program is designed to build a user polled system and find a solution to a particular problem. When customizer the system, one can specify only two options for answering the question – "Yes" or "No", and then indicate the next question and possible answers. Thus, it is necessary to build a tree for finding the answer. Thus, the logic of the system is completely set by the developer; the possibility of self-learning is excluded.
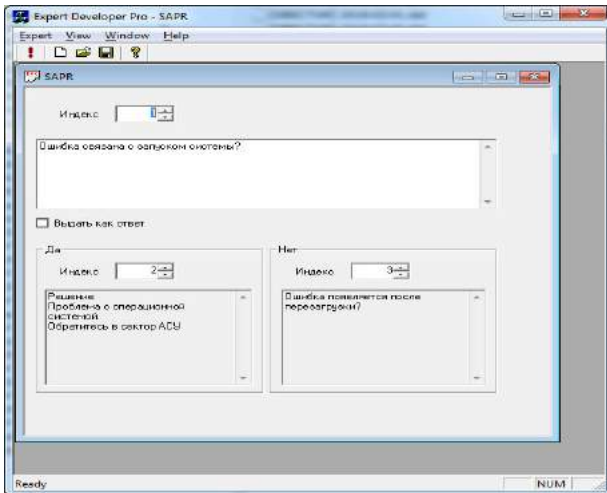
Figure 6 – Interface of ES development
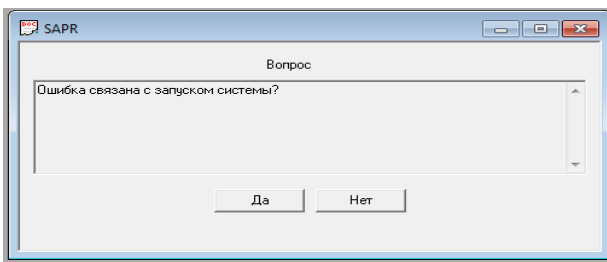
Figure 7 – Dialog window of application development
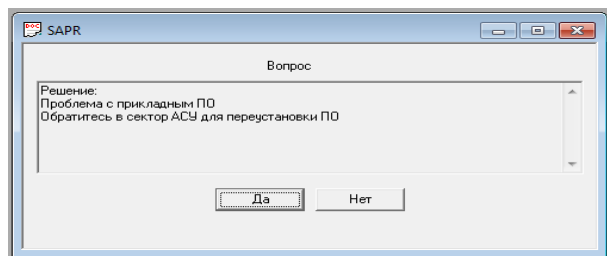
Figure 8 – Window with output of results

2.6 Exsys Corvid

Exsys Corvid is an intelligent system that can be used to develop a knowledge base in any domain. The system includes tools for program debugging and testing. Rules can exist with some probability which is expressed by the coefficient of confidence, the value is set by the expert when developing the knowledge base. The system supports the backward chaining from facts to the goal, linear programming, fuzzy logic, neural networks and has a SQL interface.
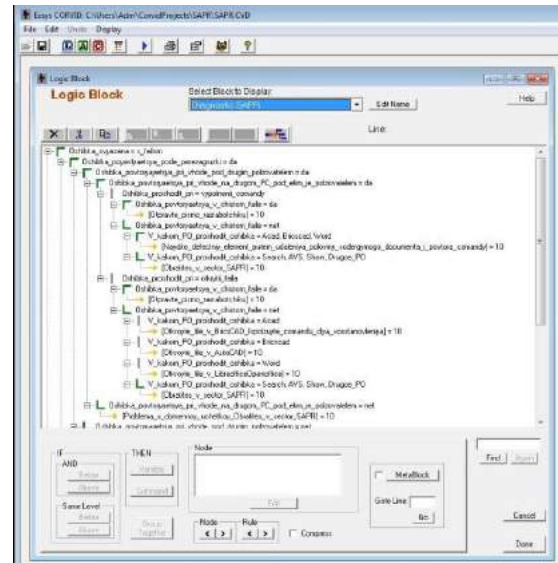
Figure 9 – Interface of ES development
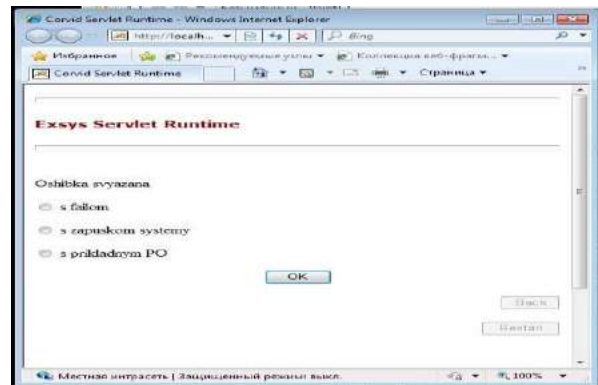
Figure 10 – Dialog window of application development
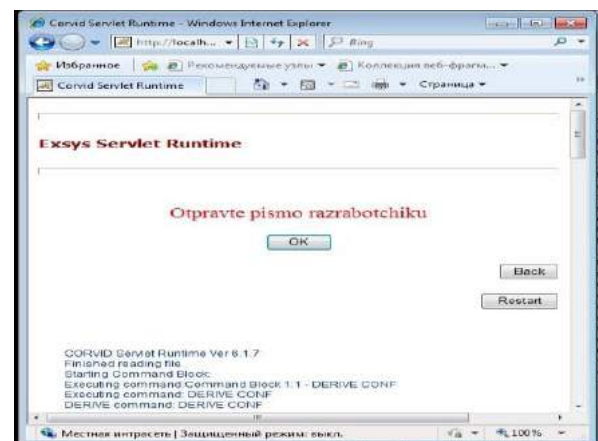
Figure 11 – Window with output of results

3 Results

Let's analyze the functionality of the selected software in relation to the declared set of criteria. The source code for CLIPS can be written in any text editor. To start the program, the shell is used. Dialogue occurs only in text mode by entering values from the keyboard. When writing a program, it is necessary to compile a list of facts and rules. At the same time when the program is working, it is possible to change the fact base which is a process of self-learning of program. It is possible to implement a graphical user interface by means of other software (for example, C ++ supports CLIPS commands).

In the Visual Prolog program shell, when writing a program, it is necessary first to describe a list of conditions (facts) during execution of which specific recommendations will be displayed. At the same time, this set is permanent; there is no change in the facts when the program is working. Dialogue with the user occurs in the console desk in text mode. Also, it was not possible to implement the work of the program on the answer "NO" and it is not possible to combine the conditions for "OR".

JESS uses the CLIPS syntax, but it runs on the Java platform, so you need to install additional software of Sun. Unlike CLIPS, the source code is closed. The use of the program is free for non-commercial use. The program runs in the console text mode.

Expert Developer Pro is a program with a graphical interface. To develop the program, it is necessary to indicate a sequence of questions, while arranging a scheme for finding the answer. The built-in system accepts only 2 variants of answer – "Yes" or "No" thus it is impossible to combine conditions automatically. The source code is closed, so no further development is possible. The advantages include the fact that you do not need to know programming languages to construct the ES, the system is constructed in the user-friendly graphic mode.

Exsys Corvid is commercial software. To work, you need a Java platform, as well install Apache server. It is necessary to build a complete tree for searching the answer, creating variables necessary for the program operation by setting up the logical and command blocks. Self-learning of program is not provided. The user interface is very diverse - you can select the answer option with the help of radio buttons, drop-down list, and active graphic zones. The advantages include the lack of the necessity to learn the programming language, but on the other hand the process of developing and configuring the ES is quite complex and time-consuming.

Table 1 – Comparison of parameters of ES shells

Software	Program operating mode	Ease for development of ES (ranking)	Convenient debugging tool	Possible improve-ment	Add	Free of charge
CLIPS	Text mode*	2	+	+	−	+
JESS	Text mode	3	–	-	+	+
Visual Prolog	Text mode	4	+	-	−	−
Expert Developer Pro	Graphic mode	1	Not required	-	−	+
Exsys Corvid	Graphic mode	5	+	-	+	−

4 Conclusions

As a result of the research, the following software products used for constructing the ES were tested: CLIPS, JESS, Prolog, Expert Developer Pro and Exsys Corvid. In terms of development ease, Expert Developer Pro and CLIPS proved to be the best. Expert Developer Pro and Exsys Corvid are characterized by graphic mode, and CLIPS can be also integrated with a graphical interface written in other software. Debugging tools are not required for Expert Developer Pro, and only JESS has no convenient debugging tool.

Only CLIPS of the entire tested software has open source code and can be implemented. The disadvantages include the need to install additional software to run the program, which is typical for JESS and Exsys Corvid.

Considering the ease of development, convenient debugging, ability to be improved, self-learning, as well as the absence of the need to install additional software and free distribution, the best choice for constructing the ES can be CLIPS.

References

1. Sviridenko, S. S. (1989). *Modern Information Technologies*, pp. 305.
2. Gavrilova, T. A., & Khoroshevskiy, V. F. (2001). *Intelligent Systems Knowledge Base*, p. 34.
3. Jackson, P. (2001). *Introduction to Expert Systems*, p. 283.
4. Gary, R. *CLIPS online documentation*, Digital resource: http://clipsrules.sourceforge.net/OnlineDocs.html.

Вибір оптимального програмного забезпечення для побудови експертних систем

Мухоїд О. В., Косторной О. С., Шифрін Д. М.

Науково-дослідний і проектно-конструкторський інститут атомного та енергетичного насособудування
АТ «ВНДІАЕН», вул. 2-га Залізнична, 2, 40003, м. Суми, Україна

Анотація. Стаття присвячена проблемі обробки інформації, пошуку і знаходженню рішень у суміжних областях наукових знань. Одним із рішень такого роду завдань є клас програмного забезпечення – експертні системи. У статті поставлено завдання розглянути представлений на світовому ринку програмний інструментарій для побудови експертних систем; оцінити наявний функціонал, визначити набір критеріїв, які впливають на вибір програмного забезпечення; провести аналіз імовірних засобів використання стосовно до областей структурування, зберігання, пошуку, зміни баз знань, що накопичуються. У статті проведено всебічний аналіз оболонок для експертних систем, що існують. У результаті аналізу розглянуті етапи життєвого циклу експертної систем; для кожного етапу обрано основні критерії. Орієнтуючись на критерії, що користуються найбільшим попитом, виконано підбір оптимального програмного забезпечення для побудови експертної системи. В обраних оболонках розроблено прототип експертної системи. Проведено оцінку трудомісткості та складності виконання прототипу. Виявлено недоліки розглянутих програмних продуктів. Параметри, за якими проводився аналіз, зведені до порівняльної таблиці. Обрана оптимальна оболонка для побудови експертних систем з урахуванням наведених критеріїв.

Ключові слова: експертна система, продукційна система, оболонки для експертних систем, аналіз.

Implementation of Efficient Artificial Neural Network Data Fusion Classification Technique for Induction Motor Fault Detection

Altaf S.[1], Mehmood M. S.[2], Imran M.[3]

[1] Sensor Network and Smart Environment Research Centre, Auckland University of Technology, Auckland, New Zealand;
[2] Sajid Brothers Engineering Industries, Awais Qarni Road, Gujranwala, Pakistan;
[3] Ministry of Industries and Production, Islamabad, Pakistan

Abstract. Reliability measurement and estimation of an industrial system is a difficult and essential problematic task for control engineers. In this context reliability can be described as the probability that machine network will implement its proposed functions under the observing condition throughout a specified time period of running machine system network. In this study single sensor method is applied for fault diagnosis depending on identification of single parameter. At early stages it is hard to diagnose machine fault due to ambiguities in modeling environment. Due to these uncertainties and ambiguities in modeling, decision making become difficult and lead to high financial loss. To overcome these issues between the machine fault symptoms and estimating the severity of the fault; a new method of artificial intelligence fault diagnosis based approach Dempster–Shafer theory has been proposed in this paper. This theory will help in making accurate decision of the machine condition by fusing information from different sensors. The experimental results demonstrate the efficient performance of this theory which can be easily compared between unsurpassed discrete classifiers with the single sensor source data.

Keywords: Dempster–Shafer theory, data fusion, fault diagnosis, artificial neural network, fast Fourier transform.

1 Introduction

In fault detection of source related to machine condition monitoring, its diagnosis and information gathering are the key steps before it goes into failure. It is also a fact that without availability of prior information machine fault cannot be recognized timely. Condition of fault is mainly dependent on time and available spectrum signature. It is always a difficult task to diagnose the machine fault at preliminary phase due to uncertainties in its modeling. In this context a method of single sensor based on signature of single parameter for diagnosis is suggested in this paper. But sometimes decision goes wrong and may cause loss of throughput and significant financial losses [1].

Yen et al, [2] have advocated the use of data fusion in CBM, since decision making using more than one sensor increases the accuracy of decision. In this scenario, Dempster-Shafer evidence combination or neural nets or fuzzy logic decision making may be used to determine the identity of fault by combining identity declaration from individual sensors.

Fan et. al in [3], studied the features extraction method from raw data, reasoning of faults and decision making derived from diagnostic knowledge. But practically, fault characteristics may be uncertain and inaccurate owing to sensor faults and some restrictions of the feature extraction approaches. Some features may not be visible when any faults are in the initial phase of development. This research introduced an improved membership function, importance of features, evidence capability issues, evidence significance, and conflicting evidences into D-S combination rule in practical application to avoid the important information loss and precision in decision making.

The Dempster-Shafer evidence theory was applied to image segmentation in a Markov field context [4]. The parameter estimation problem was considered as a classical mixture estimation problem. A generalized mixture estimation method was then applied to solve the parameter estimation problem in the context of the multisensory evidential Markov field model. The research shows that the estimated parameter based estimation is close to the true parameter estimation.

According to the Denoeux [5], D-S evidence theory differentiates between uncertainty and probability functions. These probability functions can be sub class of belief functions and the evidence theory decreases the probability theory when the probability values are well-known. Denoeux work's further extended by Yang et al in [6]. They modified the method for 3-phase induction motor system, based on current and vibration signal. To increase the performance and precision of fault diagnosis in system, they combined NN algorithm with D-S evidence theory and decision level approach. First of all, features extraction (mean, skewness, kurtosis etc) is managed by one-dimensional (1-D) discrete wavelet transform. Secondly, the extracted data are used for vibration and current inputs of the NN based on D-S theory. Finally, approximated basic belief assignment (BBA) outputs from classifiers are merged by D-S theory for improving the fault diagnosis accuracy.

In this paper, Fault diagnosis based approach Dempster–Shafer theory has been proposed to make an accurate decision of the machine condition by fusing information from different sensors. The experimental results demonstrate the efficient performance of this theory which can be easily compared between unsurpassed discrete classifiers with the single sensor source data.

2 Research Methodology

2.1 Mathematical modeling of Dempster–Shafer (D-S) evidence theory

2.1.1 Frame of discernment (Fod)

The Dempster-Shafer evidence theory employs probability theory to explain the practical uncertainty problems. The Dempster-Shafer evidence method is regarded as a generalized Bayesian theory [1]. The theory can demonstrate support not only for an object but also for the union of objects.

To compute the credibility of distribution from all kinds of faults, let assume θ be a fixed set of elements and N independent evidence element. We refer the θ like the FoD [22]; it consists all groups with the subsets of θ is known as the power of set of θ, and denoted by 2^{θ}, when θ has n elements, 2^{θ} has 2^n elements.

Suppose $\theta = \{F_1, F_2, \ldots, F_n\}$, if there is N autonomous reliable distribution function in the identical recognition framework, so $m_1, m_2, \ldots, m_n$, the combine result is [23]:

$$N = \sum_{\substack{\cap \\ i=1 \\ F_i \neq \phi}}^{n} \prod_{j=1}^{n} m_j(F_j).$$ (1)

Once the combination, the whole credit assignment function (CAF) is as given below:

$$m(F) = (m_1 \oplus m_2 \oplus \ldots \oplus m_n)(F) = \frac{1}{N} \sum_{\substack{\cap \\ i=1 \\ F_i = F}}^{n} \prod_{j=1}^{n} m_j(F_j).$$ (2)

The reliability distribution function's $m_i(F_j)$ of the first i sensor at current state F_j and reliability distribution function R is as follows [24]:

$$m_i(F_j) = \frac{C_i(F_m)}{\sum_{j=1}^{N_C} C_i(F_m) + N_S(1 - R_i)(1 - \alpha_i\beta_i)},$$ (3)

where α_i, β_i are correlation coefficients.

And reliability distribution function $m_i(\theta)$ is in the evidence body E as given below:

$$m_i(\theta) = \frac{N_S(1 - R_i)(1 - \alpha_i\beta_i)}{\sum_{j=1}^{N_C} C_i(F_m) + N_S(1 - R_i)(1 - \alpha_i\beta_i)}.$$ (4)

So, the largest correlation coefficients α_i as follows:

$$\alpha_i = \max_j \{C_i(F_m)\}.$$ (5)

And distribution correlation coefficient β_i is:

$$\beta_i = \frac{1}{N_C - 1} \left[\frac{N_C \alpha_i}{\sum_{j=1}^{N_C} C_i(F_m)} - 1 \right].$$ (6)

Sensor reliability coefficient R_i could be uncertainty of the CAF:

$$R_i = \alpha_i\beta_i / \sum_{j=1}^{N_C} \alpha_i\beta_i.$$ (7)

Before going to calculate the confidence period, compute the belief proposition function (*Bel*) and likelihood function (*Pls*) as follows [23]:

$$Bel(A) = \sum_{B \subseteq A} m(B);$$
$$Pls(A) = 1 - Bel(A) = \sum_{A \cap B} m(B),$$ (8)

Where *Bel(A)* and *Pls(A)* are the proposition of *A*'s the confidence level.

2.1.2 Dempster's rule of combination

As discussed above, Dempster's theory has been suggested for the evidence combination when the evidence from dissimilar sources has diminutive difference. Dempster's rule joins many belief functions (*Bel*) through their respective BPAs. These all belief functions are described on the identical FoD. Although, these are derived from autonomous evidence sources. This theory is based on conjunctive operation. The result of belief function combination consists of conjunctive pooled evidence [4].

Suppose sensor S_1 observes parametric data and assigns mass probabilities $[mp_1(A_0), mp_1(A_1), mp_1(A_2)]$ to the 3 propositions and sensor S_2 assigns the mass probabilities $[mp_2(A_0), mp_2(A_1), mp_2(A_2)]$ respectively. The following Table 1 summarizes the D-S combination rule for the fault diagnosis.

Table 1 – D-S combination rule's

S_2 \\ S_1	$[mp_1(A_0)]$	$[mp_1(A_1)]$	$[mp_1(A_2)]$
$[mp_2(A_0)]$	$mp(A_0) = mp_1(A_0)mp_2(A_0)$	$k_{07} = mp_1(A_0)mp_2(A_0)$	$mp(A_0) = mp_1(A_0)mp_2(A_0)$
$[mp_2(A_1)]$	$k_{06} = mp_1(A_0)mp_2(A_0)$	$mp(A_0) = mp_1(A_0)mp_2(A_0)$	$mp(A_0) = mp_1(A_0)mp_2(A_0)$
$[mp_2(A_2)]$	$mp(A_0) = mp_1(A_0)mp_2(A_0)$	$k_{10} = mp_1(A_0)mp_2(A_0)$	$mp(A_0) = mp_1(A_0)mp_2(A_0)$

The matrix elements shown in Table 1, are the joint the evidences of two sensors which assigned as per the combination rule. The joint probability for equal propositions, products of the masses are given by each of sensor.

Dempster's rule of combination [24] calculates a normalization factor nf which is the total of the masses given by the divergence propositions (Figure 1).
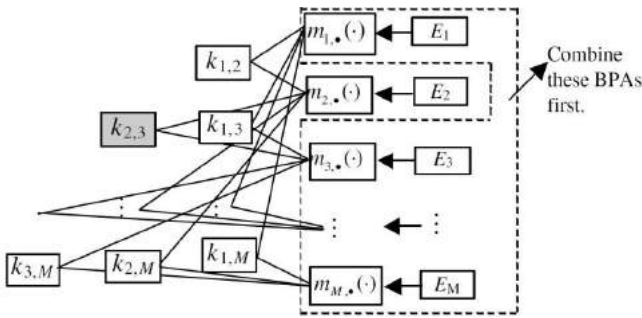
Figure 1 – Classification of evidences [1]

The Dempster's combination rule subsequently may be inscribed for two autonomous sources as:

$$mp(A_i) = \frac{\sum_{A_i | B_j = C} mp_1(A_i)mp_2(B_j)}{1 - nf}; \qquad (9)$$

$$nf = \sum_{A_i | B_j = \phi} mp_1(A_i)mp_2(B_j),$$

where Ø represent the empty set and A_i defined as a general proposition.

3 Results

We suppose the three evidences to perform the online monitoring of induction motors in MATLAB and Dempster–Shafer Engine 1.0 (DSE) is used for the fusing sensors data. For that, an enormous number of different signals exist in production line to detect the three hypotheses were chosen as faults types. Three evidences sources against these fault types in healthy and faulty motors and mass probabilities functions are shown in the following Table 2.

Table 2 – Sources of mass probabilities functions in Healthy machine

Evidences sources	Sensor number			Diagnosis result
	1	2	3	
Evidence 1	0.011	0.003	0.011	uncertainly
Evidence 2	0.001	0.000	0.000	healthy
Evidence 3	0.000	0.000	0.000	healthy

In each case the condition signal provides a qualitative indication of the sensor fault. The only significant temporal resolution of the method used to estimate the frequency spectrum. Temporal resolution can be improved by increasing the overlap of blocks but this incurs a significant computational penalty.

Figure 2 a shows the effect of a sensor hard over fault and failure which is initially detected using samples in the block 94–150 minutes, however the sensor status value is only reduced to 0.59 as the first 19 samples in the block are obtained from a healthy sensor. The status value is reduced to zero by data in the block 119–175 minutes and all subsequent blocks. In Figure 2 b, the sensor is unpredictable from 95 minutes. The sensor status output is reduced appropriately by data in the block 85–145 minutes and all subsequent blocks. Figure 2 c demonstrates that a sensor point fault at 83 minutes and the sensor status value is reduced to 0.09 by data in the block 47–139 minutes but returned to unity by data in the block 77–133 minutes. In response to the sensor fixed fault at 110 minutes the sensor status value is reduced suitably by data in the block 110–210 minutes and all subsequent blocks.

The following Tables 3, 4 shows the specification of features classification and accuracy of each fault class for network training and data testing with 100 evidence trees, with splitting one class variable for each split with their accuracy percentage against each evidence. For features classification, specific numbers of sample are taken by each sensor, and train it through proposed theory.

The following Figure 3 presents the performance errors against each targeted class. As we can observed that in classification of class 1 and 3; the required best epoch is near 32 and 26, which is not close targeted value which shows the less accuracy in training. Instead, class 2 is very adjacent and shows the healthy state of evidence class.
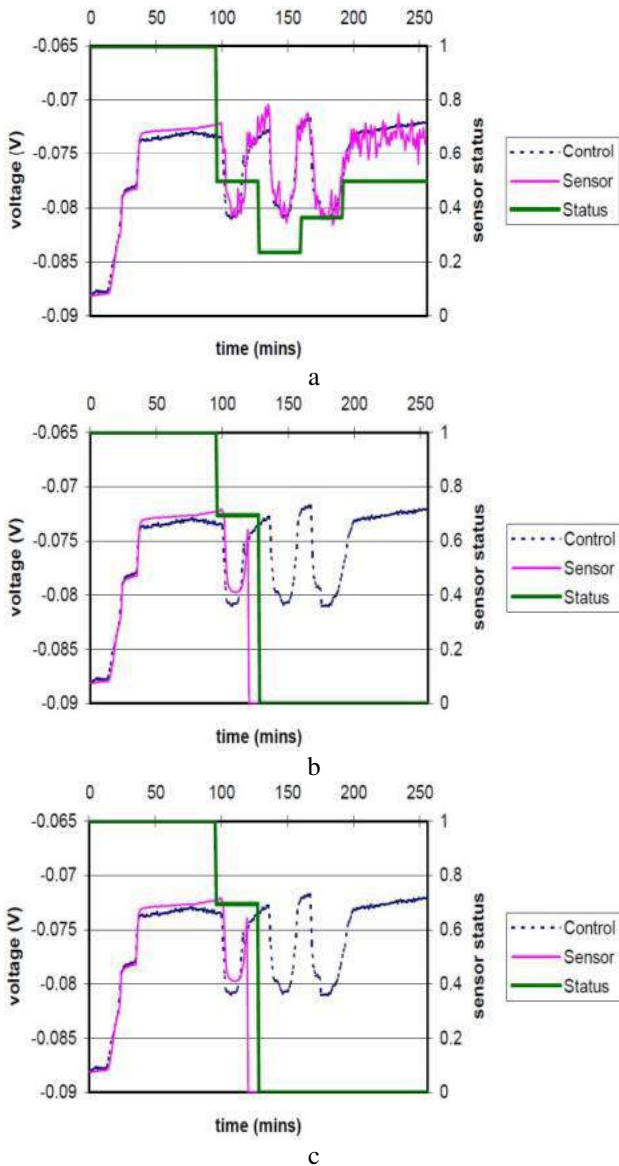
Figure 2 – Confidence in different hypothesis
at sensor 1 (a), 2 (b), and 3 (c)

Table 3 – Specification of features classification

Class	Condition	Samples	Training sample	Testing sample
1	uncertainly	10	15	15
2	healthy	10	15	15
3	uncertainly	10	15	15

Table 4 – Each fault class accuracy with trees structure

Class	Confusion matrix									
	1	2	3	4	5	6	7	8	9	10
1	10	0	0	0	0	0	5	0	0	0
2	0	10	0	0	0	4	0	0	0	0
3	0	0	10	0	0	0	0	0	10	0
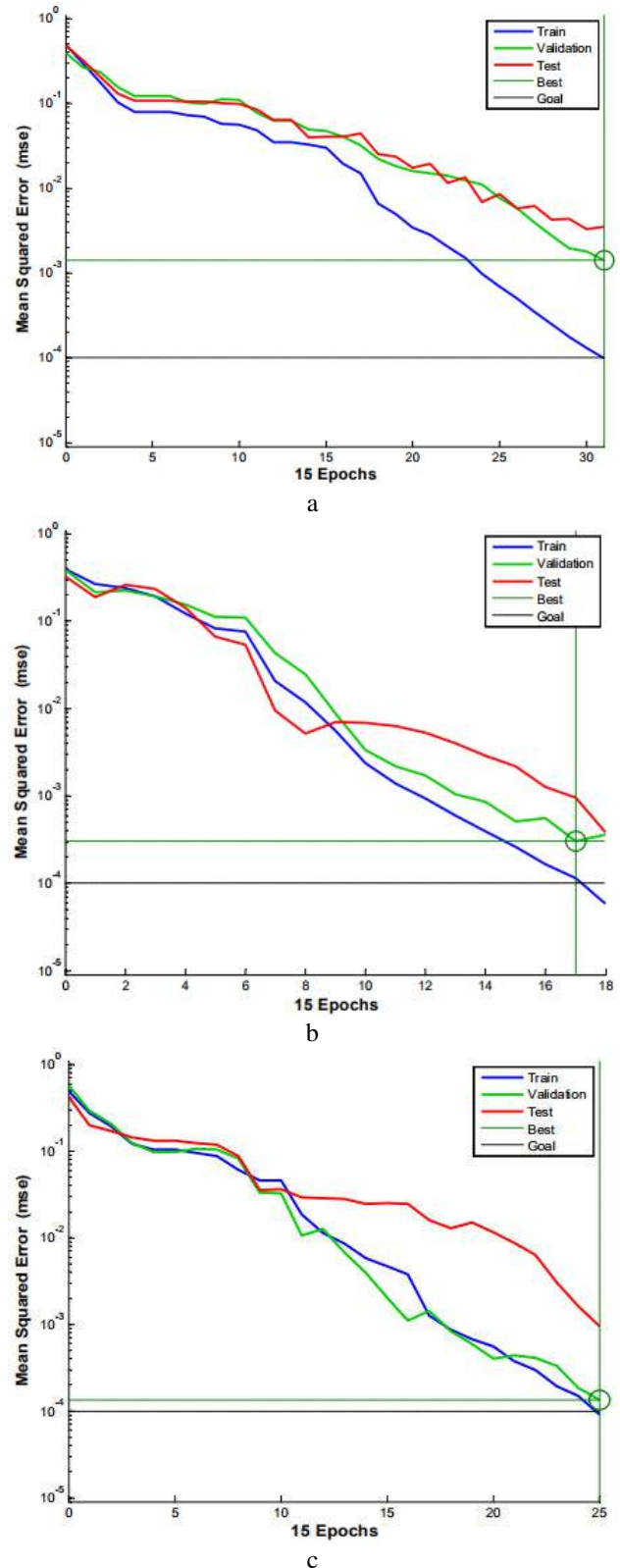
Figure 3 – Class 1 (a), 2 (b), and 3 (c) performance

Figure 4 shows the error percentage of all the evidences.
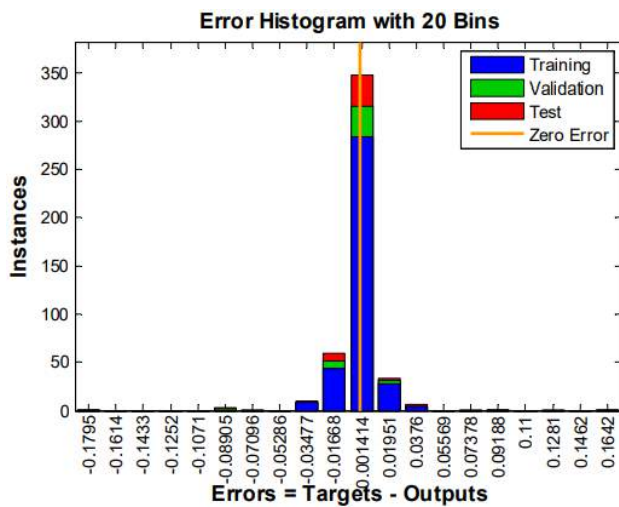
Figure 4 – Overall error percentage instances

Conclusions

This paper discussed the machine fault diagnosis using the sensor fusion technique D-S evidence theory. Through the theoretical and practically, we found this theory very efficient and realistic in machine fault diagnosis concept. A critical comparison is also performed between the different sensors fusion in respect to time which also show the accuracy percentage of D-S. The results shows that it effectively enhance the reliability of machine diagnosis and very much decreased the probability of uncertainty. It also detects the different faults timely to reduce the cause loss of throughput and significant financial losses among the industries. Therefore, it can be believed that the fault diagnosis of electric machines is a significant investigate topic with great potential for application in industry.

4 Acknowledgements

References

1. Fan, X. F., & Zuo, M. J. (2006). Fault diagnosis of machines based on D–S evidence theory. Part 2: Application of the improved D-S evidence theory in gearbox fault diagnosis. *Pattern Recognition Letters*, Vol. 27, pp. 377–385.
2. Fan, X., & Hu, Y. (2007). Target Identif ication Based on Neural Network and D-S Evidence Theory. *Transactions of Shenyang Ligong University*, Vol. 26, No. 5, pp. 33–36.
3. Yen, J. (2003). *Discussion of Dempster's–Shafer's Theory*. D. Hall, State College, PA.
4. Gestel, T. V., & Suykens, J. A, Lanckriet, K., Lambrechts, G., De Moor, B., & Vandewalle, J. (2002). Bayesian Framework for Least Squares Support Vector Machine Classifiers, Gaussian Processes and Kernel Fisher Discriminant Analysis. *Neural Computation*, Vol. 15, No. 5, pp. 1115–1142.
5. Denoeux, T. (1999). Reasoning with imprecise belief structures. *International Journal of Approximate Reasoning*, pp. 79–111.
6. Luo, H., Yang, S.-L., Hu, X.-J., & Hu, X.-X. (2012). Agent oriented intelligent fault diagnosis system using evidence theory. *Expert Systems with Applications*, Vol. 39, Issue 3, pp. 2524–2531.
7. Smets, P. (1990). The combination of evidence in the transferable belief model. *IEEE Transactions on Pattern Analysis and Machine Intelligence*, Vol. 12, No. 5, pp. 447–458.
8. Basir, O., & Yuan, X. (2007). *Engine fault diagnosis based on multi-sensor information fusion using Dempster-Shafer evidence theory*. Information Fusion.
9. Yager, R. R. (1987). On the Dempster-Shafer framework and new combination rules. *Information Sciences*, Vol. 41, No. 2, pp. 93–137.
10. Zadeh, L. A. (1986). Simple view of the dempster-shafer theory of evidence and its implication for the rule of combination. *Artificial Intelligence*, Vol. 7, No. 2, pp. 85–90.
11. Murphy, R. R. (1998). Dempster-Shafer theory for sensor fusion in autonomous mobile robots. *IEEE Transactions on Robotics and Automation*, Vol. 14, No. 2, pp. 197–206.
12. Dubois, D., & Prade, H. (1988). Representation and combination of uncertainty with belief functions and possibility measures. *Computational Intelligence*, Vol. 4, No. 3, pp. 244–264.
13. Murphy, C. K. (2000). Combining belief functions when evidence conflicts. *Decision Support Systems*, Vol. 29, No. 1, pp. 1–9.
14. Zhang, J., Fan, X., Huang, C., & Chen, T. (2008). Fusion monitoring system of locomotive wheel set state. *Journal of Traffic and Transportation Engineering*, Vol. 8, No. 6, pp. 13–19.
15. Asakura, T., Kobayashi, T., & Hayashi, S. (1999). A study of Fault Diagnosis System Using Neural Networks. *Proceedings of IMEKO-XV World Congress TC-10*, pp. 39–44.
16. Adgar, A., Cox, C., & MacIntyre, J. (1998). Automatic fault diagnosis for rotating machinery using statistical and neural network techniques. *11th International Congress and Exhibition on Condition Monitoring and Diagnostic Engineering Management "COMADEM 98"*.
17. Zolghadri, A. (1996). An Algorithm for Real-Time Failure Detection in Kalman Filters. *IEEE Transactions on Automatic Control*, Vol. 41, No. 10, pp. 1537–1539.

18. Buczak, A. L., & Uhrig, R. E. (1993). Hybrid neural network – fuzzy logic diagnosis system for vibration monitoring. *Proceedings of Artificial Neural Networks in Engineering Conference "ANNIE-93"*, pp. 757–762.

19. Siu, C. C., Shen, Q, & Milne, R. A. (1997). Fuzzy Expert System for Turbomachinery Diagnosis. *IEEE Int. Conference on Fuzzy Systems*, Vol. 1, pp. 555–560.

20. Hu, Z., Cai, Y., He, X., & Xu, X. (2005). Fusion of multi-class support vector machines for fault diagnosis. *American Control Conference*, Vol. 3, pp. 1941–1945.

21. Bendjebbour, A., & Pieczynski, W. (1998). Unsupervised image segmentation using Dempster-Shafer fusion in a Markov fields context. *Proceedings of the 1st International Conference on Multisource-Multisensor Information Fusion*.

22. Hall, D. L., & McMullen, S. A. H. (2004). *Mathematical Techniques in Multisensor Data Fusion*. Artech House Publishers.

23. Shengqiang, W., Wanlu, J. (2009). Research on Data Fusion Fault Diagnosis Method Based on DS Evidence Theory. *International Conference on Measuring Technology and Mechatronics Automation "ICMTMA'09"*, Vol. 1, pp. 689–692.

24. Shao, W. Y. H., & Wang, X. (2004). Soft sensing modeling based on support vector machine and Bayesian model selection. *Computers and Chemical Engineering*, Vol. 28, Issue 8, pp. 1489–1498.

Впровадження ефективної методики класифікації злиття даних для визначення несправностей асинхронного двигуна із застосуванням штучної нейронної мережі

Альтаф С.[1], Мехмуд М. С.[2], Імран М.[3]

[1] Дослідницький центр мережі датчиків та інтелектуального середовища,
Оклендський технологічний університет, м. Окленд, Нова Зеландія;
[2] Інженерна компанія "Sajid Brothers", шлях Авайз Карні, м. Гуджарвала, Пакистан;
[3] Міністерство промисловості та виробництва, м. Ісламабад, Пакистан

Анотація. Визначення надійності та оцінка промислової системи є важким і важливим проблемним завданням для інженерії керування. У цьому контексті надійність може бути охарактеризована як вірогідність того, що машинна мережа реалізує свої запропоновані функції в умовах спостереження впродовж певного часового проміжку, коли працює система машинної мережі. У цьому дослідженні застосовується метод одиночного датчика для діагностування несправностей залежно від ідентифікації одного параметра. На ранніх етапах важко діагностувати помилку машини через невизначеність у середовищі моделювання. З огляду на ці факти, невизначеності і двозначності в моделюванні, прийняття рішень стає складним завданням і призводить до значних фінансових втрат. Для подолання цих проблем між проявами несправності машини та оцінкою її ступеня в роботі запропоновано новий підхід із застосуванням штучного інтелекту на основі теорії
Демпстера–Шафера. Ця теорія дозволяє більш точно визначати стан машини шляхом об'єднання інформації з різних датчиків. Результати числового експерименту демонструють високу ефективність запропонованої методики у порівнянні з дискретними класифікаторами з вихідними даними одиночних датчиків.

Ключові слова: теорія Демпстера–Шафера, злиття даних, діагностування несправностей, штучна нейронна мережа, швидке перетворення Фур'є.

Kalman Filter Based Controlled Online System Identification

Ganesh E. N.

Saveetha Engineering College, Kuthambakkam, 600124 Tamil Nadu, Chennai, India

Abstract. In the development of model predictive controllers a significant amount of time and effort is necessary for the development of the empirical control models. Even if on-line measurements are available, the control models have to be estimated carefully. The payback time of a model predictive controller could be significantly reduced, if a common identification tool would be available which could be introduced in a control scheme right away. In this work it was developed a control system which consists of a neural network (NN) with external recurrence only, whose parameters are adjusted by the extended Kalman filter in real-time. The output of the neural network is used in a control loop to study its accuracy in a control loop. At the moment this control loop is a NN-model based minimum variance controller. The on-line system identification with controller was tested on a simulation of a fed-batch penicillin production process to understand its behaviour in a complex environment. On every signal process and measurements noise was applied. Even though the NN was never trained before, the controller did not diverge. Although it seemed like the on-line prediction of the NN was quite accurate, the real process was not learned yet. This was checked by simulating the process with the NN obtained at the end of the batch. Nevertheless the process was maintained under control near the wanted set-points. These results show a promising start for a model predictive controller using an on-line system identification method, which could greatly reduce implementation times.

Keywords: Kalman filter, neural network, on-line training, variance control.

1 Introduction

Most companies have limited resources as most of the large central research departments have shrunken down. Advanced control projects have to compete with other cost saving projects and therefore need to have a typical payback time of two years. Once a control system is introduced, it has to be maintained as the process configuration or process conditions can change willingly or unwanted, for example catalyst decoking. If it would be possible to have a general control tool with self-tuning capabilities for system identification and control, implementation time and thus payback times could be greatly reduced.

The proposed control and system identification system consist of a neural network with external recurrence, whose weights are adjusted by the extended Kalman filter. The neural network's prediction is fed to a second extended Kalman filter which tries to obtain the set-point at the next sampling point. This system identification scheme and control structure can be seen as an adaptive non-linear minimum variance control (Astrom and Wittenmark, 1984).

2 Research Methodology

2.1 System identification

Neural networks are known to be non-linear fitters in a certain domain. A neural network with external recurrence is normally sufficient for chemical processes as they show slow dynamics compared with electrical (Haykin, 1999).

Various neural network configurations can be seen as the non-linear correspondent of known linear models such as the models NARX, ARMAX, CARMA and state space models (Haykin, 1999; Rivals and Personnaz, 1998).

The neural network weights are adapted by the extended Kalman filter, which is implemented as the MEKA algorithm as first introduced by Shah and Palmiero in 1990, as well as later by Puskoris and Feldkamp in 1991 as the decoupled Kalman filter algorithm. In this case every neuron has its own extended Kalman filter (Figure 1).
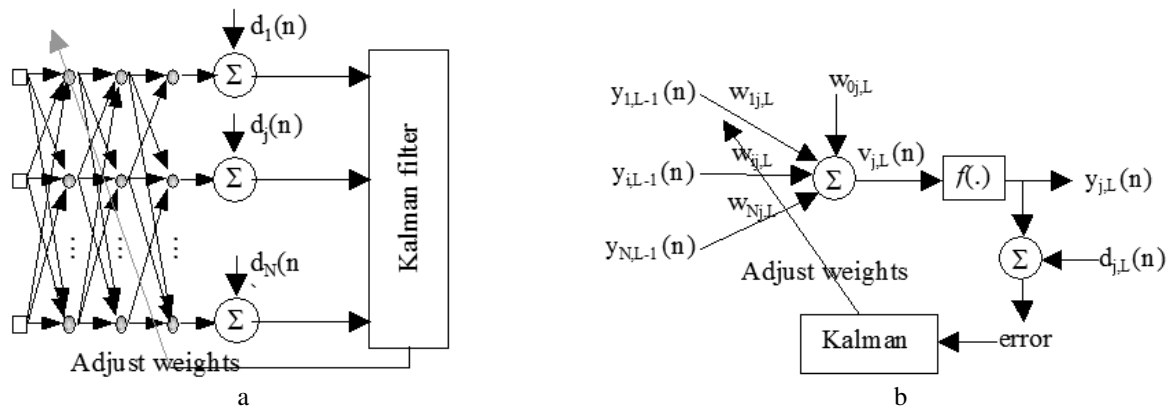
Figure 1 – Global extended Kalman Filter (a) and non-linear Kalman filtering per neuron (b)

The network weights are updated in real-time by a Multiple Extended Kalman filter algorithm to account for changes in the process, whose implementation can be found in Scheffer et al. in 2000–2001.

New development have taken place in improving de Kalman filter by replacing the derivatives for mean and variance calculations (Julier and Uhlmann, 1997) and applying this concept to neural networks (Wan and van der Merwe, 2000).

2.2 The control system

The estimate of the recurrent neural network is fed to an extended Kalman filter to estimate the controller parameters or directly the manipulated variables. Here, the latter approach is chosen and the manipulated variable is directly estimated by the following dynamical system:

$$m(k + 1) = m(k) + w(k); \qquad (1)$$

$$y_c(k) = y_{ann,c}(k) + v(k), \qquad (2)$$

where m is the manipulated variable; y_c – the controlled variable; w and v are variables with a Gaussian distribution of $(0, Q)$ and $(0, R)$ respectively.

The measurement d of the controlled variable is the desired set-point of the controlled variable. The manipulated variable is one of the inputs of the recurrent neural network. In the application of the Kalman filter, the observation equation has to be linearised every sampling instance. Thus the derivative of the controlled variable to the manipulated variable has to be calculated, which is the derivative to the recurrent neural network. The derivative of a neural network can be calculated by applying the chain rule, which results for a two layer neural network in:

$$\frac{dy_{k,j}}{dy_{k-2,h}} = f'(v_{k,j}) \cdot \sum_{i=1}^{N_{k-1}} \left[w_{k,ji} \cdot w_{k-1,ih} f'(v_{k-1,i}) \right]. \quad (3)$$

The controlled variable can now be updated by the Kalman filter:

$$m(k) = m(k) + K(k) \cdot \left[y_{c,setpoint}(k) - y_{ann,c}(k) \right]. \quad (4)$$

2.3 The penicillin production process

Fed-batch processing is a typical example of a process exhibiting non-linear process dynamics. Especially, biochemical processes are known to have a lot of interaction between their state variables and are sensible to minor changes in pH, dissolved oxygen concentration, and temperature due to the sensitivity of the biochemical catalysts. PID control behaves well in case of continuous processing but in batch processing the control parameters will never maintain optimal values due to the changing process conditions. Therefore this seems to be a challenging study case as it exhibits non-linear process dynamics and a need for a self-tuning controller (Figure 2).
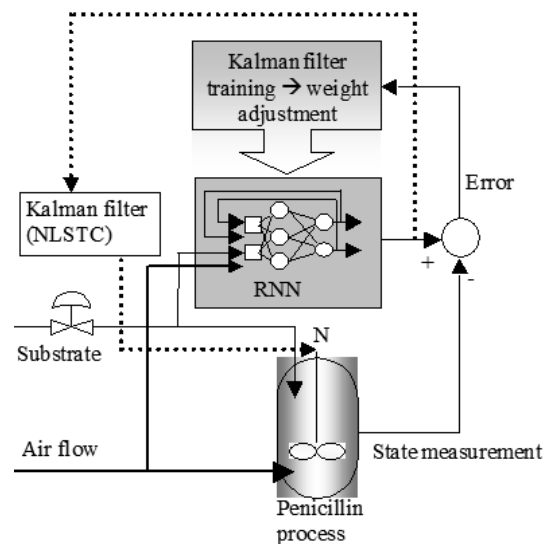
Figure 2 – The proposed non-linear self-tuning controller scheme

The emphasis is put on the production phase and not on the growing phase where an optimal feeding strategy is essential in obtaining a high concentration of penicillin. But it is essential to keep the dissolved oxygen concentration above 30 % to ensure life conditions to the fungi. In this work the feeding strategy determined by Rodrigues in 1999 is used and the control objective is to maintain the dissolved oxygen concentration at about 55 %. The

dissolved oxygen concentration is controlled by manipulating the rotation speed through the mentioned non-linear self-tuning controller.

An essential part of the non-linear self-tuning controller is the recurrent neural network identification. Three input and four state variables were taken to identify the process and are the substrate feed flow, the rotation speed and the air flow as input variables and the bio-mass concentration, the substrate concentration, the penicillin concentration and the dissolved oxygen concentration as state variables. The mentioned Kalman filter algorithm will be compared to the standard backpropagation algorithm.

3 Results

The system identification is an important part of the control structure. It is necessary to have a good prediction of the dissolved oxygen concentration of the next measurement as this is used by the minimum variance control. Therefore the on-line prediction was studied also without the control structure to understand its prediction capabilities. The standard back-propagation algorithm (SBP) is one of the few algorithms was used as a comparison as it is one of the few other recurrent algorithms. The parameters of the standard back propagation and the Kalman filter algorithms were tuned and a selection was made by ranking them on the training error or on the simulation error of all the state variables as mentioned in the former paragraph. The simulation error was obtained by simulating again after the on-line training, which is the showing of every data-point only one time to the neural network. We would like to note that it was also tried to use the standard backpropgation algorithm with momentum, but that did not result in smaller errors than with the standard backpropagation algorithm. The results are presented in Figures 3–6.

From the Figures 3 and 4 it can be seen the known fact, that the best training errors is no assurance for a good generalization error and is clearly seen the larger discrepancy between the data and the prediction in the simulation with the one-time trained neural network. But it is interesting to see that the usage of the Kalman filter algorithm results indeed in a better general learning. Additionally it can be seen that the simplification of the global extended Kalman filter to multiple local Kalman filters in the MEKA algorithm penalizes the general learning. Additionally, the MEKA algorithm shows more instability in the simulation (Figure 4).

If we turn to the tuning of the parameters, which lead to the best simulation error (Figures 5, 6) the situation becomes even more pronounced. During the training the prediction of the dissolved oxygen concentration with the backpropagation algorithm would not be suitable for control as the concentration prediction during the prediction is not good enough.

It is interesting to see that the instability in the MEKA algorithm has been transferred from the simulations error (Figure 4) to the training error for this case (Figure 5). Still the MEKA algorithm's prediction during the training follows the real concentration.
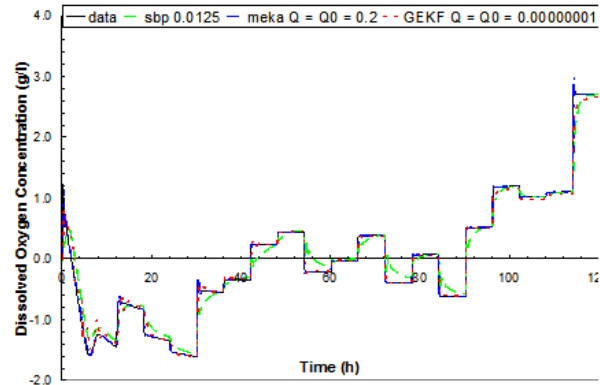
Figure 3 – Dissolved oxygen prediction of NN during the on-line training (best training error and normalized data)
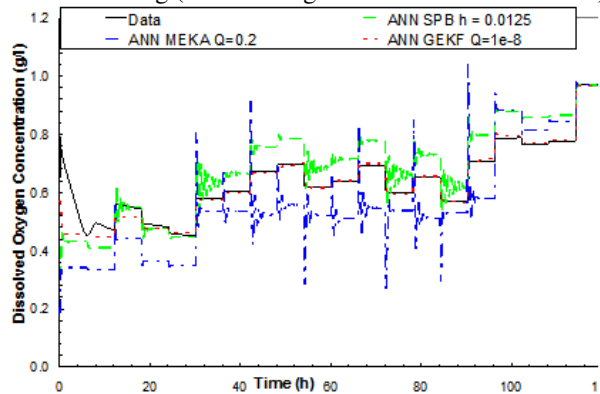
Figure 4 – Simulation of the same dissolved oxygen data with the on-line trained NN (best training error)
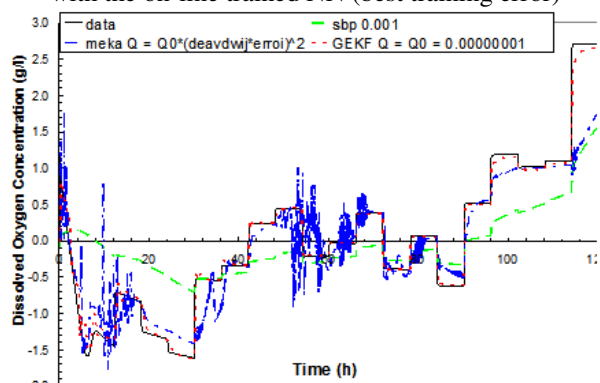
Figure 5 – Dissolved oxygen prediction of NN during the on-line training (best simulation error and normalized data)
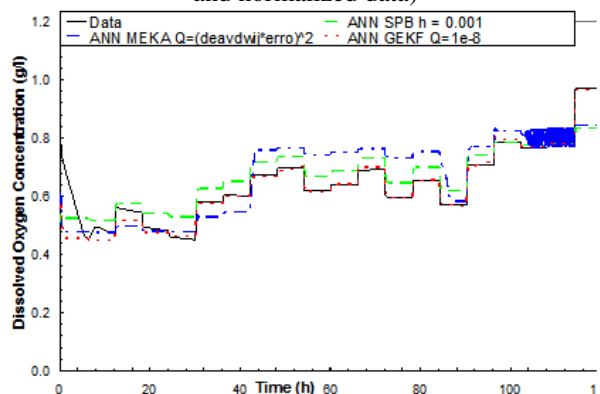
Figure 6 – Simulation of the same dissolved oxygen data with the on-line trained NN (best simulation error)

The GEKF algorithm outperforms in this case very much both algorithms. Therefore there is encouragement to implement the unscented Kalman filter (Julier et al., 1997) also, as this is an improvement over the extended Kalman filter.

In Table 1 it is shown the errors for both cases. The error summed over all the state variables (bio-mass concentration, the substrate concentration, the penicillin concentration and the dissolved oxygen concentration. From the table, it seems that the MEKA algorithm performs better than the GEKF, but that is not true due to the instabilities as shown in Figures 4, 5.

In Table 2 it is shown the calculation times of the different algorithms. Although it seems that the GEKF has a much higher computational costs, it still means that the calculation per data point is done in less than 1 second. The data is probably not faster available from the on-line measurements and therefore the GEKF would be a good candidate also for on-line control scheme or even be the favourite on-line neural network training algorithm.

Table 1 – Training errors for the best training and best simulation cases of the different algorithms

Algorithm	SBP	SBP	MEKA	MEKA	GEKF	GEKF
Parameter	Best training	Best simulation	Best simulation	Best training	Best simulation	Best training
Quality, Q	$1.25 \cdot 10^{-2}$	$1.0 \cdot 10^{-3}$	$(error \cdot d\_error/dw_{ii})^2$	0.20	$1.0 \cdot 10^{-8}$	$1.0 \cdot 10^{-8}$
Relative error	$5.09 \cdot 10^{6}$	$2.34 \cdot 10^{6}$	$1.95 \cdot 10^{5}$	$2.24 \cdot 10^{5}$	$1.35 \cdot 10^{6}$	$7.39 \cdot 10^{5}$

Table 2 – Calculation times of the different algorithms for 1 200 data points

Algorithm	SPB	MEKA	GEKF
Calculation time, s	0.08	27	409

In Figures 7 and 8 it is shown the minimum variance control of the dissolved oxygen concentration with the on-line training of the recurrent neural network at the same time. For the moment the MEKA algorithm has been used and therefore it can still be gained from using the GEKF algorithm. It can be clearly seen that the minimum variance control is better with the MEKA algorithm. The Kalman filter training algorithm assure that the neural network training is better which results in the much smaller deviations at the end of the batch run.

4 Conclusions

The on-line training of recurrent neural networks should be done preferably with extended Kalman filter algorithms. Localizing the Kalman filter to the neuron level (MEKA) affects the learning of the neural network and therefore the implementation of the unscented Kalman filter algorithm could lead even to further improvements for on-line training of neural networks. However, the simulations show that not always a good generalization is obtained. The application of the minimum variance controller with the on-line training of the neural network showed that control could be obtained on the neural networks prediction without divergence of the algorithm. Therefore, implementation or payback time could be reduced by applying on-line training.
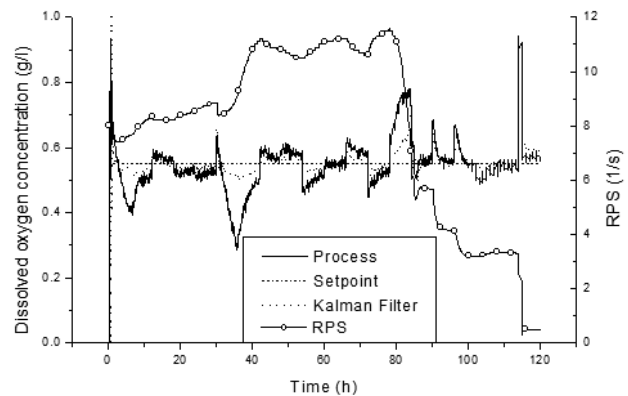
Figure 7 – Estimation and minimum variance control of the dissolved oxygen concentration concentration (the recurrent neural network is trained with the MEKA filter algorithm)
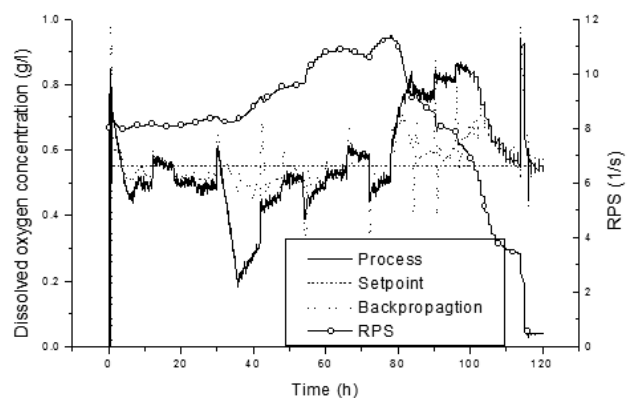
Figure 8 – Estimation and minimum variance control of the dissolved oxygen concentration concentration (the recurrent neural network is trained with the backpropagation algorithm)

References

1. Astrom, K. J., & Wittenmark, B. (1984). *Computer Controlled Systems*. Prentice-Hall Inc., New Jersey, USA.
2. Haykin, S. (1999). *Neural networks: a comprehensive foundation*. Prentice-Hall Inc., New Jersey, USA.
3. Julier, S., & Uhlmann, J. K. (1997). A new extension of the Kalman filter to nonlinear systems. *Proceedings of the 11th International Symposium on Aerospace/Defence Sensing, Simulation and Controls*.
4. Puskorius, G. V., & Feldkamp, L. A. (1991). Decoupled extended Kalman filter training of feedforward layered networks. *Proceedings of the International Joint Conference on Neural Networks*.
5. Rivals, I., & Personnaz, L. (1998). A recursive algorithm based on the extended Kalman filter for the training of feedforward neural networks. *Neurocomputing*, Vol. 20(1–3), pp. 279–294.
6. Rodrigues, J. A. D., & Filho, R. M. (1999). Production optimisation with operating constraints for a fed-batch reactor with DMC predictive control. *Chemical Engineering Science*, Vol. 54(13–14), pp. 2745–2751.
7. Shah, S., & Palmieri, F. (1990). MEKA – A fast, local algorithm for training feedforward neural networks. *Proceedings of the International Joint Conference on Neural Networks*, pp III-41–45.
8. Scheffer, R., & Filho, R. M. (2000). Training a Recurrent Neural Network by the Extended Kalman Filter as an Identification Tool. *Escape-10 Symposium Proceedings*, pp. 223–228.
9. Scheffer, R., Filho, R. M. (2001). Process identification of a fed-batch penicillin production process - training with the extended kalman filter. *Application of Neural Network and Other Learning Technologies in Process Engineering*.
10. Wan, E. A., van der Merwe, R. (2000). The unscented Kalman filter for nonlinear estimation. *Proceedings of the Symposium 2000 on Adaptive Systems for Signal Processing, Communication adn Control (AS-SPCC)*, pp. 153–159.

Контрольована онлайн-система ідентифікації на основі фільтра Калмана

Ганеш Е. Н.

Інженерний коледж ім. Савеета, м. Кутгембаккем, 600124, Індія

Анотація. Для розроблення прогностичних моделей контролерів витрачається відносно велика кількість часу та зусиль. Час окупності контролера з функцією інтелектуального прогнозування можна суттєво зменшити за наявності загальний інструменту ідентифікації, введеного до схеми контролю. У роботі була розроблена система керування, яка складається з нейронної мережі (НМ) з виключно зовнішнім повторенням, параметри якої регулюються розширеним фільтром Калмана у режимі реального часу. Вихід нейронної мережі використовується в контрольній ланці для вивчення точності контуру керування. На даний момент цей контур є контролером мінімальної дисперсії на основі НМ-моделі. Ідентифікація он-лайн системи з контролером протестована шляхом моделювання процесу виробництва пеніциліну з метою розуміння поведінки у складному середовищі. На кожному сигнальному процесі та вимірюванні застосовувався шум. Незважаючи на те, що НМ ніколи раніше не навчалась, розходження контролера не спостерігалось. Хоча онлайн-прогноз НМ був достатньо точним, реальний процес залишається досі не вивченим. Він був перевірений імітацією процесу із застосуванням НМ для отриманого кінцевого продукту. Тим не менш, цей процес тримався під контролем поруч із встановленими «розумними» точками. Отримані результати свідчать про перспективні спроби моделювання інтелектуальних контролерів із використанням методу он-лайн ідентифікації, що значно вкорочує час реалізації.

Ключові слова: фільтр Калмана, нейронна мережа, онлайн-навчання, варіативний контроль.

UDC 60:620:004.9:006

Big Data Approach Application for Steel Pipelines in the Conditions of Corrosion Fatigue

Skrynkovskyy R. M.[1], Yuzevych L. V.[2, 3], Ogirko O. I.[4], Pawlowski G.[5*]

[1] Lviv University of Business and Law, 99 Kulparkivska St., 79021 Lviv, Ukraine;
[2] Lviv Polytechnic National University, 12 Stepana Bandery St., 79013 Lviv, Ukraine;
[3] Karpenko Physico-Mechanical Institute of the NAS of Ukraine, 5 Naukova St., 79060 Lviv, Ukraine;
[4] Lviv State University of Internal Affairs, 26 Horodotska St., 79007 Lviv, Ukraine;
[5] Zaklad Handlowo-Uslugowy BHP, 17 Kostrzynska St., 69-113 Gorzyca, Poland

Abstract. This paper presents results of the use of Big Data approach and neural network for the pipelines diagnosis problem. In this case the pipeline is in the conditions of crack growth of corrosion fatigue and exposed to hydrogen. It is proposed to use graphene protective coatings. The mathematical model for estimating the changes in the effective surface energy of WPL during plastic deformation, electrochemical overstrain, polarization potential and current density of the metal dissolution reaction at the top of the crack on the pipeline surface during its mechanical loading in an aqueous electrolyte solution is given. The dissolution of the metal is considered on the juvenile surface, taking into account the anode and cathode regions based on the approaches of surface physics and electrochemistry. An element of a mathematical model is a quality functional, taking into account information flows and a sensitivity coefficient. Functional quality is used to specify the feedback between the investment project methodology and risk estimates, as well as to optimize the information flows of enterprises and improve the system of protection of metallic underground pipelines that operate under conditions of corrosion fatigue. The purpose of this project is to improve the relevant regulatory and technical documents as well as software.

Keywords: gas pipeline, monitoring, fatigue crack, corrosion, databases, Big Data, neural network, intelligent software, hardware, databases.

1 Introduction

The problem of unstructured data is related to the separation of sources, their format and quality [1, 2].

Underground metal gas pipelines that come in contact with soil electrolyte can be taken as an example. Thermomechanical processing allows the yield strengths of pipe steels to be tailored through combinations of grain refinement, precipitation hardening (micro-alloying) and phase transformations [3].

Places of maximum stresses are the tips of cracks in the metal. Near the tips of cracks appears the influence of hydrogen. The influence of hydrogen leads to hydrogen embrittlement. That can be dangerous for metal pipelines.

Once hydrogen has been absorbed into the steel at the crack tip, the mechanism(s) responsible for material damage resulting from electrochemical and gaseous charging will be similar with most of the experimentally observed differences resulting from differences in the thermodynamics and kinetics of the dissociation reactions influenc-

ing the activity of the atomic hydrogen in the crack tip process zone [3].

Control of pipelines and technical equipment should take the standards, other regulatory documents, criteria of strength and reliability into account. In result, researchers will receive large amounts of unstructured data (Big Data).

It is necessary to create new methods for analyzing flows of information and chemical components for correct organizing, integrating and processing large data of underground piping systems. This is a problem of research.

2 Literature Review

Experienced pipeline operators utilize Magnetic Flux Leakage (MFL) sensors to probe oil and gas pipelines for the purpose of localizing and sizing different defect types [4]. A large number of sensors is usually used to cover the targeted pipelines. The sensors are equally distributed

Journal of Engineering Sciences, Volume 5, Issue 2 (2018), pp. E 27–E 32

E 27

around the circumference of the pipeline; and every three millimeters the sensors measure MFL signals [4]. Thus, the collected raw data is so big that it makes the pipeline probing process difficult, exhausting and error-prone. Machine learning approaches such as neural networks have made it possible to effectively manage the complexity pertaining to big data and learn their intrinsic properties [4]. Discriminant features, which characterize different defect depth patterns, are first obtained from the raw data. Neural networks are then trained using these features. The Levenberg-Marquardt back-propagation learning algorithm is adopted in the training process, during which the weight and bias parameters of the networks are tuned to optimize their performances [4].

The real-time text processing pipeline using open-source big data tools which minimize the latency to process data streams, explain it and evaluate is proposed in paper [5]. Proposed data processing pipeline on Apache Kafka for data ingestion, Apache Spark for in-memory data processing, Apache Cassandra for storing processed results, and D3 JavaScript library for visualization is new technology [5]. Apache Kafka is a distributed data transfer system that allows to process large amounts of data in real-time. The effectiveness of the proposed pipeline under varying deployment scenarios to perform sentiment analysis using Twitter dataset is evaluated [5].

A novel model for reasoning across components of Big Data Pipelines in a probabilistically well-founded manner is proposed [6]. The interaction of components as dependencies on an underlying graphical model is presented. Different message passing schemes on this graphical model provide various inference algorithms to trade-off end-to-end performance and computational cost. The framework with an efficient beam search algorithm is instantiated. That demonstrates its efficiency on two Big Data Pipelines: parsing and relation extraction [6].

An infrastructure for parallel analyzing big data in order to search, pattern recognition and decision-making based on the use of the Boolean metric of cyberspace measurement is proposed [7]. It is characterized by using only logical operation for determining the cyber-distance by means of cyclic closing at least one object, which allows significantly increasing the speed of analysis of large data [7].

Formulation of the research goals

The purpose of this study is to organize and integrate informative resources of Big Data in the system of a gas pipeline and cathodic protection device and corresponding technological, physical and chemical processes.

System of objects and processes

The objects of a gas transport system (GTS): metallic pipes; metallic and dielectric coverages; devices of cathode defence; devices of anodic defence; compressors; devices of diagnostics and control are considered. Additional objects of research: standards and other normative documents; software; technological, physical and chemical processes for the enumerated objects and processes characteristic large amount of information (Big Data) are taken into consideration.

A problem of the Big Data obtained during diagnosis of underground gas pipelines (UGP) and devices by means of contactless current measurements (CCM) is raised [8].

3 Research Methodology

3.1 Mathematical modeling of pipelines in the conditions of corrosive fatigue

The presence of fatigue cracks on the surface of metallic underground pipelines emphasise the problem of calculation values of strength characteristics at the action of corrosive environments that did not find the complete decision nowadays. In this connection it is necessary to correct the row of defects and normative and technical documents related to insufficient actuality of corresponding.

In normative documents from exploitation of construction elements on this time the reasonable norms of legitimate values of corrosive damages, reduction of bearing strength of construction elements are absent. It creates complications in the ground of normative terms of exploitation and evaluation of the maximum state of metallic constructions, in planning of charges on exploitation of construction elements and repair and restoration work.

An object of researches is underground metallic pipelines that are in the conditions of corrosion-fatigue destruction. The subject of a study is normative document. It is expedient to specify and perfect on the basis of the information acquiring of results monitoring of underground metallic pipelines functioning.

It is important to formulate the criterion and scientifically reasonable recommendations for providing of quality of underground metallic pipelines exploitation in the conditions of fatigue and influence of aggressive environment, and also forming of normative principles in sphere of pipeline transport.

Only underground main gas pipelines in the ground electrolyte in the conditions of low cycle fatigue should be considered. For the improvement of normative documents it is expedient to build a complex mathematical model, which will unite the physical and chemical model of corrosion-fatigue processes, model of piling up description of damages in metals and theory of risks elements.

Equation that binds length of fatigue corrosive crack and amount of cycles of loading to the coefficient of intensity of mechanical tensions is used for the modeling of speed increasing of fatigue crack on the middle rectilinear area of kinetic curve. Corresponding equation is improved for a metal in corrosive environment and the pH-value of environment. The electrode potential of metal is also taken into account.

For the base model of damage accumulation for metals in the conditions of irregular deformation based on the curvilinear change of damages model and energetic characteristics are used near description of process of low cycle fatigue. It is a base on criterion of fatigue strength.

Critical specific work that answers the origin of fatigue crack is included in a criterion.

Equation, power descriptions of metal and function of relative value of amplitude intensity of tensions, that characterizes the degree of mechanism influence of fatigue on the fatigue curve is also used for description of the irregular cyclic loading of metal. Evolutional equation is written in for the modeling of low cycle fatigue of metals.

Correlation for description of low cycle corrosion fatigue of material in metallic underground pipelines is complemented by equations for the evaluation of risks within the limits of investment project that executes corresponding organization (enterprise).

The functional of quality is used for receiving a feedback in methodology of risk evaluation of investment project and for optimization of informative streams of enterprise and improvement of the defence system of metallic underground pipelines from a corrosive fatigue. The aim of that application is the improvement of the corresponding normative and technical providing and software.

In zones with non-stationary plasticity strain it is expedient to use the criteria of adhesion strength, biocorrosive aggressiveness of soils, mechanical criterion for the coefficient of intensity of tensions (the overstrain of corrosive process takes into account), the criterion of corrosive stability of pitting, criterion correlation for the evaluation of speed of stability corrosion of metal in the defect of isolating coverage together with entered by diagnostic weight of signs and diagnostic value of inspections, that will complement, specify and perfect the system of the corrosive monitoring of pipelines and be used for control of corrosive process. With their help described and regulated by a state standard optimization of terms of construction elements defence of oil and gas industry can be conducted.

As a result a new complex mathematical model in relation to upgrading of corrosion protection of metallic underground pipelines from positions of corrosion fatigue, electrochemistry, physics of surface processes, mechanics of destruction and theory of risks is offered. The conducted modeling takes piling up of damages in metals into account and allows to study the mechanisms of distribution of corrosive fatigue cracks in underground metallic pipelines that are in aggressive environments, in particular, in saltwater and ground electrolyte. The results of mathematical modeling are the basis of methodology development and improvement of normative and technical documents for metallic underground pipelines, that are under the action of the regular and irregular cyclic loading in the conditions of low cycle corrosive fatigue.

The joint use of corrosive fatigue criteria and corrosive monitoring criteria of pipelines offered in this article will allow to study in detail the mechanisms of distribution of corrosive fatigue cracks in underground metallic pipelines that are in aggressive environments from positions of corrosive fatigue, electrochemistry, physics of surface processes, mechanics of fracture and theory of risks.

For optimizing information flows P_k the functional of quality $J(P_k, FB(P_k))$ with calculation for sensitivity coefficient β is used [9]:

$$J(P_k, FB(P_k)) = \int_{t_0}^{t_k} f(\bar{y}, \bar{u}, \bar{s}, \beta) dt \Rightarrow opt, \qquad (1)$$

where $\bar{y}$ – vector of specific impacts ($y_j(t)$ – vector components (key parameters for the GTS), $j = 1, 2, \ldots, n$); $\bar{u}$ – control vector of information flows; $\bar{s}$ – vector of indeterminate perturbations; P_k – information flows for the GTS and security system ($k = 1, 2, \ldots, m$); m – total number of information flows P_k considered in the given GTS; $[t_0, t_k]$ – time interval, in which the process is considered (formation of optimal values of parameters corresponding to P_k; $f(\bar{y}, \bar{u}, \bar{s}, \beta)$ – function reflecting quality index; β – sensitivity coefficient; $FB(P_k)$ – function characterizing inverse relationship between flows P_k and project's environment with accounting for sensitivity coefficient β and expert opinions; opt – optimization symbol; t – time.

3.2 GTS protection system and Big Data

To protect the system (GTS) and related software, we recommend using the scientific work algorithm [10].

This algorithm (stages) allows the following [10]:

1. The data owner describes which data user will grant the access to certain data under specified constraints, and generates a policy rule, then sends the rule to the trusted authority.

2. The data owner encrypts the data with the encryption key, and then stores encrypted data in the database.

3. The encrypted data is sent into the Kafka cluster which is comprised of one or more servers each of which is called a broker.

4. The data consumer sends a request to the trusted authority for data access, which involves passing on the sticky policy.

5. The trusted authority checks policies, potentially including challenges to the data user.

6. If all the policy checks are fulfilled and validated, the trusted authority releases the private decryption key to the data consumer.

7. The data consumer can get the encrypted data from the kafka and decrypt it by using the decryption key.

3.3 Prospect of pipelines defence from corrosion with the help of graphene coverages

Graphene layers as corrosion resistant films are presented [10]. Mild steel coupons were coated from the synthesized graphene solution. Three layers of graphene films were able to reduce the corrosion rate by 99 % [11].

Further work needs to be done to test the durability of the graphene films and its resistance to corrosion with respect to time [12].

Besides having a unique mechanical and electronic properties [12], graphene coating has broad prospects for practical application in specific structural and functional materials [12, 13].

4 Results

An object of the research is the metal under mechanical stress with a surface crack in aqueous electrolyte solution. Destruction of passive films, a juvenile surface (JS) with width δ and zone of plastic deformation occurs at the crack tip under the action of stress [14]. A geometrical parameter δ at the crack tip in a first approximation is interpreted as its opening δ_{lC}. The crack tip and, in particular, JS spreads into the depth of body under mechanical stress and corrosive environment. The cathodic and anodic electrochemical reactions occur at the crack tip region. Corrosive dissolution corresponds to the anodic reaction of metal. The crack tip (JS) is interpreted as an anode (A), beyond it on sides it is interpreted as a cathode area (K) [14]. The system "A − K" presents an electrochemical pair.

On the basis of the correlations [14] coefficient of stress intensity (KSI) K_{1SCC} is related to crack opening δ_{lC} and overstrain ζ of reaction of dissolution of metal by next formulas (2):

$$K_{1SCC} = \sqrt{\frac{E}{1-v^2} \cdot \left(WPL - z_{si} F \rho \delta \frac{\zeta}{M} \right)} = \sqrt{E \cdot \sigma_T \cdot \delta_{1C}}, \quad (2)$$

where z_{si} – microcrack, m; M – is molecular mass of metal, g·mol^{-1}; K_{1SCC} – is a threshold value KSI, that is minimum value that corresponds to the beginning of corrosion crack propagation; WPL – is specific energy spending on the plastic deformation of surface layer of body during formation of new (juvenile) surface; E, v – is the modulus of longitudinal elasticity (Young's modulus) of material is a formal charge of the solvated ions; $F = 96\,500$ C·mol^{-1} – Faraday constant; δ – is an impending front of and Poisson's ratio.

An electrochemical overstrain is a deviation of electrode potential from its equilibrium (in relation to solution near the electrode) thermodynamics value during polarization of electrode under electric current [14].

The empiric correlation that binds KSI to WPL is set in article [14] based on research results of pin (contact) deformation of different brands of steel (Poland: 15GA, EU: 20MoCr2-2, USA: A 516-55, etc.):

$$K_{1SCC} = a_1 \sqrt{WPL} - a_2;$$
$$a_1 = 2.26 \cdot 10^8 \frac{\sqrt{N}}{m}; \quad (3)$$
$$a_2 = 6.98 \sqrt{m} \ (MPa).$$

Correlation (Kaesche) for the current density i_a in the crack tip according to the paper [14] is:

$$i_a = \frac{\alpha \cdot \chi \cdot \Delta \psi_{ak}}{\delta \cdot \ln(c/\delta)}, \quad (4)$$

where α – is an angle of the crack tip; χ – is conductivity of electrolyte; $\Delta \psi_{ak}$ – is a change of potential between anodic and cathodic parts; c – is a depth of crack. Expression (4) is submitted for a crack in a unstressed metal. In actual use of construction elements, in particular pipelines, it is necessary to take diagnostic method and

the terms of corrosion stress into account [14, 15]. Therefore correlation (4) should be generalized by addition of information about mechanical parameters and characteristics.

Correlations (1)–(4) present a mathematical model for change estimating of effective surface energy WPL during a plastic deformation, electrochemical overstrain and density of current of reaction of dissolution of metal in the crack tip on the surface of metal at its mechanical stress in aqueous electrolyte solution. Such type of research is required by the uses of Big Data.

For example we will use the experimental data that approximate dependence as Tafel correlation for the evaluation of influence of mechanical stress tension on intensity of corrosive processes in Steel 20, that is in 3 % solution of NaCl, in particular, in the crack tip in the moment of fracture of passive films, when the anodic current of i_a grows substantially [12]:

$$i_a = i_0 \exp(DE/a), \quad DE = E_0 - E_a, \quad (5)$$

where i_0 is the corrosive current; a is a Tafel parameter of anodic process; E_0, E_a is the corrosion potential and potential for anodic process. The polarization potential E_P of the metal surface (pipeline) in [8] is presented.

We will use the correlation:

$$E_P = f(DE, E_0, E_a, \zeta). \quad (6)$$

A mathematical model (1)–(6) is developed for the evaluation of surface energy of plastic deformation, overstrain, polarization potential and density of current of metal dissolution reaction in the crack tip for the metal (steel) loaded in aqueous electrolyte solution on the basis of approaches of surface physics and electrochemistry. Dissolution of metal is considered on a juvenile surface taking into account a stress intensity coefficient (KSI).

We propose to use the information of Big Data in the process of neural network spectral analysis, which is able to adapt to requirements of a specific sensor [16]. Such component features with high reliability, ability to adapt to a specific application, and usage of design principles ensuring the possibility of a simple expansion of the intelligent component potential by means of completion with new algorithmic solutions [16].

Let's formulate general information on data collection (Big Data) regarding pipelines and their processing:

1. Analysis of processes.
2. Modeling.
3. Monitoring using device БВС-К [8].
4. Data mining.
5. Optimization of information.
6. Optimization of development processes.
7. Assessment of production risks for pipelines.
8. Statistical methods of information analysis.
9. Application of methods of machine learning.
10. Obtaining stable estimates of model parameters.
11. Construction of prediction and an estimation of a resource of pipelines on the basis of the learned models.
12. Decision-making regarding repair terms.

5 Conclusions

A mathematical model (1)–(6) is developed for the evaluation of surface energy of plastic deformation, over-strain, polarization potential and density of current of metal dissolution reaction in the crack tip for the metal (steel) loaded in aqueous electrolyte solution on the basis of approaches of surface physics and electrochemistry. Dissolution of metal is considered on a juvenile surface taking into account a stress intensity coefficient.

The general principles for the selection of information concerning the monitoring of underground pipelines based on Big Data technology as a result of data processing and the corresponding algorithm are formulated.

A method of functioning of intelligent software and hardware complex for the monitoring system of a metal gas pipelines and security system using Big Data is proposed.

In this paper the Big Data methodology is improved due to functional of quality application, micro and macro processes and inverse relationships.

References

1. Chen, H., Chiang, R. H., & Storey, V. C. (2012). Business intelligence and analytics: From big data to big impact. *MIS quarterly*, Vol. 36, No. 4, pp. 1165–1188.

2. Pavlyshenko, B. M. (2016). Linear, machine learning and probabilistic approaches for time series analysis. *IEEE International Conference on Data Stream Mining and Processing (DSMP)*, Aug. 2016. doi: 10.1109/dsmp.2016.7583582.

3. Nanninga, N., Slifka, A., Levy, Y., & White, C. (2010). A review of fatigue crack growth for pipeline steels exposed to hydrogen. *Journal of Research of the National Institute of Standards and Technology*, Vol. 115, No. 6, pp. 437, doi: 10.6028/jres.115.030.

4. Mohamed, A., Hamdi, M. S., & Tahar, S. (2015). A Machine Learning Approach for Big Data in Oil and Gas Pipelines. *3rd International Conference on Future Internet of Things and Cloud*.

5. Nazeer, H., Iqbal, W., Bokhari, F., Bukhari, F., & Baig, S. (2017). Real-time Text Analytics Pipeline Using Open-source Big Data Tools. *Distributed, Parallel, and Cluster Computing*, pp. 1–6.

6. K. Raman, A. Swaminathan, J. Gehrke, and T. Joachims, "Beyond myopic inference in big data pipelines," Proceedings of the 19th ACM SIGKDD international conference on Knowledge discovery and data mining - KDD '13, 2013. doi: https://doi.org/10.1145/2487575.2487588 .

7. Hahanov, V. I., Litvinova, E. I., Chumachenko, S. V., Yemelianov, I., & Amer, T. B. (2016). Processor structures for Big Data analysis. *Radio Electronic and Computer Systems*, No. 6(80), pp. 163–175.

8. Dzhala, R. M., Verbenets', B. Y., Mel'nyk, M. I., Mytsyk, A. B., Savula, R. S., & Semenyuk, O. M. (2017). New Methods for the Corrosion Monitoring of Underground Pipelines According to the Measurements of Currents and Potentials. *Materials Science*, Vol. 52, No. 5, pp. 732–741.

9. Krap, N., & Yuzevych, V. (2013). Neural Networks as a tool for managing the configurations of tourist flow projects. *Management of Development of Complex Systems*, No. 14, pp. 37–40.

10. Thein, K. M., Nyunt, T. T., & Aye, K. N. (2017). Security of real-time Big Data analytics pipeline. *International Journal of Advances in Electronics and Computer Science*, Vol. 4, No. 2, pp. 1–5.

11. Pavan, A. S. S., & Ramanan, S. R. (2016). A study on corrosion resistant graphene films on low alloy steel. *Applied Nanoscience*, Vol. 6, No. 8, pp. 1175–1181, doi: 10.1007/s13204-016-0530-2.

12. Koman, B. P., & Yuzevich, V. M. (2015). Energy Parameters of Interfacial Layers in Composite Systems: Graphene – (Si, Cu, Fe, Co, Au, Ag, Al, Ru, Hf, Pb) and Semiconductor (Si, Ge) – (Fe, Co, Cu, Al, Au, Cr, W, Pb). *Journal of Nano- and Electronic Physics*, Vol. 7, No 4, pp. 04059-1–04059-7.

13. Novoselov, K. S., Morozov, S. V., Mohinddin, T. M. G., Ponomarenko, L. A., Elias, D. C., Yang, R., Barbolina, I. I., Blake, P., Booth, T. J., Jiang, D., Giesbers, J., Hill, E. W., & Geim, A. K. (2007). Electronic properties of grapheme. *Physica Status Solidi*, Vol. 244, No. 11, pp. 4106–4111, doi: 10.1002/pssb.200776208.

14. Yuzevych, V. M., Dzhala, R. M., & Koman, B. P. (2018). Analysis of Metal Corrosion under Conditions of Mechanical Impacts and Aggressive Environments. *Metallofizika i Noveishie Tekhnologii*, Vol. 39, No. 12, pp. 1655–1667, doi: 10.15407/mfint.39.12.1655.

15. Yuzevych, V., Klyuvak, O., & Skrynkovskyy, R. (2016). Diagnostics of the system of interaction between the government and business in terms of public e-procurement. *Economic Annals-XXI*, Vol. 160, No. 7–8, pp. 39–44, doi: 10.21003/ea.v160-08.

16. Cielen, D., Meysman, A. D. B., & Ali, M. (2016). *Introducing Data Science: Big Data, Machine Learning, and More, using Python Tools*. Manning Publications, New York, USA.

Journal of Engineering Sciences, Volume 5, Issue 2 (2018), pp. E 27–E 32

E 31

Застосування підходу Big Data для сталевих трубопроводів в умовах корозійної втоми

Скриньковський Р. М.[1], Юзевич Л. В.[2, 3], Огірко О. І.[4], Павловські Г.[5]

[1] Львівський університет бізнесу та права, вул. Кульпарківська, 99, м. Львів, 79021, Україна;
[2] Національний університет "Львівська політехніка", вул. Степана Бандери, 12, м. Львів, 79013, Україна;
[3] Фізико-механічний інститут ім. Г. В. Карпенка НАН України, вул. Наукова, 5, м. Львів, 79060, Україна;
[4] Львівський державний університет внутрішніх справ, вул. Городоцька, 26, м. Львів, 79007, Україна;
[5] Компанія "Zaklad Handlowo-Uslugowy BHP", вул. Костшинська, 17, м. Гужиця, 69-113, Польща

Анотація. У роботі подано результати використання підходів Big Data та нейронних мереж для діагностування трубопроводів. Приймаємо до уваги, що на поверхні трубопроводу знаходяться втомні корозійні тріщини і метал піддається впливу водню. Запропоновано використовувати графенові захисні покриття. Наведено елементи математичної моделі для оцінювання змін ефективної поверхневої енергії WPL під час пластичної деформації, електрохімічного перенапруження, поляризаційного потенціалу та густини струму реакції розчинення металу у вершині тріщини на поверхні трубопроводу під час його механічного навантаження у водному розчині електроліту. Розчинення металу розглядаємо на ювенільній поверхні з урахуванням анодної та катодної ділянок на основі підходів фізики поверхні та електрохімії. Елементом математичної моделі є функціонал якості з урахуванням інформаційних потоків та коефіцієнта чутливості. Функціонал якості використовуємо для конкретизації зворотного зв'язку між методологією інвестиційного проекту та оцінками ризику, а також для оптимізації інформаційних потоків підприємств та вдосконалення системи захисту металевих підземних трубопроводів, які функціонують в умовах корозійної втоми. Метою цього проекту є вдосконалення відповідних нормативних та технічних документів, а також програмного забезпечення.

Ключові слова: газопровід, моніторинг, тріщина втоми, корозія, бази даних, великі дані, нейронна мережа, інтелектуальне програмне забезпечення, апаратні засоби, бази даних.

UDC 621.3.035.4

Membrane Processes during the Regeneration of Galvanic Solution

Serdiuk V. O.[1], Sklavbinskyi V. I.[1], Bolshanina S. B.[1*], Ivchenko V. D.[2], Qasim M. N.[3], Zaytseva K. O.[1]

[1] Sumy State University, 2 Rymskogo-Korsakova St., Sumy 40007, Ukraine;
[2] Sumy National Agrarian University, 160 H. Kondratieva St., Sumy 40021, Ukraine;
[3] Institute of Technology, Middle Technical University, Baghdad, Iraq

Abstract. The process of Cd^{2+} and Zn^{2+} cations transfer through the cation exchange membrane RALEX®CM-PES 11-66 in double-chamber electrolyzer was investigated. Anodic chamber electrolyte (analyte) contained model solutions which imitates galvanic baths composition for passivation processes. The analyte contained 50 g/l sodium dichromate and 10 g/l sulfuric acid as main substances and impurities of Cd^{2+} and Zn^{2+} cations in amount of 2.5 g/l of each. The electrolyte of cathode chamber is catholyte, contained 1 % solution of sulfuric acid. The titanium grade BT-0 and lead grade C-0 were used as cathode and anode respectively. Cathode processes connected with processes of ion migration through the membrane and metal release on cathode were studied. The creation of volt-ampere curves in galvanodynamic mode was supplied by impulse potentiometer, tool for combined measurements and silver chloride reference electrode. An increase of cathode overvoltage in the presence of cadmium ions and decrease of cathode potential with the increase of temperature were proved. The pH range for intensive reduction of metals was determined during investigations. Scanning electron microscopy with X-ray analysis was used for estimation of cathode deposits elemental composition. It was established that metal atoms of cadmium and zinc were presented in cathode deposits. Transference numbers of ions through cationic membrane were calculated for cadmium and mixture of cations proved the effectiveness of chromium and zinc ions extraction from chromium containing solutions. This process provides regeneration of galvanic solutions and maintains stable composition of passivation bath.

Keywords: electrolysis, galvanic solution, ion-exchange membrane, chromium-containing solution, cadmium cations, zinc cations.

1 Introduction

High aggressivity of hexavalent chromium-based solutions in galvanic production sewage waters causes significant environmental hazard. The Cr^{6+} compounds have toxic properties, take mutagenic and carcinogenic impact on living organisms [1, 2]. The sources of such pollution are not only flushing waters, but also exhausted concentrated solutions of process baths [3]. The examples can be brightening and passivating bath solutions containing up to 100–200 g/l of hexavalent chromium compounds. Active employment of such baths results in hexavalent chromium reduction, while solutions accumulate heavy-metal ions. At the same time, the ratio of the essential components in these baths changes, that entails the need for adjustment by adding new portions of reagents. That leads to instability in bath operation and declining quality of coating [4]. In order to eliminate those defects, the contents of the baths must be replaced, while exhausted concentrated solutions are liable to be discharged into sediment tanks. The volley character of emptying doesn't allow treating facilities to neutralize toxic wastes completely that causes the risk of environmental pollution. Besides, when discharging hexavalent chromium compounds as a waste, the enterprise irretrievably loses the valuable component necessary for technological operations in the electroplating shop. The high level of solution contamination resulted from electroplating production, the presence of numerous organic compounds make it difficult to use reverse osmosis. The development and implementation of membrane-type electrochemical devices with the simultaneous return of the valuable components into production (in the form of commercial products and secondary raw materials) has been the only radical solution to the emerging problem so far. In this case, electrolysis with ion-exchange membranes is the most perspective treatment for such runoff [5, 6].

The electromembrane processes can be found in the submersible electrochemical modules. The feature of the processes taking place in these devices consists in the fact

that the separation of the components occurs with the help of anionic or cationic membranes within the electrolytic module [7, 8]. Regeneration is carried out in batch-type electrolysers (electrolytic cells) with the premium brand membranes (MK-40, MA-40) [9]. Process solutions of rinsing baths or sulfuric acid solutions [3] are used as catholyte and anolyte depending on the type of electrolyser and the purpose of the process. Electrolysis is carried out using anodes and cathodes manufactured from different materials (e. g. platinized titanium, lead, steel) [10, 11].

In order to research the impact of individual technological parameters on membranous electrolyser operation, the given research explores the voltampere characteristics of the cathode and anode process, as well as the influence of temperature, electrolyte composition and medium acidity on the migration and electrochemical reduction of metal ions. Modeling of electrolyte composition proceeded from the features of the processes in real galvanic passivating baths [11]. These processes require the solutions with hexavalent chromium compounds. In such solutions as a result of operation hexavalent chromium gets reduced to Cr^{3+} from chromate (CrO_4^{2-}) and dichromate ($Cr_2O_7^{2-}$) ions, while work zinc or cadmium coating dissolves. Consequently, ions of trivalent chromium and dissolving metal get accumulated in the solutions in accordance with the reaction equations (1) and (2):

$$3Zn + 2CrO_4^{2-} + 16H^+ \rightarrow 3Zn^{2+} + 2Cr^{3+} + 8H_2O; \quad (1)$$

$$3Cd + Cr_2O_7^{2-} + 14H^+ \rightarrow 3Cd^{2+} + 2Cr^{3+} + 7H_2O. \quad (2)$$
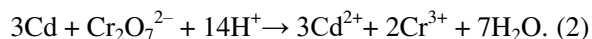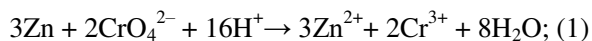
The accumulated ions of heavy metals, trivalent chromium with simultaneous deacidification make these solutions unserviceable. Considering the composition of passivating baths, as well as availability of the mentioned zinc [12, 13] and cadmium ions and trivalent chromium there, bath compositions were modeled under laboratory conditions by adding the defined amounts of salts of the specified metals to electrolyte which was subjected to electromembrane process [3, 14].

Due to the abovementioned, the objective of the work is to study the electrochemical regularities of membrane electrolysis of chromium-containing solutions which will allow to multiply the lifetime of galvanic baths and prevent the entry of toxic Cr^{6+} ions into the environment.

2 Research Methodology

In order to study the effect of different parameters on chromic solutions regeneration, the two-chamber electrolyser MECk (electrochemical cationic module) was produced inclusive of anode and cathode chambers separated by a cation-exchange membrane (Figure 1).

The external anode was dipped into the anode chamber that simulated a passivating bath. The cation-exchange membrane RALEX®CM-PES 11-66 was installed so that it formed one of the cathode chamber walls from the anode side. Filter cloth was tightly attached to the membrane from the anode side. The presence of filter cloth prevented from rapid membrane blinding [7].
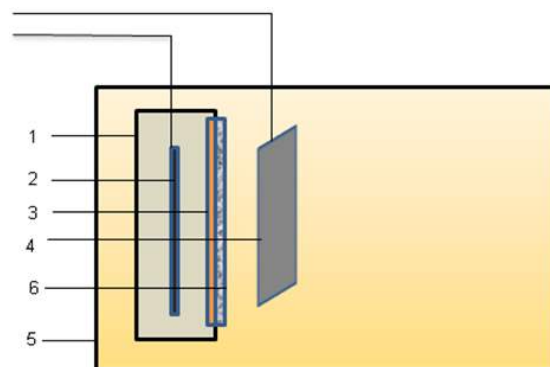
Figure 1 – The diagram of membrane external-anode electrolyser: 1 – cathode chamber body; 2 – internal electrode-cathode; 3 – ion-exchange membrane; 4 – external electrode-anode; 5 – chromic solution chamber; 6 – filter cloth

The anode material is lead (C2 grade), the cathode material is titanium. Cathode and anode areas are $S_K = 0.3$ dm^2 and $S_A = 0.72$ dm^2 respectively. The 10 dm^3 anode chamber was filled with chromic solution of the following concentration: $Na_2Cr_2O_7 - 50$ g/l, $H_2SO_4 - 10$ g/l. In order to simulate the bath operating conditions, cation-containing compounds of the respective metals Zn^{2+}, Cd^{2+} and Cr^{3+}. were added to anodic solution. The content of the added ions in anodic solution (anolyte) complied with the concentration of 2.5 g/l for each ion. The 1 dm³ cathode chamber was filled with cathode liquor (catholyte) – 1 % sulfuric acid solution. Electrolysis was carried out at current density of 0.3–3.0 A/dm^2 and 3–9 V voltage. Throughout the process, the catholyte's pH was being monitored. Cathode deposit was examined by scanning electron microscopy.

3 Results

As a primary method for studying electrical reduction of metal ions in chromic solution, we used the voltammetry method with linear potential sweep. Voltammograms were recorded in a galvanic-dynamic mode by means of the PI-50-1.1 pulse potentiostat and the Victor VC88C multimeter. To measure electrode potential drop, a silver-chloride reference electrode was employed [13]. The measurement results showed that with current strength growth, the anode potential changed insignificantly (no more than 0.1–0.2 V). The anode process is related to oxygen release and partial oxidation of trivalent chromium ions in $Cr_2O_7^{2-}$ [1].

Voltammograms of zinc and cadmium reduction on the cathode in the cathode chamber are presented in Figure 2.

Voltammograms of zinc and cadmium reduction on the cathode in the cathode chamber are presented in Figure 2. As follows from the graphs of electrode potential shift dependencies on current density, the presence of metal cation impurity reduces the overvoltage on the cathode (curves 2 and 3). However, it should be noted that the contribution of each of metal ions to the general decline in overvoltage is not the same.
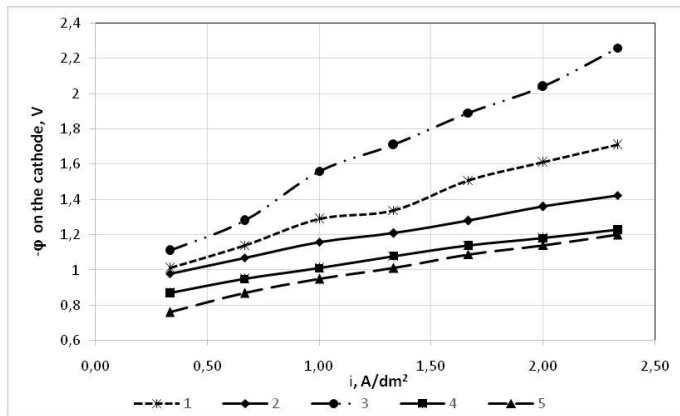
Figure 2 – Voltammogramsof cathodic electroreduction of metalsattheir migration through a cation-exchange membrane: 1, 2, 3 – at electrolyte temperature of 14 °C; 4, 5, 1 – at 30 °C – an anolyte does not contain metal ions able to be deposited on the cathode; 2 – anolyte additionally contains Zn^{2+} ions (2.5 g/l); 3 – anolyte additionally contains Zn^{2+} ions (2.5 g/l) and Cd^{2+} (2.5 g/l); 4 – anolyte does not contain metal ions able to be deposited on the cathode; 5 – anolyte additionally contains Zn^{2+} ions (2.5 g/l)

Figure 3 presents voltammograms for electrolytes separately containing zinc and cadmium cations 1 and 2 respectively. As can be seen, the presence of cadmium ions significantly extends the cathode potential which seems to be connected with the increased conductivity of electrolyte.

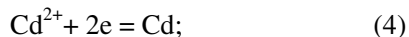Besides, the cathodic process is affected by the temperature (Figure 2). As the temperature rises, the electrolytic conductivity increases. This is connected with the reduced viscosity of solution (thinning) and increased mobility of ions. In addition, the increased temperature stimulates the increased number of active ions, contributes to the decrement of the effective radius of ions as a result of their shells dehydration.

The increase in electroconductivity reduces cathodic polarization (Figure 2, curves 4, 5). Electrode depolarization provides more active product deposition.

While studying the chemism of the ongoing electrode reactions, we can assume the resulting products. Thus, the following reactions can occur on the cathode and in cathode liquor (catholyte) during the electricity flow:

$$Zn^{2+} + 2e = Zn; \qquad (3)$$

$$Cd^{2+} + 2e = Cd; \qquad (4)$$

$$2H_3O^+ + 2e = H_2 + 2H_2O; \qquad (5)$$

$$2H_2O + 2e = H_2 + 2OH^-. \qquad (6)$$

Trivalent chromium ions which are generated in the process of chrome plating in anodic solution in practice are not expected to pass to catholyte or be deposited on the cathode. They oxidize on the anode forming $Cr_2O_7^{2-}$ [9]. However, as our research has shown, insignificant amounts of chromium compounds can still migrate to the cathode, but their presence is not more than 1 % of the total amount of precipitate on the cathode (Figures 4, 5).
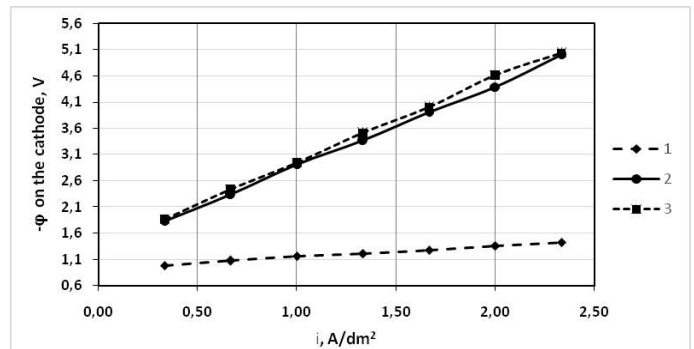
Figure 3 – Voltammograms of cathodic electroreduction of metal sat their migration through a cation-exchange membrane at electrolyte temperature of 14 °C: 1 – anolyte contains Zn^{2+} ions (2.5 g/l); 2 – anolyte contains Cd^{2+} ions (2.5 g/l); 3 – anolyte contains Cd^{2+} ions (2.5 g/l), Zn^{2+} ions (2.5 g/l) and Cr^{3+} ions (2.5 g/l)

As can be seen from the above-mentioned reactions, 5 and 6 cause the change in cathodic pH medium. Change in catholyte's acidity, its shift towards the alkaline side, leads to the drop of electrical conductivity of solution and formation of flaked insoluble metal hydroxides that result in module efficiency decrement.

X-ray microanalysis conducted using the scanning electron microscope REM-106-i (manufactured by "SELMI", Ukraine) allowed determination of chemical elements in the samples of the studied cathodic deposits on the basis of energy values of the characteristic X-ray peaks of each chemical element [15, 16]. To determine the elementary composition the samples were placed on a double-sided carbon adhesive tape. The prepared samples were placed in the electron microscope and examined at accelerating 20 kV voltage in the secondary-electron mode within the range of electro-optical magnification from 600 to 6 000 times (Figures 4, 5).

The accomplished analysis of cathode deposits formed at module operation with electron microscopy employment demonstrated that there were metal atoms in deposits which initially had not been available within catholyte. The spectrograms display the metals that were added to dichromate anodic solution – namely, cadmium and zinc. Their percentage in the deposit reaches 95–98 %. It should be noted that in case of their joint presence, cadmium content as much as 2 times exceeds zinc content. As to chromium, its presence in the deposit makes only a fraction of a percent and is considered to be negligible [11] (Table 1).

For the purpose of setting optimal pH values in catholyte, the change in the solution acidity in the process of electrolysis was under investigation. Simultaneously, the research of cathodic deposition products in the form of deposited metal was carried out at current strength of 0.7 A over the period from 1 up to 12 hours. The corresponding results are presented in Table 1.
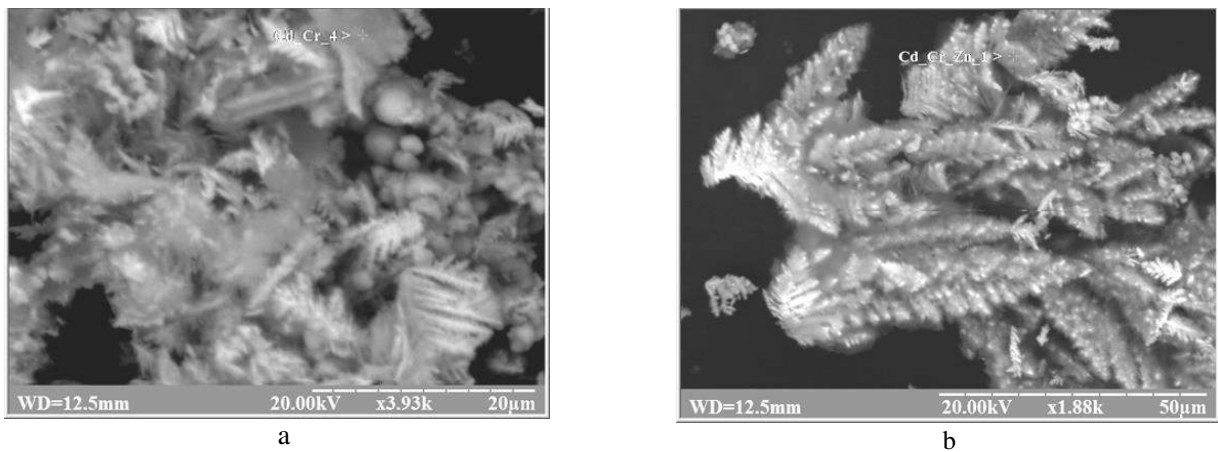
Figure 4 – REM photographs of cathodic deposit samples when the module is operated: a – anodic solution (anolyte) contains Cd^{2+} ions (2.5 g/l); b – anolyte contains Zn^{2+} ions (2.5 g/l) and Cd^{2+} (2.5 g/l)

a

b

Figure 5 – Spectrograms of cathode deposit samples and the results of microanalysis: a – the anolyte contains Cd^{2+} ions (2.5 g/l) (Figure 4 a); b – the anolyte contains Zn^{2+} ions (2.5 g/l) and Cd^{2+} (2.5 g/l) (Figure 4 b)

Table 1 – Changes in the catholyte acidity and the mass of metals deposited on the cathode at electrochemical module operation

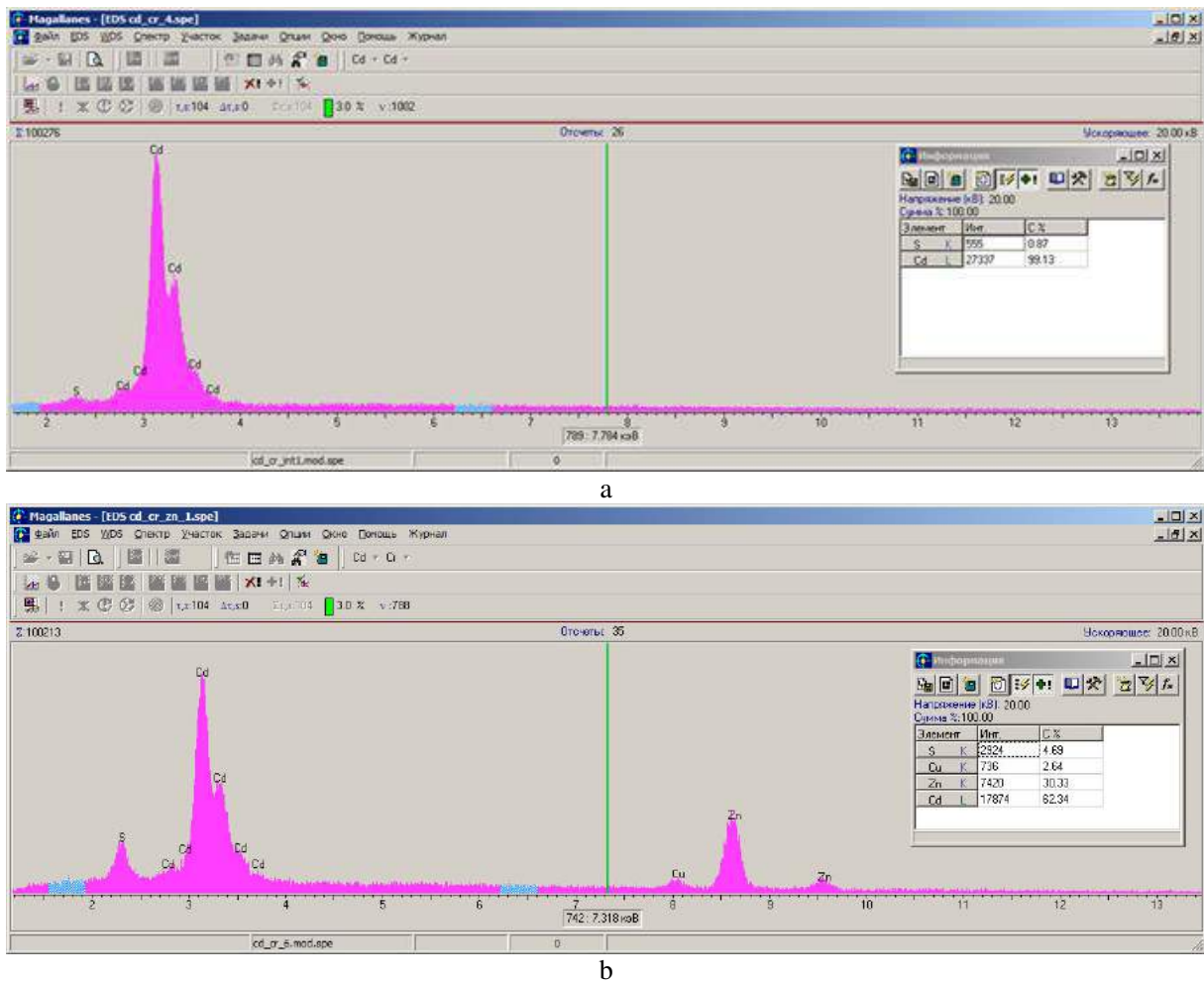| Module operating time	Catholyte pH value		Masses of metals on the cathode, (operational)	
	Anolyte with the only impurity of Cd^{2+}	Anolyte with the impurities of $Zn^{2+}, Cd^{2+} Cr^{3+}$	Anolyte with the only impurity of Cd^{2+}	Anolyte with the impurities of $Zn^{2+}, Cd^{2+} Cr^{3+}$
1	1.00	1.00	0.000	0.00
3	1.30	1.30	0.020	0.02
6	1.41	1.50	0.080	0.15
9	1.61	1.65	0.253	0.37
12	2.07	1.86	0.333	0.47

From the values presented in the table, it is possible to determine that the greatest amount of deposited metal is observed at 1.5–1.8 pH values. This corresponds to the highest electrical conductivity of catholyte solution. At a pH less than 1.5, hydrogen is actively reducts at the cathode which interferes with the metal recovery process, and at pH greater than 1.8-2, insoluble metal hydroxides begin to form in the catholyte which also inhibits with the process. Over 12 hours of module operation, the cathodic pH increases insignificantly. It should be noticed that over the next 3 hours (13th, 14th and 15th hour) pH rises dramatically up to 5-6. At the same time the release of metal on the cathode practically ceases and the presence of insoluble hydroxides in the catholyte increases [14]. In this case metal deposition on the cathode is practically terminated, whereas the presence of insoluble hydroxides in cathode liquor increases. Matching of yield of metal resulting from electrolysis for every 3 hours with the change in catholyte pH is presented on the diagram (Figure 6).
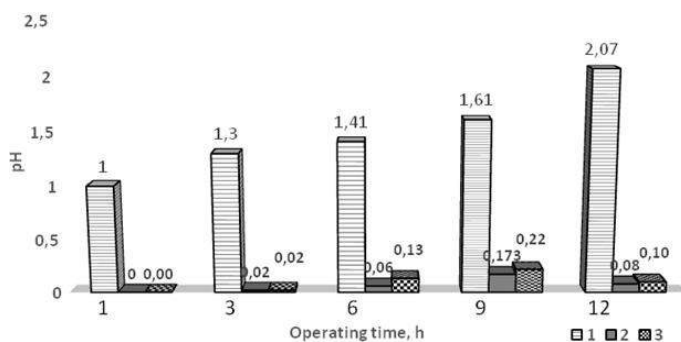
Figure 6 – Change in catholyte pH and mass of metals deposited on the cathode over the periods of module operation: 1, 3, 6, 9, and 12 hours at the electrolyte temperature of 14 °C:
1 – catholyte pH; 2 – anolyte contains Zn^{2+} ions (2.5 g/l);
3 – anolyte contains ions of Zn^{2+} (2.5 g/l) and Cd^{2+} (2.5 g/l)

The data presented in Table 1 and Figure 6 makes it possible to calculate the numbers of metal ion transfer from the regenerated solution (anolyte) to catholyte. The transfer numbers of metal ions from the anolyte to the catholyte through the cation-exchange membrane were calculated taking into account the change of the volumes of these solutions. In the electrolysis process the volume of the catholyte was slightly increasing and the anolyte volume was decreasing, which is due to the migration of water. The ion transfer numbers for both cadmium and a mixture of cations are 0.011–0.009 respectively. In spite of this, about 13 % of cadmium and 11 % of cadmium and zinc ions were removed during 12 hours of the module operation when they were both in the anolyte.

4 Conclusions

The investigation of the electrolysis of chromium-containing solutions using a module with a cation-exchange membrane showed that this process allows the solution to be regenerated by extracting metal ions that contaminates it. The study of the specific indicators and characteristics of this process showed the following.

Volt-ampere characteristics taken in galvanostatic mode indicate a significant overvoltage at the cathode in the presence of metal ions (Cd^{2+}), which is due to the membrane resistance.

Temperature affects the cathode potential. With the temperature increasing, the polarization of the cathode decreases, that contributes to a more efficient conduct of the process.

Using the method of electron microscopy with the functions of X-ray phase microanalysis it is established that cadmium and zinc metal atoms are present in the composition of cathode deposit that were in the anolyte as impurities.

The cathode metal reduction depends on the medium acidity. In the course of the research, the pH interval was assigned at which the process of electrolysis is the most intensive. It corresponds to the values of 1.5–1.8. With the further pH increasing the electrolyte conductivity decreases due to the formation of insoluble hydroxides in the catholyte. Besides, it should be noticed, that metal reduction is complicated by a parallel cathodic reaction – hydrogen release, especially at a pH of less than 1.3.

The efficiency indicators of cadmium and zinc ions extraction from chromium-containing solutions allows to maintain a stable composition of the baths and completely to eliminate the discharge of toxic substances and heavy metal compounds into the sewage.

References

1. Qian, Y., Huang, L., Pan, Y., Quan, X., Lian, H., & Yang, J. (2017). Dependency of migration and reduction of mixed $Cr_2O_7^{2-}$, Cu^{2+} and Cd^{2+} on electric field, ion exchange membrane and metal concentration in microbial fuel cells. *Separation and Purification Technology*, Vol. 192, No. 9, pp. 78–87, doi: 10.1016/j.seppur.2017.09.049.
2. Bolshanina, S. B. (2016). Chemical Industry in Ukraine, Vol. 1 (132), pp. 13 [in Russian].
3. Yao, Y., Wei, Q., Sun, M., Chen, Y., & Ren, X. (2013). The Royal Society of Chemistry, Vol. 3, Art. no. 13131.
4. Bolshanina, S. B., Ablieyeva, I. Yu., Kyrychenko, O. M., Altunina L. L., Klimanov O. B., & Serdiuk, V. O. (2016). Method of Electrolytic Regeneration of Chromium-Containing Solutions. Patent of Ukraine, No. 109623, MPC (2006.01) C02F 1/46.
5. Benvenuti, T., Krapf, R. S., Rodrigues, M. A. S., Bernardes, A. M., & Zoppas-Ferreira, J. (2014). Recovery of nickel and water from nickel electroplating wastewater by electrodialysis. *Separation and Purification Technology*, Vol. 129, No. 29, pp. 106–112, doi: 10.1016/j.seppur.2014.04.002.
6. Dimitris, P., Zagklis, E. C., Arvaniti, V. G., et al. (2013). Sustainability analysis and benchmarking of olive mill wastewater treatment methods. *Journal of Chemical Technology and Biotechnology*, Vol. 88, pp. 742–750.
7. Kruglikov, S. S., & Kolotovkina, N. S. (2013). Electroplating and Surface Treatment, Vol. 21, No. 3, pp. 63 [in Russian].
8. Kruglikov, S. S., Kolotovkina, N. S., et al. (2008). Electroplating and Surface Treatment, Vol. 16, No. 1, pp. 34 [in Russian].
9. Nekrasova, N. E., Nevmyatullina, Kh. A., Kharin, P. A., & Kruglikova, E. S. (2016). Application of a two-chamber immersion electrochemical module for increasing the stability of a lead anode in aggressive media. *Electroplating and Surface Treatment*, Vol. 24, No. 1, pp. 22.
10. Turek, M., Mitko, K., Chorazewska, M., & Dydo, P. (2013). Use of the desalination brines in the saturation of membrane electrolysis feed. *Desalination and Water Treatment*, Vol. 51, pp. 2749–2754.
11. Davoudi, M., Gholami, M., Naseri, S., Mahvi, A. H., Farzadkia, M., Esrafili, A., & Alidadi, H. (2014). Application of electrochemical reactor divided by cellulosic membrane for optimized simultaneous removal of phenols, chromium, and ammonia from tannery effluents. *Toxicological and Environmental Chemistry*, Vol. 96, Issue 9, pp. 1310–1332.
12. Carrillo-Abad, J., Garcia-Gabaldon, M., & Perez-Herranz, V. (2017). pH effect on zinc recovery from the spent pickling baths of hot dip galvanizing industries. *Separation and Purification Technology*, Vol. 177, No. 28, pp. 21–28.
13. Abbasi-Garravand, E., & Mulligan, C. N. (2014). Using micellar enhanced ultrafiltration and reduction techniques for removal of Cr(VI) and Cr(III) from water. *Separation and Purification Technology*, Vol. 132, No. 20, pp. 505–512.
14. Hu, Ch.-Y., Shih, K., & Leckie, J. O. (2010). Formation of copper aluminate spinel and cuprous aluminate delafossite to thermally stabilize simulated copper-laden sludge, *Journal of Hazardous Materials*, Vol. 181, Issue 1, pp. 399–404.
15. Durgun, I., & Ertan, R. (2014). Experimental investigation of FDM process for improvement of mechanical properties andproduction cost. *Rapid Prototyping Journal*, Vol. 20, Issue 3, pp. 228–235, doi: 10.1108/RPJ-10-2012-0091.
16. Wenner, S., Jones, L., & Marioara, C. D., Holmestad, R. (2017). Atomic-resolution chemical mapping of ordered precipitates in Al alloys using energy-dispersive X-ray spectroscopy, *Micron*, Vol. 96, pp. 103–111, doi: 10.1016/j.micron.2017.02.007.

Мембранні процеси при регенерації гальванічного розчину

Сердюк В. О.[1], Склабінський В. І.[1], Большаніна С. Б.[1], Івченко В. Д.[2], Касім М. Н.[3], Зайцева К. О.[1]

[1] Сумський державний університет, вул. Римского Корсакова, 2, м. Суми, 40007, Україна;
[2] Сумський національний аграрний університет, вул. Г. Кондратьєва, 160, м.Суми, 40021, Україна;
[3] Технологічний інститут, Технічний університет, м. Багдад, Ірак

Анотація. Досліджено процес перенесення катіонів Cd^{2+} і Zn^{2+} через кат іонообмінну мембрану RALEX®CM-PES 11-66 у двокамерному електролізері. Електроліт анодної камери (аноліт) містив модельний розчин, що імітував склад гальванічних ванн для процесів пасивації, зокрема натрій дихромат (50 г/л) і сульфатну кислоту (10 г/л) як основні компоненти, а також як домішку – катіони Cd^{2+} і Zn^{2+} у кількості по 2,5 г/л кожного. Електроліт катодної камери (католіт) містив 1 % розчин сульфатної кислоти. Як катод використовувався титан ВТ-0, як анод – свинець С-0. У результаті вивчені катодні процеси, що пов'язані із міграцією йонів крізь мембрану та виділенням металів на катоді. Використано метод побудови вольтамперних кривих у гальванодинамічному режимі за допомогою імпульсного потенціостату, приладів комбінованих вимірювань і хлор-срібного електроду порівняння. Доведено зростання перенапруги на катоді у присутності йонів кадмію та зниження потенціалу катода при підвищенні температури. У ході досліджень встановлений інтервал pH, для якого процес катодного відновлення металів є найінтенсивнішим. Використано метод скануючої електронної мікроскопії з функцією рентгенівського мікроаналізу для визначення елементарного складу катодних осадів. Встановлено, що до складу осадів на катоді входять атоми кадмію та цинку. Розраховані числа перенесення йонів крізь катіонообмінну мембрану для кадмію і для суміші катіонів, що підтверджує ефективність вилучення йонів кадмію та цинку із хромовмісних розчинів. Цей процес дозволяє регенерувати гальванічні розчини та підтримувати стабільний склад ванн пасивування.

Ключові слова: електроліз, гальванічний розчин, іонообмінна мембрана, хромовмісний розчин, катіони кадмію, катіони цинку.

Numerical Simulation of the Evaporative Air Cooler with a Capillary-Porous Structure

Arseniev V. M., Shulumei A. V.[*]

[1] Sumy State University, 2 Rymskogo-Korsakova St., 40007 Sumy, Ukraine

[*]Corresponding Author's Address:
anton.shulumey@gmail.com

Abstract. Application of evaporative air cooling in various technologies allows reducing energy costs for improving environmental performance. Considering the promise of using air coolers with a capillary-porous structure, a mathematical model of the working process for such devices of contact heat of mass transfer was developed. The model takes into account the completeness of the process with temperature efficiency equal to 0.6–0.7 at constant water temperature at the temperature level of the wet thermometer. The estimation of energy efficiency of the air cooler on the basis of the exergent method of thermodynamic analysis is proposed. As a result, the thermophysical and design model of evaporative cooling of air in air-cooled contact type with capillary-porous structures was developed. The proposed method of cooling air is characterized by the following advantages the lowest water consumption per unit of heat exchange surface compared with other methods (e. g. spray nozzles), as well as zero discharge of drip liquid, which does not require further separation. Finally, the estimation of energy efficiency of the air vent is proposed on the basis of the exergent method of thermodynamic analysis.

Keywords: evaporative cooling, capillary-porous structure, thermophysical modelling, exergy efficiency.

1 Introduction

Evaporative cooling of water and atmospheric air is one of the first ways to implement artificial cold in the history of human development. Modern problems in low-energy energy and environment require the search for alternative solutions in the field of climate technology. Evaporative cooling is a non-mechanical way, but its efficiency is significantly limited by climatic conditions. At the same time, interest in the possibilities of evaporative coolers has increased in recent years, due to their low energy consumption and environmental cleanliness [1–3].

Among the technical systems for which evaporative cooling can significantly improve the thermoeconomic efficiency are compressor and gas turbine units. As it is known, when working compressor plants with compression of atmospheric air there is a deviation of the regime parameters from the nominal due to changes in the thermal parameters of the air at the input: pressure, temperature and relative humidity.

The most negative consequences are associated with an increase in the temperature of atmospheric air. For compressors of the volume principle of operation (compressor installations of general purpose, small and medium air separation units), the increase in air temperature in the suction is primarily manifested in the reduction of mass productivity and increase in energy consumption in the intermediate and final cooling. For turbochargers (gas turbine units, compressor stations for mine and chemical production), the power of the drive significantly increases.

In the paper [4] the dependence of the relative reduction of the effective power of the gas turbine unit with increasing temperature of the intake of the cyclic air is shown, experimental for GTU of the mark LM 1600 "General Electric" with Ne, *iso* = 15 MW and calculated for GTU AL-31ST with Ne, *iso* = 16 MW

According to the graph of the increase in the temperature of air intake from 15 °C (nominal mode ISO) to 40 °C reduces the effective power GTU at 18–20 %, which corresponds to losses of about 3 MW for the considered installations.

To cool the air at the suction, air coolers of the surface or contact type are used depending on the required depth of cooling or cold water capacity.

The required cold-productivity is provided by the operation of refrigerating machines, mainly heat-discharging waste streams of heat.

Contact air coolers are suitable for technological air conditioning in premises where it is necessary to maintain high relative humidity (spinning, paper production, etc.). From the position of capital and operating costs, contact air coolers have an advantage over surface type devices for cooling cyclic air gas turbine engines.

The main disadvantage of contact air coolers is the increased attribution of droplet moisture to the air flow,

requiring its separation or ensuring its evaporation in the process of compression of air.

In this regard, air coolers with porous ceramics or capillary-porous structures of composite materials are of particular interest. Evaporative cooling using capillary-porous materials allows the film flow to be eliminated on the contact surfaces of the apparatuses and the dropping of moisture from the heat transfer surface.

2 Research Methodology

2.1 Thermophysical description of the calculation model

Figure 1 shows simplified schemes for two design variants of air coolers using capillary-porous structural elements, the heat of mass exchange between air and water.

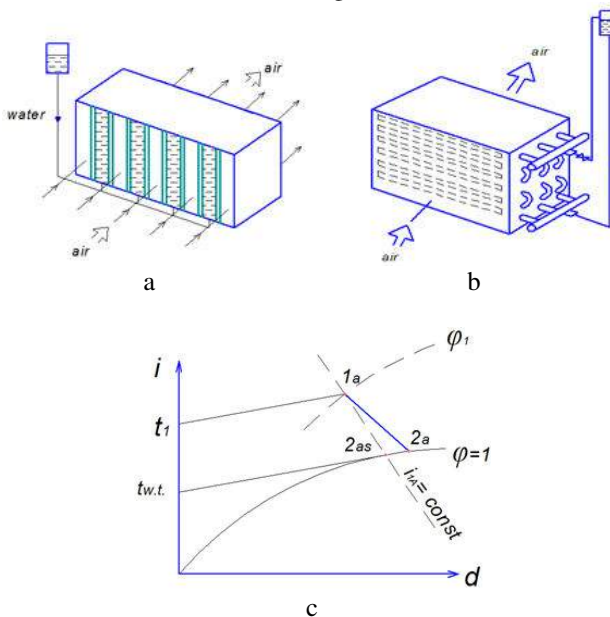a   b

c

Figure 1 – Evaporative air coolers: a – multi-channel with walls of capillary-porous materials; b – heat exchange unit with a bundle of pipes from capillary-porous materials; c – process in "i–d" diagram

According to Figure 1 a, porous walls divide flat parallel channels with water and air passage. Water in the channels is replenished as it moves through the capillaries and evaporates into the air at the expense of the reservoir of water in the tank.

A pumping movement of water through the apparatus can also be organized. Filling with water is organized through one row of channels.

According to the scheme in Figure 1 b, the heat exchange unit has a conventional constructive solution for airflow of a beam of non-circular pipes with a corridor or chess arrangement, in which the pipes are characterized by a fine porosity of 2.0–2.5 μm. Material of pipes: ceramics, plastics, composite materials. Water in pipes is supported either by gravity pressure or by pump circulation.

Taking into account a number of features inherent in the process of evaporative cooling in the capillary-porous structures, the following assumptions were adopted:

– the temperature of the liquid in the channels is constant and is equal to the temperature of the wet thermometer;

– the temperature efficiency of the process is limited by the value $E_a = 0.6$;

– there is no heating of the main mass of the liquid;

– the contact surface of the media is completely moistened with water by blurring the air flow of the meniscus volume of droplets, which flows from the water of the water;

– there is no attribution of droplet moisture;

– gas-dynamic air resistance neglected;

– in the temperature range the dependence of the partial pressure of the saturated water vapor on the temperature is taken as a linear function;

– the notion of cold productivity becomes incorrect in view of inequalities $i_{2a} > i_{1a}$, it is more correct to consider the ability to humidify the air, that is, its increase in moisture content.

The conceptual task of the calculation model is to determine the required area of the contact surface of the capillary-porous structure, on which the change of the parameters of the air flow along the line of heat - logistic relation is realized, taking into account the accepted value of the temperature efficiency of the evaporative cooling process.

For the temperature efficiency E_a parameters of air flow at the outlet of the air cooler is characterized by the expressions:

$$t_{2a} = t_{1a} - E_a(t_{1a} - t_{2as}) \quad (1)$$

where $\varphi_{2.A} = 0.98–1.00$, which allows to find the moisture content, x_{2a} and enthalpy, i_{2a} in the state of 2a and determine the thermal logic ratio:

$$\varepsilon_{AC} = \frac{i_{1a} - i_{2a}}{x_{1a} - x_{2a}} \quad (2)$$

By breaking the intervals of change in the moisture content in the apparatus, $(x_{1a} - x_{2a})$, on the elementary regions along the line ε_{AC} we obtain the possibility of determining the thermal, caloric and thermophysical parameters of air from the state 1a to 2a by the equations used in the calculations of air conditioning systems and convective drying of moist materials [7].

The very process of energy interaction between environments is described by the equation of thermal balance:

$$Q_\alpha = Q_\beta + Q_w, \quad (3)$$

which shows that the convective heat flowing away from the air flow, Q_α goes to the evaporation of the moisture from the wetted surface, Q_β and to the heating of the fluid flow in the middle of the channels or tubes of the apparatus, Q_w.

In turn, the component equations are written in the form:

$$Q_\alpha = \alpha \cdot F_\alpha \cdot (t_\alpha - t_w); \tag{4}$$

$$Q_\beta = r \cdot G_{Bw} = r\beta_p F_\beta (p_w - p_a); \tag{5}$$

$$Q_w = G_w c_w \Delta t, \tag{6}$$

where α – coefficient of heat transfer; F_α – surface area of heat transfer; $(t_a - t_w)$ – air temperature in the core of the stream and water on the surface of evaporation; r - specific heat of vaporization of water at t_w; G_{ev} – mass flow rate of evaporated water; β_p – the coefficient of evaporation is determined by the difference of partial pressure of water vapor, p_w – at the surface of water and p_a - in the core of the stream; G_w - mass flow rate of water when it is circulating through channels or pipes; c_w – average heat capacity of water in the interval of temperature changes; $\Delta t = t_{2w} - t_{1w}$ – water heating in the machine.

The heat flux to the liquid Q_w is realized under the condition

$$G_w \cdot c_w \cdot \Delta t_w = k_w \cdot F_w \cdot (t_a - t_w) \tag{7}$$

where k_w – the coefficient of heat transfer from air to water through the distribution surface, the area of F_w.

Assuming equality $F_\alpha = F_\beta = F_w$:

$$\alpha \cdot (t_a - t_w) = r \cdot \beta_p \cdot (p_w - p_a) + \frac{G_w}{F_w} \cdot c_w \cdot \Delta t_w$$

In the absence of water circulation $\Delta t_w = 0$:

$$\alpha \cdot (t_A - t_w) = r \cdot \beta_p \cdot (p_w - p_A)$$

To determine the quantities on the interface of the media, we can use the linearized approximation dependence of the partial pressure of the saturated water vapor $p_s(t)$ on the temperature as proposed in [11]:

$$p_s(t) = a + b \cdot t$$

After the appropriate changes:

$$p_w - p_a = p_s(t_a) \cdot \frac{1 - \varphi_a}{1 + \dfrac{b}{A}}$$

where the complex $A = \dfrac{\alpha}{\beta_p \cdot r_p(t)}$ – the psychometric coefficient.

For the calculation of the technical characteristics of the air cooler on the capillary-porous structures, the following expressions were obtained:

– consumption of evaporating water per unit of heat exchange surface:

$$q_F = \beta_p \cdot p_s(t_w) \cdot \frac{1 - \varphi_{1a}}{1 + \dfrac{b}{A}}, \quad \frac{kg_{H_2O}}{m^2};$$

– water consumption for evaporation:

$$G_{ev} = m_{d.a.} \cdot (x_{1a} - x_{2a}), \quad \frac{kg_{H_2O}}{m^2};$$

– area of heat exchange surface:

$$F_{tot} = \frac{G_{ev}}{g_F}, \quad m^2$$

– relative water consumption:

$$G_w = \frac{G_a}{m_a} = \frac{x_{1a} - x_{2a}}{1 + x_{1a}};$$

where the coefficient of mass return is determined from the expression:

$$\beta_p = \frac{\alpha}{Le \cdot c_{pa} \cdot P_{tot}} \tag{8}$$

In this formula, the Lewis criterion Le is considered as the ratio of the molecular diffusion coefficient at P_{tot} and the air temperature in the boundary layer to the air-cooled coefficient under the same conditions.

2.2 Energy efficiency of the evaporative cooling process

For contact type coolers, energy efficiency is considered as the relative value of air temperature differences, which takes into account the non-adiabativity of the energy conversion process. This value is called the temperature efficiency and is written as:

$$E_a = \frac{(t_{1a} - t_{2a})}{(t_{1a} - t_{2as})} \tag{9}$$

However, the magnitude of the E_a takes into account only the lack of recuperation for air cooling, due to the non-indifference of the process and does not take into account the internal irreversibility in the form of gas-dynamic resistances along the airway.

Based on the exergent method of thermodynamic analysis by J. Tsatsaronis [8] and used for refrigeration and heat pump technology [9, 10], it can be considered the exergic efficiency of power transitions in a contact air cooler.

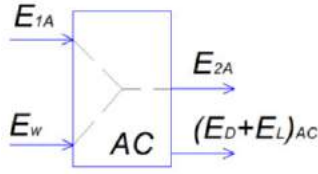Formalized scheme of exergent transformations is presented in Figure 2.

Figure 2 – Design scheme of exergent transformations in an air cooler in capillary-porous structures at $t_{1w} = t_{w.t}$

On this scheme it is indicated:

− E_{1a}, E_{2a} − exergy of the airflow on the input and output of the apparatus;

− E_w − exergy of water at the entrance to the capillary canals;

− $(E_D + E_L)_{AC}$ − exergy of destruction and loss in the air cooler.

To determine the exurance of the fuel flow, E_F and product flow E_R, according to the purpose of the apparatus can be written:

$$E_{2a} = (E_{2a})_F + (E_{2a})_P$$

where $(E_{2a})_F$ − the exergy of the wet air at t_{2a}, x_{2a}, m_{1a}; $(E_{2a})_P$ − the exergy of water vapor at t_{2a}, x_{2a} with mass flow G_{ev}.

This separation of exergy air at the outlet allows obtaining:

$$E_F = E_{1a} - (E_{2a})_F$$
$$E_P = (E_{2a})_F - E_w$$

(10)

and exergic efficiency takes the form of

$$\varepsilon_{ex} = \frac{E_P}{E_F} = \frac{(E_{2a})_F - E_w}{E_{1a} - (E_{2a})_F}$$

(11)

Considering moist air as a mixture of ideal gases, we obtain:

$$E_{1a} - (E_{2a})_F = m_{d.a} \cdot (1 + x_{1a}) \times$$
$$\times \left[c_{p,w.a}(t_{1a} - t_{2a}) - T_e \left(c_{p,w.a} \cdot \ln\frac{T_{1a}}{T_{2a}} - R_{w.a} \cdot \ln\frac{P_{1a}}{P_{2a}} \right) \right]$$

(12)

where $m_{d.a} \cdot (1 + x_{1a})$ − mass flow of moist air; $c_{p,w.a}$ − the isobar heat capacity of the wet air in the temperature range t_{1a}, t_{2a}; $R_{w.a}$ − the gas became wet air; P_{1a}, P_{2a} − air pressure at the entrance and exit of the apparatus.

The calculated equations for $c_{p,w.a}$, $R_{w.a}$, P_{2a} are given in the next section.

For the exergy stream of water vapor and water, use the equation for real gases:

$$(E_{2a})_P = G_{ev} \left[((h_{2a})_P - h_e) - T_e((S_{2a})_P - S_e) \right]$$

(13)

$$(E_{2a})_P = G_{ev} \left[(h_w - h_e) - T_e(S_w - S_e) \right]$$

(14)

where h_w, $(h_{2a})_P$ − the enthalpy of water and water vapor at the appropriate temperatures t_w, t_{2a}.

When taking environmental parameters $T_e = 273$ K and $P_e = 100$ kPa, the values of h_e, S_e for water are zero and the exergy of the product stream is written as follows:

$$(E_{2a})_P - E_w = m_{d.a} \cdot (x_{2a} - x_{1a}) \times$$
$$\times \left[((h_{2a})_P - h_w) - T_e((S_{2a})_P + S_w) \right]$$

(15)

After substituting (15) and (12) in (11) it can be obtained the following dependence:

$$\varepsilon_{ex} = \frac{(x_{2a} - x_{1a}) \cdot \left[((h_{2a})_P - h_w) - T_e((S_{2a})_P + S_w) \right]}{(1 + x_{1a}) \cdot \left[c_{p,w.a}(t_{1a} - t_{2a}) - T_e \left(c_{p,w.a} \cdot \ln\frac{T_{1a}}{T_{2a}} - R_{w.a} \cdot \ln\frac{P_{1a}}{P_{2a}} \right) \right]}$$

(16)

3 Results

Based on the results of calculations, graphic dependencies were constructed, Figures 3, 4 for both types of constructive execution.

Based on the calculations in Figure 3 the dependence of the specific wet current on the relative humidity is presented. It can be seen that with an increase in relative humidity, the specific moisture influx decreases.

Based on the calculations in Figure 4, the dependence of the exergent efficiency on the relative humidity is presented. It can be seen that when the relative humidity increases, the exergic efficiency decreases.
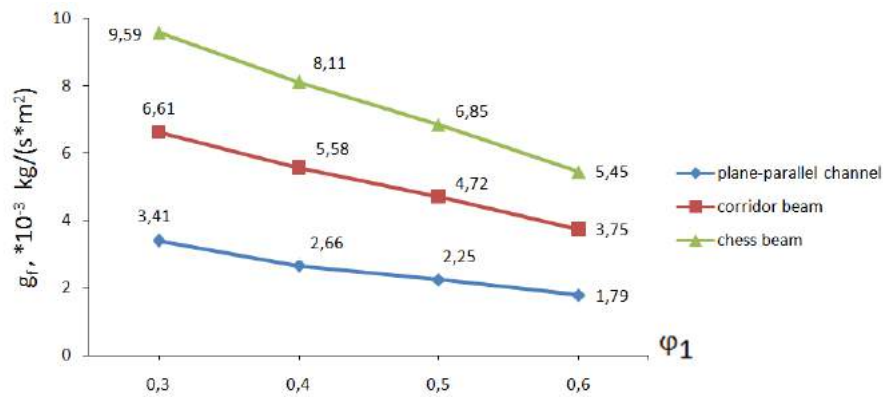
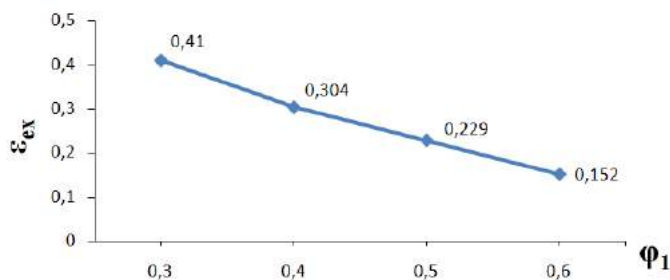Figure 3 – The dependence of specific wet current on relative humidity

Figure 4 – The dependence of exergic efficiency on relative humidity

4 Conclusions

As a result, the thermophysical and design model of evaporative cooling of air in air-cooled contact type with capillary-porous structures was developed. The following dependencies are calculated:

– water consumption per unit of heat exchange surface;

– the effect of relative humidity on exergic efficiency.

This method of cooling air is characterized by the following advantages:

– the lowest water consumption per unit of heat exchange surface compared with other methods (e. g. spray nozzles);

– zero discharge of drip liquid, which does not require further separation.

Finally, the estimation of energy efficiency of the air vent is proposed on the basis of the exergent method of thermodynamic analysis.

References

1. Gorin, A. N., & Doroshenko, A. V. (2007). *Alternative Refrigeration Systems and Air Conditioning Systems*, Nordpress, Donetsk, Ukraine.
2. Velasso, E., Rey F. I., Tejero A., & Flores F. E. (2009). Performance of three different evaporative cooling systems. *Proceedings of the 7th World Conference on Experimental Heat Transfer, Fluid Mechanics and Thermo-dynamics*.
3. Cheban, D. N., & Doroshenko A. V. (2013). Use of porous ceramics in the field of evaporative cooling and theoretical analysis of combined systems. *Refrigeration Technique and Technology*, No 2(142), pp. 4–10.
4. Arseniev, V. M., Miroshnichenko V. V., & Borisov N. A. (2015). Exergy efficiency of technogenic cooling of cyclic air of a gas turbine plant, *Refrigeration Technique and Technology*, Vol. 51, Issue 6, pp. 6–11.
5. Isachenko, V. P., Osipova, V. A., & Sukomel, A. S. (1969). *Heat Transfer*. Energy, Moscow, Russia.
6. Bykov, A. V. (1980). *Thermophysical Bases for Artificial Cold Production*. Food industry, Moscow, Russia.
7. Chumak, I. G., Laryanovsky, S. Yu., et al. (2006). *Cooling Installations*. Palmyra, Odessa, Ukraine.
8. Tsatsaronis, D. (2002). *Interaction of thermodynamics and economics to minimize the cost of the energy-converting system*. Negotiant, Odessa.
9. Morozyuk, T. V. (2006). *The theory of refrigerating machines and heat pumps*. Negociant, Odessa, Ukraine.
10. Arseniev, V. M. (2012). *Heat Pump Energy Conservation Technology*. Sumy State University, Sumy, Ukraine.
11. Gerasimov, N. A., & Kurilev, E. C. (1970). *Cooling Installations*. Mechanical Engineering, Saint Petersburg, Russia.
12. Pavlov, K. F., Romankov, P. G., & Noskov, A. A. (1964). *Examples and tasks on the course of processes and apparatuses of chemical technology*. Chemistry, Moscow, Russia.
13. Stefanov, E. V. (2005). *Ventilation and Air Conditioning*. AVOK North-West, Saint Petersburg, Russia.

14. Lipa, A. I. (2010). *Air conditioning. The basics of the theory. Modern air treatment technology*. VMV Publishing House, Odessa, Ukraine.

15. Zhuk, K. B., & Doroshenko, A. V. (2012). Prospects of use of capillary - porous structures in evaporative coolers of gases and liquids. *Sustainable development and artificial cold. Proceedings of the 8th International Scientific and Technical Conference*, pp. 510–513.

16. Cheban, A. N., & Doroshenko, A. V. (2012). Use of porous ceramics in the field of evaporative cooling. Sustainable development and artificial cold. *Sustainable development and artificial cold. Proceedings of the 8th International Scientific and Technical Conference*, pp. 174-177.

17. Doroshenko, A. (1992). *Compact heat and mass exchange equipment for refrigeration equipment (theory, calculation, engineering practice)*. Doctoral Thesis, Odessa Institute of Low-Temperature Technology and Energy, Odessa, Ukraine.

Числове моделювання випарного повітроохолоджувача з капілярно-пористою структурою

Арсеньєв В. М., Шулумей А. В.

Сумський державний університет, вул. Римського-Корсакова, 2, 40007, м. Суми, Україна

Анотація. Застосування випарного охолодження повітря в різних технологіях дозволяє знизити енерговитрати і поліпшити екологічні показники. Зважаючи на перспективність використання повітроохолоджувачів з капілярно-пористою структурою, розроблена математична модель робочого процесу для апаратів контактного тепломасообміну. У результаті розроблена термофізична модель випарного повітряного охолоджування із застосуванням капілярно-пористих структур. Запропонована модель ураховує завершеність процесу з температурною ефективністю 0,6–0,7 при постійній температурі води на рівні температури мокрого термометра. Запропоновано спосіб оцінювання енергоефективності повітроохолоджувача на основі ексергетичного методу термодинамічного аналізу. Наведений спосіб охолодження повітря характеризується такими перевагами як найнижча витрата води на одиницю поверхні теплопередачі, а також нульові витоки краплинної рідини, що не потребує подальшого розділення. У результаті запропоновано спосіб оцінювання енергоефективності запропонованої конструкції на основі ексергетичного методу термодинамічного аналізу.

Ключові слова: випарне охолодження, капілярно-пориста структура, теплофізичне моделювання, ексергетична ефективність.

Intensification of Foam Layered Apparatus by Foam Stabilization

Liaposhchenko O.[1*], Khukhryanskiy O.[1,2], Moiseev V.[3], Ochowiak M.[4], Manoilo E.[3]

[1] Sumy State University, 2 Rymskogo-Korsakova St., 40007 Sumy, Ukraine;
[2] PJSC "Ukrhimproekt", 13 Illinska St., 40009 Sumy, Ukraine;
[3] National Technical University "Kharkiv Polytechnic Institute", 2 Kyrpychova St., 61002 Kharkiv, Ukraine;
[4] Poznan University of Technology, 5 M. Sklodowska-Curie Sq., 60-965 Poznan, Poland

Abstract. In this work the expanded models are studied for foaming apparatuses with gratings made of tubes for different diameters. The problem of intensification of foam devices using coarse-grating lattices is considered. The possibility of deep cleaning and practically complete cleaning of gases from ammonia and fluoride compounds with their separate absorption is noted. The series of experimental dependencies for the main parameters of the process are given. The possibility of effective mass-exchange processes in an intensive foam layer on counter-current coarse-grating lattices is confirmed. The controversial requirements for equipment have been given despite the large number of existing machines for mass transfer processes, as well as the development of new high-intensity and efficient equipment for environmental technologies in many industries is considered.

Keywords: industrial gas emissions, hydrodynamics, mass transfer; foam apparatus, foam layer, purification process, stabilization of foam layer, intensification of the process.

1 Introduction

In modern conditions of significant anthropogenic environmental impact, it began the search for the most efficient and cost-effective methods of cleaning industrial emissions. Methods of cleaning and equipment that is being developed should take into account working possibilities in a wide range of working conditions.

In order to reduce energy consumption in systems for catching harmful and toxic substances, it is necessary to provide a reduction of hydraulic resistance while maintaining the high efficiency of gas streams cleaning.

Given the controversial requirements for equipment and despite the large number of existing machines for mass transfer processes, the development of new highly intensive and efficient equipment is of considerable interest to environmental protection technologies in many industries.

2 Literature Review

The most common method of purifying gas streams is methods for the absorption of harmful components from the released industrial gases. In this case, either the process of physical absorption occurs, or the absorbent enters a chemical interaction with the absorbed component (the process of chemisorption).

Recently, the direction associated with conducting diffuse processes in intensive regimes with developed turbulence at high speeds of gas and liquid flows has become relevant. Actually turbolization of the gas-liquid system leads to an increase in the intensity of mass-exchange devices.

One of the methods of turbination of gas-liquid systems is their transformation into mobile unstable foam due to the kinetic energy of gas.

Foam mode and foam devices of the "classical" type are described in and analyzed in the papers [1-4]. Intensified apparatuses with foam layer stabilizer have been widely used for capturing dust from gases and for gas absorption in the chemical and related industries. Due to its high efficiency, high unit capacity, good operational qualities of their application, they can improve the stages of gas purification for technological and sanitary purposes, increase the efficiency of mass transfer and the reliability of gas-cleaning equipment.

Industrial introducing the stabilization method of the gas-liquid layer significantly expands the scope of foaming devices and opens up new possibilities for intensifying technological processes with the simultaneous creation of low-waste technologies.

3 Research Methodology

Based on researching the semi-industrial models of foam machines with lattices, assembled from tubes of different diameters, a pilot sample of foam absorber with the productivity of 12 000 m^3/h of gas was designed.

One of the research directions was the absorption of ammonia by water in intensive foam modes with a stabilized foam layer. Absorption of ammonia by water is a typical process in absorber research to detect their effectiveness.

The process of absorption of ammonia in foam mode on counterproductive gratings of the usual type is quite fully studied at gas velocities up to 2.5 m/s. In order to compare the technological parameters of ammonia absorption in water under similar conditions, the work of the most common industrial counter processing grating with an area of free intersection of 0.18 m^2/m^2 and a diameter of holes of 5 mm was investigated.

The research of this grating was carried out both with the stabilizer, and without it. The research was due to the need to determine the degree of effect of the stabilization of the layer and comparison with the technological parameters of the newly developed design foam apparatus, as well as the establishment of the general nature of dependencies and kinetic parameters of the absorption process (η – efficiency of the contact stage (ECS); Ks – mass transfer coefficient) from the following basic parameters: Wg – gas velocity; L_0 – irrigation density; C_n – initial concentration; S_0 – area of the free intersection of the plate.

4 Results

The gas velocity in the complete section of the device has a significant effect on the height of the gas-discharge and the initial layer. Accordingly, the gas velocity significantly influences the mass transfer coefficient, and the nature of this dependence is determined by the solubility of the gas component in the fluid. The foregoing is confirmed by the experimental data given in Figure 1, dependence 6.

When absorbing well-soluble gases (for example, ammonia), is required a low phase of contact to achieve a high degree of absorption. Reducing the contact time of phases with increasing gas velocity in foam mode is largely offset by the turbulence of the gas-liquid layer and increasing the contact of surface phases.

Previously, in studying the absorption of ammonia by water on ordinary gratings, it was found that in the gas torch the holes in the grid transmit from 50 to 90 % of the total mass of matter [5]. This determines the "input" effect, that is, the most intense interaction between the gas and the liquid, which occurs at the time of forming a new contact surface. However, at a low altitude of the initial fluid layer on the grating of the usual type of apparatus it is possible to pass the gas without contact with the absorbent fluid, and as a consequence, a decrease in the absorption rate. This is especially true for industrial ma-

chines. As indicated, the stabilization of the foam layer makes its structure more uniform and excludes the probability of such a state.

Investigations on new types of gratings with foam layer stabilization have shown that the efficiency of the apparatus during absorption of ammonia by water practically does not depend on the value of gas velocity (Figure 1). Moreover, ECS in the new design of the device is much higher than that of conventional gratings without stabilization and even when it is installed on ordinary type gratings.
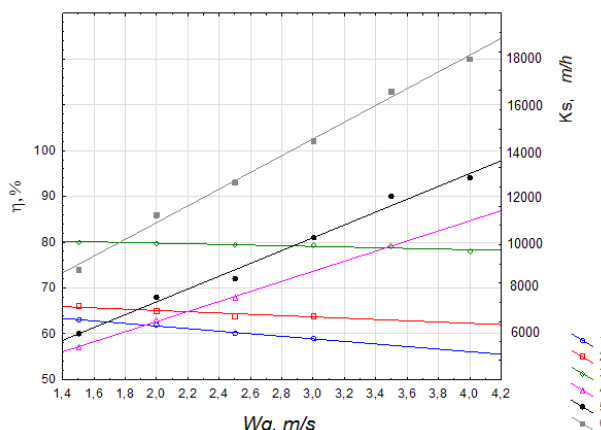

Figure 1 – Efficiency of the contact stage (1–3) and mass transfer coefficient (4–6) dependences on the gas velocity for the ammonia water system with L_0 = 5 m^3/(m^2·h):
1, 4 – d_E = 0.005 m, S_0 = 0.18 m^2/m^2 – without stabilizer;
2, 5 – d_E = 0.005 m, S_0 = 0.18 m^2/m^2 – with stabilizer;
3, 6 – d_E = 0.005 m, S_0 = 0.20 m^2/m^2 – with stabilizer

It should be noted that the difference between the values of the efficiency of the contact stage and mass transfer coefficient, referenced to the unit area of the grating, depending on the gas velocity in the complete section of the apparatus on the gratings with small holes with and without the stabilizer increases at high gas. This proves the high intensity of the process and confirms the expediency of using a stabilized foam layer on large-hinged gratings for the purification of gases in the industry.

The dependence of the of the efficiency of the contact stage by absorption on the initial ammonia concentration of the comparable contact devices (Figure 2) fully confirms the conclusions made about the effectiveness of new foaming apparatus. It is important to note that in the studied limits of variation of the initial concentration of ammonia ($C_n \leq 1$ % vol.), the efficiency of the contact stage remains constant for other equal conditions. This allows using the known methods of calculating the required number of steps to achieve the desired process efficiency.

The irrigation density (Figure 3) affects on the efficiency of the contact stage only at low values of the L_0 to 8 m^3/(m^2·h). It depends on the fact that at low irrigation density, the residence time of the liquid on the grading increases to a certain (effective) value. Further increases in irrigation density have little effect on the absorption process.
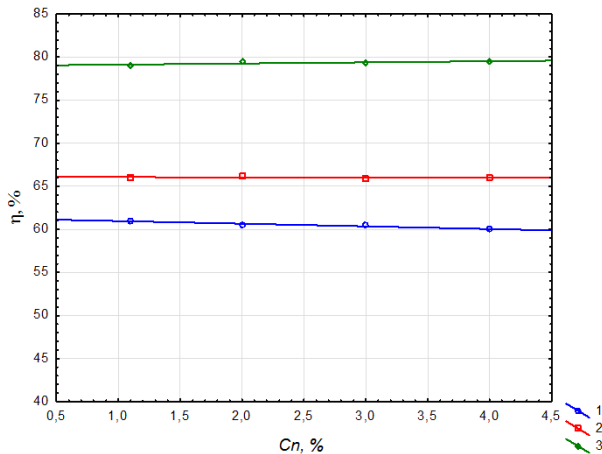
Figure 2 – Efficiency of the contact stage dependence at absorbing ammonia by water from the initial concentration of ammonia W_g = 2.5 m/s and L_0 = 5 m³/(m²·h) with the following grates: 1 – d_E = 0.005 m, S_0 = 0.18 m²/m² – without stabilizer; 2 – d_E = 0.005 m, S_0 = 0.18 m²/m² – with stabilizer; 3 – d_E = 0.005 m, S_0 = 0.20 m²/m² – with stabilizer
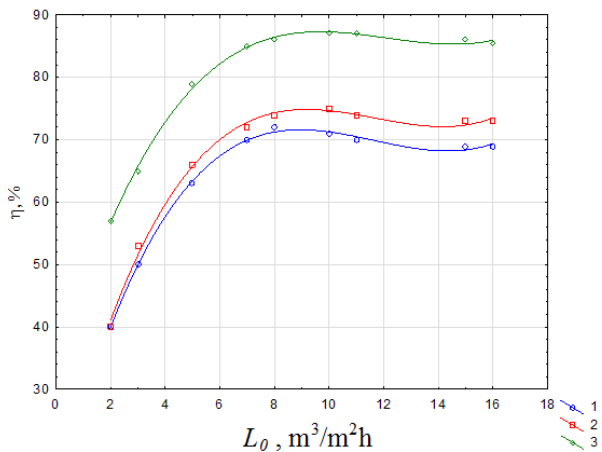

Figure 3 – Efficiency of the contact stage dependence in absorbing ammonia by water from the irrigation density: W_g = 2.5 m/s; C_n = 1–2 %. with the following grates: 1 – d_E = 0.005 m, S_0 = 0.18 m²/m² – without stabilizer; 2 – d_E = 0.005 m, S_0 = 0.18 m²/m² – with stabilizer; 3 – d_E = 0.005 m, S_0 = 0.20 m²/m² – with stabilizer

Increasing the area of the free segment leads to a decrease in efficiency (Figure 4). This confirms the correctness of the conclusions drawn in the analysis of the relationship of structural parameters.

An increase in the diameter of the grating holes 10 times when applied to the foam layer stabilization increases the efficiency of capturing ammonia by 20 % compared to conventional gratings without stabilizing the layer and by 15 % compared to conventional gratings with foam layer stabilization. It should be noted that the rate of gas processing in the investigated range from 2 to 5 m/s has virtually no effect on the magnitude of efficiency.
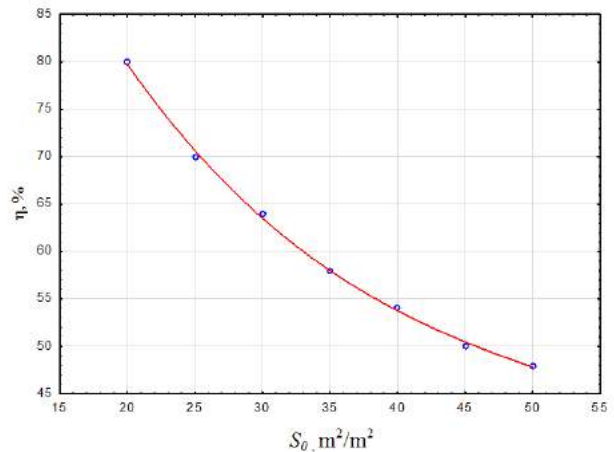
Figure 4 – Efficiency dependence at absorbing ammonia by water: W_g = 2.5 m/s; C_n = 1–2 %; L_0 = 5 m³/(m²·h)

The character of change in the mass transfer coefficient, referenced to the grating area, from the linear gas velocity is given in Figure 5, from which it is evident that W_g greatly affects K_s in the investigated boundaries W_g. Processing the experimental data was obtained the following empirical equations for the calculation of K_s, m/h:

$$K_s = 1659,8 W_g^{1,5} L_0^{0,12} d_{\hat{A}}^{0,26} S_0^{-0,71} \qquad (1)$$

To calculate the efficiency, %:

$$\eta = 0,713 \cdot 10^3 W_g^{-1,9} L_0^{0,30} d_{\hat{A}}^{-0,34} K_s^{1,27} \qquad (2)$$

Border for changing parameters:
$W_g = 2 - 4,0$ m/h, $L_0 = 1 - 20$ m³/m² · h;

$S_0 = 0,20 - 0,40$ m²/m², $d_{\hat{A}} = 0,02 - 0,08$ m.

The error of calculating by equations (1) and (2) is not more than 9 %.

The influence of hydrodynamic parameters on the mass transfer coefficient at ammonia absorption by water is given in Fig. 6, which confirms the sufficient accuracy of the obtained equations, while the dependence of the mass transfer coefficient on the height of the foam layer is described by the following equation:

$$K_s = 4742 \cdot W_g H^{0,33} \qquad (3)$$

Border for changing parameters:
$W_g = 2 - 4,0$ m/h, $L_0 = 1 - 20$ m³/m²h;

$S_0 = 0,20 - 0,4$ m²/m², $d_{\hat{A}} = 0,02 - 0,08$ m.

Equation (3) allows us to evaluate the mass transfer process under any hydrodynamic conditions, which is very important in the development and evaluation of technological schemes in industrial conditions with the use of new devices.

Experimental data confirmed the dependence obtained [1, 5] by Mukhlennov I. P.on the basis of theoretical consideration of the mass transfer in the foam layer for well-soluble gases, which is expressed by the equation:

$$K_s = nH^{0,33} \qquad (4)$$

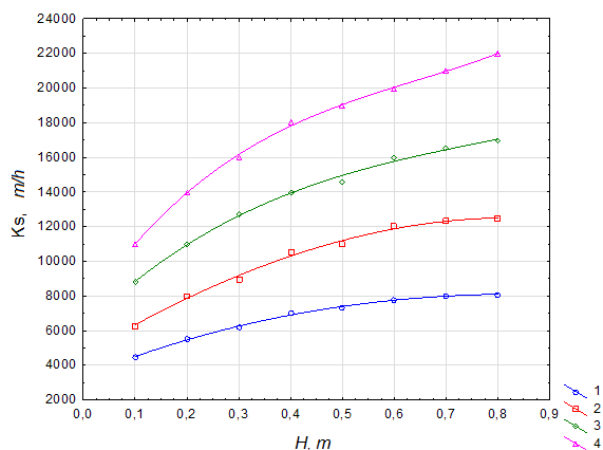Figure 5 – Dependence of mass transfer coefficient, referenced to the grading area from the height of the gas-liquid layer at different gas velocities: $1 - W_g = 2$ m/s; $2 - W_g = 3$ m/s; $3 - W_g = 4$ m/s; $4 - W_g = 5$ m/s

Figure 6 shows the dependence of the actual mass transfer coefficient on the linear gas velocity, which implies that an increase in speed leads to an increase in the mass transfer coefficient.
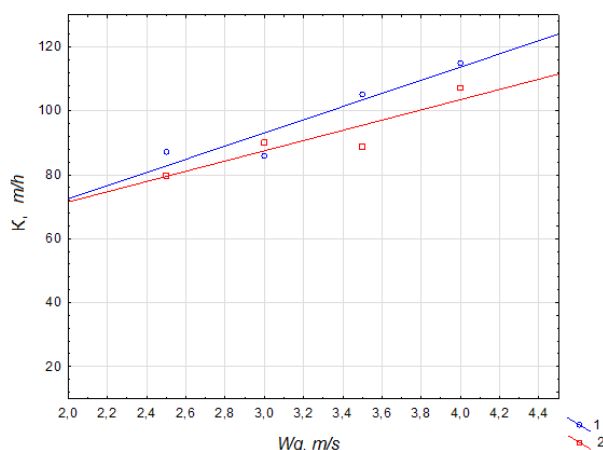

Figure 6 – Dependence of the actual mass transfer coefficient on the linear gas velocity (with stabilization) at absorbing ammonia by water: 1 – grid $S_0 = 0.25$ m^2/m^2; $d_E = 0.005$ m, $L_0 = 5$ m^3/(m^2·h)); 2 – grid $S_0 = 0.18$ m^2/m^2; $d_E = 0.005$ m; $L_0 = 5$ m^3/(m^2·h)

It should be noted that the value of the true mass transfer coefficient for apparatus with ordinary and coarse hinged gratings with stabilization of the foam layer is approximately the same.

This confirms that the contact surface of phases in the foam layer on coarse-grained grates is 1.5 times higher at a gas velocity of more than 3 m/s with an increase in the diameter of the grating holes 10 times, and confirms the possibility of efficient gas cleaning in the industry using foam machines.

5 Discussion

In order to verify the results obtained during bench tests in laboratory conditions, a cycle of pilot-industrial tests was conducted in which the main gas components were ammonia, fluoride compounds (mainly silicon tetra fluoride). In the system of purifying gases from the spray dryer, a reconstruction of the existing absorber was carried out (hollow scrubber with three tiers of nozzles). Instead of nozzles in the scrubber case, a contact step with coarse hole gratings (the holes are 0.045×0.045 m and $S_0 = 0.28$ m^2/m^2) and a foam layer stabilizer were installed (size 40×40×60 mm).

Hydrodynamic tests were initially performed, which showed that the foam absorber has stable hydrodynamic characteristics when changing the gas velocity in the free intersection of the device from 3.5 to 5.5 m/s at $L_0 = 8$ m^3/(m^2·h). The highly developed gas-liquid layer on the grating is present even at speeds less than 2.2 m/s. Measurement of the gas height -liquid layer in industrial conditions was carried out by electro-sharpening method. It should be noted at the same time that the measurements also showed good convergence with bench tests in laboratory conditions (Figure 7).
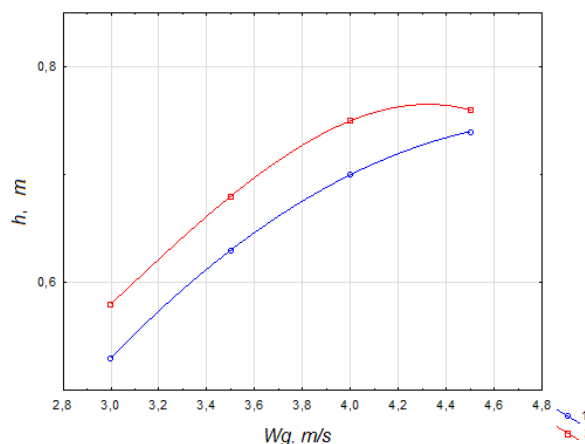
Figure 7 – Dependence of the foam layer height on the linear gas velocity of the apparatus (experimental and industrial tests): gas-pulp system with $\rho = 1.22$ kg/m^3, $L_0 = 8$ m^3/(m^2·h): 1 – experimental-industrial tests $S_0 = 0.28$ m^2/m^2; $d_E = 0.048$ m; 2 – bench tests $S_0 = 0.25$ m^2/m^2; $d_E = 0.05$ m

On this basis, for this technological scheme, optimal hydrodynamic mode of gas processing was determined which corresponded to the linear gas velocity from 3.0 to 4.9 m/s [6].

At these hydrodynamic parameters technological regimes for capturing ammonia, fluoride compounds and dust, depending on the acidity of ammonium phosphates, and also parameters in the existing technological scheme were analyzed in parallel (Figure 8).
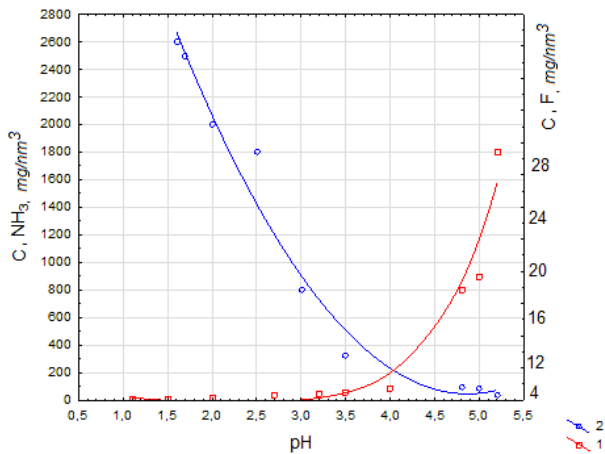
Figure 8 – Dependence of the NH_3 final content and fluoride compounds on the acidity of the irrigation solution: W_g = 4 m/s; L_0 = 8 m³/(m²·h); 1 – ammonia; 2 – fluoride compounds, C_{NH_4} = 1.0 g/nm³, C_{HF} = 0.1 g/nm³, grid: S_0 = 28 %, d_E = 0.045 m

Figure 9 – Dependence of NH_3 absorption rate and fluoride compounds on the acidity of the irrigation solution: L_0 = 8 m³/(m²·h); 1 – ammonia; 2 – fluoride compounds, initial concentration of ammonia 1.0 % vol.; W_g = 4 m/s; grid S_0 = 0.28 m²/m², d_E = 0.045 m

Figure 9 shows the dependence of the gas purification efficiency from ammonia and fluoride compounds from the acidity of the pulp, and it is evident that the degree of absorption of ammonia and fluoride compounds depends on the acidity of the irrigation solution. At pH of a solution equal to 1.4, for ammonia, the degree of absorption is 98 %, and for fluoride compounds at pH = 5.7, the efficiency is 94 %.

6 Conclusions

The conducted studies indicate the possibility of deep cleaning and virtually complete removal of harmful components from gases in their separate absorption. Dependences of NH3 final content and fluorine in the gas after treatment from ammonium phosphate acidity are shown in Figure 9, from which it is evident that the optimal mode for the absorption of these components lies within the pH of the solution from 3 to 5. In this case, the maximum permissible emission rates for ammonia are maintained. This is confirmed by the high mass exchange characteristics of the developed foam device, allowing the process of joint and effective cleaning of these components in the range of pH irrigating solution from 3 to 5. As a result of experimental and industrial tests, it is established the following: the efficiency of dust capture practically does not depend on the pH of the solution and also on the increase of the inlet dust to 4–6 g/nm³. Increasing the density of the circulating pulp of ammonium phosphates does not affect the efficiency.

The conducted studies have experimentally confirmed the possibility of effective mass exchange processes in an intensive foam layer on counter currently coarse hinged gratings.

The application of new apparatus allows radically reconstructing, with minimal cost, technological schemes for gas cleaning in the chemical and other industries to provide them with better operational and technological characteristics, while simultaneously increasing the efficiency of working with concentrated solutions, their circulation and use in the main process [7].

7 Acknowledgements

References

1. Muhlenova, I. P., & Tarata, E. Ya. (1977). *Foam mode and foam devices*. Moscow, Chemistry.

2. Tarat, E. Ya., Balabekov, O. S., & Bolgov, N. P. (1976). *Intensive colony machines for handling gases with liquids*. Saint-Petersburg State University.

3. Moiseev, V. F., Manoylo, E. V., Repko, K. Yu., & Davydov, D. V. (2017). Treatment of gas-discharge systems on tubular lattices with foam layer stabilizer. *Bulletin of the National Technical University "Kharkiv Polytechnic Institure", Series "New solutions in modern technologies"*, No. 53, pp. 114–123, doi: 10.20998/2413-4295.2017.53.17.

4. Moiseev, V. F., Manoylo, Ye. V., Ponomareva, N. G., Repko, K. Yu., & Davydov, D. V. (2018). Methodology for calculation of regime-constructive and hydrodynamic parameters of foam devices for mass transfer processes. *Bulletin of the National Technical University "Kharkiv Polytechnic Institure", Series "New Solutions in Modern Technologies"*, No. 16, pp. 165–176, doi: 10.20998/2413- 4295.2018.16.25.

5. Muhlenova, I. P., & Kovalev, O. S. (1987). *Absorption and dust extraction in the production of mineral fertilizers*. Moscow, Chemistry.

6. Moiseev, V. F., Manoylo, Ye. V., Lyaposhenko, O. O., Khukhryansky, O.M., & Ponomareva, N. G. (2018). Structure of foam layer on counteracting contact elements with stabilization. *Bulletin of the National Technical University "Kharkiv Polytechnic Institure", Series "New solutions in modern technologies"*, No. 26, pp. 83–92, doi: 10.20998/2413-4295.2018.26.37.

7. Perry, D. C., & Stevenson, P. (2015). Gas absorption and reaction in a wet pneumatic foam. *Chemical Engineering Science*, Vol. 126, pp. 177–185, doi: 10.1016/j.ces.2014.11.037.

Дослідження інтенсифікованих пінних апаратів із крупнодірчастими гратками

Liaposhchenko O.[1*], Khukhryanskiy O.[1,2], Moiseev V.[3], Ochowiak M.[4], Manoilo E.[3]

[1] Сумський державний університет, вул. Римського-Корсакова, 2, 40007, м. Суми, Україна;
[2] ПАТ «Укрхімпроект», вул. Іллінська, 13, 40009, м. Суми, Україна;
[3] Національний технічний університет «Харківський політехнічний інститут»,
вул. Кирпичова, 2, 61002, м. Харків, Україна;
[4] Технологічний університет м. Познань, пл. М. Склодовської-Кюрі, 5, 60-965, м. Познань, Польща

Анотація. У роботі досліджувалися укрупнені моделі пінних апаратів з гратками, зібраними з трубок різного діаметра. Розглядаються питання інтенсифікації пінних апаратів із застосуванням крупнодірчастих граток. Відзначена можливість глибокого очищення і практично повного очищення газів від аміаку і фтористих з'єднань при їх роздільній абсорбції. Наведено ряд експериментальних залежностей основних параметрів процесу. Підтверджена можливість ефективного проведення масообмінних процесів в інтенсивному пінному шарі на протитечійних крупнодірчастих гратках.

Ключові слова: викиди промислових газів, гідродинаміка, масообмін, пінний апарат, пінний шар, процес очищення, стабілізація пінного шару, інтенсифікація процесу.

Mathematical Modeling of Gas-Cleaning Equipment with a Highly Developed Phase Contact Surface

Plyatsuk L. D.[1], Ablieieva I. Yu.[1], Vaskin R. A.[1*], Yeskendirov M.[2], Hurets L. L.[1]

[1] Sumy State University, 2 Rymskogo-Korsakova St., 40007 Sumy, Ukraine;
[2] M. Auezov South Kazakhstan State University, 5 Tauke Khan Avenue, 160012, Shymkent, Republic of Kazakhstan

Abstract. The deposition of aerosols from process gas streams are the basis of many technologies in the chemical, petrochemical, coke, oil, gas, food etc. Industrial gases, containing aerosols of different nature of origin polydisperse solid particles (dust, smoke) or liquid particles (fog), must be cleaned. The idea of the author is to develop a mathematical model of the process of trapping waste gases, fogs in intensive nozzles with a developed surface of contact of phases. The vortex flow of the gas-liquid flow and its pulsating nature of the movement contribute to the intensification of the crushing process and coagulation of the drop gas-liquid flow in the layer of a regular moving nozzle. Methods of mathematical modeling of the process of movement of a polydisperse aerosol in a turbulent gas-liquid flow have been used. It was determined that condensation of steam in the cell occurs on the surface of the nozzle and also the formation of new germs of aerosol particles. The size distribution of aerosol particles is due to centrifugal forces. In this case, large particles are removed from the vortex region into a continuous flow, while small particles rotate in a vortex. Coagulation equation describing the change in the particle size distribution function with time, undergoing condensation and coagulation growth. The obtained results of differential and integral-differential equations can be used to describe the formation process and aerosols. Environmental and economic efficiency, as well as the optimal choice of environmental and auxiliary equipment took into account.

Keywords: "wet" cleaning technologies, regular moving nozzle, polydisperse aerosol, gas-liquid flow, condensation-coagulation integration.

1 Introduction

The activities of the chemical and petrochemical industries are accompanied by the formation and release of a wide range of pollutants into the air. The deposition of aerosols from process gas streams are the basis of many technologies in the chemical, petrochemical, coke, oil, gas, food etc. At the same time, they rather often resort not to preventive methods, but to "pipe" methods in order to achieve environmental safety standards (MPC) and technological (MPE) standards. So in the production of various formed products industrial gases containing aerosols of different nature of origin is a polydisperse solid particles (dust, smoke) or liquid particles (fog), from which the gases have to be cleaned [1].

In order to reduce the concentration of pollutants, technologies of "wet" and "dry" cleaning are used, implemented with the help of various hardware design.

The process of trapping occurs in mass transfer equipment at the end of the process. Purified dust and gas flow after exiting the cleaning equipment is released into the atmosphere and moves in the direction of the steady movement of air masses, i.e. on the wind rose, besieging at the same time.

From the point of view of environmental, economic and technological aspects, the process of "wet" cleaning of flue gases from aerosols (fumes, dust, fogs, etc.) is more efficient. Such mass exchangers include apparatuses with a nozzle, a regular nozzle, a shelf nozzle, which have a high degree of purification (trapping).

One of the main approaches to the design and development of cleaning devices is associated with the principle of heuristic modeling, which allows a number of optimization calculations to be performed under various initial conditions.

2 Literature Review

When a system-located contact elements flow around a gas-liquid flow in their root part, periodic formation and disruption of vortices occur, which form a vortex "path" of the pocket behind the streamlined contact element [2]. Depending on the shape of the cross section of the contact element, their location in the contact zone may be in a horizontal and vertical position. There may also be a case of mine location of the vortices, which predetermines the formation of a vortex wake.

The movement of the gas-liquid flow after a streamlined contact element occurs in a pulsating mode, inherent in the separated flow. The vortex flow of the gas-liquid flow and its pulsating nature of the movement contribute to the intensification of the crushing process and coagulation of the drop gas-liquid flow in the layer of a regular moving nozzle.

The results obtained in the work [3] confirm the theoretical ideas about the mechanism and regularities of the deposition of small fractions, for which the thickness of the boundary layer significantly affects the approach of particles to the deposition surface.

The study of the inadequate influence of the mechanisms of turbulent and inertial deposition allowed the researchers [1] to make a statement about the inappropriateness of increasing the velocity of the gas more than 15 m/s when trapping mist particles with a disparity dr < 0.6 microns.

Authors of the article [4] analyzed the process of coagulation of aerosol particles in turbulent aerosol flows as they flow through a layer of regularly placed turbulizing cylindrical elements (diameter d_c) installed in a plane-parallel channel (with a step t_b). Those, in the streams, where the in-phase vortex formation mode was implemented, which predetermined the extreme values of the hydrodynamic and heat and mass transfer characteristics of the flow. It is determined that when the concentration of steam exceeds 30 mg/m^3, the growth efficiency of particle sizes drops significantly.

Virtually all particles supplied by turbulent gas pulsations to the boundary of the laminar sublayer are deposited on the surface of the channel walls. The proximity of the dispersed composition of the initial and final aerosols [5] indicates the predominant role of diffusive sedimentation of particles. The aerosol particles, which are supplied by turbulent gas pulsations to the interface, have significant inertia and, as a result, can penetrate into the boundary layer.

In the contact zone, the principle of longitudinal partitioning is implemented using various nozzle designs. The most effective is a regular mobile nozzle. The turbulizing nozzle allows a high degree of purification from fogs, aerosols and polydisperse gas and liquid streams.

The nature and intensity of movement of the main carrier gas-liquid flow in direct-flow interaction of the phases determines the hydrodynamics of the gas cleaning apparatus.

In the article [6] are derived equations for calculating the thickness of the descending liquid film, starting from the balance of forces acting on the liquid film formed on the elements of the regular nozzle during the direct-flow mode of phases (both upward and downward), as well as the resistance of a plate-shaped cap coated with a film. However, these mathematical models and algorithms for calculating devices with a regular moving nozzle do not take into account the polydisperse composition of the droplet component of the surface of the contact phase.

To solve equations of the mathematical model related to the removal efficiency of a Venturi scrubber scientists [7] used an upwind control-volume method. This method is applicable to convection and diffusion equations when the Peclet number is greater than 2. For high Peclet numbers, the common numerical error of false diffusion can be neglected and, in spite of the simplicity of the upwind scheme, the numerical results are valid.

Authors of the article [8] made an attempt for application of the system-element approach in building a physical and mathematical model of a chemical process to create an ecologically safe equipment. However, the paper presents only the structure and algorithm of the mathematical description of the coagulation processes (including condensation-coagulation integration) and the deposition of aerosols, without mathematical models.

The aim of the work is to develop a mathematical model of the process of trapping waste gases, fogs in intensive nozzles with a developed surface of contact of phases.

3 Research Methodology

Consider the process of movement of a polydisperse aerosol in a turbulent gas-liquid flow. The enlargement of the aerosol is due to the condensation mechanism. Condensation of steam in the cell occurs on the surface of the nozzle and also the formation of new germs of aerosol particles.

The total balance for the pair can be written as:

$$Q_s^{(f)} = Q_s^{(in)} - \sum_{i=1}^{n} Q_i \tag{1}$$

where $Q_s^{(in)}$ is the initial quantity of steam, J; $Q_s^{(f)}$ is the final quantity of steam, J; the sum is the amount of steam going to condensation, J:

$$\sum_{i=1}^{n} Q_i = Q_1 = Q_2 + Q_3 \tag{2}$$

where Q_1 is the amount of steam condensing on the nozzle, J; Q_2 is the amount of steam condensing on the surface of the aerosol, J; Q_3 is amount of condensed steam, J.

To determine the condensed steam on the surface of the nozzle elements, we use the mass transfer equation:

$$\frac{dQ_1}{dt} = \frac{\beta_s F}{R_g T_{sg}} \left(P_s - P_w \right) \tag{3}$$

where Q_1 is the amount of steam condensing on the nozzle, J; t is time, sec; β_s is steam mass transfer coefficient; F is the surface of the contact phase (condensation), m^2; P_s is steam partial pressure, Pa; P_w is steam partial pressure at the

wall, Pa; R_g is universal gas constant; T_{sg} is steam gas mixture temperature, K.

The amount of condensed steam on the particles is determined using the dependencies:

$$\frac{dQ_2}{dt} = N_r \int_0^\infty \frac{dQ_r}{dt} f(r,t) dr \tag{4}$$

where dQ_2/dt is the amount of steam condensing on a single particle; N_r is the total number of particles involved in the condensation process; $f(r, t)$ is distribution function of aerosol particles in size.

The initial distribution function of aerosol particle size is subject to the normal-logarithmic distribution [9], in the initial period of condensation:

$$f = (r,0) = \frac{1}{r \ln \sigma \sqrt{2n}} \exp\left[-\frac{(\ln r - \ln \bar{r})^2}{2 \ln^2 \sigma}\right] \tag{5}$$

where $\bar{r}$ is the average geometric radius of particles, m; σ – standard deviation.

The change in mass of a single particle [10] is determined by

$$\frac{dQ_r}{dt} = \frac{4\pi \beta_s M_s r}{R_g T_{sg} \varphi} \left[P_s - \rho_g (T_g) \right] \tag{6}$$

where M_s is the molecular mass of steam, kg/kmol; ρ_g is gas density, kg/m³.

In this equation the Knudsen number K_n is introduced for determining the following parameter:

$$\varphi = 1 + \frac{1,33 K_n + 0,71}{1 + K_n}$$

To change the radius of particles in time, we convert equation (6) into formula (7):

$$\frac{dr}{dt} = \frac{3\beta_s M_s}{r R_g T \varphi \varphi_g} \left[P_s - P_g (T)_g \right] \tag{7}$$

The temperature and pressure of the steam-gas mixture will be determined based on the mixing balance:

$$T = \frac{T_g + ab T_s}{1 + ab} \tag{8}$$

$$P = \frac{P_g + ac P_s}{1 + ac} \tag{9}$$

where $a = Q_s/Q_g$, $b = C_s/C_g$, $C = M_s/M_g$, and C_s, C_g are the heat capacities of steam and gas, respectively, J/(kg·K).

4 Results and Discussion

The solution of equation (7) together with equations (8) and (9) has a physical meaning in the case of a uniform distribution of temperature and pressure in the volume of the conventional cell, with a laminar flow of the

gas-steam mixture. In the case under study, the gas-liquid (steam-gas) mixture is in an intense turbulent mode, which causes pressure drops (fluctuation), flow temperatures over the cross section and in the volume of the contact zone.

Considering the flow in a single vortex and based on the principles of theoretical hydrodynamics [4], we assume that the vortex consists of a nucleus rotating according to the law of a solid body and a vortex field (Fig. 1).

To change the linear velocity of motion from the radius of the vortex, we can write:

1) for the vortex core ($R_i < R$):

$$\int_s U_i dS^{(Q)} = \omega \pi R_i^2 \tag{10}$$

2) for the vortex field ($R_b > R$):

$$\int_s U dS^{(Q)} = \omega \pi R^3 \tag{11}$$

where S is sectional area of the vortex, m²; ω is angular velocity, s⁻¹; U, U_i – constants on the corresponding vortex circles.
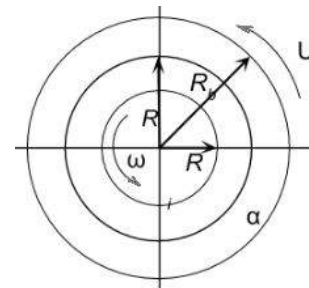
Figure 1 – Scheme of vortex motion

For the vortex core we write the equations

$$2\pi R_i U_i = \omega \pi R_i^2 \tag{12}$$

for the vortex field

$$2\pi R_B U = \omega \pi R^2 \tag{13}$$

Then for the vortex core we get

$$U_i = \frac{\omega R_1}{2} \tag{14}$$

for the vortex field

$$U = \frac{\omega R}{2 R_2} \tag{15}$$

Substituting in equations (14), (15) the value of the angular velocity equal to

$$\omega = I / \pi R^2 \tag{16}$$

where $I = U_c^2/(2f) = U_g d_c/(2Sl)$ is the intensity of the circulation rate, m²/s; f –vortex breakdown frequency, s⁻¹; Sl – Strouhal number.

Will get

$$U_i = \frac{IR_i}{2\pi R^2} \qquad (17)$$

$$U = \frac{I}{2\pi R_B} \qquad (18)$$

Knowing the laws of variation of the linear flow velocity along the vortex radius, we determine the pressure drop in the core and the vortex field.

The law of conservation of momentum in cylindrical coordinates can be written in the form:

$$\rho \frac{U}{R} = \frac{\partial P}{\partial R} \qquad (19)$$

Substituting in the equation (19) the value of the linear velocity from equations (17), (18) and integrating over pressure from P_0 to P, as well as along the vortex radius from 0 to R, we get

$$P = \frac{I^2 R^2 \rho_g}{8\pi^2 R_B^4} + P_0 \qquad (20)$$

where P_0 is the pressure in the center of the vortex, Pa; P is gas pressure, Pa.

Then for the field of the vortex dependence will be:

$$P_R = P_g - \frac{I^2 \rho_\Gamma}{8\pi^2 R^2} \qquad (21)$$

for P_0, we can write the expression

$$P_0 = P_g - \frac{I^2 \rho_g}{4\pi^2 R_B^2} \qquad (22)$$

and for the vortex we write the following relation

$$P_{R*} = P_g - \frac{I^2 \rho_g}{4\pi^2 R_B^2}\left(1 - \frac{R_*^2}{2R_B^2}\right) \qquad (23)$$

Finally, for a steam-gas flow around a nozzle element with a geometric dimension d_c, the pressure drop in a single vortex will be written:
1) for the vortex core

$$P_{R*} = P_g - \rho_g \left(\frac{U_c d_c}{4\pi R_6 Sl}\right)^2 \left(1 - \frac{R_*^2}{2R_B^2}\right) \qquad (24)$$

2) for the vortex field

$$P_R = P_g - \frac{\rho_g}{8}\left(\frac{U_g d_c}{4\pi R_6 Sl}\right)^2 \qquad (25)$$

In the case of an adiabatic steam – gas mixture, a similar solution together with the adiabatic equation allows one to obtain pressure drops:

$$\Delta P_{R*} = \frac{k-1}{k}\rho_g \left(\frac{U_c d_c}{4\pi R_6 Sl}\right)^2 \left(1 - \frac{R_*^2}{2R_B^2}\right) \qquad (26)$$

$$\Delta P_R = \frac{k-1}{k}\frac{\rho_g}{8}\left(\frac{U_g d_c}{4\pi R_6 Sl}\right)^2 \qquad (27)$$

where k is the adiabatic index.

To obtain the dependences on the temperature variation of the steam-gas mixture in a single vortex when solving equations (26) and (27) together with the equation of state of an ideal gas $P \cdot V = R \cdot T$, we obtain for the core

$$\Delta T_{R*} = \frac{k-1}{k}\frac{1}{R_g}\left(\frac{U_g d_c}{4\pi R\, Sl}\right)^2 \left(1 - \frac{R_*^2}{2R^2}\right) \qquad (28)$$

for the field

$$\Delta T_R = \frac{k-1}{k}\frac{1}{2R_g}\left(\frac{U_g d_c}{4\pi R\, Sl}\right)^2 \qquad (29)$$

In equations (26) – (29) the size of the radius R_B and vortex core R_* can be determined by the formulas:

$$R_B = 0,25 d_c \qquad (30)$$

$$R_* = \left(5,04 v_g t_B\right)^{1/2} \qquad (31)$$

where t_B is the formation time of the vortex, s; v_g is the coefficient of kinematic viscosity, m^2/s.

The formation of each vortex, breaking with the nozzle element and its formation time is equal to:

$$t_B = 0,5 d_c / U_B \qquad (32)$$

where $U_B = 0.86 U_g$ is the speed of the vortex, m/s.

The size distribution of aerosol particles is due to centrifugal forces. In this case, large particles are removed from the vortex region into a continuous flow, while small particles rotate in a vortex.

Using a number of assumptions, we will calculate the structure of a two-phase flow with the determination of the trajectory of the particles inside the vortex, the critical radius of aerosol particles, and the time of formation of the vortex.

To describe the process of movement of particles, apply the equation

$$\frac{d^2 x}{dt^2} + \frac{1}{A}\frac{dx}{dt} - \frac{1}{x^3} = 0 \qquad (33)$$

where $x = R/R_B$; $t = t_c \cdot U_{pt}/R_h$ is the dimensionless quantity; U_{pt} is tangential velocity of the particle, m/s. The parameter A can be evaluated by the following formula:

$$A = \frac{r_p\left(\rho_p - \rho_g\right)U_{pt}}{72\mu_g R}$$

Equation (33) is a nonlinear differential equation; it has no analytical solution. If we neglect the second-order differential, divide the variables and integrate t from 0 to t and x from x_1 to x_2, and substitute the values $U_{pt} = U_g$ from equation (17), then we can determine the critical particle radius for the vortex core:

$$r_{cr} = 4,08 Sl \left(\frac{\mu_g}{\rho_p - \rho_g} \right)^{1/2} \left(\frac{dy}{U_g} \right)^{1/2} \tag{34}$$

The process of coagulation of aerosol particles in the cell volume is not the only one in volume. The presence of turbulent pulsations and Brownian motion of particles leads to growth. Given these conditions, the coagulation equation describing the change in the particle size distribution function with time, undergoing condensation and coagulation growth

$$\frac{\partial f(r_p, t)}{\partial t} + \frac{\partial}{\partial r} \left[f(r_p, t) \frac{dr}{dt} \right] =$$
$$= \int_{r=0}^{r=r_p/\sqrt[3]{2}} K_C \sqrt[3]{r_{av}^3 - r^3}, r \times$$
$$\times f\left(\sqrt[3]{r_p^3 - r^3}, t \right) f(r, \tau) \left(\frac{r}{\sqrt[3]{r_p^3 - r^3}} \right)^2 dr -$$
$$- \int_{r=0}^{r=\infty} K_C (r_p, t) f(r_p, t) f(r, t) dr +$$
$$+ \frac{Q}{V_c} \left[f(r, 0) - f(r, t) \right] \tag{35}$$

where r is the current radius of the aerosol particle, m; Q is aerosol consumption, m³/s; V_c is cell volume, m³; K_C is coagulation coefficient due to turbulent and Brownian mechanisms, m³/s.

The coagulation coefficient K_C is calculated as the sum of the coefficients by turbulent K_T and Brownian coagulation K_B

$$K_C = K_T + K_B \tag{36}$$

$$K_B = \frac{4 k_b T_g}{3 \mu_g}, \tag{37}$$

where k_b is the Boltzmann constant.

The coefficient of turbulent coagulation [8] is determined by:

$$K_T = 1,67 (r_p + r)^3 \sqrt{E/\nu_g} \tag{38}$$

The energy dissipation E in the volume of the cell E is defined as:

$$E = \frac{N_B}{V_c \rho_{sg}} \tag{39}$$

Here N_B is the power of the vortex formed when a nozzle flows around a continuous flow.

The vortex power is determined by the equation:

$$N_B = C_L \sqrt{\frac{C_L}{C_D}} \rho_{sg} l_c dy \frac{U_g^3}{2} \tag{40}$$

where C_L is the lift coefficient; C_D is coefficient of resistance; U_g is true gas flow rate, m/s; l_c is geometrical size of the nozzle, m.

Cell volume is:

$$V_c = b \cdot I_c \cdot t_{b.c}, \tag{41}$$

where b is the width of the plane-parallel channel, m; $t_{b.c}$ is cell height equal to the center distance between the elements of the nozzle, m.

Substituting the expressions (40) and (41) into equation (39) we get

$$E = \frac{C_{LD}}{2b} \frac{dy}{t_b} U_g^3, \tag{42}$$

where

$$C_{LD} = C_L \sqrt{\frac{C_L}{C_D}}$$

The developed models make it most likely to establish the mechanism of interaction of dispersed particles with a continuous flow, taking into account the structural features of the developed apparatus.

5 Conclusions

On the basis of the conducted substantiation and calculations, it is possible to obtain a system of differential and integral-differential equations, which make it possible to describe the formation process and aerosols due to condensation and coagulation growth. In this way, it becomes possible to carry out the calculation of the effective capture of waste gases, fogs in intensive packing devices with a developed surface of the contact of phases.

The design and performance parameters of the developed apparatus were calculated to determine the environmental and economic efficiency, as well as the optimal choice of environmental and auxiliary equipment, without which the assembly of the unit, installation and production line is impossible.

References

1. Yeskendirov, M. Z., Sadyrbaev, A. S., Turebekova, A. M., & Vozzhaeva, N. S. (2017). *Studies of trapping of aerosols in turbulent two-phase flows*. Retrieved from https://www.eduherald.ru/pdf/2017/3/17215.pdf.
2. Kafarov, V. V., & Dorokhov, I. N. (1976). *System analysis of chemical technology processes*. Science, Moscow, Russia.
3. Sabyrkhanov, D. S. (1996). *Development, calculation and implementation of mass transfer and dust collecting devices with a movable and regular packing*. Shymkent.
4. Sadyrbaeva, A. S., Eskendirov, M. Z., Usipbaev, U. A., Asylbek, N. U., & Asylbek, G. U. (2017). Studies of the integration of aerosol particles in turbulent two-phase flows. *International Student Science Journal*, Vol. 5. Retrieved from http://www.eduherald.ru/ru/article/view?id=17314.
5. Golubev, V. G., & Brener, A. M. (2002). Features of film condensation from a dusty steam-gas mixture. *Theoretical foundations of chemical technology*, Vol. 36, Issue 2, pp. 141–146.
6. Sadyrbayeva, A. S., Eskendirov, M. Z., Ussipbayev, U. A., et al. (2017). Investigation of the hydrodynamic characteristics of the liquid film flow. *Bulletin of the Eurasian National University named after L. N. Gumilyov*, Vol. 4 (119), pp. 175–177.
7. Talaie, M. R., Fathikalajahi, J., & Taheri, M. (1997). Mathematical modeling of SO_2 absorption in a Venturi scrubber. *Journal of the Air and Waste Management Association*, Vol. 47 (11), pp. 1211–1215, doi: 10.1080/10473289.1997.10464066.
8. Altukhov, A. V., Balabekov, O. S., Volnenko, A. A., & Balabekov, M. O. (2013). *Methodology for the study and calculation of an environmentally perfect unit*. Scientific research and their practical application. Modern state and ways of development.
9. Dzyubenko, B. F., Kuzma-Kichta, Yu. A., Holpanov, L. P., et al. (2008). *Intensification of heat and mass transfer at the macro, micro and nano scales*. TSNIIATOMINFORM, Moscow, Russia.
10. Sadyrbaeva, A. S., Yeskendirov, M. Z., Usipbaev, U. A., Sadyrbaeva, A. S., Ormanova, G. M., & Asylbek, N. U. (2017). Turbulent-diffusion mechanism for aerosol deposition in the presence of a water steam concentration gradient. *Bulletin of the Eurasian National University named after L. N. Gumilyov*, Vol. 4 (119), pp. 178–182.

Математичне моделювання газоочисного обладнання з високорозвиненою поверхнею контакту фаз

Пляцук Л. Д.[1], Аблєєва І. Ю.[1], Васькін Р. А.[1], Єскендіров М.[2], Гурець Л. Л.[1]

[1] Сумський державний університет, вул. Римського-Корсакова, 40007, м. Суми, Україна;
[2] Південно-Казахський національний університет ім. М. Ауезова,
просп. Тауке Хан, 5, 160012, м. Шимкент, Республіка Казахстан

Анотація. Осадження аерозолів з технологічних газових потоків лежить в основі багатьох технологій хімічної, нафтохімічної, коксохімічної, нафто-газової, харчової промисловості тощо. Промислові гази, що містять аерозолі різної природи походження, полідисперсні тверді частинки (пил, дим), або рідкі частинки (туман) необхідно очищувати. Авторська ідея полягає у розробленні математичної моделі процесу захоплення відхідних газів, туманів в інтенсивних насадках з розвиненою поверхнею контакту фаз. Вихровий газо-рідинний потік та пульсуючий характер його руху сприяють інтенсифікації процесу дроблення і коагуляції при падінні газорідинного потоку в шарі традиційної рухомої насадки. Використовуються методи математичного моделювання процесу руху полідисперсного аерозолю в турбулентному газорідинному потоці. Встановлено, що конденсація пари у комірці відбувається на поверхні насадки, а також утворюються нові зародження частинок аерозолю. Розподіл частинок аерозолю відбувається завдяки відцентровим силам. У цьому випадку відносно великі частинки видаляються з вихрової області до безперервного потоку, а невеликі частинки обертаються у вихорі. Рівняння коагуляції, що описує зміну функції розподілу за розміром частинок з часом, ураховує конденсацію і зростання коагуляції. Отримані результати диференціальних та інтегро-диференціальних рівнянь можуть бути використані для опису процесу формування аерозолів. Ураховано екологічну та економічну ефективність, а також оптимальний вибір екологічного та допоміжного обладнання.

Ключові слова: технології «мокрого» очищення, насадка з регулярним переміщенням, полідисперсний аерозоль, газорідинний потік, конденсатно-коагуляційна інтеграція.

SUMY STATE UNIVERSITY

TECHNOLOGY AND MECHANIZATION OF THE UNIT FOR PRODUCTION OF COMPLEX LIQUID FERTLIZERS

Purpose and Scope of Application

The device is developed for production of complex liquid nitrogen and phosphorus fertilizers of various grades, in particular with high nitrogen content, on the mobile industrial block-modular unit.

Main Characteristics of the Device

Mobile unit for production of complex liquid nitrogen-containing fertilizers provides the opportunity to obtain the commercial product with high nitrogen content (up to 30%). Flexible technological line enables to produce complex liquid nitrogen-containing fertilizers with a wide range of nitrogen and phosphorus content (up to 20% of nitrogen and 8.5% of phosphorus), and, if necessary, trace elements can be added. Production line performance is up to 15 tons per hour for the finished product.

## Main Advanatges of the Unit

The production of complex liquid fertilizers instead of traditional mineral fertilizers involves reducing of the economic and energy costs on processing agricultural areas. Less technological passages of equipment on the farmed area are required and less transport costs are necessary for the delivery of liquid complex fertilizers to the place of use or such automobile delivery of fertilers will not be needed at all. Liquid fertilizers increase the efficiency of useful substances assimilation by plants in comparison with solid mineral fertilizers.

Intellectual Property Protection Status

There are issued 2 patents of Ukraine on the production unit (№ 1155895, №121362).

Market Demand

Mobile unit for production of liquid complex fertilizers can be used by agrarian enterprises to cover their own needs in mineral complex fertilizers as well as by fertilizer producers for sale to third-party consumers.
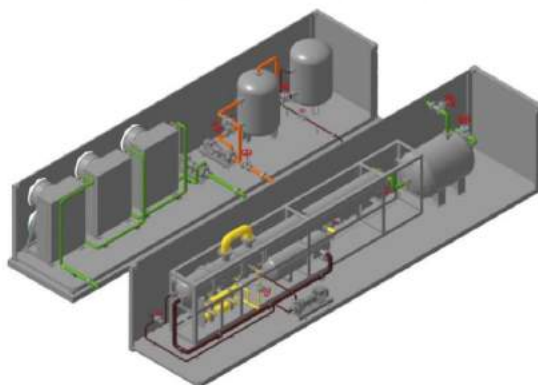
Readiness State of the Developed Unit

A set of design and technological documentation for the production of the main technological equipment of the unit has been developed. Experimental and industrial samples are being tested. The developed unit is ready for introduction.

International Collaboration

ENGITEC

Modernizing Higher Engineering Education in Georgia, Ukraine and Uzbekistan to meet the Technology Challenge

(530244-TEMPUS-1-2012-1-SE-TEMPUS-JPCR)

Partners

Characterization and Degradation of Viton Fuel Hose Exposed to Blended Diesel and Waste Cooking Oil Biodiesel

Samuel O. D.[1*], Emovon I.[1], Idubor F. I.[1], Adekomaya O.[2]

[1] Federal University of Petroleum Resources, P.M.B. 1221, Effurun, Delta State, Nigeria;
[2] Tshwane University of Technology, Pretoria 0001, South Africa

[*]**Corresponding Author's Address:**
samuel.david@fupre.edu.ng

Abstract. Degradation and material incompatibility between biodiesel and fuel system are the major concern associated with the adoption of biodiesel. In this research, effects of different mixture of waste cooking oil biodiesel/diesel blends (B10, B20 and B40) were investigated on the basic fuel properties such as density, kinematic viscosity (KV), flash point (FP), pour point (PP), cloud point (PP), freezing point (FRP) and sulphur content (SC). Viton fuel hose exposed to different fuel of types and their degradation characteristics, total acid number and change in the surface morphology were studied. It was found that density, KV, FP, FRP, CP and PP increased while SC decreased with increasing biodiesel content in the blends. The biodiesel concentration was noticed to affect the properties of elastomers, causing swelling of Viton fuel hose. The exposure of Viton fuel hose to fuel types of increasing biodiesel content led to reductions in tensile strength, harness and compressive strength.

Keywords: degradation, Viton hose, biodiesel, hardness, compressive strength, swelling.

1 Introduction

Increase demands for alternative energy and pollution problem caused by the widespread usage of fossil fuel have stimulated increasingly development of alternative source of energy. Biodiesel has marked a realistic option among other biofuel because of its environmental friendliness, readily available feedstock and technical feasible [1]. Biodiesel synthesized from lipid feedstocks (e. g., waste cooking oil). is considered as potential feedstock because of its biodegradability, higher flash point, lubricity, less exhaust emission, higher cetane, and almost zero sulphur content [2]. The adoption of up to 20 % biodiesel has been implemented in many developed country, but there is practical step towards exploring of higher blends for the future heavy-duty vehicles capable of up to 40 % (B40) [3, 4]. Biodiesel, although a biodegradable and sustainable fuel, often associated with degradation of automotive elastomers and corrosion of automotive parts when exposed to biodiesel [5, 6]. Degradation of automotive rubbers implies irreversible deterioration of the physical and chemical properties [7]. Notable factors that cause degradation are temperature, light, ionizing, radiation, humidity, fluids, bio- organism, mechanical stress and electrical stress [8]. In addition, the corrosiveness and

degradation nature of automotive parts have been aggravated by the presence in the molecules in biodiesel [9]. In spite of the numerous advantages of biodiesel over fossil diesel, rubber automotive material is prone to wear and degradation when exposed to biodiesel. Polymers such as elastomers and plastic can degrade because of pure biodiesel contact [10]. As a result of degradation, mechanical properties such as hardness, tensile strength, cracking and chemical disintegration of petroleum products are being affected [10, 11]. Moreover, the degree of degradation of automotive rubber has been attributed to high level of biodiesel contact [12]. The impact of employing high blends of biodiesel has been identified to cause several problems of corrosion, degradation, filter clogging, pour combustion, low performance, and so on by several authors [13, 14]. In addition, insufficient information regarding compatibility of biodiesel and elastomers has been causing set-backs in an automotive industry [12].

Several researchers have investigated the degradation nature of elastomers in different types of fuel and its blends [15–20]. Besse and Fay [21] investigated the effect of soya biodiesel-diesel fuel blends on the tensile strength, hardness, elongation and swelling on different polymers. Their results showed that nitrile, nylon 6-6, and high density polypropylene change in physical prop-

erties while Teflon, Viton 401-C, and Viton GFLT did not cause a significant change. Alves et al. [18] investigated the effect of biodiesel from palm and soy bean oil on the degradation behaviour and sealing capacity of nitrile rubber (NBR) and fluorocarbon (FKM). They reported a decrease in mass of the NBR for all biodiesel. Trakampruk and Porntangjitlikit [22] studied effect of biodiesels on six kinds of elastomers properties related to fuel systems. The researchers remarked that the biodiesel has negligible impact on the properties of co–polymer FKM, and terpolymer FKM. Haseebet al. [23] compared degradation properties of five types of elastomers (EPDM, NBR, CR, SR and PTFE) in palm biodiesel / diesel fuel. Their results demonstrated that the compatible elastomers in palm biodiesel to be PTFE > SR > NBR > EPDM > CR. Haseebet al. [24] investigated the degradation of various elastomers in palm biodiesel. Their analysis showed that mechanical properties such as tensile strength, elongation and hardness were reduced for both nitrile rubber and polychloroprene while little changes were observed for fluoro-Viton. Nuneset al. [25] determined the effect of biodiesel on nitrile rubber with three kinds of acrylonitrile contents at 28 %, 33 % and 45 %. Their analysis demonstrated that the higher content of acrylonitrile makes the nitrile rubber more resistance to biodiesel degradation. However, none of these studies analyzed degradation of Viton fuel in the spectrum range of blends of waste cooking oil methyl ester and fossil diesel. It is worth knowing that information associated with degradation of the Viton fuel hose system will provide base data information for biodiesel stakeholders in automotive industry. The present work aimed to investigate the degradation characteristic of Viton fuel hose in waste cooking oil biodiesel/diesel fuel blends. This analysis further verified the influence of exposition to the fuel and the changes in the mechanical and degradation properties were also studied.

2 Research Methodology

2.1 Blend preparation and characterization

The biodiesel employed in this work was synthesized in a reactor shown in plate 1. Basic alkaline transesterification was adopted on waste cooking oil (WCO) using oil / methanol molar ratio of 5:99, with 1.1 % potassium hydroxide by weight as the catalyst. The reaction duration and temperature were 78 min and 60 °C respectively. The fossil diesel was procured from Jocceco Filling station, Warri, Delta State, Nigeria. The splash method was adopted to prepare three blends of waste cooking oil methyl ester (WCOME) and fossil diesel (B0) at proportions of B10 (10 %), B20 (20 %) and B40 (40 %) on volume basis. In order to ensure homogeneous mixture, required volume of WCOME and B0 was mixed and agitated as described elsewhere [26–28].

The blend properties of fuel types were analyzed following the ASTM standards. Density was measured in accordance with ASTM D1250 [29] using calibrated glass API gravity hydrometers. Viscosity was determined following ASTM D445 standard [30] using a Model

VSTA-2000 Chongqing viscometer (Gallekamp model A345, UK).The Flash point was determined according to the procedures in ASTM methods D56 [31] using a Model 750/AUT Pensky-Martens flash tester (USA, 0.1 °C accuracy). Acid value (AV, mgKOH/g) was determined as indicated in ASTM D664 [32] using an automated titration system (Toledo, USA). Cloud (CP, °C), pour (PP, °C) and freezing points (FP, °C) analyzed were made in accordance with ASTM standards D2500, D97 and D5901 [32] (ASTM, 2007) respectively, using a Model 664 Lawler CP, PP and FP analyzer (USA, 0.1 °C accuracy). Sulphur content was measured in accordance with ASTM D129 [33] using a Horiba sulphur analyzer (Tokyo, Japan).

Schematic set up diagram for transesterification is presented in Figure 1.
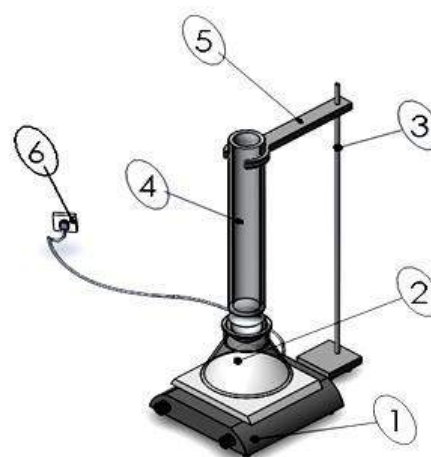

Figure 1 – Schematic set up diagram for transesterification:
1 – heating mantle; 2 – reactor; 3 – tripod stand;
4 – condenser; 5 – clamp; 6 – power source

2.2 Elastomer preparation

The test was conducted using 10 test coupons 7×100 mm, cut from a Viton fuel hose, as set by ASTM D471 [34]. Two jars per coupon were used for immersion test and the Viton fuel hoses were suspended by stainless safety wire, via 2.5 mm hole in the end of each one, so that they were completely immersed but were not rested on the bottom of the jar.The mass of the automotive rubber types before swelling of the test coupon were subsequently determined using an analytical balance (Contech, India). The temperature was maintained constant during the exposure time for 720 hours, as stipulated by the standard using circulating water bath. The ten time coupons were kept in the dark. The coupons were removed from the vessel and suspended outdoor to enable fuel evaporate, so that other final mass after swelling was then carried out. Finally, the percentage mass changes were calculated by the following equation:

$$\Delta_m = \frac{m_2 - m_1}{m_1} \cdot 100 \%, \qquad (1)$$

where Δ_m – change rate of mass; m_1 – sample mass before immersion; m_2 – sample mass after immersion.

2.3 Mechanical parameters evaluation

The mechanical properties testing of duplicate test elastomers were conducted before and after swelling experiment. Mechanical properties such as hardness testing and compression testing with Rockwell hardness testing machine (Excel B34H, England) and universal tensiometer machine (TM 415, England), situated at the University of Nigeria, Nsukka, respectively.

2.4 Degradation of the fuel types and surface morphology

The changes in the surface morphology of the coupons Viton fuel hose after being exposed to the fuel types were investigated by JCM 100 mini scanning electron microscope (SEM) (Joel, USA) at the Chemical Engineering Department, Ahmadu Bello University, Zaria, Kaduna State, Nigeria.

Moreover, degradation of the different biodiesel / diesel fuel types was assessed before and after using total acid number.

3 Results

3.1 Characterization of waste cooking oil methyl ester and diesel fuel blends

Presented in Figures 2–9 are the variations of basic fuel properties and biodiesel content. Fuel properties of the experimental data were correlated as a function of biodiesel concentration. The effect of biodiesel concentration was investigated on the following key properties: such as density, kinematic viscosity (KV), flash point (FP), acid value, water content, pour point (PP), cloud point (CP), freezing point and sulphur content (SC).

Density increased as the content of WCOME increased in the blends. As the content of WCOME–fossil diesel shifted from 10 % to 40 %, the density of the biodiesel blends advanced from 862.6 to 871.2 kg/m^3 but they are within the specification of EN14214 standard (860–900 kg/m^3). Second-degree equation was found suitable to correlate the variation of densities and WCOME–diesel fuel blends. The coefficient of determinant (R^2) from the density regression model shows that over 99.6 % of the data is captured in the empirical equation. Hammare and Yamin [35] reported that more fuel is injected as the fuel density increase.

The kinematic viscosity (KV) of the WCOME–diesel fuel blends certified the density norms of the ASTM D6751 (1.9–6.0kg/m^3) and EN14214 (3.5–5.0 kg/m^3) specification even though the KV of the WCOME increased as the content of biodiesel in the blends increased. The third-degree model equation was found adequate to correlate the variation of KV and WCOME-diesel fuel blends. Similar observation was also reported by Alptekin and Canacki [36]. The high R^2 (0.978) indicates that over 97.8 % of the data is captured by the empirical equation.

The flash point (FP) increased as the content of WCOME increases in the blends. The increasing trend reveals that the fuels are safe to transport and store. A third-degree polynomial equation was utilized to correlate the variation of FP with biodiesel content at any blend. The R^2 of 0.999 reveals that over 99.9 % of the measured FP was captured by the FP regression equation.

The cloud and pour points values increased as the content of waste cooking oil methyl esters advance in the blends. A second-order degree equation and third-degree equation were developed for the respective cloud point and pour point variation with biodiesel percentage. The high R^2 (0.999) and R^2 (0.995) resulting from the pour point regression model and cloud point polynomial, respectively reveal that not less than 99 % of the experiment data were captured for the cloud and pour points measured.

The freezing point increased from –15 °C to –12 °C as the percentage of biodiesel advanced from B10 to B40. The values of freezing point of WCOME (2 °C) were higher than that of the diesel fuel (–16 °C). The measured freezing points are found to be correlated by the third-degree equation and a high R^2 (0.999) indicates that over 99.9 % of the data are captured by freezing point regression model.

The sulphur content of the WCOME-diesel blends certified the sulphur content norms of the ASTM D6751and EN14214 (0.05 mg) specification, even though the sulphur content of the WCOME decreased as the content of biodiesel in the blends increased. The result is in consistent with the findings of sulphur content of loofa oil ethyl ester blends [37]. Sulphur (IV) oxide is expected to reduce if fossil diesel is fuelled with WCOME blends. The third degree model equation was found adequate to correlate the variation of sulphur content and methyl ester in the blends. The high R^2 (0.9999) indicates that 99.9 % of the experiment was captured by the sulphur content model equation.
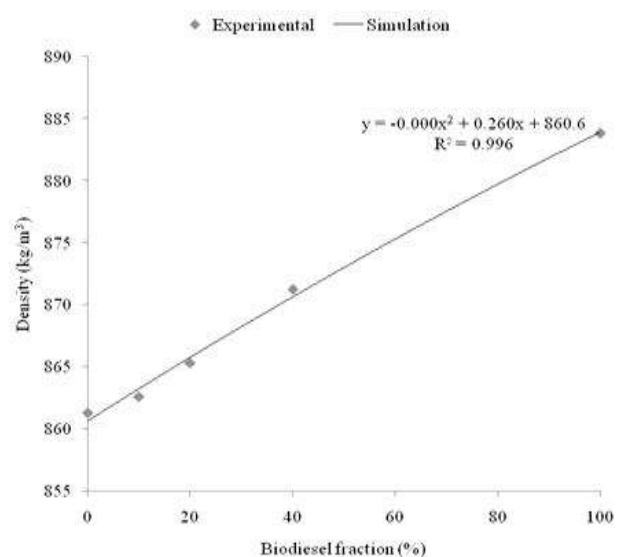

$$y = -0.000x^2 + 0.260x + 860.6$$
$$R^2 = 0.996$$

Figure 2 – Variation of density with biodiesel fraction
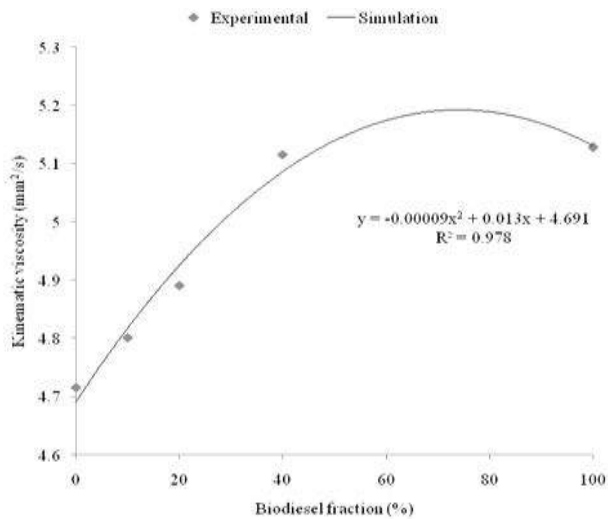
Figure 3 – Variation of kinematic viscosity with biodiesel fraction

$$y = -0.00009x^2 + 0.013x + 4.691$$
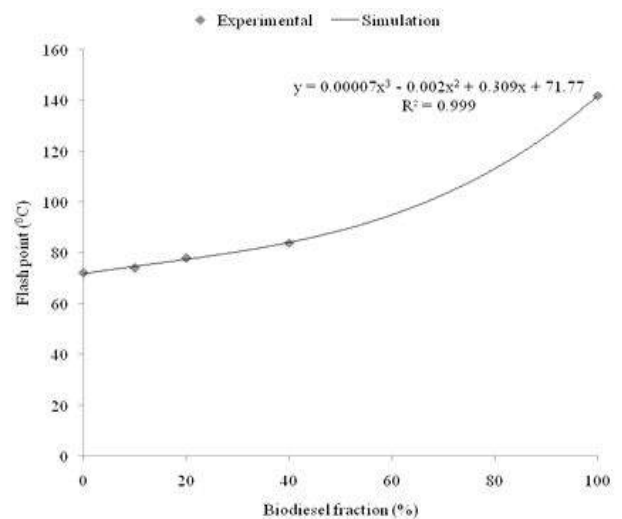$$R^2 = 0.978$$

Figure 4 – Variation of flash point with biodiesel fraction

$$y = 0.00007x^3 - 0.002x^2 + 0.309x + 71.77$$
$$R^2 = 0.999$$
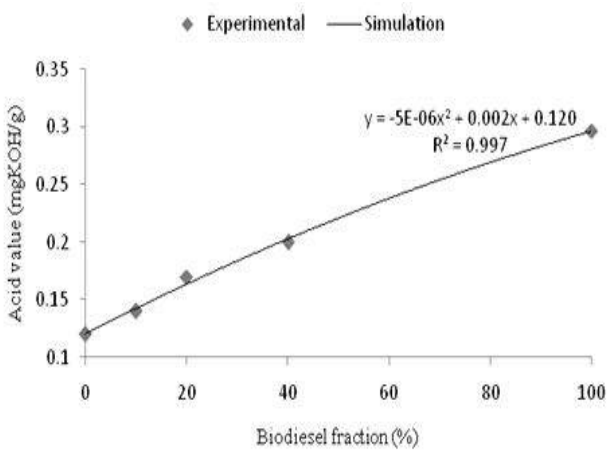
Figure 5 – Variation of acid value with biodiesel fraction

$$y = -5E\text{-}06x^2 + 0.002x + 0.120$$
$$R^2 = 0.997$$
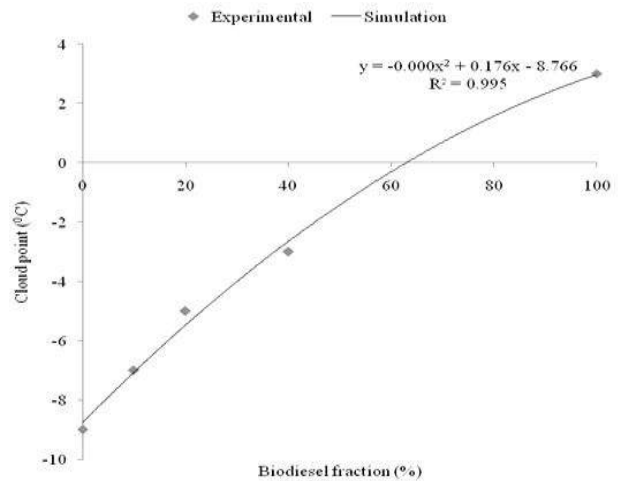
Figure 6 – Variation of cloud point with biodiesel fraction

$$y = -0.000x^2 + 0.176x - 8.766$$
$$R^2 = 0.995$$
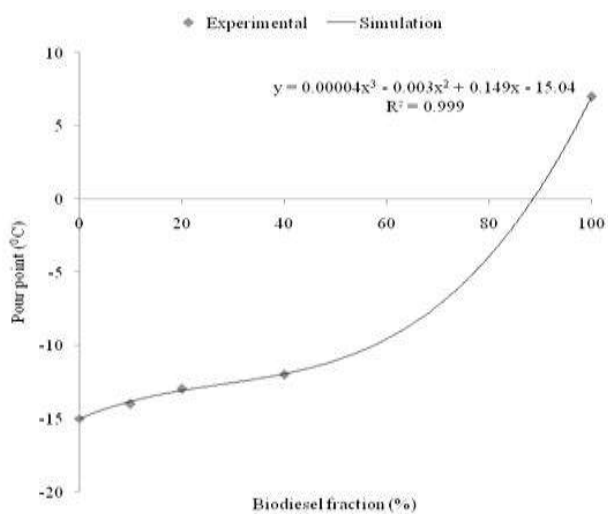
Figure 7 – Variation of pour point with biodiesel fraction

$$y = 0.00004x^3 - 0.003x^2 + 0.149x - 15.04$$
$$R^2 = 0.999$$
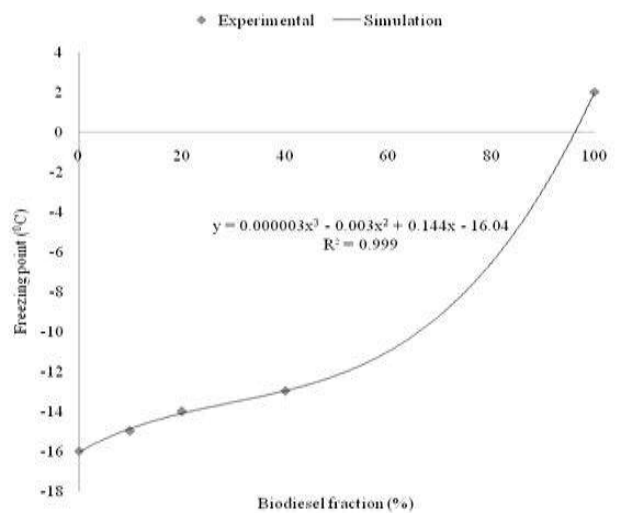
Figure 8 – Variation of freezing point with biodiesel fraction

$$y = 0.000003x^3 - 0.003x^2 + 0.144x - 16.04$$
$$R^2 = 0.999$$

Figure 9 – Variation of sulphur content with biodiesel fraction

3.2 Mass change rate and mechanical properties of Viton fuel hose

To obtain a detailed overview on degradation potential of diesel fuel (B0), waste cooking oil biodiesel/diesel fuel blends(B10, B20, and B40) and waste cooking oil biodiesel (B100),percentage change in mass, change in hardness, change in compressive strength and tensile strength were determined. Figure 10 shows mass change of Viton fuel hose after being exposed to B0, B100 and its blends at 35 °C for 720 hours. As can be observed in Figure 10, mass change of Viton fuel hose exposed to the fuel types increased as the biodiesel content increased. Coronado et al. [11] attributed the phenomenon to the solvent absorption and relaxation of polymer chain. Haseeb et al. [24] further attributed the increase in mass change to the interaction of ester present in the biodiesel with elastomer through dipole-dipole interaction, causing swelling.

Presented in Figures 11–13 are the variations of change in hardness, compressive strength and tensile strength, respectively at 35 °C for 720 hours. Figure 11 depicts the hardness change of Viton hose exposed to different fuel types. This indicates increasing biodiesel concentration; consequently decreased the hardness change of Viton hose. As can be observed in Figure 11, the hardness change of Viton hose in B10, B20, B40 and B100 is lower than that of B0.This can be attributed to dissolution of linkage agents between the polymeric chains, resulting in a reduction of hardness of Viton hose exposed to high concentration of biodiesel [11]. This observation is consistent with the report of Sellden [38]. Percentage change in hardness quadratically decreased with increasing biodiesel content. Owing to this variation, a second degree model equation was found adequate to correlate the variation of change in hardness versus WCOME-diesel fuel blends. The high R^2 (0.993) indicates that 99.3 % of the experiment was captured by the change in hardness model equation for Viton fuel hose.

The variation between percentage change in compressive strength and biodiesel fraction is presented in Figure 12. The change in compressive strength of Viton fuel hose decreased with increasing biodiesel content in

the blend. The adopted compressive strength model equation has high R^2 (0.982) indicates that 98.2 % of the compressive strength measured was captured by the compressive strength regression equation for Viton fuel hose.

Presented in Figure 13 is the relationship between tensile strength and biodiesel/diesel fuel types. As noticed in Figure 13, the percentage change in tensile strength for Viton fuel hose decreased with increasing biodiesel content in the blends. The reduction in tensile strength of the Viton exposed to higher biodiesel content was attributed to the higher loss of cross-linkage between polymeric chains [16, 18]. The second degree model equation was found adequate to correlate the variation of tensile strength Viton fuel hose with WCOME-diesel fuel blends. The high R^2 (0.993) indicates that 99.3 % of the experiment was captured by the tensile strength model equation for Viton fuel hose.

Figure 10 – Relative change in mass of Viton fuel hose with biodiesel fraction

Figure 11 – Variation of hardness test on Viton fuel hose with biodiesel fraction
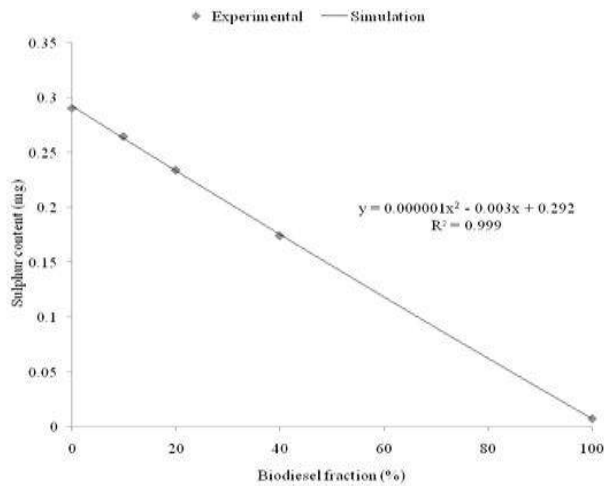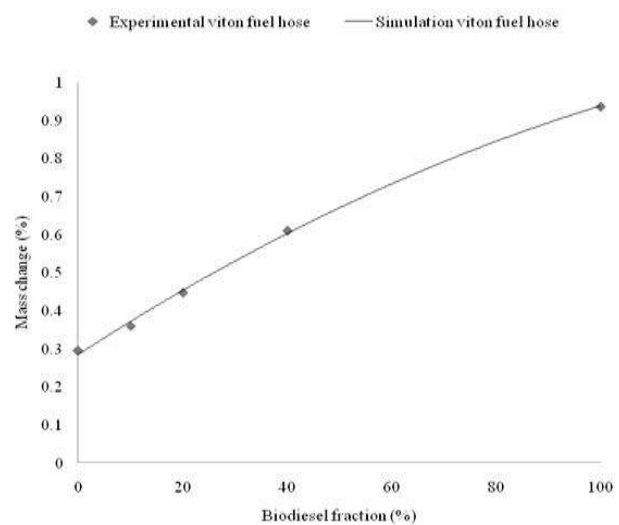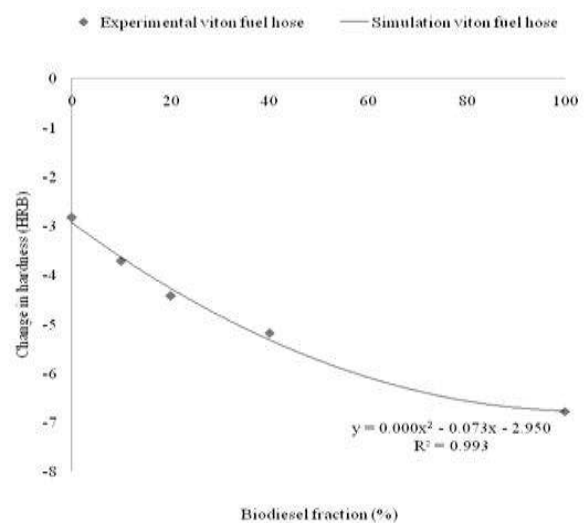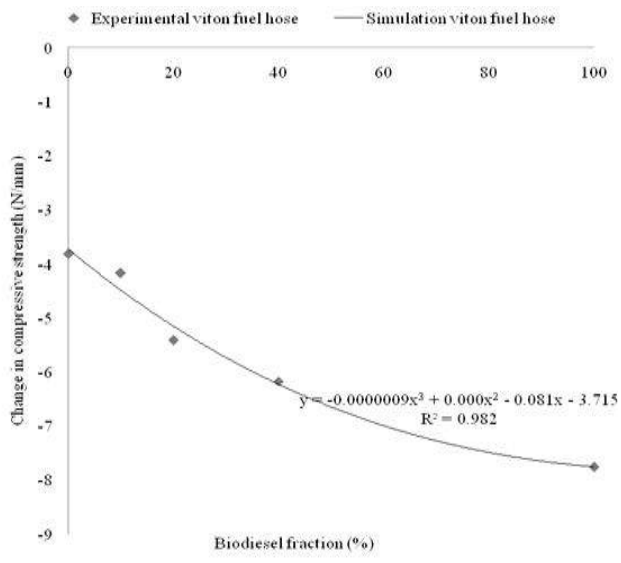
Figure 12 – Variation of Viton fuel hose compressive strength with biodiesel
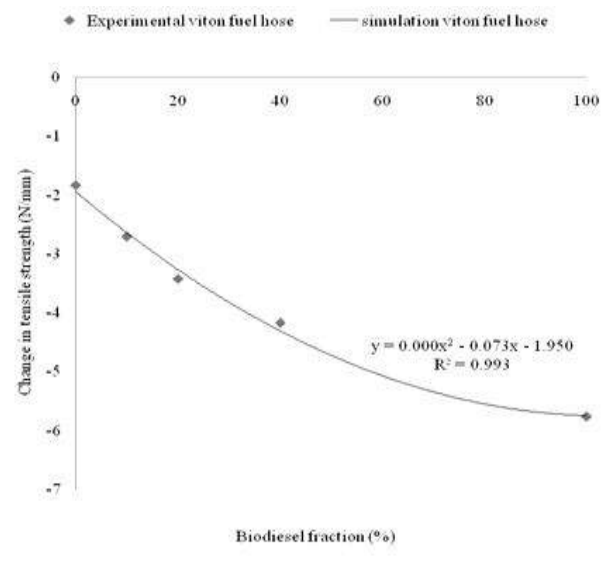
Figure 13 – Variation of Viton fuel hose tensile strength with biodiesel fraction

3.3 Acidity change of different fuel and surface morphology of Viton fuel hose

Figure 14 depicts fuel acidity change after Viton fuel hose has been exposed to biodiesel/diesel fuel blends. As can be observed, blends B10, B20, B40 and B100 showed remarkable change in acidity to diesel fuel. These results are in consistent with earlier reports by other researchers [11, 24]. Their results indicated that biodiesel is more prone to oxidation than fossil diesel.

Presented in Figure 15 is the surface morphology of Viton fuel hose (VFH) before and after exposed to different fuel types. Deterioration of VFH is accentuated when the biodiesel content increased in the fuel types. This is evident by more pits and crack observed in VFH in biodiesel and its blends compared to diesel fuel. Hence, this study recommends the use of low biodiesel content to be blended with diesel exposed to VFH.

Figure 14 – Acid number of the different fuels prior and after the immersion tests

Figure 15 – SEM micrographs of Viton hose surface and after exposed to diesel (B0), B10, B20, B40, B100 blends at 35 °C for 720 hours: a, d – Viton hose before; b, e – Viton hose / B0; c, f – Viton hose / B10

4 Conclusions

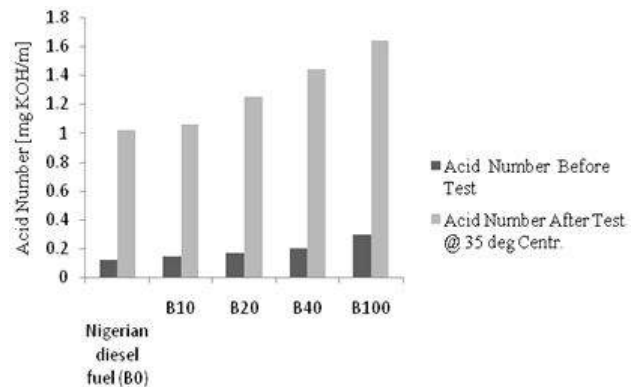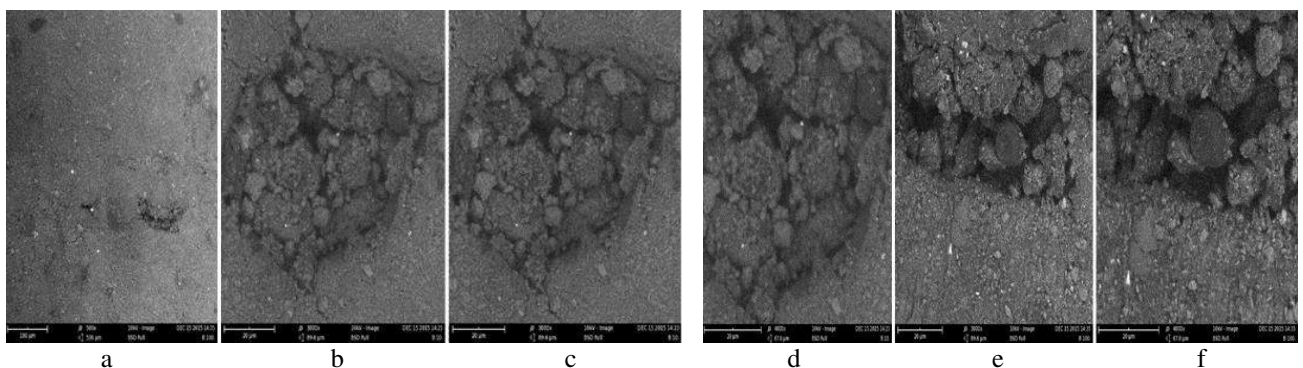The following conclusions can be deduced from results obtained from blend characterization of diesel and waste cooking oil biodiesel and its effecton degradation of Viton hose system. Blend density, kinematic viscosity, flash point, cold flow properties, freezing point increases while sulphur content decreases with increasing biodiesel percentage. The density and cloud point variations with biodiesel fraction in the blends follow second degree equation, while those of kinematic viscosity, flash point, pour point, freezing point and sulphur content are found to be well fitted by third degree regression equation. Mass change increased while hardness, compressive strength and tensile strength of Viton fuel decreased with increasing content of biodiesel in the blends.

References

1. Nadeem, M. K., Ahmed, S., Nadeem, S., Ishfaq, M., & Fiaz, M. (2014). Assessment of insecticides resistance in field population of Bactrocerazonata (saunders) (diptera: tephritidae). *The Journal of Animal and Plant Sciences*, Vol. 24, pp. 172–178.

2. Moser, B. R. (2009). Biodiesel production, properties, and feedstocks. *In vitro Cell Biol. Plant*, Vol. 45, pp. 229–266.

3. Agarwal, A. K. (2007). Biofuels (alcohols and biodiesel) applications as fuels for internal combustion engines. *Progress in Energy and Combustion Sciences*, Vol. 33, pp. 223–271.

4. Sorda, G., Banse, M., & Kemfert, C. (2010). An overview of biofuel policies across the world. *Energy Policy*, Vol. 38, pp. 6977–6988.

5. Coronado, M., Montero, G., Valdez, B., Stoytcheva, M., Eliezer, A., Garcia, C., Campbell, H., & Perez, A. (2014). Degradation of nitrile rubber fuel hose by biodiesel use. *Energy*, Vol. 68, pp. 364–369.

6. Chew, K. V., Haseeb, A. S. M. A., Masjuki, H. H., Fazal, M. A., & Gupta, M. (2013). Corrosion of magnesium in palm biodiesel: A comparative evaluation. *Energy*, Vol. 57, pp. 478–483.

7. Brown, R. P. (2001). *Practical guide to the assessment of the useful life of rubbers*. Shrewsbury, Rapra Technology.

8. Brown, R. P. (2002). *Rubber product failure*. Shrewsbury, Technology.

9. Jafari, H., Idris, M. H., Ourdjini, A., Rahimi, H., & Ghobadian, B. (2011). EIS study of corrosion behavior of metallic materials in ethanol blended gasoline containing water as a contaminant. *Fuel*, Vol. 90, pp. 1181–1187.

10. Chucwumenogor, O. (2016). *Characterization and corrosion behaviour of copper, aluminium and brass exposed to waste cooking oil biodiesel*. B. Eng. Thesis, Federal University of Petroleum Resources, Effurun, Nigeria.

11. Bhardwaj, M., Gupta, P., & Kumar, N. (2014). Compatibility of metals and elastomers in biodiesel: a review. *International Journal of Research*, Vol. 7, pp. 376–391.

12. Singh, B., Korstad, J., & Sharma, Y. C. (2012). A critical review on corrosion of compression ignition (CI) engine parts by biodiesel and biodiesel blends and its inhibition. *Renewable and Sustainable Energy Review*, Vol. 16, pp. 3401–3408.

13. Fazal, M. A., Haseeb, A. S. M. A., & Masjuki, H. H. (2011). Effect of temperature on the corrosion behaviour of mild steel upon exposure to palm biodiesel. *Energy*, Vol. 36, pp. 3328–3334.

14. Kass, M. D., Janke, C., Connatser, R., Lewis, S., Keiser, J., & Theiss, T. (2015). Compatibility assessment of elastomeric infrastructure materials with neat diesel and a diesel blend containing 20 percent fast pyrolysis bio-oil. *SAE International Journal of Fuels and Lubricants*, Vol. 8, No. 2015-01-0888, pp. 50–61.

15. Sorate, K. A., Bhale, P. V., & Dhaolakiya, B. Z. (2015). A Material Compatibility Study of Automotive Elastomers with high FFA based Biodiesel. *Energy Procedia*, Vol. 75, pp. 105–110.

16. Dubovsky, M., Bozek, M., Olsovsky, M. (2015). Degradation of aviation sealing materials in rapseed biodiesel. *Journal of Applied Polymer Science*, pp. 1–7.

17. Alves, S. M., Mello, V. S., & Medeiros, J. S. (2013). Palm and soybeans biodiesel compatibility with fuel system elastomers. *Tribology International*, Vol. 65, pp. 74–80.

18. Cursaru, D. L., Branoiu, G., Ramadan, I., & Miculescu, F. (2014). Degradation of automotive materials upon exposure to sunflower biodiesel. *Industrial Crops and Products*, Vol. 54, pp. 149–158.

19. Zhang, X., Li, L., Wu, Z., Hu, Z., & Zhou, Y. (2009). Material Compatibilies of Biodiesels with Elastomers. Metals and Plastics in a Diesel Engine. *SAE Technical Paper*, Art. no. 2799.

20. Bessee, G. B., & Fey, J. P. (1997). Compatibility of elastomer and metals in biodiesel fuel blends. *SAE Technical paper*, Art. no. 971690.

21. Trakampruk, W., & Porntangjitilikit, S. (2008). Palm oil biodiesel synthesized with potassium loaded calcined hydrotalicite and effect of biodiesel blend on elastomers properties. *Renewable Energy*, Vol. 33, pp. 1558–1563.

22. Haseeb, A. S. M. A., Masjuski, H. H., Siang, C. T., & Fazai, M. A. (2010). Compatibility of elastomers in palm biodiesel. *Renewable Energy*, Vol. 35, pp. 2356–2361.

23. Haseeb, A. S. M. A., Jun, T. S., Fazal, M. A., & Masjuki, H. H. (2011). Degradation of physical properties of different elastomers upon exposure to palm biodiesel. *Energy*, Vol. 36, pp. 1814–1819.

24. Nunes, F., Lourenco, H., & Nagib, C. (2013). Study of compability rubber with Brazilian biodiesel. *Energy*, Vol. 49, pp. 102–106.

25. Moser, B. R. (2012). Efficacy of specific gravity as a tool for prediction of biodiesel – petroleum desel blend ratio. *Fuel*, Vol. 99, pp. 254–261.

26. Giwa, S. O., Chuah, L. A., & Adam, N. M. (2014). Fuel properties and rheological behavior of biodiesel from egusi (colocynthiscitrullus L.) seed kernel. *Fuel Processing Technology*, Vol. 122, pp. 42–48.

27. Samuel, O. D., Giwa, S. O., & El-Suleiman, A. (2016). Optimization of coconut oil ethyl esters reaction variables and prediction model of its blends with diesel fuel for density and kinematic viscosity. *Biofuels*, Vol. 7, pp. 723–733.

28. ASTM D1250-08. *Standard guide for use of the petroleum measurement tables*. ASTM international, West Conshohonken, PA, retrieved from; http://www.stm.org.

29. ASTM, American Society for Testing and Material, Designated D445. *Standard Method of Test for kinematic viscosity of transparent and opaque liquids (and the calculation of dynamic viscosity*. ASTM International West Conshocken PA, USA.

30. ASTM, American Society for Testing and Material, Designated D56. *Standard Method of Test Methods for Flash Point by Pensky-Martens*. ASTM International West Conshocken PA, USA.

31. ASTM, American Society for Testing and Material, Designated D97. *Standard Method of Test Methods for pour point by lawler cloud point analyzer*. ASTM International West Conshocken PA, USA.

32. ASTM, American Society for Testing and Material, Designated D129-13. *Standard test method for sulphur in petroleum products (General High pressure Decomposition device method)*. ASTM International West Conshocken PA, USA.

33. ASTM, American Society for Testing and Material, Designated D471. *Standard Test Method for Rubber Property-Effects of Liquids*. ASTM International West Conshocken PA, USA.

34. Alptekin, E., & Canakci, M. (2008). Determination of the density and the viscosities of biodiesel-diesel fuel blends. *Renewable Energy*, Vol. 33, pp. 2623–2630.

35. Al-Hammare, Z., & Yamin, J. (2014). Parametric study of the alkali catalyzed transesterification of waste frying oil for biodiesel production. *Energy Conversion and Management*, Vol. 79, pp. 246–254.

36. Bamgboye, A.I., & Oniya, O. O. (2012). Fuel properties loofah (Luffa Cylindrica L.) biofuel blended with diesel. *African Journal of Environmental Science and Technology*, Vol. 6, pp. 346–352.

37. Sellden, E. (2013). *Life assessment of rubber articles in fuels*. M.Sc. Thesis, Uppsala University, Sweden.

Характеристика та деградація паливного шлангу, що піддається випливу суміші дизельного палива з відпрацьованими відходами

Самуель О. Д.[1], Емовон І.[1], Ідубор Ф. І.[1], Адекомайа О.[2]

[1] Федеральний університет нафтових ресурсів, м. Еффурум, Р.М.В. 1221, Нігерія;
[2] Технологічний університет ім. Тшване, м. Преторія, 0001, Південно-Африканська Республіка

Анотація. Деградація та несумісність біодизеля з паливною системою є головною проблемою, пов'язаною із застосуванням першого. У цьому дослідженні були досліджені основні властивості палива, такі як щільність, кінематична в'язкість, точка займання, вміст сірки тощо у результаті змішування біодизеля / дизельного палива (зокрема, В10, В20 і В40) з відходами. Паливні шланги, що піддаються впливу різних типів палива та їх характеристик деградації, загальної кількості кислот та зміни морфології поверхні. Знайдено вищезазначені параметри, значення яких збільшуються від зменшення вмісту сірки при збільшенні вмісту біодизельного палива у суміші. Зазначено, що концентрація біодизелю впливає на властивості еластомерів, що призводить до випинання паливного шлангу. Встановлено, що експлуатація шлангів для палива з підвищеним вмістом біодизельного палива призводить до зменшення міцності на розрив, жорсткості та міцності при стисканні.

Ключові слова: деградація, паливний шланг, біодизель, твердість, міцність на стискання, випинання.

Features of Geochemical Migration of Chemical Elements after Technogenic Loading of Pyrogenic Nature

Buts Yu. V.

S. Kuznets Kharkiv National University of Economics, 9-A Nauky Av., 61166 Kharkiv, Ukraine

*Corresponding Author's Address:
butsyura@ukr.net

Abstract. The study of the concentration of trace metals in soils by atomic absorption analysis was carried out. The results indicate the transformation of their migration properties. The diversity and versatility of behavior of chemical elements in environmental components after the fire was noted. In different ecological conditions, it is possible to observe a wide range of quantitative values of geochemical migration or accumulation of any particular chemical element. Analytical results show that the contents of migrant elements, pH values, areas of incidents, which are approximately in the same conditions, but passed by the grass or upper fire differ quite tangibly. Trace metals that hit the environment can form difficult soluble hydroxides. In addition, in the soil solution, there is a probability of the formation of hydroxocomplexes with different amounts of hydroxide ions by metals. The range of precipitation of hydroxides and the region of predominance of soluble hydroxocomplexes have been studied by constructing concentration-logarithmic diagrams. On the basis of the calculations it can be argued that the influence of the technogenic loading of pyrogenic origin on the geochemical migration of trace metals takes place. The obtained calculations can be used to predict the geochemical migration of trace metals in soils after the man-made consequences of emergencies of pyrogenic origin.

Keywords: chemical element, hydroxocomplex, migration ability, concentration-logarithmic diagram.

1 Introduction

At present, in Ukraine, studies focused on studying the man-made load due to the action of the pyrogenic (literally "generated by fire") factor on the environment, are given insufficient attention to. At the same time, the number of natural fires and their consequences increases from year to year. In the process of the restoration of natural ecosystems, it is the soil that determines both the type of vegetation and the dynamics of plant communities; hence the influence of natural fires on the properties of soils is one of the important tasks in the field of soil science.

The purpose of this paper is to study the geochemical aspects of the accumulation of trace metals under the influence of the man-caused load of pyrogenic origin.

2 Literature Review

There is no single-valued explanation for the causes that affect the behaviour of trace elements, in particular trace metals (TM), under the influence of technogenic

effects. Literature data analysis allows noting the diversity and versatility of the behaviour of chemical elements in the components of the environment after fire damage. At various environmental conditions, a wide range of quantitative values of geochemical migration or accumulation of any specific chemical element can be observed [1]. For example, the concentration of mercury in soil after a ground fire is from 27.3 to 64.3 %. The discrepancy is almost by a factor of 2.36 [2].

As a rule, anionogenic elements have the best migration characteristics. Naturally they exist in the form of anions and highly soluble salts. For example, these are molybdenum and boron. Cationogenic elements, like zinc, copper, manganese and cobalt, migrate in the form of cations in the composition of highly soluble salts, sols, complex compounds and salts of fulvic acids [3].

The bulk of TM, like Cu, Hg, Cd, As, Pb, etc., migrates in the composition of dust and aerosols. But when it comes to single cases of the minor migrations of ore elements, like Cr, Ni, Co, Mg, etc., which most often passively accumulate in the lithogenous basis of burned and/or adjacent area, so the role of large dust particles [4] should be recognized.

The type of fire and its intensity affect the migration of chemical elements. The higher firepower, the higher the quantitative parameters of the air migration of chemical elements. It is obvious that there are other factors that determine the behaviour of TMs in fires in ecosystems.

Analytical results showed that areas of fires being under approximately the same conditions but traversed by ground or crown fire differ significantly in the content of migrating elements (mg/kg) and pH values.

In a general crown fire, a number of chemical elements, for example, mercury, cadmium, selenium and artificial radionuclides are taken out of the fire zone, their contents are 30–45 % of their concentration in the areas of a ground fire [2]. The pH value increases by 6–10 %. Undoubtedly, this is due to the increase in the amount of ash that has an alkaline reaction, but it could be partially removed from the soil cover of the burned area by aeolian or hydrological processes. For this reason, it is not possible to correctly establish the relationship between the amount of ash and the pH value in the burned areas in a given time after the fire. The above examples of geochemical migration processes convincingly evidence that in addition to the type of fire as a factor in the migration of chemical elements from burned areas, the state of light-combustible materials, namely, the moisture content of the forest litter, is played a presentable role. This allows us to formulate one more reason determining the behaviour of TMs in forest fires: the physical state of ground forest combustible materials also serves as one of the factors determining geochemical migration in a natural fire.

It is known that different plants accumulate different microelements in different ways. That is, the nature of the distribution of trace metals in terrestrial plant parts should be taken into account. This determines the quantitative indicators of geochemical migration of chemical elements in a fire. The most characteristic is the radial distribution of most TMs in the soil profile, including the upper soil horizons with interlayers of steppe mat and forest litter. And in this event there is a significant fluctuation of TM content in radial differentiation within the soil profile.

Burnout of the upper parts of steppe mat, mosses, lichens and forest litter is accompanied by a weak emission of migrating trace elements not only because the upper layers of surface combustible materials dry out faster than the lower ones, but also because in these horizons their elevated concentrations are in the lower intervals but not in the upper ones.

Consequently, it should be emphasized that the complex interaction of chemical elements with each other, the state of ground combustible materials and the distribution of elements in soil vertical profiles are responsible for the behaviour of chemical elements during fires in ecosystems.

In windless weather, during the spread of a fire in the ecosystem, the chemical elements held by the fiery convection current migrate vertically to the upper atmospheric layers and, as it cools, settle on the burned area. The wind promotes the spread of the smoke plume beyond the pyrogenically affected area. This also makes it possible to recognize the role of weather conditions as one of the factors determining the migration of chemical elements from burned areas. However, in our opinion, this factor can be applied only to small fires, since the general crown fires are accompanied by the formation of vortex air currents tightening cold air masses from the areas adjacent to the fire. At the same time a horizontal advection movement of the smoke plume in such fires can not only be predicted but also almost impossible to take into account during a fire. At the same time, dry and warm weather will be favourable for atmospheric migration, while foggy and rainy weather will facilitate the rapid washout and deposition of dust and aerosol particles of the smoke plume. All presented analyzed information allows confirming the existence of another factor, of which the spread of the smoke plume depends on during the fire in the ecosystem: weather conditions affecting the migration or accumulation of separate chemical elements within the burned area.

There is no doubt that the transformation of steppe mats, forest litter, mosses, lichens, etc. in various combustion products (ash, coal, dust, aerosols, etc.) under the influence of high temperatures, natural fires are able to affect the migration of all the chemical elements.

It is proved that in the components of natural systems chemical elements occur in different states: sorption, absorption, and complex organo-mineral compounds, etc. But, since it is referred to natural fires, and consequently high temperatures, I.V. Alekseenko [2] considers their behaviour as depending on the temperatures of their boiling and evaporation. He associates active migration of cadmium and mercury with their low boiling points, whereas in such TMs as copper, chromium, nickel and cobalt it is an order of magnitude higher, namely they tend to be geochemically accumulated in the lithogenous basis of the burned area (°C): Hg = 357, As = 610, Cs = 690, Cd = 765, Zn = 907, Mg = 1 107, Pb = 1 744, Mn = 2 151, Sr = 1 384, Cr = 2 482, Cu = 2 595, Ni = 2732, V and Co = 3 000.

However, manganese falls from the above trend: having a high boiling point, it easily migrates. On the other hand, the migration of arsenic is low, although sublimation of this chemical element already occurs at a temperature of 610 °C. The reason for the low values of this indicator can be staying of arsenic within the mineral part of the forest litter and an expressed close connection with iron. The behaviour of sodium and potassium, which accumulate in the soils of burned areas but have a low temperature gradient, does not correspond to this pattern too.

Thus, the analysis of the above data allows us to conclude that the behaviour of trace metals during fires in ecosystems depends on many factors, the main of which are the following: the type of fire, the state of forest fuels, weather conditions, the geochemical properties of chemical elements and the nature of their distribution in components of the ecosystem.
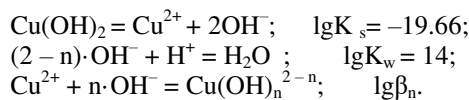
During fires, the top few centimeters of soil are exposed to high temperatures, so the most drastic changes occur in the litter and in the upper part of the humus horizon. In the process of combustion, there is a significant loss of soil organic matter. Under the influence of high temperatures during a fire, most of carbon from the organic substance is oxidized to gaseous forms (mainly CO_2) and volatilizes. During intense fires, the organic matter of the above the soil surface horizons and the upper part of the humus horizon are destroyed while the formation of a large number of carbonate compounds of alkaline and alkaline-earth elements, which causes an increase in the pH response, takes place. As

noted by Yu. M. Krasnoschekov, et al. [5], the shift in soil acidity after a fire can be very considerable, it was recorded events from pH = 5.7–5.9 before a fire to pH = 8.7 after passing a ground fire. Two months after the fire, pH of the surface horizon remains to be 8.0, and only in the burned areas 10 years after fire the reaction of the upper organogenic horizons is restored. In addition to the microelements, which are of vital significance for plants, entering soil after passing through fire, large amounts of Fe, Al, Zn, Mn and other trace metals are supplied together with ash.
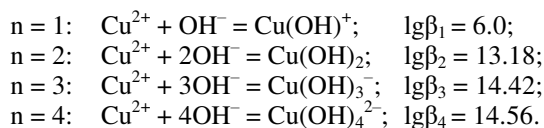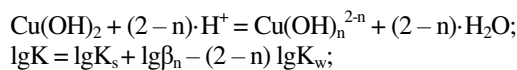
3 Research Methodology

Let us examine in more detail the conditions for the formation of mobile forms of trace metals in soils, which will allow us to conclude of their migration or accumulation in the geochemical environment.

Trace metals that enter the environment can form hardly soluble hydroxides. In addition, in the soil solution there is the possibility of the formation of hydroxocomplexes by metals with different amounts of hydroxide ions [1]. The range of precipitation of hydroxides and the ranges of the predominance of soluble hydroxocomplexes have been studied by plotting concentration-logarithmic diagrams (CLDs) [6]. The dissolution of metal hydroxide illustrated with the example of the formation of copper hydroxide and the formation of its complex compounds is described by three main reactions as follows:

$$Cu(OH)_2 = Cu^{2+} + 2OH^-; \quad lgK_s = -19.66;$$
$$(2-n) \cdot OH^- + H^+ = H_2O ; \quad lgK_w = 14;$$
$$Cu^{2+} + n \cdot OH^- = Cu(OH)_n^{2-n}; \quad lg\beta_n.$$

Lumped reaction:

$$Cu(OH)_2 + (2-n) \cdot H^+ = Cu(OH)_n^{2-n} + (2-n) \cdot H_2O;$$
$$lgK = lgK_s + lg\beta_n - (2-n) lgK_w;$$

$n = 1: \quad Cu^{2+} + OH^- = Cu(OH)^+; \quad lg\beta_1 = 6.0;$
$n = 2: \quad Cu^{2+} + 2OH^- = Cu(OH)_2; \quad lg\beta_2 = 13.18;$
$n = 3: \quad Cu^{2+} + 3OH^- = Cu(OH)_3^-; \quad lg\beta_3 = 14.42;$
$n = 4: \quad Cu^{2+} + 4OH^- = Cu(OH)_4^{2-}; \quad lg\beta_4 = 14.56.$

To calculate the equilibrium constant of the total reaction, logarithms of the products of hydroxide solubility and the stability constants of metal complexes and hydroxide ions were used.

The equilibrium concentrations of metal-containing particles will be the following:

$$lg[Cu(OH)_n^{2-n}] = lgK_s + lg\beta_n - (2-n) \cdot lgK_w - (2-n) \cdot pH;$$

$n = 0: \quad lg[Cu^{2+}] = lgK_s - 2lgK_w - 2pH = 8.34 - 2pH;$
$n = 1: \quad lg[Cu(OH)^+] = lgK_s + lg\beta_1 - lgK_w - pH = 0.34 - pH;$
$n = 2: \quad lg[Cu(OH)_2] = lgK_s + lg\beta_2 = -6.48;$
$n = 3: \quad lg[Cu(OH)_3^-] = lgK_s + lg\beta_3 + lgK_w + pH = -19.24 + pH;$
$n = 4: \quad lg[Cu(OH)_4^{2-}] = lgK_s + lg\beta_4 + 2lgK_w + 2pH = -33.1 + 2pH.$

Thus, from the diagrams shown in Figure 1, it is possible to clearly determine the ranges of maximum precipitation of metal hydroxides. The condition for the precipitation of Me^{z+} is considered that it achieves concentration of the order of 10^{-5} mol/l in the soil solution. From Figure 1, at pH ≤ 6.8, copper is in a dissolved form, at higher pH values, copper precipitates in the form of hydroxide $Cu(OH)_2$, and at very high levels (pH > 13), hydroxocomplexes $Cu(OH)_3$ are formed but their concentration is very low, which allows us to conclude that copper compounds in neutral medium have a high migration capacity and their fixation at pH ≥ 6.8. Calculations have been made and corresponding diagrams have been plotted for a number of other metals.
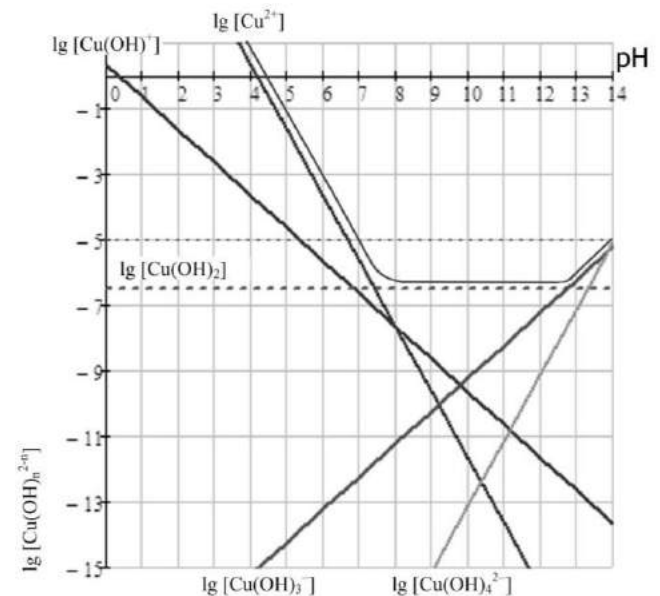

Figure 1 – The concentration-logarithmic diagram (CLD) of forming copper hydroxocomlexes

4 Results

The precipitation ranges of hydroxides calculated by us with the aid of CLDs are in good agreement with the experimental data obtained by Yu. Lurie [7].

In neutral soil, most metals, such as Al, Cr, Zn, Cu, Fe (II), Co and Ni, are in hardly soluble forms (in the forms of hydroxides), at this their migration capacity is not large, which leads to the accumulation of chemical elements in soils. Under such conditions, trace metals are not washed out of soils, they are not assimilated by plants, instead their accumulation in soils occurs [1].

If a significant shift in pH occurs, as for example was recorded by Yu.M. Krasnoschekov et al. [5], the behaviour of copper compounds will change dramatically. At pH = 5.7 before the fire, the concentration of $[Cu^{+2}] = 0.01$ mol/l, at pH = 8.7 after the fire, all copper in an insoluble form will accumulate in soils.

Fe^{2+} ions migrate easily in acidic, neutral and even slightly alkaline medium up to pH = 9.5, and only in strongly alkaline medium hydroxide $Fe(OH)_2$ is formed.

5 Conclusions

On the basis of our calculations, it can be argued that the effect of the man-made load of pyrogenic origin on the geochemical migration of trace metals takes place. Compounds of Fe^{3+} at pH = 4.5–14.0, Cu^{2+} at pH = 7–14, Cr^{2+} at pH = 7–9, Zn^{2+} at pH = 8–11, Ni^{2+} at pH = 8–14, Pb^{2+} at pH = 9–12, Fe^{2+} at pH = 9.5–14 have the lowest migration abilities. In a more acidic environment, soluble substances are formed, but with an increase in pH = 0.5–1.0 only, their mobility can decrease by an order of magnitude, which contributes to their concentration in soils after fire.

In neutral in their reaction soils most of trace metals, like Cr, Zn, Cu, Fe (II), Ni, are in hardly soluble forms as hydroxides, at this their migratory abilities are low, which leads to accumulation of these elements in soils.

Trace metals, which are mobile in a neutral medium, such as Fe (II), Cd, Co, Mg and Mn should be allocated in a separate group. Any increase in the level of pH facilitates their fixation.

The calculation results obtained can be used to predict the geochemical migration of trace metals in soils in consequence of the man-made emergencies of pyrogenic origin.

References

1. Buts, Yu. V., & Krayniuk, E. V. (2017). Geochemical transformation of migration properties of heavy metals under the influence of technogenic loading of pyrogen. *Ecological Safety*, Vol. 24, pp. 95–100 [in Ukrainian].
2. Alekseenko, I. V., & Gamova, N. S. (2015). Influence of forest fires on the properties of soils of taiga landscapes of the Khamar-Daban ridge. *Biogeochemistry of Technogenesis and Modern Problems of Geochemical Ecology*, Vol. 1, pp. 171–174 [in Russian].
3. Trofimov, I. T., & Bakharev, I. Yu. (2007). Peculiarities of post-pyrogenic transformation of sod-podzolic soils in the southwestern part of bandar forests of the Altai Territory. *Bulletin of the AGAU*, No. 11(37), pp. 31–35 [in Russian].
4. Bryanin, S. V. (2014). Migration and accumulation of ash elements in forest landscapes under the influence of periodic fires on the Amur-Zeisk plain. *Fundamental Studies*, Vol. 8, pp. 859–863 [in Russian].
5. Krasnoschekov, Yu. N., Valendik, Ye. N., Bezkorovajnaja, I. N., Verhovec, S. V., Kisiljahov, E. K., & Kuz'michenko, V. V. (2005). Influence of controlled burning of silk crackers on the properties of sod-podzolic soils in Nizhny Novgorod. *Forestry*, Vol. 2, pp. 16–24 [in Russian].
6. Goronovskiy, I. T., Nazarenko, Yu. P., & Nekryach, Ye. F. (1974). *Brief Chemical Handbook*. Kyiv, Naukova Dumka [in Russian].
7. Lurie, Yu. (1989). *Handbook on Analytical Chemistry*. Moscow, Chemistry [in Russian].

Особливості геохімічної міграції хімічних елементів при техногенному навантаженні пірогенного характеру

Буц Ю. В.

Харківський національний економічний університет ім. С. Кузнеця, просп. Науки, 9-А, 61166, м. Харків, Україна

Анотація. Відзначено різноманітність поведінки хімічних елементів у довкіллі після ураження пожежами. Можна спостерігати широкий діапазон кількісних значень геохімічної міграції або акумуляції хімічного елемента. Важкі метали, що потрапили у довкілля, можуть утворювати гідроксиди або гідроксокомплекси, від яких залежить міграційна здатність. Діапазон осадження гідроксидів та області переважання розчинних гідроксокомплексів вивчені за допомогою побудови концентраційно-логарифмічних діаграм. Створено прогнозування геохімічної міграції сполук міді у ґрунтах після пірогенного впливу. На підставі розрахунків можна стверджувати, що має місце вплив техногенного навантаження пірогенного характеру на геохімічну міграцію важких металів. Отримані розрахунки можна використовувати для прогнозування геохімічної міграції важких металів у ґрунтах після техногенних наслідків надзвичайних ситуацій пірогенного походження.

Ключові слова: хімічний елемент, гідроксокомплекс, міграційна властивість, концентраційно-логарифмічна діаграма.

Recovery of Pyrolytic Oil from Thermal Pyrolysis of Medical Waste

Som U.[1], Rahman F.[2], Hossain S.[3*]

[1] Jessore University of Science and Technology, Churamonkathi–Chaugachha Rd., Jessore-7408, Bangladesh;
[2] Jahangirnagar University, Savar, Dhaka-1342, Bangladesh;
[3] Khulna University of Engineering and Technology, Khulna-9203, Bangladesh

Abstract. In this paper, potential of beneficial products recovery was investigated from plastic medical waste (PMW) by pyrolysis process. Disposable plastic is one of the chief items in the medical waste. High density polyethylene and Polypropylene is the main component of several PMW. These plastics have a higher latent as hydrocarbons sources for chemical industry. Pyrolysis of PMW was accomplished at a temperature range of 200–300 °C in a batch reactor make up of stainless steel. The chemical and physical properties of the pyrolysis liquid were much closer to the commercial fuel like diesel, petrol etc. The density is 840 kg/m3, the gross calorific value is $4.13 \cdot 10^4$ kJ/kg flash point is 39 °C in produces pyrolytic oil. This liquid can be used as alternative sources of fuel.

Keywords: plastic medical waste, pyrolysis, pyrolytic oil, alternative fuel.

1 Introduction

The major problems we facade these days are energy crisis and environmental concern due to the fast growth of population and industrialization. Massive quantity of solid wastes have been refused every day from various sources like household wastes, industrial wastes, municipal wastes, medical wastes, etc. These wastes can be transformed into energy by following appropriate methods; that would be usable for the next generation. Recovery of alternative fuel and reducing plastic waste, the technologies are developed day by day, which are suitable from the environmental viewpoint and cost–effective, has recognized to be an inflexible challenge because of the obscure characteristic in the recycle of polymers [1].Plastic materials, for instance, encompass a progressively increasing proportion of the municipal and industrial wastes. The yearly plastic consumption of the sphere has augmented about 20 times since 5 million tons in 1950s to approximately 100 million tons in latest time [2]. Medical wastes are categorized as solid and liquid states. Plastic medical wastes are the solid type of medical wastes, such as vials, saline pots, saline pipes, covers, medicine containers, packets, etc. Medical wastes are infectious and hazardous. It retains severe threats to the environment and needs specific treatment and management prior to its final disposal [3]. The safe dumping and

handling of medical wastes has been ignored in Bangladesh. Medical waste is proficient of causing diseases and disorder to people, either through straight contact or ultimately by contaminating soil, surface water, groundwater and air [4]. Medical waste, consequently, possesses a risk to human, communities and the surroundings if not carefully handled. According to [5], the medical waste management procedure includes handling, segregation, disinfection, storage, transportation, collection and final disposal. Various methods such as land filling, biological recycling, mechanical recycling, thermo–chemical recycling, etc. are used for medical waste management. Land filling is not a suitable option for positioning plastic wastes because of their relaxed degradation rates. Mechanical recycling can be actual process but it is limited to thermoplastics, contamination level, homogeneity of the types and color similarity [6]. Chemical recycling of plastic wastes is one of the most remarkable plastic wastes management methods. Incineration and pyrolysis are usually employed to obtain bio–fuel from plastic materials. Of them, pyrolysis method is one of the most effective and promising techniques to obtain liquid fuel from the plastic medical waste. Incineration is a critical procedure, in which hydrocarbons are altered to their combustion products, whereas, pyrolysis may be employed to change them into inferior hydrocarbons, which may be made use of as fuel and other different materials [7]. Pyrolysis is a thermal method by less or deficiency of oxygen. In the pyrolysis

method, the organic constituents of the decomposable material yield gaseous and liquid products, which can be used as a source of chemicals and fuels [8]. Products acquired from pyrolysis of plastics depend on the nature of plastics, residence time, feeding arrangement, reactor type, condensation arrangement and temperatures employed [9]. Very diverse experimental processes have been used to acquire liquid products from plastic–based medical waste by thermal pyrolysis method. Numerous reactor schemes have been established and used for instance batch/semi batch, fluidized bed, spouted bed, fixed bed, microwave and screw kiln. Semi–batch, batch and fixed bed reactors have been used by numerous researchers as a result of its simple design and informal operation. Consequently, we selected batch type pyrolysis reactor to convey out the process.

Not much written in the literature about the pyrolysis process to produce fuel from waste plastics. Butler et al. [10] discussed the review of waste polyolefin plastics. Dash et al. [11] studied on the thermal pyrolysis of medical waste (plastic syringe) for the production of useful liquid fuels. However, nobody explored the present issue as of conversion of plastic medical waste into energy in details, so far.The objective of the work was to manage plastic wastes as well as to reduce environmental emissions. The aim of this research is to explore an alternative source of energy from plastic medical wastes through thermal pyrolysis method using a fixed-bed reactor. The properties of the fuel has been studied and compared with commercial fuels.

2 Research Methodology

2.1 Raw materials

Plastic–based medical waste, used as feed material throughout the experiment, was collected from the local Hospital of Bangladesh. The plastic materials were cleaned successively with water and hydrochloric acid and finally washed with distilled water. They were shredded into four different sizes such as 0.65, 0.975, 1.3, and 1.95 cm^3. Every plastic content were chopped cross–section wise. Then they were used as raw material for thermal pyrolysis process.

2.2 Experimental procedure

The layout of the experiment can be seen in Figure 1. The apparatus used in the pyrolysis of wastes plastic consisted of batch reactor made of carbon steel of 8 cm length, 14 cm inside diameter and 28 cm outside diameter. Thermocouple (type K) with digital temperature recorder connected to the reactor of 10 cm deep was used to measure inside temperature of the reactor. The heat was supplied to the reactor by 2 kW external electrical heaters (1.5 kW heater in the bottom of the reactor and 0.5 kW heater surrounding the reactor) to get the required reaction temperature. At the top end of the reactor, a tubing system was connected with two gate valves.

Figure 1 – Feed material for pyrolysis

All tubes, having a diameter of 0.5 inch made by copper, were used as condenser. Pyrolysis of medical waste (plastic content) was conducted by a batch type fixed–bed system. This procedure was conducted for variety of feed quantity and temperature. The plastic–based medical wastes were shredded into equal size which was fed (1 kg) to the reactor. The thermal recycling pyrolysis process carried out under inert atmosphere. Prior to starting the experiment, the pressure cooker was purged by flowing N_2 gas for 5min to remove air inside. During the experiment, the pressure in the flow meter and reactor chamber were remained same but slightly higher than that of atmospheric pressure just to maintain continuous flow of N_2 gas.

The heat was supplied (room temperature to 500 °C) in consistence basis and vapor forms in the reactor. The gas movement line was completely opened from the reactor to the condenser. Cooling water was supplied on the surface of the condenser on continuous basis. At the outlet of reactor, a condenser was attached to condense the vapors coming out of it. The condensed vapors were collected in a container as the liquid product, whereas, there was some amount of non–condensable gases which were simply left out. The schematic diagram of fixed bed pyrolysis plant is shown in Figure 2.

Fiureg 2 – Schematic diagram of a fixed bed pyrolysis plant

When the pyrolysis process of all samples was completed, supply of N_2 gas was stopped and switched off the heater of the reactor. Then wait for a while to cool the reactor and collected the char product. After that the char product and liquid were weighted. The weight of the gas was determined

by subtracting the total weight of char product and liquid obtained after condensation of vapor from the full amount of feedstock.

3 Results and Discussion

3.1 Elemental and proximate analysis of PMW

Elemental and proximate analysis PMW is very important to determine numerous properties of PMW. The heating rate and volatile constituents are the vital factors for PMW pyrolysis. The Elemental and proximate analyses of PMW with higher calorific rate are showed in below Table 1.

Table 1 – Proximate and elemental analysis PMW, wt %

Proximate analysis		Elemental analysis	
Moisture	0.82	Carbon (C)	72.56
Volatile	62.70	Hydrogen (H)	11.17
Fixed carbon	32.31	Nitrogen (N)	5.82
Ash	4.17	Sulphur (S)	0.23
H.C.V, MJ/kg	33.30	Others	10.22

3.2 Effect of temperature on pyrolysis product yield

Pyrolysis of medical waste (plastic) in batch type fixed-bed reactor, the experimentations was directed in the temperature range of 200–300 °C. The investigations were directed to detect the significance of pyrolysis temperature on yield.
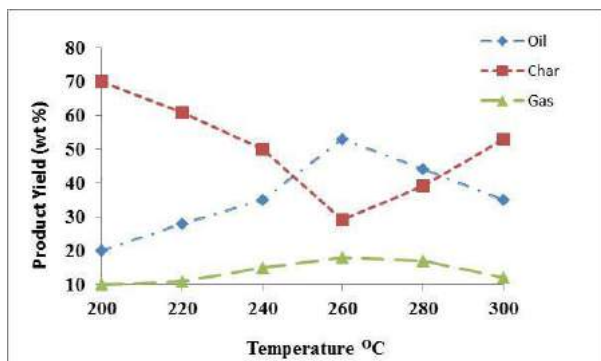

Figure 3 – Effect of temperature on pyrolytic yields for feedstock size 0.65 cm^3

At diverse temperature of numerous feedstock sizes (0.65, 0.975, 1.30, and 1.95 cm^3), there were achieved three types of pyrolysis yields such as liquid oil, solid and gas are presented in Figure 3 for feedstock 0.65cm^3 due to straightforwardness. It is stated from the figure that when the escalation of temperature occur, the rate of

liquid manufacture augmented up until it attained a maximum value and formerly reduced. All the data denote alike nature. Among the 4 sample sizes, the excellent result was attained for the feed size of 0.65 cm^3. When the temperature augmented from 200 to 260 °C, the production of liquid augmented first from 20 wt % to a maximum value of 53 wt % and then reduces to 35 wt % at a temperature of 300°C. The gas production augmented from 10 to 18 wt % over the entire temperature range, whereas char yield declined from 70 to 29 wt %, formerly remain residues were almost constant. It is pragmatic that a properly sharp optimum occurs in temperature at which supreme production of liquid was attained possibly because of strong cracking of plastic at 260 °C temperature. The gas manufacture augmented over the whole temperature range to a uppermost value of 18 wt % at 260 °C, whereas, char yield decayed up to 300 °C and formerly remained just about constant.

3.3 Fuel properties of the liquids

The obtained synthetic oil obtained from pyrolysis of plastic content of medical wastes had strong acrid smell and appears dark brown with. Comparison to commercial fuel kerosene oil and diesel, the fuel properties of the pyrolysis oil which are generally consumed in Bangladesh, are shown below in Table 2. This table shows that the pyrolysis oil density was found approximately similar to other commercial oil like diesel fuel and kerosene oil.

Table 2 – Fuel properties of the pyrolysis oil compared to commercial fuels

Property	Pyrolytic oil	Diesel	Kerosene
Density, kg/m^3	840	870–950	780–810
Gross calorific value, kJ/kg	41 325	44 800	35 000
Flash point, °C	39	52	37–65
Pour point, °C	14	−9…+9	−40

4 Conclusions

Recovery of liquid fuel from PMW through thermal pyrolysis was explored in the present issue quite effectively that added value to the energy sector. A limited number of trial runs were done at several operating conditions for the maximum liquid yield. The maximum yield of pyrolysis oil from the medical plastic waste was 53 wt % at a temperature of 260 °C with the feed size of 0.65 cm^3. It was observed that fuel properties of pyrolysis oil were comparable to that of diesel and furnace oil. There was possibility to have some impurities in the oil such as wax, water, higher hydrocarbons, etc. need to be removed. The pyrolysis oil can be suggested as a probable alternative fuel to commercial diesel as well as successful management of PMW toward safe environment.

References

1. Hossain, M., Som, U., Hossain, J., Rahman, M. W., & Iqbal, S. A. (2017). Recovery of Alternative Fuel from Thermal Pyrolysis of Medical Wastes. *Proceedia of the ICERIE International. Conference on Engineering Research, Innovation and Education*, pp. 683–688.
2. UNEP (2009). *Converting waste plastics into resource: Compendium of technologies*. United Nations Environment Programme, Osaka.
3. Hossain, M., Ahmed, S., Rahman, K. A., & Biswas, T. K. (2008). *Pattern of medical waste management: existing scenario in Dhaka city, Bangladesh*. BMC Public Health, pp. 1–10.
4. PRISM (2005). *Bangladesh, Survey Report on Hospital Waste Management in Dhaka City, Unpublished Report Dhaka*. PRISM, Bangladesh.
5. Dash, A. (2012). *Study on the thermal pyrolysis of medical waste (plastic syringe) for the production of useful liquid fuels*, Doctoral dissertation.
6. Aguado, J., & Serrano, D. (1999). *Feedstock Recycling of Plastic Wastes*. The Royal Society of Chemistry, UK.
7. Howell, G. S. (1992). A ten year review of plastics recycling. *Journal of Hazardous Materials*, Vol. 29, pp. 143–641.
8. Lopez, A., Marco, I., Caballero, B. M., Laresgoiti, M. F., & Adrados, A. (2011). Influence of Time and Temperature on Pyrolysis of Plastic Wastes in a Semi–Batch Reactor. *Chemical Engineering Journal*, Vol. 173, pp. 62–71.
9. Lee, K.-H., & Shin, D.-H. (2006). A Comparative Study of Liquid Product on Non-Catalytic and Catalytic Degradation of Waste PlasticsUsing Spent FCC catalyst. *Korean Journal of Chemical Engineering*, Vol. 23, pp. 209–215.
10. Butler, E., Devlin, G., & McDonnell, K. (2011). Waste Polyolefins to Liquid Fuels Vie Pyrolysis, *Waste Biomass Valor*, Vol. 2, pp. 227–255.
11. Dash, A., Kumar, S., & Singh, R. K. (2012). *Recovery of gasoline range hydrocarbons by thermal pyrolysis of plastic syringe waste.* Asia-Pacific Journal of Chemical Engineering, Wiley Publications.

Відновлення піролітичної олії з термічного піролізу лікарських відходів

Сом У.[1], Рахман Ф.[2], Хоссейн С.[3*]

[1] Джессорський університет науки і технології, Чурамонкаті–Чагач'я роуд, 7408, м. Джессор, Бангладеш;
[2] Університет Джахангірнагар, 1342, м. Савар, Bangladesh;
[3] Університет інженерії та технології м. Кхулна, 9203, м. Кхулна, Бангладеш

Анотація. У роботі досліджено потенціал відновлення корисних продуктів із пластичних медичних відходів (ПМВ) за допомогою піролізу. Одноразовий пластик є одним з найважливіших предметів у медичних відходах, а поліетилен високої щільності та поліпропілен – основними компонентами деяких ПМВ. Ці пластмаси мають більш високі приховані джерела вуглеводнів для хімічної промисловості. Піроліз ПМВ здійснювався в інтервалі температур 200–300 °C у паровому реакторі з нержавіючої сталі. Хімічні та фізичні властивості піролізної рідини були суттєво ближчими до комерційного палива, зокрема дизельного палива та бензину. Властивості піролітичної олії: густина 840 кг/м^3, питома енергоємність 4.13·10^4 кДж/кг, температура займання 39 °C. Також отриману рідину можна використовувати як альтернативне паливо.

Ключові слова: пластичні медичні відходи, піроліз, піролітична олія, альтернативне паливо.

Analysis of Technogenic Load of Oil and Gas Production on Caspian Region

Plyatsuk L. D.[1], Gabassova S. M.[1], Ablieieva I. Yu.[1*], Mamutova A.[2]

[1] Sumy State University, 2 Rymskogo-Korsakova St., 40007 Sumy, Ukraine;
[2] Al-Farabi Kazakh National University, 71 Al-Farabi Av., 050040 Almaty, Republic of Kazakhstan

Abstract. The problem of intensive pollution of the Caspian Sea has been continued to be one of the most significant and serious for the region. The rising of pollution level of the Caspian Sea coast with oil hydrocarbons has a particular concern. The purpose of this paper is to assess the pollution degree of the Caspian coast with petroleum hydrocarbons. The idea of the author is to provide a comprehensive analysis of the environmental destructive factors of the oil production process on natural complexes, including the effect of chemical pollution of the water basin with petroleum hydrocarbons on local hydrobionts. Methods of mathematical modeling of the oil films spreading on the water surface aimed to the prediction of the influence area, and methods of toxicological studies and assessment of the dose-effect relationship have been used. It was determined that the waters of the Caspian Sea, associated with offshore oil production, are areas of increased environmental risk. In the cases the concentration of hydrocarbons is above 1 mg / l, physiological changes are observed in the majority of dominant groups of hydrobionts. Areas of increased risk level for marine ecosystems caused by gas and oil industry development are connected with north and west-south parts of the Caspian Sea. The obtained results can be used to develop programs to ensure the environmental safety of the studied region.

Keywords: oil pollution, offshore oil production, marine biota, ecological risk, spills, Caspian Region, oil film, risk assessment, biodegradation, mathematical modelling.

1 Introduction

The discovery and development of a new oil and gas subprovince on the continental shelf of the Caspian Sea brought the region to the rank of one of the most promising areas for oil production in the 21st century [1]. The Caspian Sea is the largest in the world, unparalleled inland water area of more than 398 thousand square kilometers, not connected with the World Ocean. Currently, the proven oil reserves of the Caspian region are estimated at 5.4 billion tons (3.2 % of the world total), gas reserves are at the level of 8 trillion cubic meters (5 % of the world total) [2] (Figure 1).

Intensive oil production in the Caspian [3] entails a number of environmental problems. The technogenic load on the natural environment of the region is expressed both in the direct influence on the biota of chemical and physical factors, and indirectly by changing the habitat of marine hydrobionts.
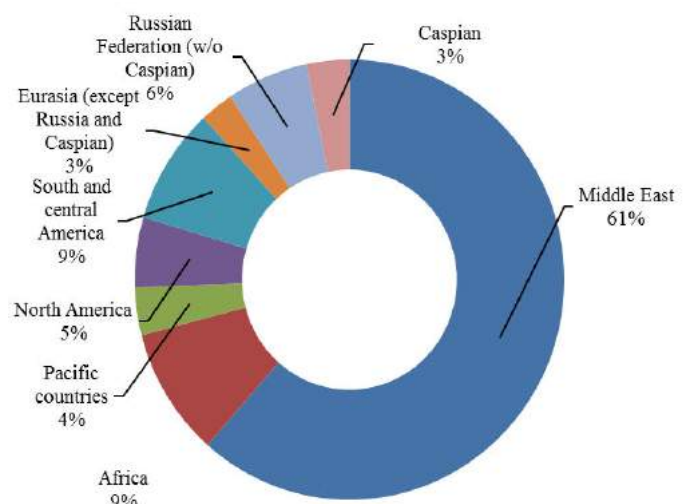

Figure 1 – Distribution of proven oil reserves

According to the Caspian Regional Thematic Center for Pollution Control (Caspian Environmental Program), up to 122.35 thousand tons of oil products enter the sea annually from various sources [4].

The situation is complicated by the ongoing processes of accumulation, decomposition and burial of incoming toxicants, which is typical of drainage reservoirs. Once released into the environment, oil may undergo a variety of natural processes that may act to reduce the severity of a spill, or accelerate the decomposition of the spilled oil into forms that are less environmentally hazardous. Five natural processes have been identified as particularly important to the fate of oil in the environment: weathering, evaporation, oxidation, biodegradation, and emulsification [5]. By their biological nature, products of oil transformation in the aquatic environment and their further combined interaction with other toxicants represent a high environmental hazard [6]. The development of toxic effects in aquatic organisms is determined mainly by the bioavailability of xenobiotics, the physicochemical parameters of the environment, and mainly the individual characteristics of the organism. The degree of susceptibility depends on the level of organization and physiological indicators of various taxonomic units. Some types of bacteria have appropriate enzymatic systems that ensure the involvement of petroleum hydrocarbons in metabolic reactions, and as a result of their biodegradation. Researchers [7–9] proved the high efficiency of using the consortium of bacteria Aquimarina, Polaribacter, Salegentibacter, Sulfitobacter, Idiomarina, which have significant oil destructive ability at low temperatures, as well as other bacteria that play a key role in reducing the concentration of oil in water.

According to research [10] on average 80 % of fish biomass and 86 % of secondary fish production would be retained after partial removal, with above 90 % retention expected for both metrics on many platforms. Partial removal result in the loss of fish biomass and production for species typically found residing in the shallow portions of the platform structure.

When assessing the level of anthropogenic pressure on the Caspian marine ecosystem due to offshore oil production, one of the unresolved issues is the determination of the zone of active pollution or the zone of maximum impact. Today, models of Fei, Johansen and Elliot, Blocker and others are known for evaluating the spreading field of oil film on the water surface when oil is supplied in various quantities [11], but the influence of oil is only one component of technological risk.

The purpose of the paper is to comprehensively assess the oil production activities in the Caspian environment.

2 Research Methodology

2.1 Materials

When oil / oil products enter the sea, they form oil films, and those in turn are smoothing areas on the sea surface or slicks. At the beginning of the era of remote sensing of the ocean, all the spots-slicks on the sea surface and, accordingly, dark spots on radarlocation images (RLI) were considered as films of oil or oil products. In the first hours of film existence, physicochemical processes for the removal of petroleum hydrocarbons from the surface of water dominate [12]. Components with a low boiling point quickly evaporate, dragging fractions with a higher boiling point. In the first few days, depending on the composition of the oil and hydrometeorological conditions, 30–70 % of the oil is lost, mainly the C_4–C_{12} fraction. Chemical transformations of oil in the water column are oxidative, often accompanied by photochemical reactions under the influence of the ultraviolet part of the solar spectrum and can be catalyzed in the presence of certain trace elements, such as vanadium, and inhibited by sulfur compounds. The final oxidation products (hydroperoxides, phenols, carboxylic acids, ketones, aldehydes, etc.) usually have an increased solubility in water and are highly toxic. Photo-oxidative reactions initiate the polymerization and destruction of the most complex molecules in the composition of oil, increase its viscosity and the content of tar and asphaltene products and contribute to the formation of solid oil aggregates.

Films of crude oil and heavy oil products (including emulsions) are very thick and can reach a thickness of several millimeters on the sea surface, ranging in color from dark brown to metallic gray. Crude oil is capable of forming emulsions on the sea surface, which can contain up to 80 % of water (visually from light brown to orange). The shapes and sizes of the spots of oil and oil products are extremely diverse. These contaminants may appear near oil platforms, floating storage facilities, terminals, pipelines, wells, other operating or abandoned offshore oil and gas facilities; they are formed as a result of exploration, drilling, production, transportation and other operations with oil and oil products, as well as result of accidents with tankers and oil platforms. A significant part of oil and oil products can be carried with river runoff in cases where leaks and accidents occur on land.
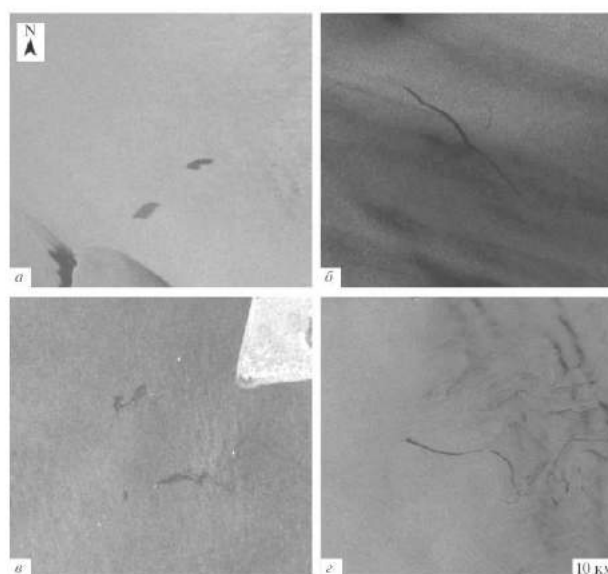

FIgure 2 – Examples of film pollution found in the Caspian Sea

Oil slicks glittering on the surface of the sea and thousands of hectares of soil penetrated by oil leaking from abandoned wells are just part of the pollution that people living around the Caspian Sea must endure. In addition there are various industries, particularly chemicals and mining, large-scale irrigated farming and untreated household waste. Combined with the effects of the oil, all these forms of pollution have a serious impact on the well-being of humans and wildlife.

Another source of oil products in the Caspian Sea is the industrial and economic flow of cities and towns along the coastal strip of the sea. 200 large cities with more than 220 sources of pollution of the water basin are concentrated in the Caspian region. Here, about 39 cubic kilometers of wastewater is discharged annually, of which almost 8 cubic kilometers are polluted. Together with sewage, up to 30 tons of petroleum hydrocarbons are

dumped into the sea. Beyond the scope of statistical reporting, rainfall runoff of settlements, as well as emergency discharges [13].

2.2 Factors affected on the behavior and fate of petroleum compounds

Figure 3 shows the interrelationships among the physical, chemical, and biological processes that crude oil undergoes when introduced into the marine environment, subsequently weathers, and is then transported away from the source. Processes involved in the weathering of crude oil include evaporation, emulsification, and dissolution, whereas chemical processes focus on oxidation, particularly photooxidation. The principal biological process that affects crude oil in the marine environment is microbial oxidation.
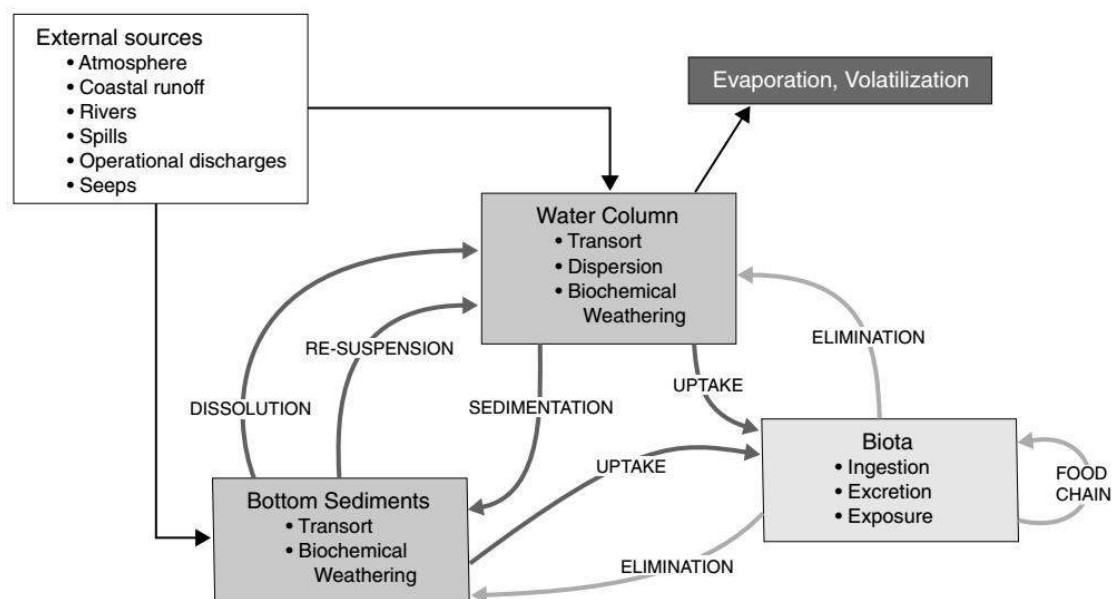

Figure 3 – Detailed interactions of a conceptual model for the fate of petroleum in the marine environment [14]

The kinetics of the breakdown of oil and petroleum products in the marine environment is determined by the influence of external factors related to the properties and characteristics of the environment in which the oil falls. Experiments have shown that the temperature factor is decisive in the kinetics of the breakdown of petroleum and petroleum products. In general cases, the rate of chemical reactions with a temperature increase of 10 °C increases by 2–4 times, and a decrease in the temperature of the medium significantly inhibits not only the physicochemical, but also the biochemical processes associated with the destruction and transformation of various substances. This is explained by the fact that temperature conditions have an undoubted effect on the rate of reproduction of the bacterial mass – as the temperature decreases, the total number and number of heterotrophic organisms decreases.

An increase in the salinity of seawater also adversely affects the biochemical oxidation of petroleum hydrocarbons. The changing of salinity by 1 % causes the half-life

of petroleum hydrocarbons changes by 22 hours. However, for each marine region, changes in salinity are generally very small, and sharp salinity gradients are observed mainly in the zones of influence of river flow and melting (formation) of ice. The same can be said about the effect of pH on the biochemical oxidation of petroleum hydrocarbons. Thus, the effect of a change in the half-life of petroleum hydrocarbons on temperature is 25 times more than on changes in pH and 8 times more than on changes in salinity.

If the hardly soluble oil residues, together with the inorganic and organic impurities included in them, approach the density of sea water (or exceed it), then in this case they are sedimented. As a result, oil aggregates can sink to the bottom or leach onto the shore, which leads to the purification of the water column. In turn, the bottom sediments during wave roiling can be a source of pollution of marine waters.

2.3 Methods of mathematical modeling of the spreading of the oil film on the water surface

It is advisable to simulate the spreading of oil film to predict the scale of emergency oil spills in the sea, and as a consequence, the zone of maximum damage to the ecosystem. The process of spreading the oil film over the sea surface occurs under the action of various forces, but to simplify the task, we take into account the force of gravity and viscous friction. The main characteristics of the oil film will be its radius and thickness. The process is described using the mass conservation equation for the elemental volume of an oil film and the equation of motion of a viscous Newtonian fluid [15]. The equation of mass conservation for the mathematical model of the process under consideration in the axisymmetric case can be represented as

$$\frac{\partial h}{\partial t} + \frac{1}{r}\frac{\partial (ruh)}{\partial r} = 0. \tag{1}$$

The equation of fluid motion is

$$\frac{\partial u}{\partial t} + u\frac{\partial u}{\partial r} = -g\delta\frac{\partial h}{\partial r} - \frac{\tau}{\rho_0 h}. \tag{2}$$

where h is oil film thickness, m; u is film speed averaged over film thickness, m/sec; τ is shear stress at the bottom of the film; g is acceleration of gravity, m/s²; $\delta = (\rho_w - \rho_o)\rho_o^{-1}$; ρ_w, ρ_o is density of water and oil respectively, kg/m³; r is radial coordinate; t is time, sec.

The solution of the differential equations (1) and (2) from the specified initial conditions by analytical methods allowed us to obtain a formula for determining the final radius $r_k(t)$ of the oil film at a certain point in time as the ratio

$$r_k(t) = \xi_0 \left(\frac{V_0^3 \alpha t}{8\pi^3}\right)^{1/8}. \tag{3}$$

Oil spill modeling is based on GIS technology. Modeling is done using software ArcGIS for Desktop Advanced v.10.2 and ADIOS® (Automated Data Inquiry for Oil Spills) is NOAA's oil weathering model. It's an oil spill response tool that models how different types of oil weather (undergo physical and chemical changes) in the marine environment. Working from a database of more than a thousand different crude oils and refined products, ADIOS quickly estimates the expected characteristics and behaviour of spilled oil.

2.4 Methods to assess impact concentrations of chemicals

The greatest source of uncertainties in deriving assessment end points (e.g. a PNEC; the concentration below which organisms in the area of interest are unlikely to be adversely affected) is the extrapolation of laboratory bioassay results to the natural environment. The requirement to both culture and maintain test species in the la-

boratory restricts the selection of possible test species and the species used are often not very representative for the large spectrum of species, with varying degree of sensitivity that may occur in natural ecosystems. This exercise of extrapolation therefore involves many often untested assumptions (Figure 4).
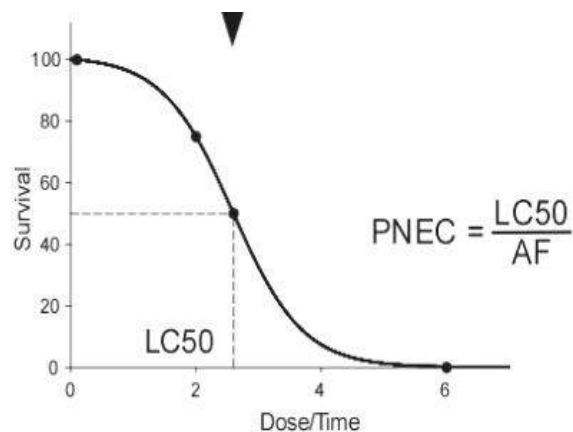

Figure 4 – Dose-response relationship based on laboratory toxicity test (bioassay), here fish

The outcome is often that the PNECs may be either overprotective or underprotective, depending upon the biological and environmental conditions that apply at each natural site [16, 17]. This severely limits the usefulness of the chemical criteria in Ecotoxicological Risk Assessment (ERA). The two main approaches used to extrapolate lab data to field data to obtain an estimate of the field Predicted No Effect Concentration (PNEC) is (1) using an assessment factor approach or, when sufficient data are available, (2) from statistical extrapolation.

LC50 is the lethal concentration to 50 % of the individuals but any level of biological organization (e.g. molecular, cellular, organ and organism), effect level (e.g. NOEC, the highest concentrations with no observed effect and LOEC, the lowest concentration with observed effect) and life history variable (growth, reproduction, swimming speed etc.) can be used to estimate an effect concentration.

Experience shows that different species differ in their sensitivity towards a single chemical. This may be due to differences in life history, physiology, morphology and behavior. The species sensitivity distributions (SSDs) approach is a statistical description of the variation among a set of species in toxicity of a certain compound or mixture (Figure 5). SSDs consider variation between species and not within species and do not attempt to explain why species differ in sensitivity. It is a probabilistic approach in contrast to the deterministic procedure of assessment factors.

As mentioned [18] forward use $(x \rightarrow y)$ in risk assessment and inverse use $(y \rightarrow x)$ in EQC is indicated.
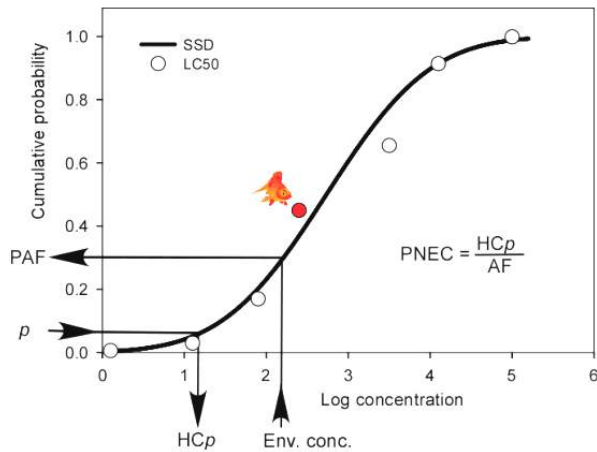
Figure 5 – Species sensitivity distribution combining results from various single species bioassay

2.5 Methodology of oil toxicity studies

Under the Chemical Response to Oil Spills: Ecological Research Forum (CROSERF) [19] is often used to determine lethal concentrations. In general, field studies allow for less control of environmental variables but allow for investigations that may not be possible in most laboratory experiments (e.g., multi-species assemblages). Field experiments are also more costly and regulatory approvals

from various stakeholders are sometimes difficult to obtain.

Multivariate analysis and the biotic index (BIOSTRESS) Multivariate analysis is regarded as the most sensitive technique for distinguishing site groupings of disturbed assemblages related to oil activity. Subtle effects induced by pollutants may be reflected in changes in the community composition that may be identified using the biological criteria discussed above (e.g. similarity matrixes, species response models) together with multivariate techniques (e. g. ordination and classification) [20].

3 Results

Studies on natural models in the Caspian Sea have shown that physicochemical oxidation plays a significant role in the breakdown of petroleum hydrocarbons, which is consistent with the results of the practical development of a system for protecting the biological diversity of the Caspian Sea from oil pollution [22].

A summary of the processes that affect the fate of petroleum hydrocarbons from seven major input categories is shown in table 1. Each input is ranked using a scale of high, medium, and low that indicates the relative importance of each process. The table is intended only to convey variability and is based on many assumptions.

Table 1 – Processes that move petroleum hydrocarbons away from point of origin

Input Type	Seeps	Spills	Light distillates	Crudes	Heavy distillates	Produced water	Vessel operational	Atmospheric
Persistence	years	days	days	months	years	days	months	days
Horizontal Transport or Movement	H	L	M	M	H	L	M	H
Vertical Transport or Movement	M	NR	L	M	H	L	L	NR
Evaporation	H	H	M	M	L	M	M	H
Emulsification	M	NR	L	M	M	NR	L	NR
Dissolution	M	M	H	M	L	M	M	M
Oxidation	M	L	L	M	L	M	L	M
Sedimentation	M	NR	L	M	H	L	L	NR

Note: H = high; L = low; M = moderate; NR = not relevant.

The resulting (integral) film pollution maps found in the Northern Caspian in 2009–2013, 2014–2015, are shown in Figures 6 a, b. For the convenience and simplicity of the analysis on these maps the boundaries of state sectors (economy zones), the main ship routes and license areas are plotted. They were created by combining all the vector contours of the found pollution for one year into one layer and then merging the annual maps into one.

National Caspian Action Plan of Azerbaijan, 2002; National Action Programme on Enhancement of the Environment of the Caspian Sea, Kazakhstan 2003–2012; Environmental Performance Review of Kazakhstan, UNECE, 2000; Environmental Performance Review of

Azerbaijan, UNECE, 2003; Study for; Safe Management of Radioactive Sites in Turkmenistan, NATO, 2005; Environment and Security: Transforming Risks into Cooperation, Case of Central Asia, 2003 ; Global Alarm: Dust and Sandstorms from the World´s Drylands, UNCCD, 2001.

The concentration of SPAR in the water area was higher when it was calm (0.45 mg/l) than under the conditions of the northern (0.31 mg/l), southern (0.26 mg/l), western (0.23 mg/l) and east (0.13 mg/l) winds [22]. Moreover, the content of oil components in the west (0.34 mg/l) of the region always exceeded their indicators in its eastern and central (0.14 mg/l) parts. The NU con-

tent in the water area decreased from weak (0.15–0.32 mg/l) to moderate (0.09–0.24 mg/l), significant (0.07–0.19 mg/l), and severe disturbances. The effect of the latter in calm is also combined with a decrease in the oil content in the range (0.09–0.27 mg/l). Integrated map of film pollution is shown in Figure 6.
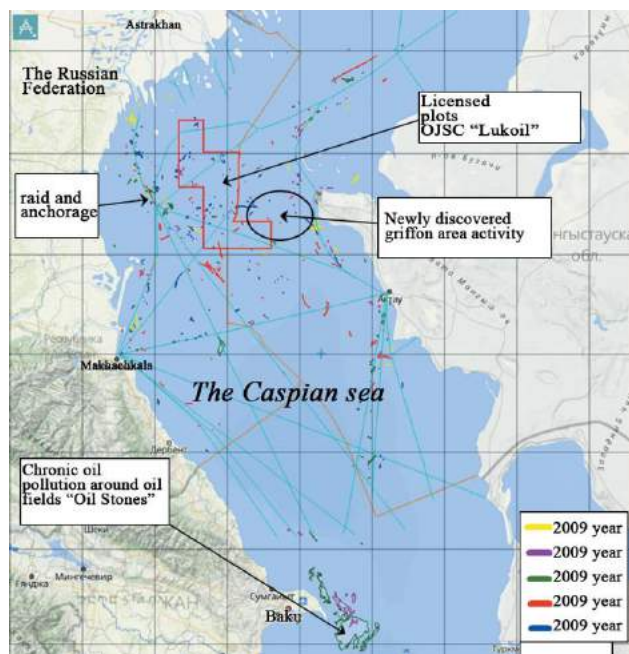

Figure 6 – Integrated map of film pollution found in the Caspian Sea in 2009–2013: light brown lines are the boundaries of public sectors, blue ones are the main ship routes; red is licensed blocks of OAO "Lukoil"

4 Discussion

In the northern part of the Caspian Sea, where oil is being actively extracted, no films of crude oil were found (Figures 6 a, b). This, in general, is explained by effective industrial and environmental safety measures that Lukoil uses during exploration and production of oil in the Caspian Sea. (According to company representatives, the risk of emissions of crude oil is virtually zero.) 6a shows a map of the distribution of film contamination in the sea for 5 years, from which it follows that the largest pollution areas were found in the main shipping routes and approaches to the Caspian ports of Russia and Kazakhstan. They are also ship-based and can be mining, bilge water and other liquid waste, due to commercial transport and fishing, and, to some extent, tanker shipments of oil. This is also confirmed by rice, and Figure 6 b is for 2014–2015.

The results of experiments in the Caspian Sea showed that lowering the temperature of the aquatic environment by 10 °C lengthens the half-life of dissolved forms of oil by 2 times, and a change in the temperature of the medium by 1 °C changes this period by 40 hours. Thus, with a decrease in water temperature from 28 °C to 0 °C, the half-life period is extended by 1.12 hours.

The wind speed is important for the spread of oil spills on the surface of the Northern Caspian, along with the direction. With its increase in the area of water there is a decrease in the concentration of oil impurities from weak (0.15–0.32 mg/l) to moderate (0.08–0.18 mg/l) and strong (0.07–0.15 mg/l) winds [23]. However, in the case of continuous operation of the source of pollution with the same wind, the amount of petroleum hydrocarbons first decreases and then increases again, stabilizing at the original level.

The inertia of levels of sea pollution associated with the action of winds is noted. With the duration and constancy of the volumes and the quality of the anthropogenic runoff, after some decline, the concentration of toxicants is restored. At the same time, the dual role of winds and waves in self-purification and secondary pollution of sea waters as a result of their mixing and stirring up of bottom sediments can be traced. Other things being equal (distance from the source of pollution, depth of occurrence, physical properties) the content of harmful impurities in bottom soils depends on the degree of their dispersion, the predominance of fine or coarse fractions.

Despite the relatively small losses of hydrocarbons during their production on the shelf, emergencies at drilling rigs remain inevitable so far, and with emergency and technological discharges of oil products into the sea from drilling rigs, pollution is mostly local in nature. However, near the source, the concentration of petroleum hydrocarbons may be tens or hundreds of times higher than the norm established for fishery bodies of water. On average, during the development of fields, 30–120 tons of oil comes from a single well into the marine environment. In cases where local pollution becomes chronic, oil not only pollutes water, but also bottom sediments.

Studies have revealed the dependence of the toxic effects of wastewater, drilling mud and sludge on the organisms of the Caspian Sea on their composition and habitat conditions. Oil hydrocarbons at a concentration of 0.05–0.5 mg/l, as a rule, do not affect the survival of marine organisms if their toxic effect is not aggravated by the action of other toxicants. At the same time, almost all tissues and organs show physiological and biochemical changes that become irreversible with an increase in the concentration of oil from 0.5 mg/l to 50 mg/l. Already at the very bottom of this interval (0.5–1.0 mg/l), changes in physiological and biochemical parameters are accompanied by impaired growth and development, as well as fish fertility. Reduced fertility is manifested to a greater extent in subsequent generations. The stability of aquatic and benthic organisms to the toxic effects of oil depends on their taxonomic identity and stage of development, the concentration of hydrocarbons, the duration of exposure, and its combination with other factors and environmental conditions.

Figure 7 – Hazards in and around the Caspian

5 Conclusions

The ecological state of the Caspian Sea is deteriorating due to the intensification of oil production on the sea shelf. The influx of petroleum hydrocarbons into the aquatic environment occurs additionally due to river flow. It is determined that the components of oil undergo transformations under the influence of physical, chemical and biological processes. Under the conditions of temper-ature, salt and wind regimes characteristic of the Caspian, these reactions are based on photo-oxidation processes. Nevertheless, biodegradation plays an important role. Ana-lyzed models of spreading oil film, allowing to determine and predict contaminated areas. The main ways of xenobi-otic influence on hydrobionts are considered.

According to the results of the assessment of the techno-genic load on the natural environment of the Caspian Sea, zones of high, moderate and low levels of environmental risk were identified (Figure 7).

References

1. Mercheva, V. S. (2012). Environmental responsibility in the development of oil and gas fields in the Caspian region. *Astrakhan Bulletin of Environmental Education,* Vol. 3, Issue 21, pp. 94–101 [in Russian].

2. Kuramshin, D. R. (2016). Estimation of hydrocarbon reserves in the countries of the Caspian region. *University Bulletin*, Vol. 7–8, pp. 82–87 [in Russian].

3. Petrov, M. P., & Lubenko, V. N. (2008). Prospects for offshore oil and gas production on the shelf of the Northern Caspian Sea and possible ways of their transportation. *ASTU Bulletin*, Vol. 43, Issue 2 [in Russian].

4. Zakirov, S. N., & Korotaev, Yu. P. (1985). Principles of development of the Caspian deposits. *The gas industry,* Issue 11, pp. 5–8 [in Russian].

5. EPA (2004). *The Fate of Oil, Office of Emergency Management, Oil Program, Washington, D.C*. Retrieved from: http://www.epa.gov/oilspill/oilfate.htm.

6. Abdurakhmanov, G. M., Akhmedova, G. A., & Gasangadzhieva, A. G. (2006). Pollution of the western part of the Middle Caspi-an by oil hydrocarbons and biological diversity. *ASTU Bulletin,* 2006, Vol. 32, Issue 3 [in Russian].

7. Fasca, H., de Castilho, L. V. A., de Castilho, J. F. M., et al. (2008). Response of marine bacteria to oil contamination and to high pressure and low temperature deep sea conditions. *MicrobiologyOpen*. Retrieved from: https://doi.org/10.1002/mbo3.550.

8. Santisi, S., Cappello, S., Catalfamo, M., Mancini, G., Hassanshahian, M., Genovese, L., Giuliano, L., & Yakimov, M. (2015). Biodegradation of crude oil by individual bacterial strains and a mixed bacterial consortium. *Brazilian Journal of Microbiology*, Vol. 46, pp. 377, doi: 10.1590/S1517-838246120131276.

9. Fathepure, B. Z. (2014). Recent studies in microbial degradation of petroleum hydrocarbons in hypersaline environments. *Fron-tiers in Microbiology*, Vol. 5, pp. 173. doi: 10.3389/fmicb.2014.00173.

10. Claisse, J. T., Pondella, D. J., Love, M., Zahn, L. A., Williams, C. M., & Bull, A. S. (2015). Impacts from Partial Removal of Decommissioned Oil and Gas Platforms on Fish Biomass and Production on the Remaining Platform Structure and Surrounding Shell Mounds. *PLoS ONE*, Vol. 10 (9), no. e0135812, doi: 10.1371/journal.pone.0135812.

11. Dmitrenko, A. B., Pavlov, A. A., & Chernyaev, A. B. (2007). Integrated model for computer analysis of the consequences of emergency oil spills from pipelines. *Information technology modeling and management,* Vol. 8, pp. 970–975 [in Russian].

12. Ivanov, A. Yu., Kucheiko, A. A., Filimonova, N. A., Kucheiko, A. Yu., Evtushenko, N. V., Terleeva, N. V., & Uskova, A. A. (2017). Time-spatial distribution of film pollution in the Black and Caspian Seas according to the space radar data: a compara-tive analysis. *Earth Study from Space*, Issue 2, pp. 13–25 [in Russian].

13. Report on the state and use of water resources of the Republic of Dagestan in 2002 (2003). *Federal State. Department of Water Management of the Republic of Dagestan "Dagvodresursy"*, Makhachkala, Russia.

14. Transportation Research Board and National Research Council (2003). *Oil in the Sea III: Inputs, Fates, and Effects*. The National Academies Press, Washington, USA, doi: 10.17226/10388.

15. Hamzayev, Kh. M. (2009). Modeling the spreading of oil film on the sea surface. *Applied mechanics and technical physics,* Vol. 50. Issue 3, pp. 127–130 [in Russian].

16. Kapustka, L. A., Clements, W. H., Ziccardi, L., Paquin, P. R., Sprenger, M., & Wall, D. (2004). *Issue paper on the ecological ef-fects of metals*. U.S. Environmental Protection Agency, Washington, USA.

17. Crane, M., Kwok, K. W. H., Wells, C., Whitehouse, P., & Lui, G. C. S. (2007). Use of field data to support European water framework directive quality standards for dissolved metals. *Environmental Science and Technology*, Vol. 41 (14), pp. 5014–5021.

18. Posthuma, L., Traas, T. P., & Suter, G. W. (2001). *General introduction to species sensitivity distributions. In: L. Posthuma, G.W. Suter and T.P. Traas (Editors), Species Sensitivity Distributions in Ecotoxicology*. CRC Press, Boca Raton, Florida, USA.

19. Singer, M., Aurand, D., Bragin, G., Clarks, J., Coelho, G., Sowby, M., & Tjeerdema, R. (2000). Standardization of the prepara-tion and quantitation of water-accommodated fractions of petroleum for toxicity testing. *Mar. Pollut. Bull.*, Vol. 40, pp. 1007–1016.

20. Dupuis, A., & Ucan-Marin, F. (2015). *A literature review on the aquatic toxicology of petroleum oil: An overview of oil properties and effects to aquatic biota*. DFO Can. Sci. Advis. Sec. Res. Doc.

21. Sokolsky, A. F., Popova, N. V., Kolmykov, E. V., & Kurapov, A. A. (2005). *Bioecological foundations and practical development of the system for protecting the biological diversity of the Caspian Sea from oil pollution*. CaspNIRKH, Astrakhan, Russia.

22. Mehtiyev A. Sh., & Gul, A. K. (2006). *Technogenic pollution of the Caspian Sea*. Elm Publishing, Baku, Azerbaijan [in Russian].

23. Gul, A. K., & Faradzheva, L. N. (2010). On the distribution of technogenic impurities in the Northern Caspian. *Caspian Bulletin*, Issue 3, pp. 35–41 [in Russian].

Аналіз техногенного навантаження від нафто-газової промисловості на Каспійський регіон

Пляцук Л. Д.[1], Габбасова С. М.[1], Аблєєва І. Ю.[1], Мамутова А.[2]

[1] Сумський державний університет, вул. Римського-Корсакова, 40007, м. Суми, Україна;
[2] Казахський національний університет ім. Аль-Фарабі,
просп. Аль-Фарабі, 71, 050040, м. Алмати, Республіка Казахстан

Анотація. Проблема інтенсивного забруднення Каспійського моря продовжує залишатися однією з найважливіших і найсерйозніших для регіону. Особливе занепокоєння викликає підвищення рівня забруднення нафтовими вуглеводнями узбережжя Каспійського моря. Мета даної статті полягає в оцінці ступеня забруднення прибережної зони Каспію нафтовими вуглеводнями. Авторська ідея полягає у забезпеченні комплексного аналізу екодеструктивних факторів процесу нафтового видобутку на природні комплекси, зокрема впливу хімічного забруднення нафтовими вуглеводнями водного басейну на місцеві гідробіонти. У роботі використані методи математичного моделювання поширення нафтових плівок на поверхні води, спрямовані на прогнозування області впливу, а також методи токсикологічних досліджень та оцінювання взаємозв'язку «доза – ефект». Встановлено, що води Каспійського моря, пов'язані з видобутком нафти, є районами підвищеного екологічного ризику. У випадках, коли концентрація вуглеводнів перевищує 1 мг/л, фізіологічні зміни спостерігаються у більшості домінуючих груп гідробіонтів. Зони підвищеного рівня ризику для морських екосистем, спричинені розвитком газової та нафтової промисловості, пов'язані з північною та південно-західною частинами Каспійського моря. На підставі проведених досліджень одержані результати, необхідні для розроблення програм забезпечення екологічної безпеки досліджуваного регіону.

Ключові слова: нафтове забруднення, видобуток нафти на морському шельфі, гідробіонти, екологічний ризик, витоки, Каспійський регіон, нафтова плівка, оцінювання ризиків, біодеградація, математичне моделювання.

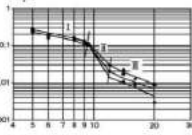## Department of Applied Ecology
Main Research Areas of the Department

Development of technologies and mass transfer equipment for purification of gas emissions

Developing ways to improve the environmental situation of cities and industrial zones

Comprehensive approach to the prevention and control of environmental pollution. Implementation of the methodology "Clean Production"

Modeling and assessment of environmental risks caused by environmental pollution

Biotechnology of technogenic waste recycling and environmental protection

Bioindication research of urban ecosystems condition
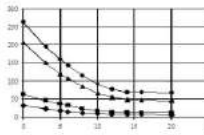
Laboratory Facilities

Laboratory of biochemical investigations

Laboratory of atomic absorption analysis

Laboratory bench of gases purification

Laboratory bench of multicomponent mixtures separation

Laboratory bench of electrochemical treatment of sewage

Cooperation with industrial sector:

- developing of mass transfer and and gas cleaning equipment;
- implementation of environmental management systems;
- drafting environmental documentation and assistance in obtaining permits etc.;
- ISO certification;
- development and optimization of the protected sites network, ecological network area.

http://ecolog.sumdu.edu.ua

Copyright Agreement

We, the Authors of the Manuscript publishing in the Journal of Engineering Sciences, in the case of acceptance for publication, transfer to Founders and Editorial Board the underlined rights:

– publishing this article in English and distribution of the printed version;

– English translation of the article (for articles in Ukrainian or Russian) and distribution the hard copy of the translation;

– distribution of the electronic version of the article, as well as electronic version of English translation (for articles in Ukrainian or Russian) through any electronic means (by hosted on the official web-site of the Journal, in electronic databases, repositories, etc.).

We reserve the rights without the consent with the Editorial Board or Founders:

– to use the article materials in whole or partly for educational purposes;

– to use the article materials in whole or partly to write own dissertations;

– to use the article materials for thesis preparing, conference materials, as well as for presentations;

– to post electronic copies (including the final electronic version downloaded from the official web-site of the Jounal):

– on the personal web-sources of the all co-authors (web-sites, web-pages, blogs, etc.);

– on the web-sources of authors working organizations (including electronic institutional repository);

– on the International Scientometric Databases (CrossRef, DOAJ, Index Copernicus Indexing, etc.);

– on non-commercial Open Access sources (e.g. arXiv.org).

In all cases, the presence of citations to the article or hyper-link to the electronic copy of on the official web-site of the journal is obligatory.

By this agreement we also certify that the submitted manuscript:

– does not violate the copyrights of other persons or organizations;

– has not been published previously in other publishing houses and submitted for publication in other Journals.

Dear Authors of the Journal of Engineering Sciences!

The Editorial Board of the Journal of Engineering Sciences pays special attention to the structure of the articles according to the "Enhancement of requirements to specialized editions registered in the databases of Ukrainian State Commission for academic degrees" (minutes No. 7-05/1 from January 15, 2003). Only original articles by the authorship of up to 5 authors are accepted for the publication according the **Template** with the following elements:

– general statement of the problem and its relation with the important scientific or practical problems;

– analysis of the recent investigations and publications in the same research field;

– statement of the significance of the general problem that were not solved before;

– statement of the purpose of the research article;

– description of the initial data of the research with the justification of the achieved scientific results;

– conclusions and ways for further development of the research.

All the articles are reviewed by the independent double-blind procedure.

All the authors should sent via e-mail jes@sumdu.edu.ua the electronic version of the following materials:

– article **in English** according to the **Template**;

– information about authors and their affiliation with the related address.

ATTENTION!

If one of the mentioned components is not sent or there are many stylistic, orthographic and grammatical errors, the article will not be taken into consideration by the Editorial Board and will not be reviewed.

Minimum size of the materials:

1. Scientific – theoretical articles (up to 25 000 symbols, about 14 pages) that deal with the theoretical research and descriptions of physical laws concerning the investigated phenomena; theoretical generalizations and fundamental principles proved by the experimental research data.

2. Scientific-practical articles (up to 10 000 symbols, about 6 pages) that deal with scientific experiments and real experience. They include the statement of the proposed methods for the experimental research or means for the observation of the studied phenomena. An essential part of these articles is the description of the achieved results and their explanation acquired in the process of immediate interaction with the object of investigations, its significance and practical implementations.

3. Scientific-methodological articles (up to 15 000 symbols, about 8 pages) that deal with the review of processes, methods, instruments for solving scientific and applied problems; the statement of the new methodology, results of which allow creating more precise methodology on the basis of up-to-date methodology for the implementation of discovered laws.

JOURNAL OF ENGINEERING SCIENCES

ЖУРНАЛ ІНЖЕНЕРНИХ НАУК

ЖУРНАЛ ИНЖЕНЕРНЫХ НАУК

Scientific Journal

Науковий журнал

Научный журнал

State registration certificate of the print mass-media No. 20499-10299 ПР.